Experimental study of pressure grouted soil nail system

By

Mohammad Zahidul Islam Bhuiyan

M.Eng.Sc. (Geotechnical Engineering)

B.Sc. (Civil Engineering)

A thesis submitted in the partial fulfilment of the requirements for the degree of **Doctor of Philosophy** in Civil Engineering

THE UNIVERSITY OF NEWCASTLE AUSTRALIA

Faculty of Engineering and Built Environment

School of Engineering

June 2020

Experimental study of pressure grouted soil nail system

Statement of Originality

I hereby certify that the work embodied in the thesis is my own work, conducted under normal supervision. The thesis contains no material which has been accepted, or is being examined, for the award of any other degree or diploma in any university or other tertiary institution and, to the best of my knowledge and belief, contains no material previously published or written by another person, except where due reference has been made. I give consent to the final version of my thesis being made available worldwide when deposited in the University's Digital Repository, subject to the provisions of the Copyright Act 1968 and any approved embargo.

Mohammad Zahidul Islam Bhuiyan

Experimental study of pressure grouted soil nail system

Acknowledgement of Authorship

I hereby certify that the work embodied in this thesis contains published papers of which I am a joint author. I have included as part of the thesis a written declaration endorsed in writing by my supervisors, Professor Shanyong Wang and Emeritus Professor John P. Carter, attesting to my contribution to the joint publications.

By signing below I confirm that Mohammad Zahidul Islam Bhuiyan contributed those publications as listed under the List of Publications section.

____
Professor Shanyong Wang

____
Emeritus Professor John P. Carter

Abstract

Soil nailing is a reinforcement technique, used to reinforce in situ ground to stabilize it more effectively and economically, in which the reinforcing slender elements (typically steel bars), called soil nails, are inserted into a soil mass by different installation methods such as driving, jacking or pre-drilling. The nailing technique is extensively applied for slopes, excavations and retaining walls. Conventionally, frictional soil nails (e.g., driven, drilled and grouted nails) are commonly used in practice, based on the soil conditions, project cost and construction flexibility, and the pullout resistance of the frictional nails primarily comes from the frictional resistance developed at the nail/soil (driven nail) or grout/soil interface (drilled and grouted nail). The frictional soil nails do not show any end bearing resistance and, thus, soil-nailed structures have the potential to undergo a relatively large lateral deflection after construction. Therefore, the frictional resistance is considered an important parameter for the design and safety assessment of conventional soil-nailed structures. In soil nailing practice, primarily, this parameter is still evaluated using field-based experience rather than a detailed scientific knowledge of nail-soil interactions.

Nowadays, pressure grouting is being progressively used for soil nailed structures as an alternative to the frequently used conventional gravity/low pressure grouting, since this grouting technique has the ability to increase the bond strength significantly, which in turn increases the pullout resistance of a grouted soil nail. The objective of this research is to develop a reliable and efficient method for enhancing the pullout resistance of soil nails through experimental research.

This thesis concentrates on the experimental study of pressure-grouted anchor-type nail systems, which are being developed in the Priority Research Centre for Geotechnical Science and Engineering, The University of Newcastle, Australia. To conduct the fully instrumented experimental study, a new volume-controlled injection system was developed and the existing apparatus was redesigned and modified for pullout testing of the pressure-grouted nail system. The physical model study was comprised of three test groups. The underlying objective of Group 1 was to evaluate the effects of grout injection rates on the pressure-grouted soil nail system. To assess the grouting rate effects on the grout injectability and the pullout resistance of the pressure-grouted soil nail, pressurized grout (w/c = 0.50) was injected through the pre-buried soil nail by the newly developed volume-controlled injection pump at different injection rates, viz. 4.0 L/min, 5.0 L/min, and 6.5 L/min. Note that a latex membrane was used as a liner around the grouting outlets of the pre-buried hollow nail to form a Tube-a-Manchette (TAM) for direct injection of grout into the surrounding soil, simulating compaction grouting, which resulted in the formation of a grout bulk around the outlets (injection points). The results obtained from this experimental study (Group 1) revealed that the volume of injected grout (i.e., grout penetration) increased as the injection rates increased, and thus the pullout resistance of the pressure-grouted soil nail also increased with the injection rate. It was found that the pullout resistance of the nail was governed by the injected grout volume rather than the injection pressure and the grouted nail acted as an anchor, showing a significant strain-hardening behaviour in pullout resistance. In addition, the results indicated that the expulsion (seepage) of water from the pressurized neat cement grout was directly and proportionally related to the injection rate, i.e., the higher the injection rate, the higher the seepage of water.

In the case of Group 2, a series of fully instrumented physical model tests were conducted to evaluate the performance of the grout, including its bleeding resistance, propagation and pressure transfer mechanism into the surrounding soil under pressurized injection conditions. Like Group 1, a pre-buried soil nail with a Tube-a-Manchette (TAM) facility was used for direct injection of the pressurized additive-mixed grout into the soil surrounding the nail to evaluate the grout-soil interaction in sand. As a grouting fluid, three different grout compositions with water/solid (cement + additive) ratio (w/s) varying from 0.30 to 0.50 were used and the performances of these grouts were compared with a traditionally used neat cement grout (w/c = 0.50). The results of Group 2 indicated that addition of an additive (a blend of superplasticizers and suspension agents) in a neat grout mix decreased the viscosity of the grout significantly by reducing the agglomeration tendency of the cement particles in suspension. The viscosity of the cementitious grout increased exponentially as the water solid (w/s) ratio decreased, whereas fluidity increased by increasing the w/s ratio. Consequently, the injectability (penetration) of the grout into a soil mass increased with decreases in viscosity of the injecting grouts. Furthermore, it was found that the volume of grout injected not only influenced the pullout capacity of pressure-grouted nails but the shape of the bulb formed inside the compacted fill also affected this type of nail performance, since highly fluid grouts (e.g., w/s = 0.40 and 0.50) formed irregular grout bulbs (deformed bulbs) that failed easily due to the stress concentration at a very small pullout displacement without mobilizing its maximum pullout capacity for a specified grout volume. Therefore, an additive-mixed cementitious grout of w/s ratio 0.30 was suggested as an effective and alternative grouting fluid compared with the conventional neat grout (w/c = 0.50) for the pressure grouted nail system because of its high bleed resistance, high compressive strength, high bond strength, low shrinkage and high fluidity.

Based on the performance of the pressure-grouted (pre-buried) soil nail with and without an additive-mixed grout (Test groups 1 and 2), an innovative driven and grouted soil nail (termed here the x-Nail) was designed and developed. The innovative x-Nail is a hybrid soil nail that introduces compaction grouting in a purely frictional driven nail. The innovative design makes it possible to drive the x-Nail into in situ ground, together with a latex balloon that is used for compaction grouting in order to form a grout bulb at the driven end of the nail to improve its pullout resistance. The ultimate objective of Group 3 was to investigate the performance of a newly developed driven and grouted soil (termed here the x-Nail) compared to a conventional driven soil nail (purely frictional nail). For compaction grouting, a special type of additive-mixed cement grout (w/s = 0.30) was used because of its zero bleeding and high bond strength, which was injected by the developed volume-controlled injection system to control injection volume. The pullout testing results of the innovative x-Nail showed that the pullout capacity of the grouted x-Nail was much higher compared with the conventional driven (purely frictional) soil nail. The pullout force of the grouted driven nail increased almost linearly with increases in diameter of the grout bulb (i.e., the larger the bulb diameter, the higher the pullout force), since the grout bulb provided a significant amount of end-bearing resistance that resulted from the passive resistance of the soil situated in front of the bulb. Almost 90% of pullout force was resisted by the expanded grout bulb. Consequently, the grouted x-Nail worked as an anchor instead of a frictional nail and showed a displacement-hardening behaviour in pullout force. Overall, it could be said that the x-Nail is a promising alternative means of soil reinforcement, which might be capable of withstanding a relatively large deformation before failure.

Dedication

This thesis is dedicated to the memory of my late father
Mohammad Nurul Islam Bhuiyan…

Acknowledgements

It is a great pleasure for me to acknowledge the people who provided assistance and support to me in completing my PhD degree at the University of Newcastle in Australia. I wish to thank everyone who aided me in any way throughout the duration of my PhD research with inspiration, advice, or a helping hand, and I cannot leave the University without mentioning their contributions towards this research.

First and foremost, I would like to offer my deepest gratitude to my principal supervisor, Professor Shanyong Wang, for his guidance, encouragement, advice and continuous support. I am extremely grateful to him for believing in me and providing me with a wonderful opportunity to work as a PhD student at the Priority Research Centre for Geotechnical Science and Engineering in the University of Newcastle. His great patience, unlimited availability, constant inspiration and delightful companionship made my PhD research life impressive, smooth, dynamic and pleasing.

I am also deeply indebted to my co-supervisor, Emeritus Professor John P. Carter, for his valuable comments, suggestions and corrections in reviewing my paper writing, which improved my writing skills and enthusiastically inspired me in writing a number of conference and journal papers throughout this research. His expertise, positive criticisms and insightful recommendations enriched and shaped my research investigation in several ways. I consider myself extremely fortunate to have a professor like him as a co-supervisor. I believe that the completion of this research project would not have been possible without the consistent support and proper supervision of my supervisors.

I gratefully acknowledge the financial support of the University of Newcastle for awarding me a University of Newcastle International Postgraduate Research Scholarship (UNIPRS) with a University of Newcastle Postgraduate Research Scholarship (UNRSC 50:50) that helped me to conduct my PhD study. I also acknowledge the partial financial support for this study provided by an ARC Future Fellowship grant FT140100019 and an ARC Discovery Project grant DP140100509 awarded to the principal supervisor.

I would like to extend my sincere thanks to Lachlan Bates, laboratory manager, Mick Goodwin, laboratory craftsman, Ross Gibson, instrumentation specialist, and Dr Michele Spadari, geotechnical professional officer, for their technical support and advice regarding fabrication and automation of the test facility. Special thanks to Andy Sullivan, senior technical officer, for his help in purchasing some testing materials. I must also thank Tabassum Mahzabeen Raka, volunteer research assistant, for assistance in conducting the physical model experiments.

I would also like to extend my gratitude to my colleagues and friends for their friendly assistance and motivations. I am especially grateful to Dr Xinyu Ye, Dr Qiong Wang and Dr Xiong Xiao for their practical suggestions regarding sensor calibration, instrumentation and pullout testing. I am also thankful to Kirstin Dunncliff and Jo Midwinter for their endless support throughout my study.

Finally, I would like to extend my deepest gratitude to my mother, brother and sisters for their unconditional love, faithful support, encouragement, vast patience and sacrifice, and for allowing me to work freely over the years. My special thanks go to my cute wife, Putla, for her love, endurance and for tolerating me in all situations. I am sorry, Putla, for blemishing your countless weekends and holidays.

Mohammad Zahidul Islam Bhuiyan

The University of Newcastle, Australia

June 2020

Table of Contents

List of Figures

List of Tables

List of symbols and nomenclature

ACF	Apparent coefficient of friction
A_p	Area of perimeter of a nail (m^2)
AS	Australian Standards
ASTM	American Society for Testing and Materials
c'	Effective apparent cohesion of soil (kPa)
c'_{cv}	Constant-volume effective cohesion (kPa)
c'_{des}	Design value of soil cohesion (minimum conceivable value in the field)
c_a	Nail-soil adhesion (kPa)
C_c	Coefficient of curvature
CDG	Completely decomposed granite
CFRP	Carbon fibre-reinforced polymer
CPT	Cone penetration test
C_r	Relative compaction
C_u	Coefficient of uniformity
D_{10}	Diameter of 10% finer soil particle (mm)
D_{15}	Diameter of 15% finer soil particle (mm)
D_{30}	Diameter of 30% finer soil particle (mm)
D_{50}	Diameter of 50% finer soil particle (mm)
D_{60}	Diameter of 60% finer soil particle (mm)
d_{85}	Diameter of 85% finer grout particle (mm)
DEPC	Diaphragm-type earth pressure cell
D_{eq}	Equivalent width of the flat reinforcement strip
e	Void ratio
EPC	Earth pressure cell
f_b	Coefficient of roughness (bond coefficient)
f_c	Coefficient of adhesion
FHWA	Federal Highway Administration
f_k	CPT sleeve friction (kPa).
FM	Fineness Modulus
FoS	Factor of safety

f_r	Coefficient of friction
FRP	Fibre-reinforced polymer
f_ϕ	Coefficient of friction(δ/ϕ')
GFRP	Glass fibre-reinforced polymer
G_s	Specific gravity of solid
k	Fitting parameter
K	Permeability (m/s)
k_a	Coefficient of active earth pressure
k_l	Coefficient of lateral earth pressure
k_o	Coefficient of earth pressure at rest
L_a	Anchorage length of the nail (m)
LMG	Low mobility grouting
LVDT	Linear variable displacement transducer
N	SPT value (N)
NRCS	Natural resources conservation service
P_l	Limit pressure (MPa)
PMT	Pressuremeter test
P_u	Ultimate pullout capacity (kN)
q_u	Ultimate mobilized shear strength at nail-soil interface (kPa)
RMS	Roads and Maritime Services
S	Degree of saturation (in ratio)
S_h	Horizontal spacing of soil-nails
SMS	Soil moisture sensor
SPT	Standard penetration test
S_r	Degree of saturation
S_u	Undrained shear strength (kPa)
TAM	Tube-a-Manchette
T_u	Maximum pullout force (kN/m)
$u_a - u_w$	Matric suction/soil suction
VWC	Volumetric water content
w	Water content (%)
w/c	Water-cement ratio
w/s	Water-solid ratio
ρ_{dry}	Dry density (Mg/m^3)

σ'	Effective normal stress (kPa)
σ'_n	Average effective normal stress around a soil nail beyond the slip surface (kPa)
σ'_v	Theoretical overburden pressure (vertical stress) at the mid-depth of a nail in anchorage zone
τ_o	Threshold shear stress of grout
τ_{loose}	Shear stress of loose sand
ϕ'	Effective angle of internal friction of soil
ϕ'	Effective angle of internal friction of soil (degrees)
ϕ'_{cv}	Constant-volume effective friction angle (degrees)
ϕ'_{des}	Design value of soil friction (minimum conceivable value in the field)
α	Sliding factor
α_ι	Inclination angle of nail (degrees)
β_{sat}	Bjerrum-Burland coefficient in saturation condition
δ	Angle of interface friction or angle of skin friction (degrees)
ϕ^b	Angle of internal friction with respect to soil suction
λ_p	Pullout factor
μ^*	Apparent coefficient of friction
θ	Perimeter of a soil-nail (driven/grouted)
υ	Poisson's ratio of the soil
ψ	Angle of dilatancy (degrees)

List of Publications

Some materials of this PhD work have already been published fully or partially in several conferences and some of the material presented in this PhD thesis have recently been submitted for publication, which are under review. The publications related to this doctoral thesis is listed below:

Journal articles

1. Bhuiyan, M. Z. I., Wang, S., and Carter, J. P. (2020). Experimental study of an innovative driven and grouted soil nail (x-Nail). *Canadian Geotechnical Journal*. (Accepted).
2. Bhuiyan, M. Z. I., Wang, S., and Carter, J. P. (2020). Test facility for studying the behaviour of pressure grouted soil nails. *Geotechnical Testing Journal.* (Under review).

Conference proceedings

1. Bhuiyan, M. Z. I., Wang, S., Sloan, S. W., Sheng, D. and Ming, L. K. (2018a). Gravity grouting and its future alternative for soil reinforcement systems. In: Wu W., Yu HS. (Eds) *Proceedings of China-Europe Conference on Geotechnical Engineering*. Springer Series in Geomechanics and Geoengineering. Springer, Cham (pp. 898-901). https://doi.org/10.1007/978-3-319-97115-5_4
2. Bhuiyan, M. Z. I., Wang, S., Sloan, S. W., Sheng, D. and Michel, H. (2018b). Calibration of earth pressure cell for a specified laboratory application. *International Conference on Geotechnique, Construction Materials and Environment*, Kuala Lumpur, Malaysia (pp. 263-268). https://www.researchgate.net/publication/329356964_CALIBRATION_OF_EARTH_PRESSURE_CELL_FOR_A_SPECIFIED_LABORATORY_APPLICATION
3. Bhuiyan, M. Z. I., Wang, S., Sloan, S. W., Carter, J. and Raka, T. M. (2019). Effects of grout injection techniques in pressure grouted soil nail system. *7th*

International Symposium on Deformation Characteristics of Geomaterials, Glasgow, UK. (pp. 1-6). https://doi.org/10.1051/e3sconf/20199217010

4. Bhuiyan, M. Z. I., Wang, S., Carter, J. P. and Raka, T. M. (2020a). An innovative driven soil nail (x-nail): a promising alternative to conventional soil nails. *Geo-congress 2020*, Minnesota, USA (pp. 383-393). https://ascelibrary.org/doi/abs/10.1061/9780784482797.038
5. Bhuiyan, M. Z. I., Wang, S., Carter, J. P. and Raka, T. M. (2020b). Calibration and assessment of capacitance-based soil moisture sensors. *Geo-Congress 2020*, Minnesota, USA (pp. 754-766). https://ascelibrary.org/doi/abs/10.1061/9780784482797.074

Chapter 1 Introduction

1.1 Background

Soil nailing is an effective earth reinforcement technique used to reinforce and stabilize in situ soil with the application of passive reinforcing elements (typically steel bars), known as soil nails. Over the decades, the technique has achieved popularity due to its cost-effectiveness and speed of construction, and it has been extensively used in different geotechnical applications around the world, for example, slope stabilization, deep excavation or retaining walls, and tunnelling (Schlosser and Unterreiner 1991; Watkins and Powell 1992; Elias and Juran 1991; Bruce and Jewell 1986; Juran 1987; Wood et al. 2009). The fundamental mechanisms of soil nails are the development of their reinforcing effects through frictional resistance, or shear resistance (bond strength), mobilized at the nail-soil interface due to the ground movement, which in turn generates the tensile forces (pullout forces) in the nails (Dey 2015). In the geotechnical design of soil nails, it is considered that the axial resistance (tensile force) plays a vital role in maintaining the internal stability of a soil-nailed structure. The most common type of internal failures of soil nails are pullout failures, i.e., tensile failure due to insufficient axial resistance (Johnson et al. 2002; Su 2006; Kim et al. 2014; Dey 2015; Zhou 2015). Therefore, the pullout force, i.e. the bond strength of the nail-soil interface, is an important parameter that controls the design and safety of soil-nailed structures (Chu and Yin, 2005).

Conventionally, soil nails are inserted into the ground by two types of frequently used methods, viz., driving and drilling-grouting techniques, based on the soil conditions, project cost and construction flexibility (Geo, 2008). Currently, however, the drilled and grouted soil nail is the most popular nailing technique on the basis of simplicity of construction compared to the classical driven soil nail (Franzen 1998; Lazarte et al. 2003; Kim et al. 2014; Zhou 2015). Figure 1.1 shows the basic difference between a driven soil nail and a drilled and grouted soil nail. The pullout resistance of both soil nails comes primarily from the frictional resistance developed at the nail/soil and grout/soil interface, respectively.

In the drilled and grouted soil nail system, a neat cement grout (a mixture of water and general purpose cement) with a water cement (w/c) ratio ranging from 0.40 to 0.50, is injected by gravity or low pressure into the pre-drilled holes where the nails are inserted centrally. Thus, grouting into a pre-drilled hole leads to significantly higher pullout resistance due to the enlarged frictional surface area (Lazarte et al. 2003; Zhou 2015). However, Cheng et al. (2009) suspected that the application of gravity in drilled and grouted soil nail system may decrease the bond strength significantly caused by the shrinkage of the neat grout. Moradi and Zadkarim (2016) also reported that the effectiveness of gravity grouting with the neat cement grout was not as satisfactory as expected because the grout probably shrank after setting, which caused a reduction in the frictional resistance between the grout and the surrounding soil. Moreover, the application of gravity grouting used in the grouted soil nail system might have very limited effects on the bond strength enhancement and thus the gravity-grouted earth reinforcement system might undergo a significant amount of lateral deflection after construction, as suggested by Bhuiyan et al. (2018a) from a case study of a gravity-grouted anchored wall used for stabilization of an approximately 19.5 m deep excavation.

Furthermore, Lazarte et al. (2003) reported that the bond strength (interface shear resistance) of the drilled and grouted soil nails could be improved significantly using pressurised injection of grout into pre-drilled holes. They also pointed out that the bond strength of a pressure-grouted soil nail for a grouting pressure less than 350 kPa could be two times that of the resistance found from conventional gravity grouting, i.e., zero grouting pressure. Recently, a number of studies have been conducted to evaluate pressure grouting effects on the pullout resistance of grouted soil nails and they have reported that the peak bond strength of a pressure-grouted soil nail increases almost linearly with the grouting pressure. This increased pullout resistance probably results from the compaction or densification of the surrounding soil, as well as grout penetration into the surrounding soil, leading to enhanced bond strength at the grout-soil interface (Yin et al. 2009; Seo et al. 2012; Hong et al. 2013).

Wang et al. (2017a,b) proposed an innovative compaction-grouted soil nail where pressurized grouting was employed instead of conventional gravity grouting to compact the surrounding soil. Importantly, for this innovative nail system, the pressurized grout was directly injected into an inflatable latex balloon (i.e., a grout bag) using a pressure-controlled injection system in order to prevent pressure filtration (i.e., seepage of water from the grout paste) and propagation of the neat grout (w/c = 0.50) into the surrounding soil. One of the key features of the compaction-grouted soil nail is that this nail shows a strain hardening behaviour in pullout resistance and approximately 80% of total pullout resistance comes from the end bearing resistance provided by the expanded grout bulb (hardened grout) (Ye et al. 2017). Consequently, the nail performs as an anchor rather than a purely frictional nail (e.g., driven and gravity grouted nail), which makes it possible for the nail to withstand a relatively large lateral deformation before ultimate failure. However, the installation technique used for the compacted-grouted soil nail is fundamentally similar to the drilled and grouted soil nail, since for both nail systems pre-drilled holes are required. A study of Su et al. (2010) showed that pre-drilling into the ground reduced the beneficial effect of overburden pressure on an installed soil nail. After the drilling process, the overburden pressure, i.e., the effective vertical stress in the compacted soil, decreased to almost zero at the nail/soil interface due to stress release at the hole surface. Consequently, the normal stress acting around the grouted nail is reduced, which ultimately reduces the pullout resistance of the grouted nail. The pullout resistance of the drilled and grouted soil nail depends almost completely on the normal stress acting around the drilled hole rather than the applied overburden pressure (Su et al. 2008). In addition, Schlosser (1982) reported that the normal stress acting at the nail-soil interface was almost equal to the applied overburden pressure for a driven soil nail.

Lazarte et al. (2003) recommended using neat cement grout (w/c = 0.40 to 0.50) in the grouted soil nail system where the nail was grouted by gravity or low pressure grouting. However, the cement grout used in compaction (or pressure) grouting exhibits significant pressure filtration, which consequently hampered the flowability and workability of the pressurised grout (Bezuijen 2010; Seo et al. 2012; Wang et al. 2016). In addition, Warner (2004) reported that the cement grout with a w/c ratio greater than 0.35 generally exhibited excessive shrinkage and low bond strength. Considering all of these factors, i.e., flowability, bond strength, and pressure filtration, it can be concluded that a cement grout with a w/c ratio of 0.50, as used previously by Wang et al. (2017a) for a compaction-grouted soil nail, is not a suitable grouting fluid for high pressure grouting. Moreover, some specifications, e.g., the NSW Roads and Maritime Services (RMS, 2018), recommend that the grout used for soil nailing applications should have high bleed resistance, low shrinkage and high fluidity. Thus, it is necessary to introduce a special type of additive-mixed cement grout for the soil nailing application that conforms to RMS requirements and optimizes the grouting performances in pressured-grouted nail systems.

The experimental study conducted by Wang et al. (2017a,b) only included the injection of the grout into a membrane bag using a pressure-controlled injection system that was unable to control the volume of the injected grout. They did not consider the direct injection of grout into the surrounding soil, and further study is therefore required to identify the performance of a compaction-grouted soil nail without a grout bag facility. In addition, the influences of grout injection rate and grout viscosity have not been studied on the compaction-grouted soil nail yet. To evaluate the effects of grout injection volume on the pressure-grouted soil nail system (i.e., compaction-grouted soil nail system), a volume-controlled injection must be developed. Furthermore, a detailed experimental investigation is necessary to quantify the performances, including measurement of bleeding resistance, propagation and the pressure transfer mechanism of the grout with different viscosities under pressurized injection into the soil.

In this study, an innovative soil nail (described here as the x-Nail) has been proposed in order to study the behaviour of a driven soil nail with its own grouting facility (Figure 1.1c). The developed soil nail combines the capabilities of a purely frictional driven nail (Franzen 1998) and a compaction-grouted soil nail (Wang et al. 2017a,b). The innovative design allows the x-Nail to be driven into the ground with a latex balloon attached that is later used for compaction grouting in order to form a grout bulb at the driven end of the nail to improve its pull-out resistance. Thus, the newly developed soil nail minimizes the pre-drilling effects at the nail/soil interface and maximizes the compaction of the surrounding soil in two ways: (1) by the driving process and (2) by pressure grouting. For the conventional driven soil nail (Figure 1.1a) and drilled and grouted soil nail (Figure 1.1b), the pullout resistance mainly comes from the frictional resistances developed at the nail/soil (f_1) and grout/soil (f'_1) interface, respectively. As a comparison, the pullout resistance of the x-Nail is contributed to by three different parts: firstly, the frictional resistance at the nail/soil interface (f_1); secondly, the passive resistance (f_2) provided by the enlarged grout bulb and thirdly, the frictional resistance between the grout bag and the soil (f_3). It is expected that, among the three components, the second one will contribute the most to the pullout resistance of the x-Nail because, under the pullout loading, the more the solidified grouting bag compresses and densifies the soil in front of it, the higher will be the resistance (f_3) that will be created, which is much higher than the frictional resistances (f_1 and f'_1) developed at the interfaces in the classical frictional soil nails.

In this work, a series of fully instrumented pullout tests were conducted with the newly developed apparatus to investigate the performance of pressure-grouted soil nails, with the grout being injected at different rates and having different viscosities. A latex membrane was used as a liner around the grouting outlets of the pressure-grouted soil nail to form a Tube-a-Manchette (TAM) for direct injection of grout into the surrounding soil. The grout-soil interaction mechanisms, including bleeding, propagation and soil responses (i.e., soil stress states and moisture contents), were evaluated during different stages of the physical model tests. In addition, to evaluate the performance of the innovative x-Nail with respect to the purely frictional driven soil nail, a number of physical model tests were conducted and the nail-soil interaction was continuously monitored using the provided instrumentation facility.

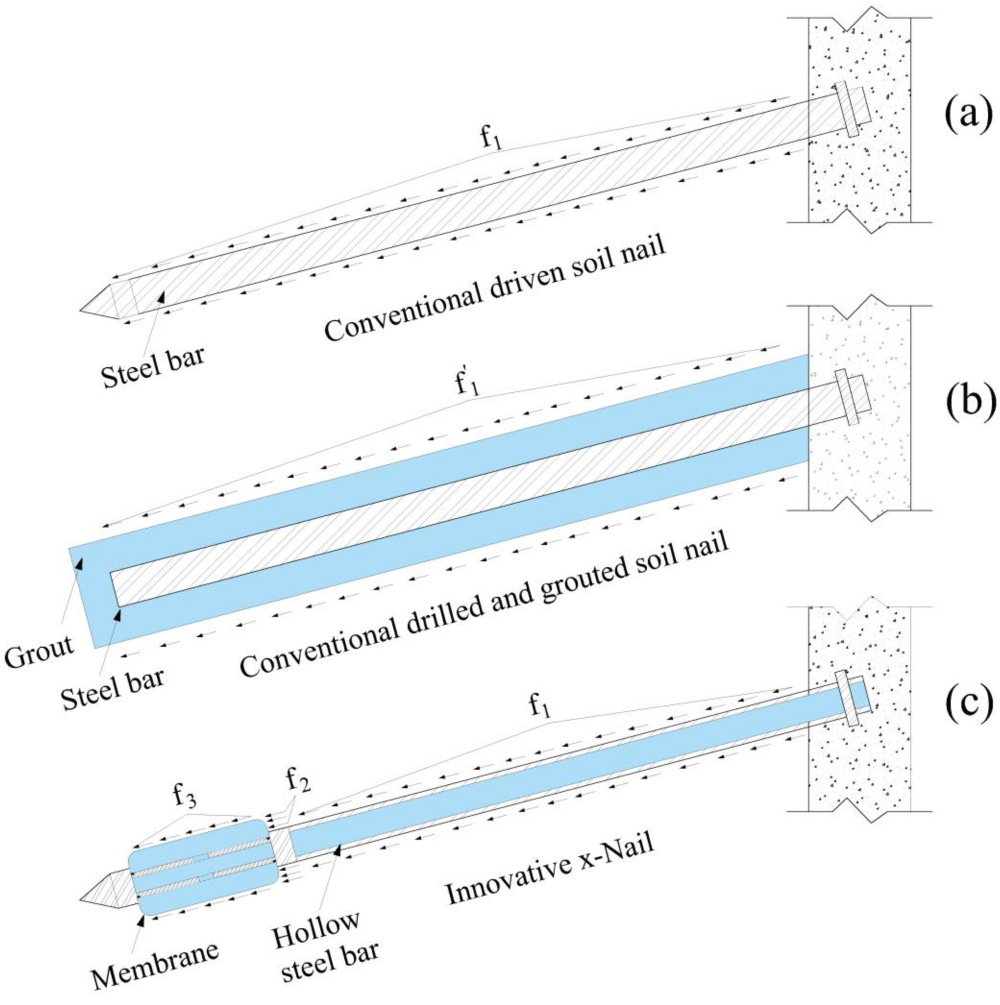

Figure 1.1: Comparison of (a) classical driven soil nail, (b) conventional drilled and grouted soil nail, and (c) innovative x-Nail

1.2 Research objectives

The principal purpose of this research was to develop an innovative driven and grouted soil nail system (x-Nail) that employs the pressure/compaction grouting used in the conventional driven soil nail, as described earlier. In this study, the following objectives were carried out to address the specific issues in the pressure-grouted nail system:

1. To design and develop a new grouting pump to control the grout injection rate and to monitor the grout injection pressure.
2. To study the grout injection rate effects on the pressure-grouted soil nail system and evaluate its performance in unsaturated sand in terms of pullout resistance.
3. To investigate the grout viscosity effects on the grout injectability into sand and thus assess the performance of pressure-grouted soil nails with different types of cementitious grouts (with and without a special type of additive).
4. To develop an innovative driven and grouted soil nail (x-Nail) and investigate its pullout resistance in cohesionless soil.

1.3 Thesis overview

The thesis is structured in eight chapters, as follows:

Chapter 1 outlines the background of soil nailing techniques and the motivation for the study, and specifies the scope and objectives of the research.

Chapter 2 gives a comprehensive literature review of conventional frictional soil nails and the factors that influence the pullout resistance of frictional soil nails. This chapter also discusses the limitations of the existing soil nailing systems and recent advancements in soil nailing techniques.

Chapter 3 describes the physical properties of the sand, neat cement grout and additive-mixed cement grout used in the laboratory investigation. The viscosities of the additive-mixed grouts with water solid (w/s) ratios varying from 0.30 to 0.50 are compared with a normally used neat cement grout with a w/c ratio of 0.50.

Chapter 4 details the experimental setup, consisting of a soil chamber, a modified overburdened pressure system, an updated “two-in-one” pullout system and an innovative volume-controlled injection system. The testing procedures with a detailed instrumentation facility for the physical model study are described.

Chapter 5 presents a number of pullout tests conducted to investigate the performance of pressure-grouted soil nails, with the neat grout (w/c = 0.50) being injected at different rates. The results of physical model tests are presented and discussed in detail during the surcharging, grouting, and pullout processes. In addition, the performance of the developed apparatus is evaluated.

Chapter 6 focuses on the application of a special type of additive-mixed cement grout with different w/s ratios ranging from 0.30 to 0.50 in a pressure-grouted soil nail system. The results of a series of physical model tests conducted to evaluate the performance of the grout, including its bleeding and propagation under pressurized injection conditions, are presented and discussed. Moreover, the performance of these additive-mixed grouts is compared with a traditionally used neat cement grout (w/c = 0.50).

Chapter 7 introduces a newly developed driven and compaction-grouted soil nail (termed here the x-Nail), which is a hybrid soil nail, combining the facilities and capabilities of a purely frictional driven nail and a compaction-grouted nail. The performance of the x-Nail is compared to a classical driven soil nail. The experimental results obtained at different stages, i.e., compaction, driving, surcharging, grouting, and pullout processes, of the physical model study are described.

Chapter 8 finally summarises the main conclusions of this research and outlines recommendations for future research works.

Chapter 2 Literature review

2.1 General

This chapter introduces the existing soil nailing techniques and mechanisms, followed by a review of the experimental and theoretical studies previously conducted on conventional soil nailing systems. Furthermore, the chapter provides an overview of the factors that influence soil nail pullout capacity. Finally, a number of works related to the recently developed compaction-grouted soil nail are discussed.

2.2 Soil nailing techniques

Soil nailing as an in-situ earth reinforcement technique has been increasingly applied in the field of soil excavation and slope stabilization due to its cost effectiveness and ease of construction (Pradhan et al., 2006; Schlosser and Unterreiner, 1991). Soil nailing systems can save approximately 10-30% of the construction cost up to an excavation depth of 10 m compared to the other ground anchorage systems, as reported by Bruce and Jewell (1986). The nailing system consists of passive inclusions (reinforcements), typically high-yield steel bars, referred to as a 'soil nail', which are inserted in situ into the ground, usually horizontally or sub-horizontally, by driving or drilling boreholes into the soil. In 1960, the idea of soil nailing was developed during underground tunnel constructions in which steel bars were used to reinforce the tunnel construction. However, the first soil nailing application was successfully completed in 1972 in France where an excavation was supported by grouted soil nails (Chu, 2003). Over the decades, various soil nailing structures have been applied successfully in different construction and remedial projects all over the world e.g., France, Germany, USA, Hong Kong and Australia (Guilloux and Schlosser, 1982; Gässler, 1983; Bruce and Jewell, 1986, 1987; Chu, 2003; Cheng et al., 2016). According to Su (2006), in Hong Kong nearly 80% of the slopes are stabilized using soil nailing techniques. Figure 2.1 compares in-soil ground reinforcement techniques (e.g., soil nail walls) and reinforced earth techniques, e.g., mechanically stabilized earth walls, in which fill material (frictional or cohesive soil) is compacted in layers by placing geosysthetic sheets or metallic strips inside it (HA68/94, 1994).

According to Lazarte et al. (2003), soil nails can be classified into five types by their basic installation methods, such as drilled and grouted soil nails, driven soil nails, self-drilling soil nails, jet grouted soil nails and launched soil nails. The selection of a specific type of soil nail depends on the soil conditions, project cost and construction flexibility (Geo, 2008).

For the drilled and grouted method, the threaded solid or hollow steel bar, with a nominal tensile strength of 420 MPa and a diameter range of 19 to 43 mm, is inserted centrally into a pre-drilled hole (100–200 mm in diameter) and then the hole is grouted using a neat cement grout (w/c = 0.40 to 0.50) under gravity or low pressure in order to provide corrosion protection to the steel bar as well as to improve the load transfer between the grouted nail and the surrounding soil (Lazarte et al., 2003). The pre-drilling method used in this nail system overcomes possible ground obstructions (e.g., the presence of corestones) and thus the soil nails of longer length can be easily installed for temporary and permanent applications. However, the pre-drilled hole has the possibility of collapsing and, therefore, a casing may be required to protect the hole (Geo, 2008).

In the case of the driven technique, a steel bar with a diameter ranging from 19 mm to 25 mm is driven directly into the existing ground using different mechanical methods, such as percussive and vibratory methods. This technique is faster and more economical compared to the drilled and grouted method. However, these nails are relatively short and are used for temporary applications only. In addition, they are susceptible to corrosion due to their direct contact with the ground (Lazarte et al., 2003; Geo, 2008).

In the self-drilling method, the soil nail consists of a hollow bar with a sacrificial drill bit that is directly drilled into the ground and grouted simultaneously by injecting grout through the hollow bar. The installation of this type of soil nail is quite rapid compared to drilled and grouted soil nails and the application of grouting provides corrosion protection to some extent. Like driven soil nails, self-drilling soil nails are also commonly applied as temporary nails (Lazarte et al., 2003; Geo, 2008).

The jet grouting method combines vibro-percussion driving and high pressure grout (> 20 MPa) to erode the soil and thus form a hole with a grouted soil where a steel bar is inserted centrally. This technique provides hydraulic fracturing and re-compaction of the surrounding soils, and thus significantly increases the pullout resistance of the nail, as claimed by Juran (1987).

Launched soil nails are a special type of driven soil nail in which steel bars, with a diameter of 19-25 mm and length up to 8 m, are launched into the ground at a very high speed of about 320 km/h using a compressed air launcher. Similar to the driven technique, this method is fast, flexible and economical, and can be used for temporary applications (Lazarte et al., 2003; Dey, 2015). The detailed installation procedures for the launched soil nail (also known as a Ballistic soil nail) can be found in a publication reported by Mcllveen (n.d.)

Currently, however, the drilled and grouted soil nail is the most popular nailing technique on the basis of simplicity of construction, and it is commonly used in practice because of its higher pullout resistance compared to the conventional driven soil nail (Franzen 1998; Lazarte et al. 2003; Geo, 2008; Kim et al. 2014; Zhou, 2015). For both soil nail systems, the pullout resistance primarily comes from the frictional resistance developed at the nail/soil or grout/soil interface (Franzen, 1998; Lazarte et al., 2003). Figure 2.2 illustrates the typical top-to-bottom construction sequence applied for soil nailing. However, in soil nailing practice, this factor is still predominantly estimated using field experience rather than a rigorous scientific knowledge of nail-soil interactions.

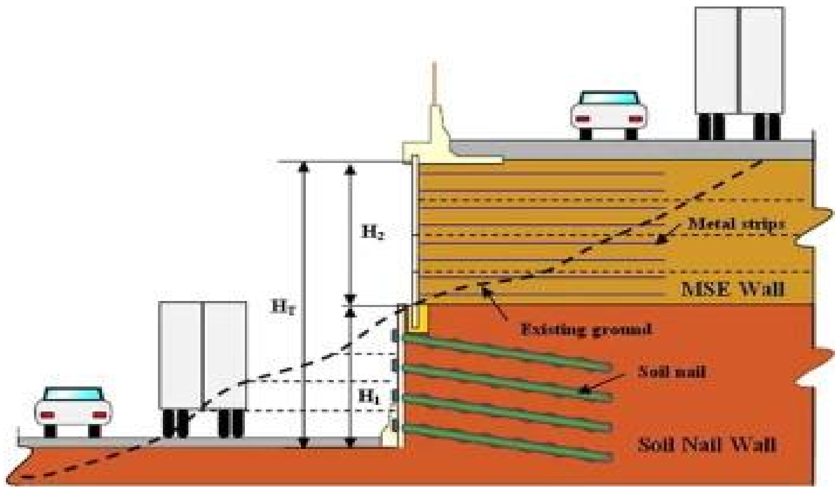

Figure 2.1: Schematic of a soil nail wall used for a retaining wall (adapted from Wood et al., 2009).

2.2.1 Mechanism of soil nailing

As can be seen in Figure 2.3, tensile forces (axial force) in the soil nails develop through interface friction between nail and surrounding soil, which is the fundamental mechanism of a soil nailing system. The critical failure surface at the back of the facing element divides the soil nail system into active and passive zone (anchorage zone). During the lateral displacement of wall or slope, the axial forces mobilized in the active zone try to pull the nails out from the ground, and this is resisted by the portion of the soil nail embedded in the anchorage zone (or resistant zone). Therefore, adequate anchorage length for the soil nails is provided after the critical failure surface (slip surface) in its design estimation.

Understanding soil nail interaction behaviour and its interface shear strength at the nail-soil or grout-soil interface is a foremost concern for the stable and cost-effective design of a soil nailing system. Shear resistance (skin friction) mobilized at the interfaces estimates the pullout capacity of the soil nail systems as well as assesses the internal stability of the soil nailed structures. Hence, the pullout capacity is a key parameter that controls the design and deformation of the soil nailed structures.

The mobilized shear strength (bond strength) totally depends on the in-situ soil conditions and it is uncertain if it will quantify the representative bond strength in laboratory conditions. In this case, simple field load tests (Ultimate load tests) are performed to evaluate consistent bond strengths, which consequently estimate and verify the typical bond strength needed in the design of the pullout capacity of soil nails (Lazarte et al., 2003).

2.2.2 Design methods for soil nailing

A number of methods have been developed, based on the classical limit equilibrium method used for slope stability analysis, for the analysis and design of soil nailed structures. According to Zhou (2015), the most frequently applied design methods are the German method (Stocker et al., 1979), the French method (FHWA, 1993), the modified Davis method (Bang et al., 1980), the Federal Highway Administration (FHWA) design method (Lazarte et al., 2003), the U.K. method (HA68/94, 1994) and the Hong Kong (H.K.) method (Geo, 2008). All methods check the internal and external stability and mainly differ by the assumption of the failure surface (slip surface). In the FHWA design manual, the slip surface is considered to be bilinear and circular, whereas a bilinear slip surface is only assumed as a failure surface for the German and the UK methods. On the contrary, the French and modified Davis methods use circular and parabola slip surfaces, respectively. In the Hong Kong method, any shape of slip can be considered for the soil nail design. In addition, for internal stability, most of the design methods consider the axial (tensile) resistance of the nail except the French method, where both the tensile and shear resistance are considered for the stability analysis. Johnson et al. (2002) also reported that axial resistance is a main contributing factor for maintaining the stability of a soil nailed structure and the shear or bending resistance makes no significant contribution to the nail stability, which can easily be neglected at the service limit state or ultimate limit state condition. The effect of shear and bending resistance can only be considered when exorbitant deformation is experienced on site, otherwise these two factors can be neglected in soil nailing design (Su, 2006).

A study of Yeo and Leung (2001) reports that the German and Davis methods are quite conservative compared to the other methods. Zhou (2015) stated that the pullout resistance (axial resistance) of a soil nail was estimated using several methods, including effective stress methods (Hong Kong and the U.K.), empirical correlation with SPT-N values (Japan), correlation with pressuremeter tests (France), and correlation with soil types (USA). However, Pun and Shiu (2007) noted that the pullout resistance estimated using the effective stress method adopted in the H.K. and U.K. design method was significantly lower compared to the actual pullout resistance obtained from the pullout test results. They pointed out that a number of unknown factors, namely soil dilatancy, moisture content, soil arching, roughness and grouting pressure, had the possibility to influence the actual pullout resistance, which were not considered in the effective stress method. Moreover, Franzen and Jendeby (2001) commented that the best way to estimate the pullout resistance of a soil nail is to conduct a field pullout test.

It is quite practicable that the interface shear strength at the nail/soil interface could be affected by different factors, such as soil types, stress conditions, drilling methods and others (Lazarte et al., 2003; Su, 2006). A detailed literature study for the estimation of pullout capacity is conducted in the subsequent sections to identify the influencing factors over the bond strength. Following that, a comprehensive review is also reported here on the findings of previous research (field and laboratory) related to soil nailing that has been carried out over previous decades.

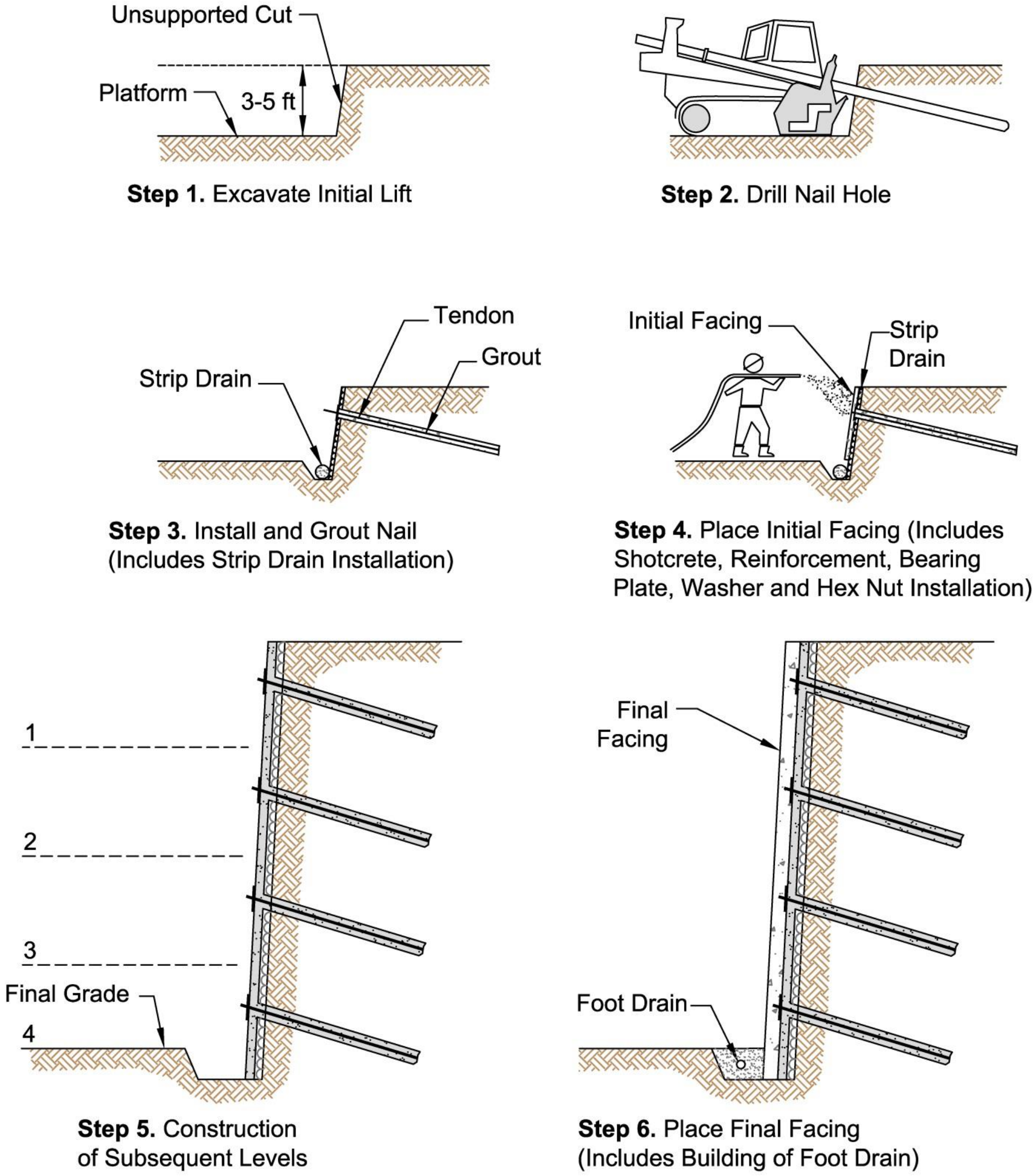

Figure 2.2: Typical construction sequence (top-to-bottom) for soil nailing (adapted from Lazarte et al., 2015).

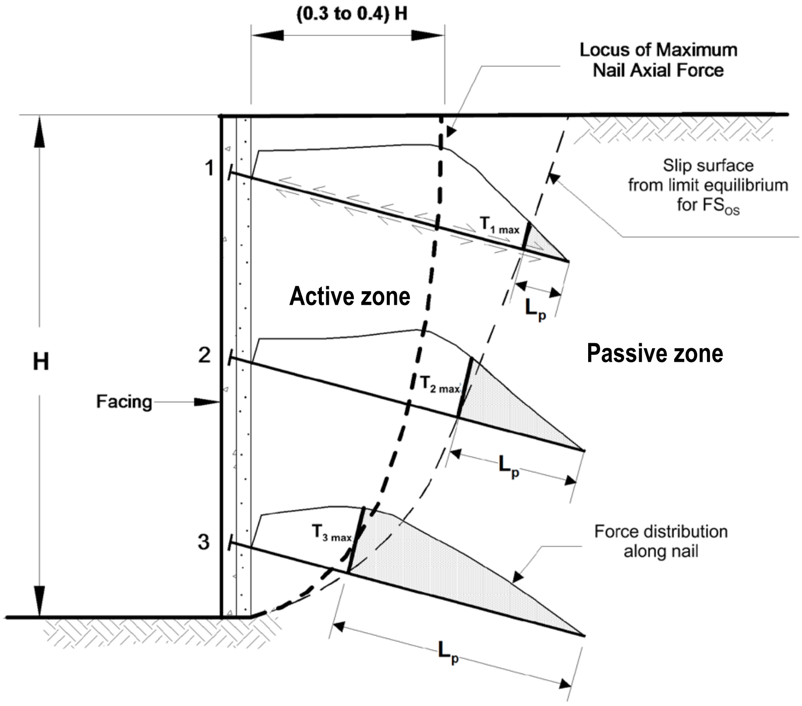

Figure 2.3: Variation of axial force along the nail showing active and passive zones (adapted from Lazarte et al., 2003)

2.3 Estimation of pullout capacity

As discussed earlier, the pullout capacity of the soil nail systems predominantly depends on the shear resistance (bond strength) mobilized at the nail-soil interface. For preliminary design, the estimation of pullout capacity and bond resistance of a soil nail could be evaluated using empirical and analytical approaches based on the experiences of professional engineers. The estimated parameters are always justified by verification load tests (field trial pullout tests) and revised accordingly during the erection since there are always uncertainties in the actual soil nail interaction mechanism.

For the frictional type soil nails, the ultimate pullout capacity (P_u) of a soil nail can be estimated using the simplified formula, as illustrated in Equation 2.1.

$$P_u = q_u A_p L_a \tag{2.1}$$

where q_u is the ultimate mobilized shear strength at the nail-soil interface, A_p is the area of perimeter of a nail, and L_a is the anchorage length of the nail.

2.3.1 Empirical methods

Soil nailed structures are usually designed based on the assumption of constant skin friction at the nail/soil interface. The predicted skin friction is recommended based on design engineers' experiences and data available from previous soil nailing projects under different soil conditions. One of the major concerns of the predicted shear resistance is the possibility of underestimation of actual design capacity, which leads to uneconomical design of soil nailing structures. The best estimation of pullout resistance can be achieved through full-scale field pullout tests at the construction sites. However, sometimes it is difficult to carry out due to practical and economic constraints. In this case, an empirical method can be a realistic and economical solution, if it is possible to establish a correlation between in-situ soil properties and pullout resistance.

In the case of a soil nailing system, the features of an empirical relation are to correlate the pullout capacity and bond resistance with specific in-situ tests, for example, Pressuremeter Test (PMT), Standard Penetration Test (SPT) and Cone Penetration Test (CPT).

Based on the literature study, it is found that empirical correlations between pullout capacity (or bond strength) and in-situ tests are very limited, and it is not commonly implied to predict the pullout capacity of a soil nail. Few researchers have made different attempts to correlate the pullout capacity with in-situ tests, which are mentioned here.

Heymann et al. (1992) proposed an empirical relationship between ultimate shear stress (q_u) and SPT value (N) obtained from residual andesite soil (a clayey silt), which was defined as:

$$q_u = 2N \tag{2.2}$$

$$P_u = 2N \tag{2.3}$$

Stroud (1974) recognized a correlation between SPT values (N) and undrained shear strength (S_u) for cohesive soils as follows:

$$N = 0.2S_u \tag{2.4}$$

Now combining Equation 2.2, 2.3 and 2.4, the ultimate pullout capacity can be expressed in the following formula:

$$P_u = 0.4 S_u A_p \tag{2.5}$$

Franzen (1998) examined a correlation between shear resistance and sleeve friction (f_k) of cone penetration test (CPT) based on horizontal CPTs under laboratory conditions. This empirical relation was actually recommended for driven soil nails in sandy soil (loose or dense) as formulated in Equation 2.6

$$P_u = f_k A_p \tag{2.6}$$

where f_k = CPT sleeve friction (kPa).

For grouted soil nails, Lazarte et al. (2003) reported an empirical relation between ultimate bond stress (q_u) and limit pressure (P_l) recorded by pressuremeter test (PMT), which is not commonly practiced, however, and this correlation is not limited to specific types of soil.

$$q_u(kPa) = 14 P_l(MPa)[6 - P_l(MPa)] \tag{2.7}$$

2.3.2 Simplified analytical methods

In the design stage of a soil nailing system, the pullout capacity of a soil nail is estimated analytically by different approaches suggested by several researchers based on soil parameters and stress conditions. It is a theoretical method to find out the bond strength or pullout capacity directly rather than using the empirical calculations. Even though there are a number of analytical methods to calculate the interface shear strength, these are fundamentally based on the Mohr-column failure criterion of a shear-normal stress model. The details of the analytical procedures proposed are discussed in the following paragraphs.

By considering the three basic parameters (e.g., effective normal stress, apparent adhesion and angle of internal friction) along with calibrating coefficients, the generic equation of the shear-normal stress transfer mechanism could be written as:

$$q_u = \sigma_n' \, f_r tan\phi' + f_c c' \tag{2.8}$$

$$c_a = f_c c' \tag{2.9}$$

$$f_r = \frac{tan\delta}{tan\phi'} \tag{2.10}$$

where:

f_c = coefficient of adhesion (0 ~ 1)

c' = effective apparent cohesion of soil

σ'_n = average effective normal stress around a soil nail beyond the slip surface

f_r = coefficient of friction

ϕ' = effective angle of internal friction of soil

c_a = nail-soil adhesion

δ = angle of interface friction (angle of skin friction)

Combining Equations 2.8, 2.9 and 2.10, the nail/soil interface shear strength can be simplified as:

$$q_u = \sigma'_n \; tan\delta + c_a \tag{2.11}$$

Potyondy (1961) studied skin friction between different types of soils and construction materials where three types of soils were used, namely coarse-grained soil (sand), fine-grained soil (clay) and mix-grained soil (cohesive-granular). The study revealed that interface friction between soil-materials was lower than soil-soil friction. For skin friction, he proposed a shear-normal stress transfer model similar to Equation 2.8, with two sliding factors for the soil cohesion and angle of internal friction as illustrated in Equation 2.12.

$$q_u = \sigma' tan\, f_\phi \phi' + f_c c' \tag{2.12}$$

Where:

σ' = effective normal stress

f_ϕ = δ/ϕ'=coefficient of friction (0.40~1.0)

ϕ' = effective angle of internal friction of soil

Cartier and Gigan (1983) examined the behaviour of a driven soil nailed wall in silty sand and correlated the mobilized skin friction with the apparent coefficient of friction (μ^*) by considering the role of constrained dilatancy of coarse grained soil as demonstrated in Equation 2.13. The correlation is commonly implied in Hong Kong to estimate the pull out capacity of grouted soil nails (Chu and Yin, 2005a; Pradhan, 2003).

$$q_u = \frac{2D_{eq}}{\theta}\sigma_v'\mu^* + c' \tag{2.13}$$

$$\mu^* = tan\phi' \tag{2.14}$$

where, θ is the perimeter of a soil nail (driven/grouted), D_{eq} is the equivalent width of the flat reinforcement strip and σ'_v is theoretical overburden pressure (vertical stress) at the mid-depth of a nail in the anchorage zone.

A simplified approach was provided by Jewell (1990) for the calculation of limiting bond stress (ultimate shear stress) in coarse grained soil, which includes a factor for bond roughness in between the nail and surrounding soil. The analytical model can be written as:

$$q_u = \sigma_n' \, f_b tan\phi' \tag{2.15}$$

For lightly overconsolidated soil, average effective normal stress acting on the soil nail:

$$\sigma_n' = (0.7{\sim}1.0)\sigma_v' \tag{2.16}$$

where, f_b, coefficient of roughness (bond coefficient), varies from 1.0 for fully rough interface (soil-grout) to 0.2~0.4 for smooth interface (soil-metal nail).

Heymann et al. (1992) proposed a similar approach to Jewell (1990) for the estimation of ultimate skin friction of a soil nail (Equation 2.15) in which bond coefficient was neglected by adding effective cohesion of soil.

$$q_u = \sigma_n' \, tan\phi' + c' \tag{2.17}$$

HA68/94 (1994) provided a model for evaluating limiting bond resistance for soil nails by considering a pullout factor *(λ)* related to a sliding factor *(α)*, which varies depending on the types of passive inclusions used in soil reinforcement. The average effective normal stress (σ'_n) acting on inclusion beyond the potential failure surface is typically considered to be equal to the effective overburden pressure (σ'_v) for strip and geosynthetic reinforcements.

In the case of soil nails, the method considers that an active stress is developed perpendicular to the slope, along with plain strain conditions acting parallel to the slope. Then, the average effective normal stress, called average radial effective stress for circular inclusions, is derived by calculating the coefficient of lateral earth pressure (k_l) parallel to the slope, that is, equal to the average of vertical and active stress coefficients. The evaluation of average effective stress could be expressed in the following equations.

$$\sigma'_n = \frac{(1 + k_l)\sigma'_v}{2} \tag{2.18}$$

$$k_l = \frac{(1 + k_a)}{2} \tag{2.19}$$

$$k_a = \frac{(1 - sin\phi'_{des})}{(1 + sin\phi'_{des})} \tag{2.20}$$

So, the limiting bond resistance of the grouted soil nail into granular and cohesive soil can be stipulated as:

$$q_u = \lambda_p(\sigma'_n\ tan\phi'_{des} + c'_{des}) \tag{2.21}$$

$$\lambda_p = \frac{\pi D_{DH}}{S_h}\alpha \tag{2.22}$$

$$\alpha = \frac{\sigma'_n\ tan\delta + c_a}{\sigma'_n\ tan\phi'_{des} + c'_{des}} \tag{2.23}$$

where:

k_a = coefficient of active earth pressure

λ_p = pullout factor

ϕ'_{des} = design value of soil friction (min. conceivable value in the field)

c'_{des} = design value of soil cohesion (min. conceivable value in the field)

α = sliding factor

S_h = horizontal spacing of soil nails

For the case of granular soil, Equation 2.21 may underestimate the bond resistance in which the design value of internal friction is recommended to be equal to the critical state angle of friction without considering the positive effects of constrained dilation, which in turn makes the method more conservative. It is also observed that the average normal stress experienced at the soil/grout interface might be substantially less than the calculated one (Equation 2.18) due to the arching effects of the soils ($c \geq 0$) around the drill hole. Therefore, this method recommends checking the design value of ultimate bond strength through a drained pullout trial test at site.

For granular fills, the critical angle of friction varies from 30° to 35°, and substituting the values in Equation (2.20), it is found that average normal stress is about $0.7\sigma'_v$, which is analogous to the simple formula suggested by Jewell (1990) in Equation (2.16). The sliding factor can also be replaced by f_b, coefficient of roughness, if soil cohesion or adhesion is neglected (Equation 2.23).

2.4 Factors affecting the bond strength of the frictional soil nail

The soil nail interaction behaviour is complex and influenced by different uncertainties present in actual field conditions. From the simplified analytical model (Equation 2.8), it is found that mobilized bond resistance is a function of normal stress, angle of internal friction and apparent adhesion, and these basic parameters are significantly controlled by the soil types, type of soil nails, method of nail installations, interface friction, relative density of soils (shear strength of soil), overburden pressure (confining stress), inclination of soil nails, degree of saturation of soil and grouting pressure. A detailed literature review on these influencing factors is discussed in the following subsections.

2.4.1 Effect of soil types

Franzen (1998) observed that types of soils significantly influence the interface shear resistance of the soil nail, and it was found that for the same type of soil nail installed using identical methods into silty clay, sand and sandy gravel, shear resistances of approximately 40-80 kPa, 100 kPa and 200 kPa, respectively, were evaluated. Similarly, Guilloux and Schlosser (1982) commented that granular soils exhibited higher ultimate shear stress compared with cohesive soils.

The increment of shear resistance in coarse-grained soil compared to fine-grained soil may have resulted from the dilatancy of granular soil. Soil dilatancy is the volume increment of soil when shear strain is mobilized in soil, and this change in volume occurs through the rotation and rearrangement of particles in soil. If this dilatancy is restrained by the surrounding soil of a nail, referred to as constrained dilatancy, then it may increase the normal stress acting in the vicinity of the nail, which in turn increases the interface shear resistance (Schlosser, 1982). The detailed effects of dilatancy are described in the following subsection. Therefore, it could easily be concluded that the shear resistance of drilled and grouted nails in cohesionless soil is affected by the nature of the granular soil, especially the friction angle. The penetrability of cement grout into surrounding soils is greatly influenced by the particle size distribution of soils which, in turn, enhances soil nail adhesion. Winterkorn and Pamukca (1991) reported that the ratio of 15% soil particle size (D_{15}) to 85% grout particle (d_{85}) should be greater than 24 to obtain a good penetration.

The soil categories that are well fitted for soil nailing may include residual soil, weathered rocks (i.e. completely decomposed granite), dense sand and gravel with some cohesion, and stiff cohesive soil (such as clayey silts), since successful applications of soil nailing in those types of soils have been experienced. In addition, it is better to avoid soil nailing (permanent constructions) in loose clean granular soils, soft clays and organic silts due to very low soil nail interface shear resistance (Su, 2006; Bruce and Jewell, 1986).

2.4.2 Effect of soil density and soil dilatancy

The influences of relative density and/or dilatancy of sandy soils are expressed by the apparent coefficient of friction (μ^*) since it is difficult to measure the increment of normal stress due to constrained dilatancy of coarse grained soils. The value of apparent coefficient of friction is controlled by the soil types (especially the granular soils), and their water content and degree of compaction. It is quite problematic to evaluate this value using classical laboratory tests instead of field pullout tests (Schlosser, 1982). Schlosser (1982) reported that the increment of normal stress acting around the soil nail, due to constrained dilatancy, could be as high as ten times the applied initial normal stress (<100 kPa). This phenomenon was also described and confirmed by Schlosser and Unterreiner (1991) using the extensive field and laboratory experiments.

Chu and Yin (2005b) reported that the apparent coefficient of friction (ACF) for the grouted soil nail decreased significantly with the increase in applied overburden pressure in dense silty sand (Figure 2.4) and after a certain overburden pressure/soil depth (approximately 5 m) it became constant, as testified by Cartier and Gigan (1983) in the case of driven steel nails, and they claimed that the decrease in the ACF was possibly compensated by the increased overburden pressure. This may be the result of the restraining effects of the applied high overburden pressure that might reduce the tendency of soil dilatancy behaviour. Luo et al. (2000, 2002) theoretically proofed that normal stress acting at the soil nail interface increased due to the soil dilatancy, and the apparent coefficient of friction decreased with the increasing overburden pressure applied in a soil nail. They also noted that the effects of the soil dilatancy dropped significantly when the nail diameter increased from 50 mm to 300 mm. In addition, they claimed that the soil dilatancy effects could be insignificant or diminished for the pullout resistance of a soil nail when its diameter was found to be greater than 100 mm in loose sand and 300 mm in dense sand.

For the completely decomposed granite (CDG) soils (granular soils), Pradhan et al. (2006) found that pullout resistance of grouted soil nails in granular soil increased significantly with the increment of relative density (or compaction), and densely compacted filling materials exhibited the higher interface shear resistance, almost 2-3 times, compared with the loose fill materials (e.g., loose sand), as shown in Figure 2.5. It is suspected that the higher relative density (compaction of about 80~95%) of the sand may result in the increased angle of internal friction, which in turn possibly increases the normal stress due to the effect of constrained dilatancy and, thus, the increase in pullout resistance in densely compacted sandy soil is expected.

Franzen (1998) reported similar behaviour for driven soil nails in sand with the relative densities of 15% and 84%. Similarly, Milligan and Tei (1998) reported that the interface friction and dilation angle were proportional to the relative density of a coarse-grained soil, e.g., sand. They also concluded that the pullout capacity of soil increased in dense soil due to dilatancy effects.

Chai and Hayashi (2005) reported that the constrained dilatancy of sandy clay greatly influenced the normal stress acting at the nail-soil interface, which was greater than the applied initial overburden pressure, and this additional normal stress was mobilized during the pullout testing. A good agreement was observed between the measured ultimate bond resistance found from the pullout tests and the calculated one estimated using the final mobilized normal stress acting on the nail surface. In Figure 2.6, it can be seen that the dry soil exhibited unexpectedly high mobilized normal stress compared with the wet soil, in which the increment of mobilized normal stress due to restrained dilatancy was insignificant with respect to the applied initial normal stress. In addition, Gässler (1983) pointed out that Mohr-Coulomb's failure criterion could not directly estimate the ultimate bond resistance of a soil nail embedded in a dense granular soil since the maximum shear strength developed at the nail/soil interface was partially influenced by the restrained dilatancy of the soil, excluding the effects of angle of internal friction and the overburden pressure. Therefore, he recommended conducting in situ pullout tests in order to estimate the shear resistance precisely at the nail-soil interface.

Su et al. (2010) simulated a finite element model for pullout testing of a grouted soil nail in sandy soil for a wide range of dilatancy angles varying from 0-29°. The results of this comprehensive parametric study illustrated that the bond shear resistance increasesd with the increment of dilatancy angle at the shearing zone.

The additional effective normal ($\Delta\sigma'_n$) mobilized due to constrained dilatancy can be computed theoretically using the formula proposed by Wang and Richwien (2002), as shown in Equation (2.24).

$$\Delta\sigma'_n = \frac{2(1+\nu)}{(1-2\nu)(1+2k_o)} q_u tan\psi \qquad (2.24)$$

where, ν = poisson's ratio of the soil and k_o = coefficient of earth pressure at rest.

It is found that angle of dilatancy (ψ) is mainly influenced by density of sandy soils and its value can be calculated from an empirical correlation suggested by Vermeer (1990):

$$\psi = \phi' - 30^o \qquad (2.25)$$

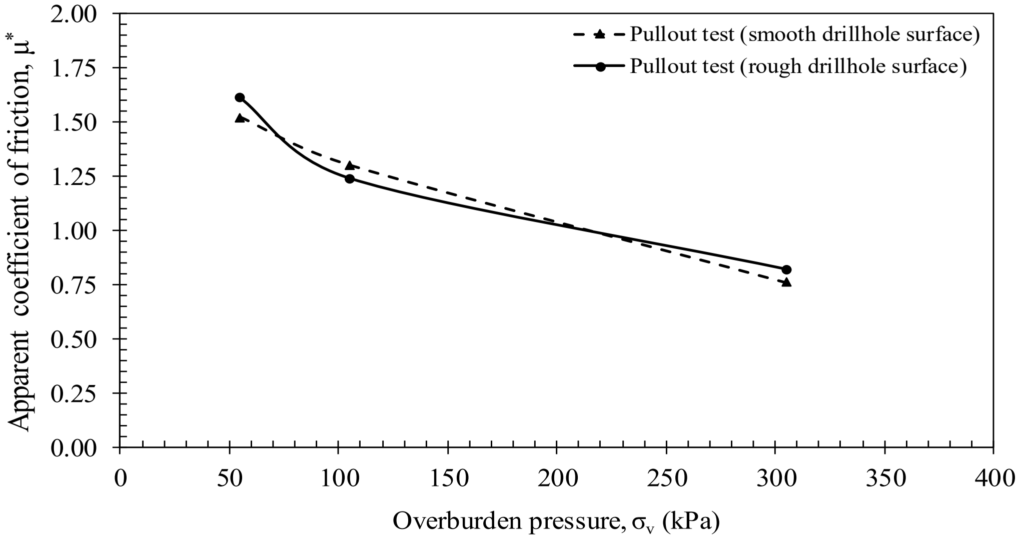

Figure 2.4: Apparent coefficient of friction (ACF) vs overburden pressure for grouted soil nail (after Chu and Yin, 2005b)

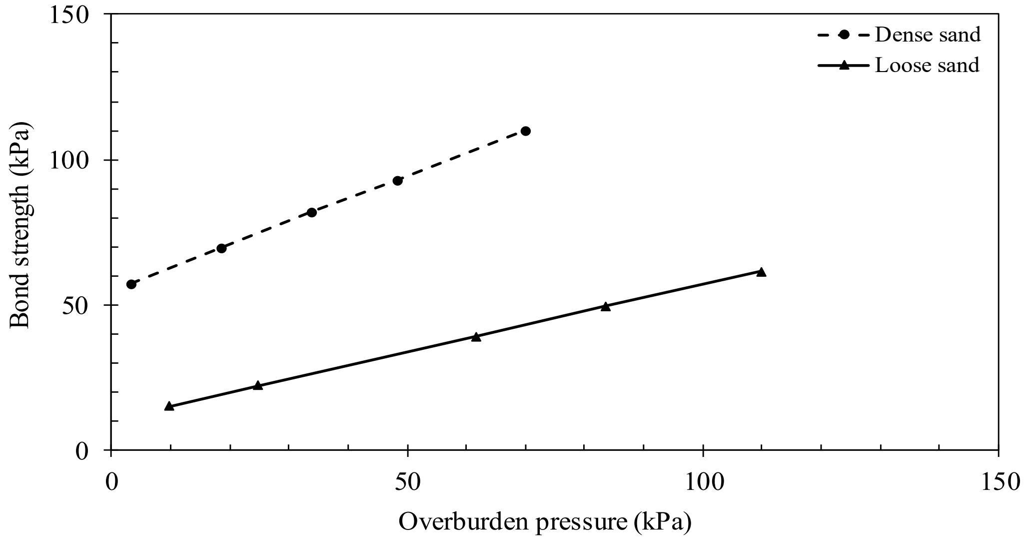

Figure 2.5: Comparison of bond strength in sandy soil (loose and dense) against overburden pressure (after Pradhan et al., 2006)

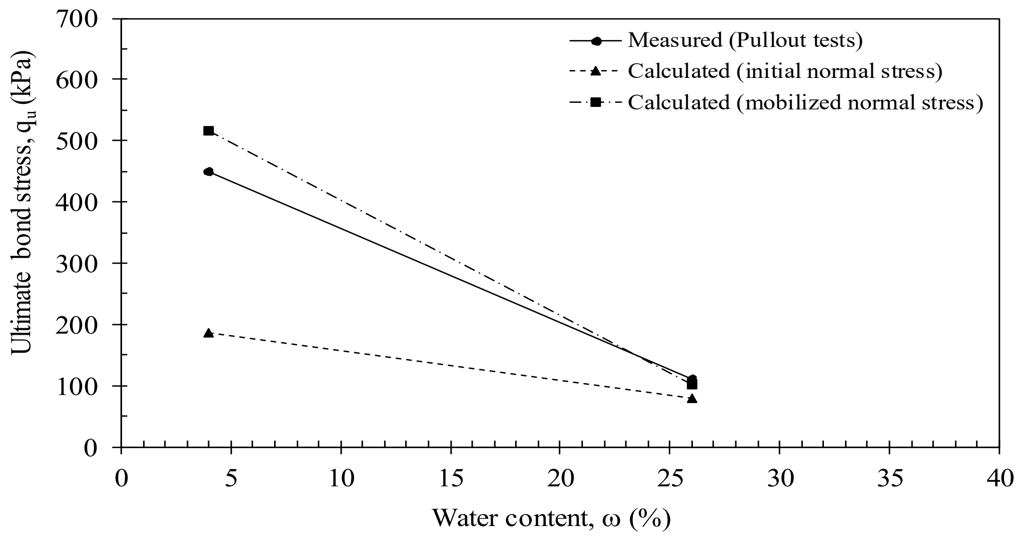

Figure 2.6: Comparison of ultimate bond resistance against moisture content for constrained dilatancy (after Chai and Hayashi, 2005)

2.4.3 Effect of overburden pressure

The influence of overburden pressure on pullout resistance, or bond shear resistance, is quite contradictory for soil nailing techniques, since some researchers have found its positive effect and others have reported insignificant effects in different types of soil nailing techniques. Su et al. (2008) performed laboratory pullout tests for the drilled and grouted soil nails in dense, completely decomposed granite (CDG) fill at different overburden pressures (40 kPa, 80 kPa, 200 kPa and 300 kPa) and found that pullout shear resistance was independent with respect to the applied overburden pressures, indicating pullout resistance at different soil depths. The study reported that drilling hole into the soil for the grouted nail reduced the vertical stress (i.e., the applied overburden pressure before drilling) around the drilled hole due to arching effects, which ultimately resulted in lower normal stress (or confining stress) acting at the grout-soil interface and, thus, the bond resistance for this type of soil nail remained unchanged with the increments in applied overburdened pressure. Hence, the simplified analytical formula (Equation 2.13) conventionally used in soil nailing overestimates the interface shear resistance of drilled and grouted soil nails. Figure 2.7 compares the measured bond resistance mobilized during the pullout testing and the resistance estimated using Equation 2.13 against the overburden pressures.

On the other hand, Pradhan et al. (2006) reported that the pullout shear resistance of drilled and grouted soil nails in loose CDG granular fill increased with the applied overburden pressures varying from 17-94 kPa, which is quite inconsistent with the findings reported by Su et al. (2008). Note that, in this study, a hole was pre-drilled into the compacted fill and then the inserted nail was grouted prior to the application of the desired overburden pressure. Chu and Yin (2005a) also described how the pullout resistance of the drilled and grouted soil nails in dense CDG fill increased when increasing the surcharge pressures (varying 0-300 kPa) where the nail installation procedure was similar to Pradhan et al. (2006), applying the overburden pressure after pre-drilling the hole and grouting. Therefore, the arching effect caused by the pre-drilling process (Su et al. 2008) was not observed in the investigations conducted by Chu and Yin (2005a) and Pradhan et al. (2006). Moreover, for the driven soil nails, Franzen (1998) concluded that the increase in overburden pressure increased the pullout shear resistance of the driven nails in sandy soil.

Heymann et al. (1992) performed forty field pullout tests for the grouted soil nails to evaluate the actual shear resistance in different types of residual soils (granite and andesite) with different soil parameters (cohesions and angle of internal frictions). The results of field investigations indicated that the interface shear resistance was independent of the soil depth (Figure 2.8). The study also concluded that the traditional analytical method (Equation 2.17) used for the estimation of pullout capacity of a soil nail was extremely conservative compared to the actual measured capacity. For the driven soil nails, Guilloux and Schlosser (1982) and Schlosser (1982) have reported that the maximum shear stress (skin friction) mobilized at the nail/soil interface during the in situ pullout testing in granular soils was constant with the increased soil depth (i.e., increasing overburden pressure). This may be attributed to the constrained dilatancy of granular soils and the effect of the constrained dilatancy becoming insignificant at high overburden pressures (Guilloux and Schlosser, 1982; Schlosser, 1982). From the laboratory pullout tests of the driven soil nails in sand conducted by Sharma et al. (2019), it was found that the pullout resistance of the driven soil nail in sand increased with the increment of the applied surcharge pressures due to the constrained dilatancy of the soil for the surcharge pressure ranges of between approximately 8-99 kPa, indicating the significant dilatancy effects on the pullout resistance of the driven nail up to the applied overburden pressure of 100 kPa, as noted by Schlosser (1982).

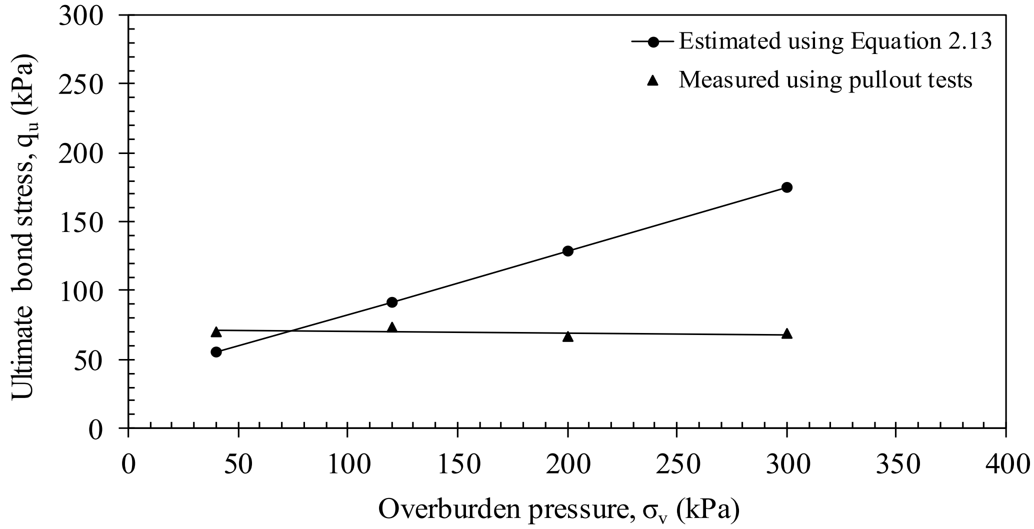

Figure 2.7: Ultimate shear stress (calculated and tested) vs overburden pressure (after Su et al., 2008)

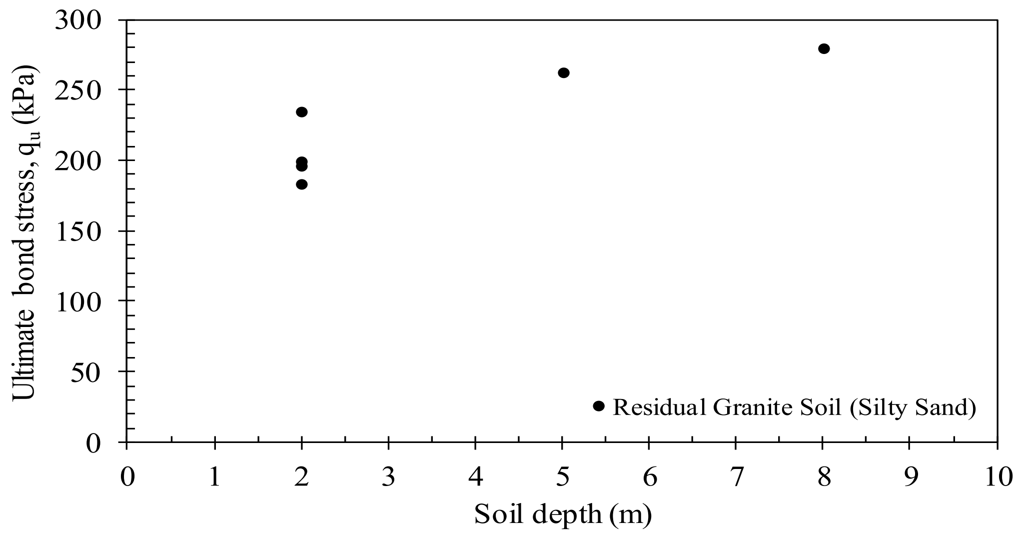

(a)

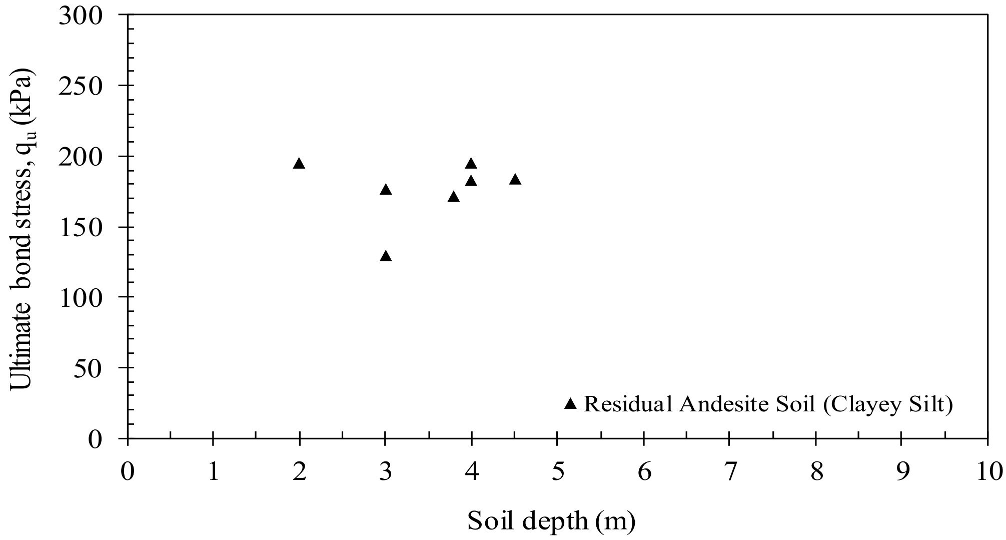

(b)

Figure 2.8: Ultimate shear resistance against soil depth for residual soils: (a) silty sand and (b) clayey silt (after Heymann et al., 1992)

2.4.4 Effect of method of installation and nail types

Installation methods significantly influence the pullout capacity of the soil nail. Schlosser (1982) stated that the normal stress (i.e., confining stress) acting at the nail/soil interface is influenced by the methods of installation used for the soil nails. The study concluded that the acting normal stress found for the driven soil nail is almost equal to the applied overburden pressure, whereas the value of the normal stress can be very low for the drilled and grouted soil nail and the value stays nearly constant with respect to the soil depth (i.e., overburden pressure).

Franzen (1998) performed the pullout tests of soil nails installed by the driving and jacking processes in dry, homogeneous, poorly graded fine sand. The study reported that the peak pullout capacity for the driven nail was approximately 50% higher than that for the jacked nail, and the former showed more strain softening behaviour. However, the residual pullout capacities for both nails were independent of installation methods. Mcllveen (n.d.) commented that the insertion of a driven nail into the ground using an air or hydraulic impact hammer has the possibility to reduce the skin friction of the driven nail due to the soil disturbance caused by the repetitive percussive impacts.

Generally, the drilled and grouted nail and the jet-grouted nail provide higher pullout resistance compared to the driven or jacked nail due to the increased frictional area and roughness at the grout/soil interface (Franzen, 1998; Lazarte et al., 2003; Su, 2006; Zhou, 2015). Byrne et al. (1993) commented that the normal stress acting on the grouted nails at a depth greater than 3m is independent of the applied overburden stress, indicating that the pre-drilling process reduces the effect of the overburden pressure applied in the grouted nail system at higher depths and this may be attributable to the arching effect of the soil, as mentioned earlier (Su et al., 2008). Gässler (1983) also noted that any types of pre-drilling methods in soil may result in a significant change of the initial normal stress situated around the soil nail. Therefore, he proposed performing an in situ pullout test for the soil nail to find out the actual shear resistance mobilized at the shearing zone, since it cannot be accurately calculated using available analytical methods at the present time.

2.4.5 Effect of degree of saturation

Su et al. (2007) conducted the pullout test of a drilled and grouted soil nail in compacted silty sand at different degrees of saturation (38, 50, 75 and 98%) and reported that the moisture content of the soil significantly influenced the bond strength of the soil nail. Based on the experimental results, it was found that grouted nails provided higher bond strength at a degree of saturation (S_r) of 75% (close to optimum moisture content). However, the shear strength reduced dramatically in fully saturation conditions, as shown in Figure 2.9.

A series of small scale field and laboratory pullout tests of grouted soil nails (8 mm diameter) were conducted by Chai and Hayashi (2005) in sandy clay. The results of the study revealed that ultimate bond resistance (maximum shear stress) reduces with the increment of water content and dropped sharply after a moisture content of about 18-20%. For the fine grained soil under saturated condition, the interface shear strength totally depends on undrained cohesion, which is usually inadequate to develop sufficient shear resistance.

One of the reasons for abrupt dropping of bond shear resistance could be the reduction of soil nail interface adhesion with high moisture contents, as reported by Pradhan (2003). Similarly, Junaideen (2001) reported that the interface adhesion disappeared for the loose CDG fills when the moisture content increased to almost saturation conditions (S_r =100%). In addition, the other reason could be the interface friction angle, which decreases significantly with increasing degree of saturation (Chu and Yin, 2005a). According to Potyondy (1961), the interface angle of friction obtained from the direct shear tests was found to be a lower value for the fully saturated soil compared to that value obtained under dry soil conditions. These are the basic parameters influencing the maximum bond resistance (Equation 2.11) and, therefore, the decreased values of the parameters consequently reduce the pullout capacity of a soil nail in saturated soil.

On the other hand, Zhang et al. (2009) and Gurpersaud et al. (2013) have reported that soil suction greatly influences the pullout capacity of a soil nail in unsaturated soil, which is not normally neglected in the conventional analytical formula, as illustrated in Equation 2.11. Zhang et al. (2009) contended that the soil suction may be high at shallow depths (< 2 m) even during the wet season and, for instance, it could be more than 50 kPa in the dry season. Therefore, the bond strength of the soil nail installed above ground table could be higher than the estimated one calculated using Equation 2.11. According to Zhang et al. (2009), the maximum bond stress of the grouted nail in the unsaturated soil was much higher than that in the saturated soil. By considering the uncertainties (e.g., soil suction and soil dilatancy), Zhang et al. (2009) modified Equation 2.13 adopted for soil nailing design in Hong Kong as follows.

$$q_u = \frac{2D_{eq}}{\theta} \frac{\sigma_v' \, tan\phi'}{1-\left[\frac{2(1+\upsilon)}{(1-2\upsilon)(1+2k_O)}\right] tan\psi \, tan\phi'} + [c' + (u_a - u_w) tan\phi^b] \tag{2.26}$$

where:

$u_a - u_w$ = matric suction/soil suction

ϕ^b = angle of internal friction with respect to soil suction

The experimental study of Gurpersaud et al. (2013) also revealed that the pullout capacity of the grouted nail in unsaturated compacted sandy soil was almost 1.3 to 1.7 times higher than that found in the saturated soil, which indicates a strong relation between pullout capacity and matric suction. Hence, a semi-empirical formula (Equation 2.27) was proposed for the estimation of the pullout capacity of the grouted soil nail in unsaturated soil using the saturated interface shear strength parameters (c_a and δ):

$$q_u = (c_a + \beta_{unsat}\sigma_v') + (u_a - u_w)S^k \tan(\delta + \psi) \tag{2.27}$$

Where:

β_{sat} = Bjerrum-Burland coefficient in saturation condition = $k_o\ tan(\delta+\psi)$

$\beta_{unsat} = 2\beta_{sat}$

S = degree of saturation (in ratio)

k = fitting parameter

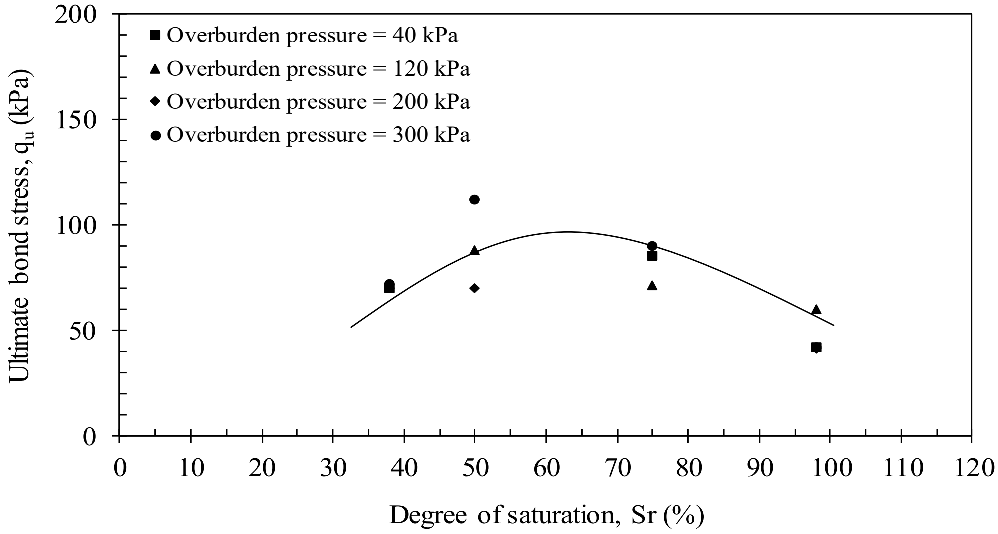

Figure 2.9: Comparison of peak shear resistance against degree of saturation under various overburden pressures (after Su et al., 2007)

2.4.6 Effect of interface roughness

To find out the effects of nail roughness on the pullout capacity of soil nails, Junaideen et al. (2004) conducted a laboratory study in loose silty sand, completely decomposed granite (CDG), for three different types of steel nails (e.g., ribbed rebar, knurled tube round and smooth rebar) under a wide range of overburden pressures (12-110 kPa). In this study, the steel bars were pre-buried horizontally in the soil during the soil placement and compaction in order to minimize surrounding soil disturbance as observed in the case of the driven nails. The study concluded that the ribbed soil nail provided the higher pullout capacity, followed by the knurled tube and round smooth bar. This is may be attributed to the ribs that provide active interlocking against the soil mass at the nail/soil interface. A good explanation is due to the presence of extremely rough surface (ribs) on the ribbed nail; the friction is probably mobilized outside the nail-soil frictional surface or partly at the nail-soil interface and the soil-soil interface. Consequently, the angle of internal friction (ϕ') dominates over the interface friction angle

(δ), which in turn increases the interface shear resistance (Figure 2.10). Sharma et al. (2019) conducted a similar investigation to Junaideen et al. (2004) for pre-buried driven soil nails with different surface roughnesses and they reported that the increase in surface roughness significantly increased the pullout capcity of a nail. Moreover, the results of the direct shear box tests conducted by Franzen (1998) revealed that the angle of interface friction, δ, for ribbed bar was almost equal to the internal friction angle, ϕ', indicating migration of the failure surface into the soil matrix. Similarly, Hong et al. (2003) reported a correlation between the surface roughness of the steel nail and the maximum shear stress (bond strength), where the bond strength increased almost linearly with the increasing surface roughness. In addition, Hong et al. (2016) reported that peak shear resistance of the drilled and grouted nail increased virtually linearly with increases in the drilled hole roughness/interface roughness angle (varying from 0 to 37°). This is consistent with the findings of Chu and Yin (2005b), who concluded that the grouted nail with irregular drilled hole surface exhibited higher bond stress compared to the grouted nail with smooth drilled hole surface, as shown in Figure 2.11.

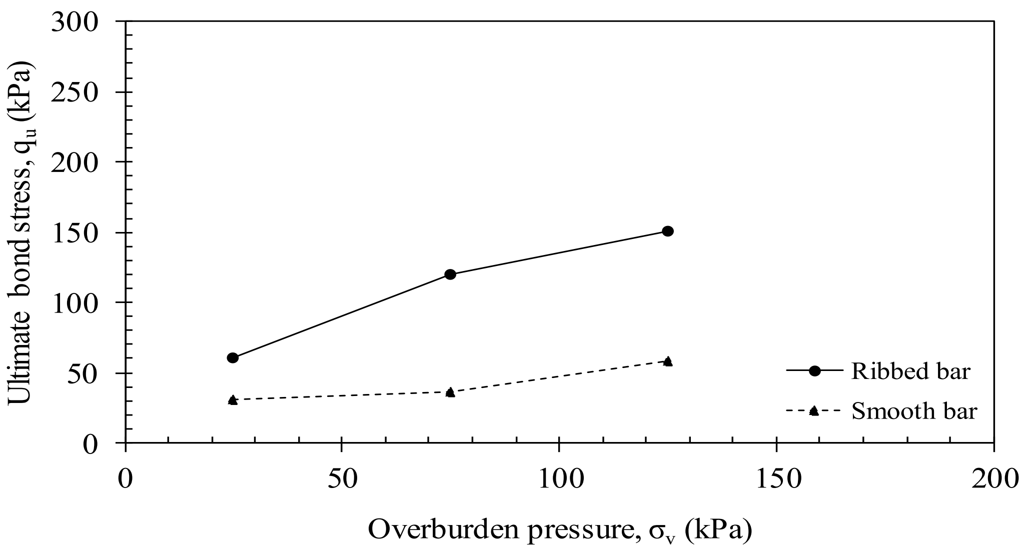

Figure 2.10: Ultimate shear stress vs overburden pressure for driven nails (after Franzen, 1998)

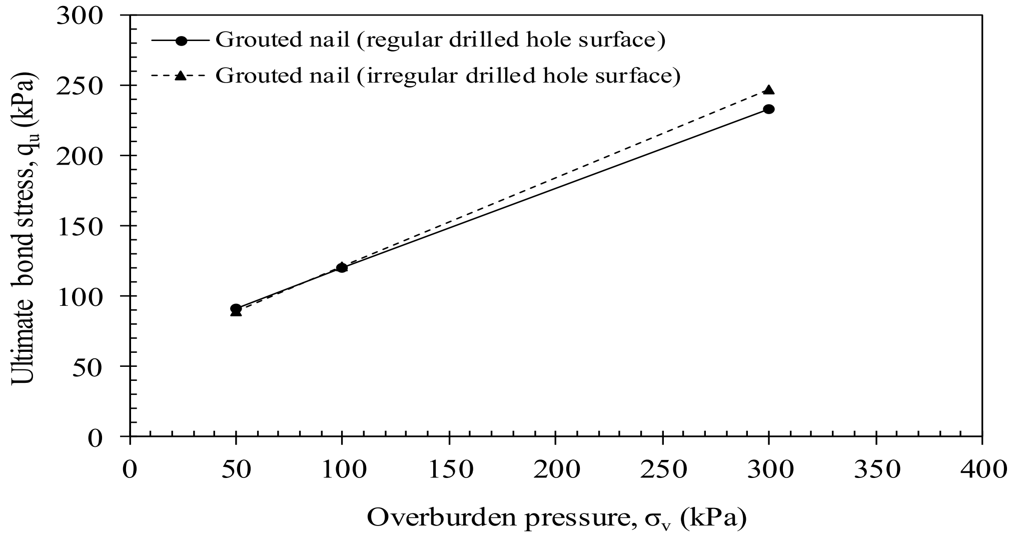

Figure 2.11: Comparison of peak shear strength for grouted nail with drilled hole roughness (after Chu and Yin, 2005b)

2.4.7 Effect of nail inclination

A numerical study was conducted by Shiu and Chang (2006) to demonstrate the effects of soil nail declination to the horizontal using a 2-D finite difference code, FLAC. The study found that the inclination of the soil nail significantly affected the tensile, or pullout, force of a soil nail. The increase in nail inclination reduced the tensile force mobilized at the nail-soil interface (Figure 2.12), consistent with the experimental results of Jewell and Wroth (1987). They suspected that, in the case of steeply inclined soil nails, the axial compression force could be induced instead of axial tensile force. Consequently, the factor of safety (ΔFoS) due to the soil nailing reduced ominously with increases in the nail inclination angle (α_l) and it became almost zero at an angle of inclination of about 65°. Therefore, it was recommended that the soil nail should be inclined as close as possible to the horizontal. An angle of inclination of 10-20 degrees is highly suggested for better reinforcing effects and gravity grouting facility. A series of field pullout tests of normally grouted soil nails conducted by Cheng et al. (2016) supported this numerical finding. The results showed that the nail inclined at 20° experienced higher pullout capacity than that the nail with an inclination angle of 30°.

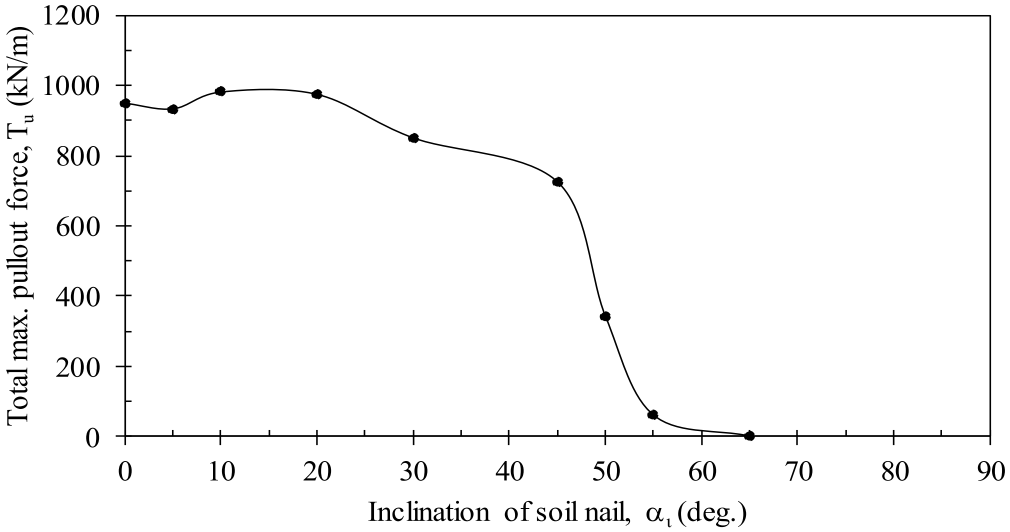

Figure 2.12: Variation of tensile forces with angle of inclination of soil nail (after Shiu and Chang, 2006)

2.4.8 Effect of pressure grouting

As mentioned above, the pre-drilling process causes a significant reduction of skin friction in a drilled and grouted soil nail system owing to the arching effect of soil. Lazarte et al. (2003) reported that for a grouting pressure less than 350 kPa in a pre-drilled hole in soil, interface shear resistance could be as high as two times that resulting from gravity grouting. Moradi and Zadkarim (2016) also reported that the effectiveness of gravity grouting with neat cement grout is not as satisfactory as expected because the grout probably shrinks after setting, which causes reduction in frictional resistance between the grout and the surrounding soil, and thus the grouted nail (i.e., frictional nail) might be susceptible to creed deformation (i.e., lateral displacement of a soil nailed structure over time under sustained loading). Moreover, the application of gravity grouting used in the grouted soil nail system might have very limited effects on the bond strength enhancement, and thus the gravity grouted earth reinforcement system might undergo a significant amount of lateral deflection after construction (i.e., creep displacement), as suggested by Bhuiyan et al. (2018a) from a case study of a gravity-grouted anchored wall used for stabilization of an approximately 19.5 m deep excavation.

Nowadays, pressure grouting is being progressively used for soil nailed structures as an alternative to frequently used conventional gravity/low pressure grouting, since this grouting technique has the ability to increase the bond strength significantly. Yin et al. (2009) conducted an experimental study of the drilled and grouted soil nail in CDG soil in order to evaluate the effects of grouting pressures varying from 0-130 kPa on the nail bond strength behaviour. They reported that the peak bond shear resistance increased almost linearly with increasing grouting pressures. The study concluded that the increment of pullout shear resistance could result from the infiltration of cement grout into the soil surrounding the drill hole due to the pressurized injection grout, and consequently enhance the soil adhesion parameter as well as compaction of the surrounding soil. They also mentioned that grouting pressure has the possibility to increase the interface roughness and diameter of grouted nails slightly compared with the initial drilled hole diameter. Similar findings were reported by Hong et al. (2013) based on the field tests in sandy soils for grouting pressures varying from 0 to 140 kPa, as shown in Figure 2.13. From the study, it was found that the interface failure surface migrated into the surrounding soils by about 16 mm and the diameter of pressure-grouted soil nails was much larger (110-130 mm) compared to the initial drilled hole diameter of 100 mm, indicating enlargement of the pre-drilled hole. In addition, the results also revealed that the apparent coefficient of friction increased with the increase in grouting pressures, which confirm the increase in surface roughness due to pressurized grouting.

To simulate a worst-case scenario, an experimental study of pullout tests for the drilled and grouted soil nail under high injection pressures (varying 80-300 kPa) was conducted by Yin and Zhou (2009) in nearly saturated compacted CDG soils. The results revealed that the higher grouting pressure provided the normal stress acting at the grout-soil interface, which resulted in an increased bond shear strength. It was also observed that the influence of overburden pressure on the interface shear resistance became prominent when the grouting (or injection) pressure was higher than 130 kPa, otherwise the increment of the overburden pressure became insignificant on the mobilized interface shear stress, as reported by Su (2006). In addition, Zhou et al. (2011) found a good agreement between the finite element analysis and the experimental results of Yin and Zhou (2009). In addition, Seo et al. (2012) reported that, for grouting pressure of about 500 kPa, the drilled and grouted nail exhibited approximately 36 % higher pullout force compared to the gravity grouted nail (i.e., the nail was grouted in a pre-drilled hole with zero grouting pressure) and they concluded that this increase in the pullout resistance resulted from the increased roughness, enlarged diameter and the compaction of the surrounding soil caused by the pressurized injection of grout. The results of the field pullout tests of the pressure-grouted soil nail reported by Seo et al. (2012) were further verified by a numerical investigation conducted by Kim et al. (2013), who found a reasonably good agreement between the field and numerical results.

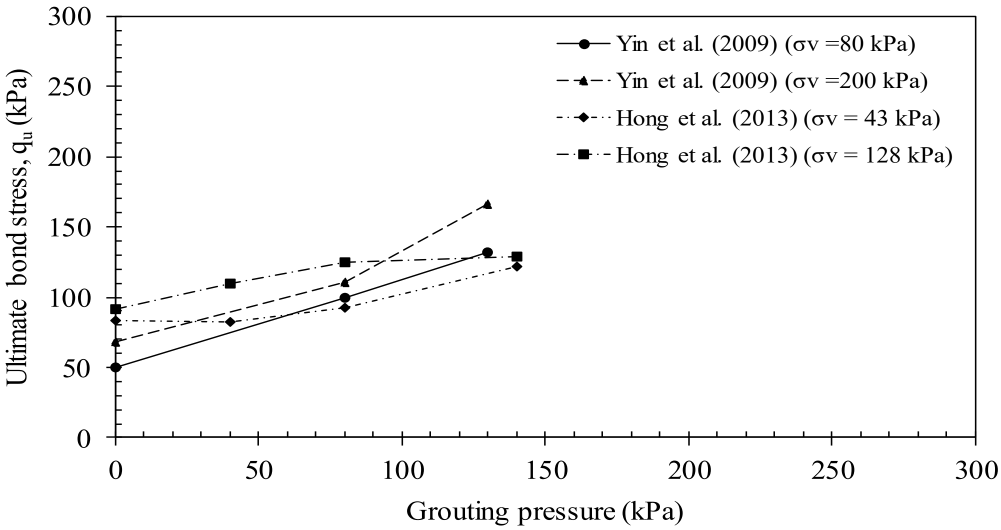

Figure 2.13: Relation between peak shear stress and grouting pressure (after Hong et al., 2013)

2.5 Limitations of frictional soil nails

From the comprehensive literature review on frictional nails, it was found that despite having different advantages, the conventional frictional soil nails possess some inherent limitations. The interaction mechanism between the soil and nail in the passive zone of a retaining soil is of utmost importance and this is affected by many factors, as mentioned in detail in the previous subsections. The impacts of some of these factors are not well understood and are likely to be ignored in the simplified design methods. To understand the interface mechanism, mainly pullout and direct shear tests are investigated to find out the estimated bond (or shear) resistance in controlled conditions as well as in comparison with actual field conditions. The important limitations that need to be considered for the application of frictional nails are summarized as follows:

1. A grouted or driven soil nailing system is not always applicable for all types of soils, especially soft clays, loose clear clean granular soils and organic silts due to very low nail-soil interface shear strength.

2. Method of installation greatly influences the interface shear capacity. It damages the influence of overburden pressure for the drilled and grouted soil nail. Pullout capacity completely depends on the acting normal load around the soil nail instead of applied vertical pressure (i.e., overburden pressure).
3. Skin friction of soil nails is drastically affected by the moisture content (or degree of saturation) of the soils. Therefore, the application of the frictional nails may be unsafe for soils with high moisture contents.
4. Pullout resistance is affected by the constrained dilatancy of granular soils to some extent. However, its effect becomes insignificant with the increase in overburden pressure or soil depth.
5. Interface roughness and grouting pressure greatly enhance the interface shear resistance of frictional soil nails.
6. Frictional soil nails do not show any end-bearing resistance and, thus, soil nailed structures have the potential to undergo a relatively large lateral deflection after construction.

2.6 Grouting and its application

Grouting is the injection of fluidized materials into the voids of soil or rock masses to change the physical properties of the masses. The key objective of grouting in soil is to strengthen the soil formation by means of improving densification, cohesion, reinforcement and reducing permeability (Warner, 2004; Samaiklang and Fuenkajorn, 2013). Three basic types of grouting can be distinguished based on their injection modes into soil and purposes, as illustrated in Figure 2.14. Permeation grouting, also known as chemical grouting, is a form of grouting technique in which high mobility grout (low viscosity) is injected into granular soil at a low pressure to solidify it by reducing permeability without causing any deformation of ground structures (Littlejohn, 2003; Keong, 2006).

Similarly, compensation grouting (e.g., compaction and fracture grouting) is also a well establish grouting technique used in different geotechnical applications, such as densification of loose granular fills, controlling liquefaction and rectification of settlements for different structures (Walker et al., 1997; Essler et al., 2000; Nomoto et al., 2000; Lee, 2002). Compared to compaction grouting, fracture grouting is mainly applied to prevent excessive soil settlement due to underground construction works, e.g., tunnelling (Drooff et al., 1995; Bezuijen et al., 2007). Selection of the grouting techniques is mainly dependent on the types of in-situ soils, as illustrated in Figure 2.15. It is seen that compaction grouting, low mobility grouting (LMG), is mainly used in granular soil, especially loose sand and soft soil, whereas fracture grouting can be applied to a wide range of soil textures. Grout injection pressure and grout viscosity are the two main controlling parameters for the grouting techniques. In the case of compaction grouting, high viscosity cement grout (low water-cement ratio) is used to provide displacement and densification of the surrounding soil. Therefore, high injection pressure is required for this type of grouting to overcome the friction between injection pipe and grout. On the other hand, the fracture grouting technique involves the injection of pressurized low viscosity grout to produce deliberate hydro-fracture in the soil, resulting in a network of interconnected root-like lenses of grout. Thus, it additionally works as permeation grouting due to infiltration of fluid suspension (cement grout) into surrounding soil. The application of the fracture grouting technique in soil nailing is very new and still under development. Littlejohn (1980) documented a conceptual application of different grouting techniques in a ground anchorage system, as shown in Figure 2.16.

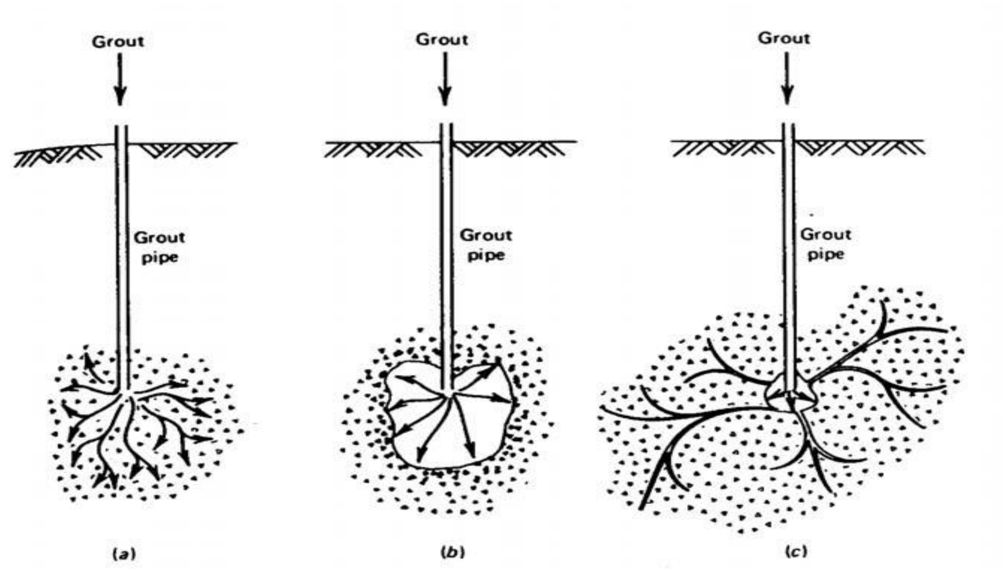

Figure 2.14: Grouting types (a) permeation grouting, (b) compaction grouting and (c) fracture grouting (adapted from Koerner, 1984)

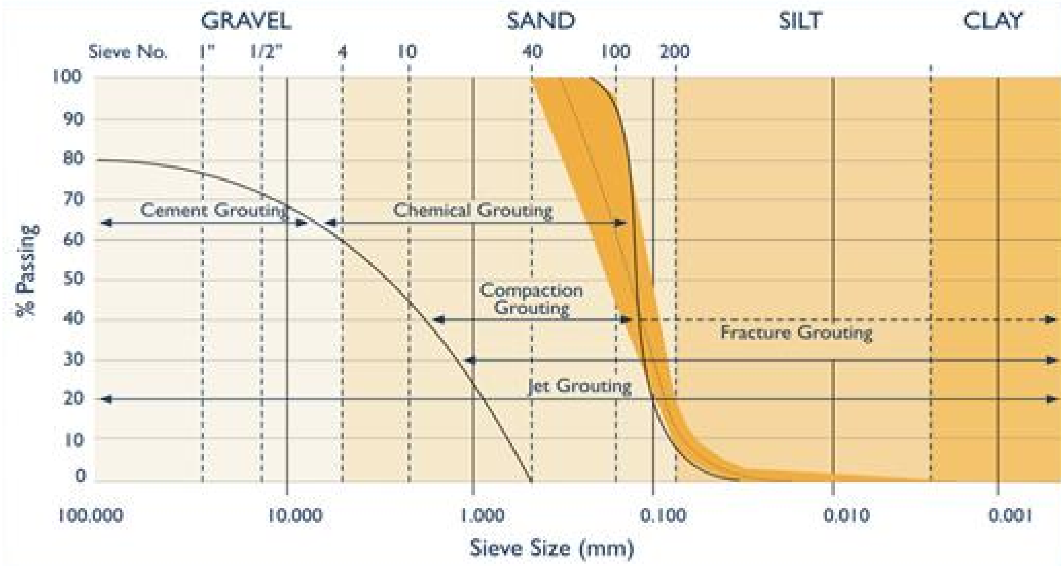

Figure 2.15: Suitable grouting techniques for different types of soil textures (Courtesy to Sin Dong Geological Engineering)

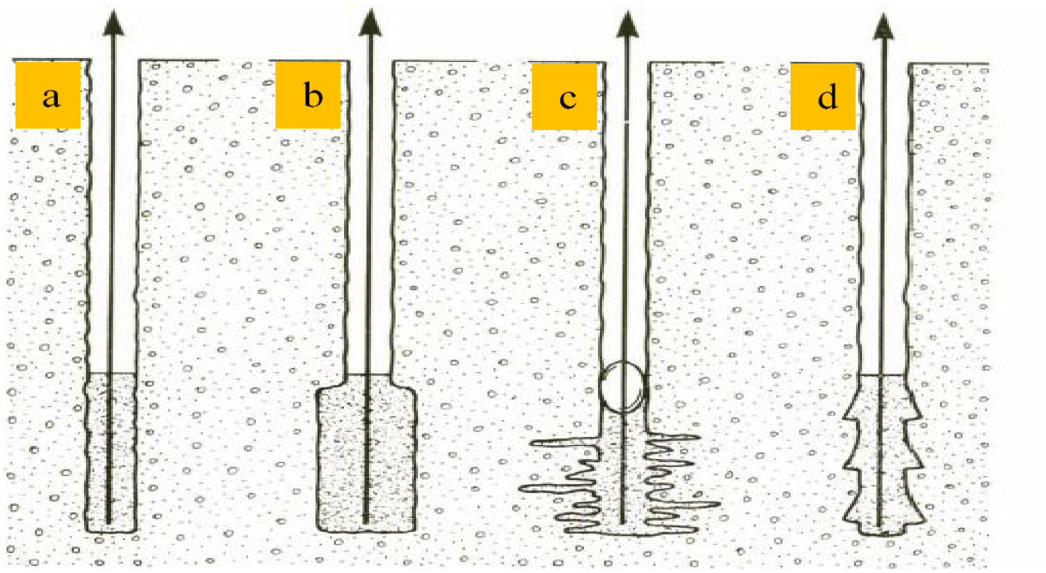

Figure 2.16: Grouting techniques for ground anchor (a) tremie (or gravity) grout, (b) pressure grouting, (c) fracture grouting and (d) tremie grouting with under-reams (adapted from Littlejohn, 1980)

2.7 Developments in soil nailing

Over the last two decades, some advancements have been made in soil nailing techniques in order to improve the performance of conventional soil nails (i.e., frictional nails) by addressing specific issues and limitations of the traditional frictional nails. For example, several researchers have proposed the application of fibre-reinforced polymer (FRP) bars and tubes as an alternative to the classical steel bars used in grouted soil nail systems due to their excellent corrosion resistance, high strength, light weight and easy site manoeuvrability (Yeung et al., 2007; Zhu et al., 2011; Cheng et al., 2016). Zhu et al. (2011) conducted a series of field pullout tests of the glass fibre-reinforced polymer (GFRP) soil nails to evaluate their performance with respect to conventional steel nails and found that the GFRP nail exhibited excessive deformation compared with the steel nail during the pullout testing. This may be attributed to the reduced Young’s modulus of the GFRP, which results in almost four times higher elongation in the GPRP with respect to the steel at specified tensile load. They also noted that, for the grouted GFRP nail, the slippage or deboning at the grout-GFRP interface might have occurred due to the thickness and roughness of the GFRP pipe. The results of full-scale pullout tests investigated by Yeung et al. (2007) and Zhu et al. (2011) indicate that the GFRP nail can be successfully applied in slope and excavation stabilization but attention is needed to the shortcomings of the GFRP nail such as low stiffness, creep and fatigue potentials. In addition, Cheng et al. (2016) investigated the performance of carbon fibre-reinforced polymer (CFRP) soil nails and glass fibre-reinforced polymer (GFRP) soil nails and evaluated their applicability in soil nailing systems in terms of strength, load transfer mechanism and cost. They recommend that the GFRP soil nail may be used as a good alternative to the conventional steel nail for normal stabilization works over the CFRP nails because of the latter’s extremely high cost, poor grout-CFRP bond strength and low shear strength (Ortigao, 1996; Burgoyene and Balafas, 2007; Cheng et al. 2009).

In addition to the FRP soil nails, an innovative two-stage pressure technique (i.e., post-grouting) has been introduced for the drilled and grouted FRP soil nail system by several researchers (Yeung et al., 2007; Cheng et al., 2009; Zhu et al., 2011) in order to increase the bond strength at the grout-soil interface. For this post grouting technique, at first a perforated GFRP pipe used as a soil nail is inserted in a pre-drilled hole and then the annular space between the nail and the hole is grouted using conventional gravity grouting. In the second stage, a packer system is inserted into the pipe bore, which works as a Tube-a-Manchette (TAM) tube (Warner, 2004), and after a few hours (about 4-8 hours) of curing the grout, a post-grouting is conducted at high pressures varying from 1000-1500 kPa at a desired location to fracture the annular grout and further penetrate the pressurized grout into the surrounding soil. This post-grouting technique is also known as the Tube-a-Manchette (TAM) grouting method (Warner, 2004; Cheng et al. 2009). Cheng et al. (2009) reported that this two-stage grouting technique, a combination of conventional gravity grouting (Stage 1) and pressure grouting (Stage 2), not only reinforces the soil but also improves its properties (e.g., cohesive strength and elastic modulus) and thus a smaller number of soil nails are required, which ultimately can save 5-10% of construction costs. Similarly, Parsapajouh et al. (2012) reported a case study of excavation stabilization in clayey soil where a high pressure (~5000 kPa) post grouting was employed to increase the pullout capacity of grouted anchors by fracturing the grout body.

Furthermore, a study by Cheng et al. (2013) reports the successful application of fracture grouting, actually post grouting, in an innovative Geonail system in a tunnel construction project in Australia, where GFRP bars were employed together with fracture grouting to stabilize the soft clay due to its low strength. They stated that this fracture grouting significantly improved the soil strength due to compaction effects and the penetration of the grout into the surrounding soil caused by the fracturing. Consequently, the pullout resistance of the grouted GFRP soil nail increased noticeably and it was found that the fracture-grouted Geonail exhibited approximately 20% higher pullout resistance compared to the gravity-grouted Geonail.

Based on the performance of pressure grouting in soil nail systems, Cheng et al. (2016) recommends that, for soil stabilization and reinforcement, conventional gravity grouting (i.e., zero pressure grouting) is not always suitable for all types of soil except for stable sandy soil. However, post grouting and fracture grouting (i.e., high pressure post grouting) could be a competitive alternative for loose sandy soils and clayey soils, respectively.

Aziz and Stephens (2013) developed a special type of hollow driven nail, termed the spiral nail, which is a twisted square steel pipe with helix fabricated by cold-rolling square steel pipe. The spiral nail is directly driven into the ground using a percussion hammer and thus no grout is required to develop bond strength with the surrounding soil, which makes it possible for the nail to carry the internal and external loads immediately. They believe that the nail is able to offer both frictional and mechanical resistance to the pullout load due to its geometry. The frictional resistance is expected to develop at the soil nail interface, whereas mechanical resistance may come from the mobilized passive resistance of the helical ribs induced by the axial movement of the nail relative to the surrounding soil. Stephens et al. (2013) reported that this dual resistance (frictional + mechanical) significantly improved the internal stability of the spiral nailed structures and it was found that almost 75%, on average, of the bond strength was contributed by the mechanical resistance of the spiral nail.

Deardorff (2010) reported an application of a helical soil nail in excavation stabilization. A helical nail is a groutless nailing technique, which is considered to be a comparatively innovative alternative to the conventional grouted soil nail systems. The helical soil nail consist of a shaft and multiple helix flights (or plates) attached to the nail shaft, and thus the helix plates offer bearing resistance. The nail is installed by a gear motor to provide sufficient torque to drive the helical nail into the ground. However, the estimation of pullout capacity for the helical nail with multiple helix plates is similar to the grouted nail (i.e., drilled and grouted nail) where a cylindrical failure surface at the outer edge of the helix plates is considered along the nail to evaluate the bond stress of the helical nail (Deardorff, 2014).

Tokhi and Li (2016) conducted an experimental study of screw soil nails (i.e., helical nails) in sand and compared their performance with respect to the drilled and grouted soil nails. They reported that the typical pullout force-displacement behaviour for the helical nail was different compared to that for the conventional grouted soil nail. The results of pullout tests indicated that helical nails did not exhibit any defined peak forces (i.e., yield value) followed by a drop in the residual force, as found for the grouted soil nails (Su et al., 2008). In comparison with the grouted soil nail (Su et al., 2008), the pullout shear resistance of the helical nail followed the Mohr-Coulomb failure criterion, i.e., the bond strength increased with increases in the overburden pressure. Similar findings were reported by Sharma et al. (2017) in a separate study of helical soil nails with different helix diameters and shaft roughness. A study of Sharma et al. (2019) shows that the pullout capacity of helical soil nails was higher than that of conventional driven soil nails.

2.7.1 Previous works relevant to current research

Wang et al. (2017a,b) developed an innovative grouted soil nail, which was termed a compaction-grouted soil nail, where compacting grouting was employed instead of conventional gravity grouting to compact the surrounding soil. The pressurized grout was directly injected into an inflatable latex balloon (i.e., a grout bag) in order to prevent pressure filtration (i.e., seepage of water from the grout paste) and propagation of the neat grout into the surrounding soil. Unlike the drilled and grouted soil nails, a small pre-drilled hole is required for the installation of the newly developed compaction-grouted soil nail, and thus it is also a drilled and grouted soil nail in some aspects. The results of the laboratory pullout testing indicated the pullout force of the new grouted soil nail increased almost linearly with increases in grouting pressure (or grout injection pressure), since the injection of grout into the grout bag was proportionally related to the grouting pressure. Consequently, with increases in the injection pressure, more grout was injected by compacting and displacing the surrounding soil, which resulted in enlarged diameter grout bulbs (solidified grout) around the injection points (Wang et al., 2017a,b). In addition, Ye et al. (2017) reported that the pullout resistance of the compaction-grouted soil nail exhibited a displacement hardening behaviour (i.e., no yield point) and almost 80% of total pullout resistance was resisted by the expanded grout bulb, which indicates this grouted nail behaves as an anchor rather than a completely frictional nail (e.g., drilled and grouted nail) and thus makes it possible for the nail to sustain a comparatively large deformation before failure. Furthermore, Ye et al. (2019a) compared the pullout capacity of the compaction-grouted soil nail with the conventional drilled and grouted soil nail and found that the pullout resistance for both grouted nails increased with increases in grouting pressure. However, for the compaction-grouted nail, the rate of increase in pullout resistance was relatively higher than that for the conventional nail, which indicates that the application of higher grouting pressure in the compaction-grouted nail is more effective than that employed in the conventional nail. An experimental study by Ye et al. (2019b) shows that the injection of grout into the unsaturated soil mass decreased with the increment of degree of saturation and thus decreased the pullout capacity of the compaction-grouted soil nail due to the formation of a smaller diameter grout bulb. Ye et al. (2019c) conducted a numerical study for the compaction-grouted soil nail with multiple grout bulbs of different diameters. They reported that, for the nail with two grouted bulbs, the pullout resistance increased with increases to the grout bulb diameter and the spacing between the grout bulbs. In addition, the pullout resistance for the nail with a larger and smaller grout bulb at the back and front, respectively, was found to be higher.

In summary, based on experimental and numerical investigations of the innovative compaction-grouted soil nail, it is found that the compaction-grouted soil exhibited better performance compared to the conventional drilled and grouted soil nail in terms of pullout resistance, and the innovative nail works as an anchor due to its end bearing resistance provided by the enlarged grout bulb. Therefore, it is believed that the grouting pressure may not have any direct effects on the pullout capacity for this anchor-type nail and the main contribution factor expected to influence it significantly is the volume of injected grout (i.e., size of the grout bulb). The experimental study conducted by Wang et al. (2017a,b) only included the injection of the grout into a membrane bag using a pressure-controlled injection system that was unable to control the volume of the injected grout. They did not consider the direct injection of grout into the surrounding soil, since the latex grout bag has the possibility to break during the installation of the compaction-grouted soil nail. Further study is therefore required to identify the performance of the compaction-grouted soil nail without a grout bag facility. In addition, the influences of grout injection rate and grout viscosity have not been studied on the compaction-grouted soil nail yet. To evaluate the effects of grout injection volume on the pressure-grouted soil nail system (i.e., compaction-grouted soil nail system), it is necessary to develop a volume-controlled injection. Furthermore, a detailed experimental investigation is necessary to quantify the performances, including bleeding resistance, propagation and the pressure transfer mechanism of the grout with different viscosities under pressurized injection into the soil.

Chapter 3 Materials

3.1 General

This chapter reports the properties of the materials used in the laboratory-scale pullout study for pressure-grouted soil nail systems. In this investigation, pullout tests were conducted in sand since it is easy to prepare moist soil samples and to control its dry density. As a grouting material, cement grout with and without a special type of additive is used. Hence, the physical properties of the sand, cement grout and additive-mixed cement grout are described in this chapter.

3.2 Soil

In this laboratory study, a silica sand, widely known as Stockton beach sand, is used as a soil, which was collected from Stockton beach, Newcastle, Australia. Aialloeian et al. (1996) have investigated the physical and mechanical properties of this type of sand in detail. However, a comprehensive investigation was conducted here to identify the basic properties of the sand for physical modelling of the pullout study. The particle size distribution curve is illustrated in Figure 3.1, which demonstrates that this sand is uniformly graded (coefficient of uniformity, $C_u < 4$) with a very narrow range of particle sizes, varying from approximately 0.3 mm to 0.6 mm. In accordance with the Australian standards (AS1289.3.6.1, 2009), the sand could be classified as clean fine to medium sand, since there are no fines in the sand mass. In addition, the sand can also be classified as a poorly-graded sand (SP) as per the Texas Department of Transportation specification (Tex-142-E, 1996). Table 3.1 summarizes the physical properties of the sand.

Sand is highly permeable soil and the average permeability of the Stockton beach sand was characterized by a laboratory permeability test using the constant head method (AS1289.6.7.1, 2001). Table 3.1 shows that the coefficient of permeability of the sand is $5x10^{-4}$ m/s, which falls within the range of $10x10^{-5}$ m/s to $10x10^{-3}$ m/s, as reported by Coduto (1999) for sandy soil.

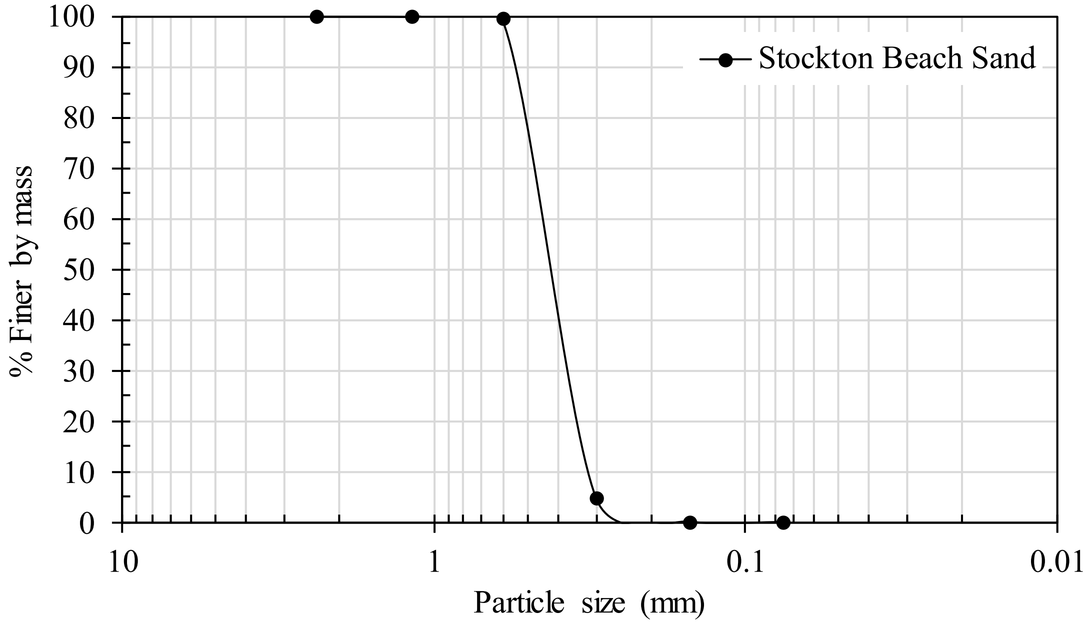

Figure 3.1: Particle size distribution curve for sand.

Table 3.1: Physical properties of the Stockton beach sand.

Parameter	Value
Diameter of 10% finer particle, D_{10} (mm)	0.325
Diameter of 30% finer particle, D_{30} (mm)	0.375
Diameter of 50% finer particle, D_{50} (mm)	0.425
Diameter of 60% finer particle, D_{60} (mm)	0.450
Coefficient of uniformity, C_u	1.38
Coefficient of curvature, C_c	0.96
Specific gravity of solid, G_s	2.66
Minimum dry density, $\rho_{dry\ (\mathrm{min.})}$ (Mg/m^3)	1.49
Maximum dry density, $\rho_{dry\ (\mathrm{max.})}$ (Mg/m^3)	1.70
Maximum void ratio, e_{max}	0.788
Minimum void ratio, e_{min}	0.563
Permeability, K (m/s)	$5\mathrm{x}10^{-4}$
Fineness modulus (FM)	2.95

Note: Density unit, Mg/m^3 = g/cm^3

The results of gradation tests reported that the soil studied is completely clean and uniform sand, and there are no fines (particles < #200 sieve) in the sand mass. The Natural Resources Conservation Service (NRCS) (2016) reported that soil compaction does not have any significant effects on the dry density of a soil having 12% or fewer fines for a wide range of water contents. This may have resulted from the small percentage of fines in the clean sand, which are not sufficient to hold water in the soil mass. To observe the moisture content effects on the clean sand, a series of standard compaction tests (AS1289.5.1.1, 2003) was performed at different water contents ranging from 0% to 15% by weight of dry sand. The variation of dry density and void ratio against the moisture contents are demonstrated in Figures 3.2-3.3. Figure 3.2 illustrates that the compaction graph of the clean sand forms a concave shape and the change in dry density values at intermediate water contents is insignificant. This may have resulted from the capillary stresses that arose in soil voids for intermediate moisture contents, and that consequently resisted compaction of the clean sand, as reported by The Natural Resources Conservation Service (NRCS) (2016). Coduto (1999) also reported a similar compaction characteristic for the clean sand. Moreover, for intermediate moisture contents (5-10%), the clean sand possessed a much higher void ratio (~0.673) than that (~0.563) of the dry condition. Based on the compaction test results, it can be said that the dry density of the moist sand is not significantly affected by the soil compaction, as mentioned previously.

A series of direct shear tests was performed to evaluate the critical state (ultimate state) angle of friction of the dry sand for a wide range of applied normal stresses. In accordance with the Australian standards (AS1289.6.2.2, 1998), loose sand specimens for direct shear tests were prepared by raining dry sand into a 60 mm of square shear box, and the sand was spread and levelled using a steel straight edge. Special measures were taken to lessen vibration and disturbance of the shear box during filling and handling. In this investigation, the sand specimen was sheared at a displacement rate of 1mm/min, which is equal to the pullout displacement speed of 1mm/min recommended in the Federal Highway Administration (FHWA) guidelines (FHWA, 1993). Figure 3.4 illustrates the ultimate shear stresses of the loose sands for different normal stresses, and it shows that the shear stress reaches maximum value after a significant amount of shear displacement, varying approximately 5 mm to 10 mm, consistent with the typical displacements (5 mm to 8 mm) at peak shear stress for loose sand, as outlined in the Australian standards (AS1289.6.2.2, 1998). The critical angle of friction of the dry sand was evaluated from the shear-normal stress relationship (Figure 3.5) and the resulting friction angle was found to be 31.5°, which is almost equal to that (31.1°) reported by Ajalloeian et al. (1996). The Highway Agency of United Kingdom (HA, 68/94) recommends that soil strength parameters (ϕ', c') adopted in the design of soil nail projects should be the minimum plausible values experienced in the field, and thus the critical state parameters (ϕ'_{cv}, c'_{cv}) can be considered as design values. The guideline reports that the critical state angle of friction (constant-volume friction angle, ϕ'_{cv}) for sandy soil generally lies between 30 to 35 degrees (HA68/94, 1994).

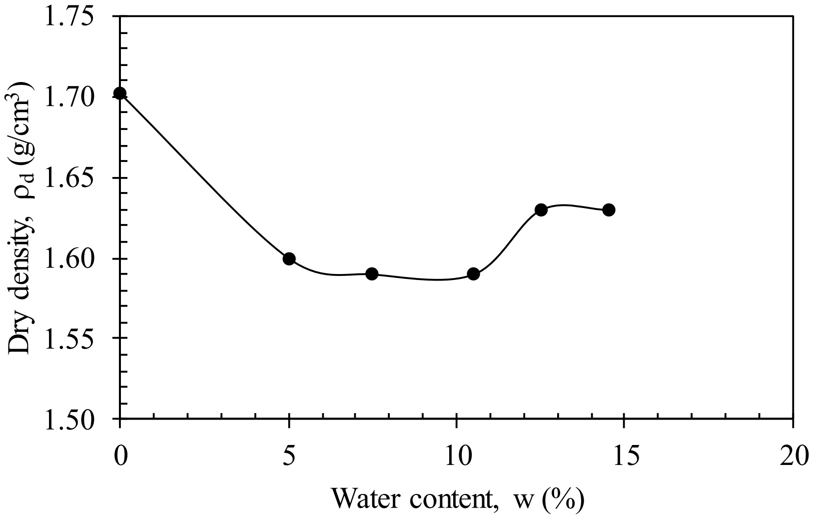

Figure 3.2: Compaction curve for sand.

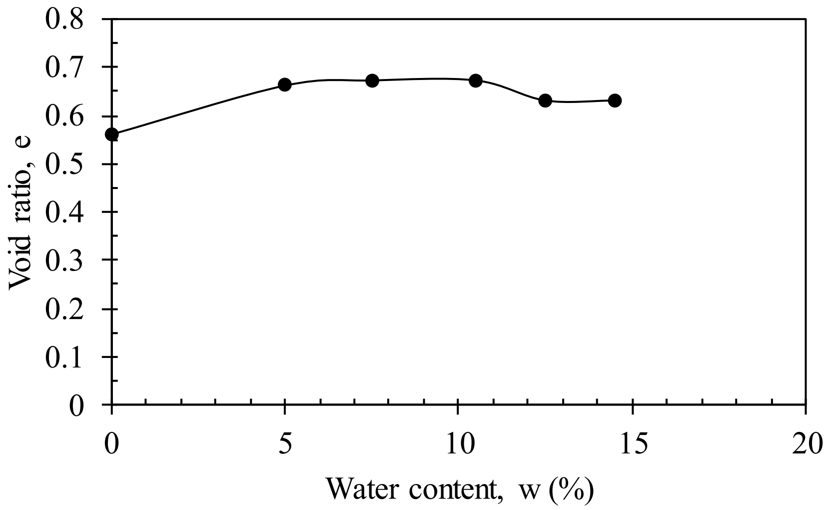

Figure 3.3: Void ratio versus moisture content for sand.

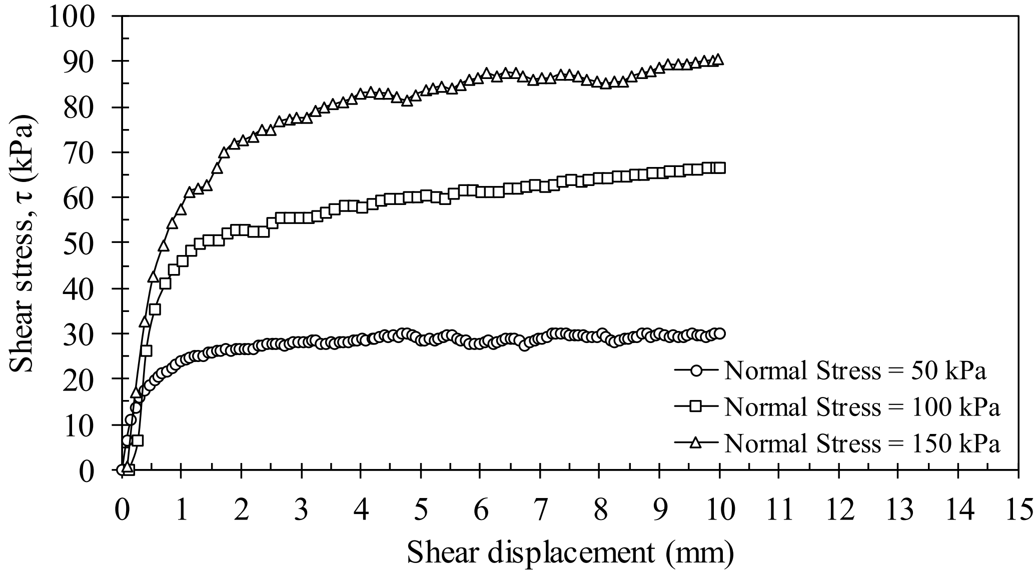

Figure 3.4: Shear stress versus shear displacement.

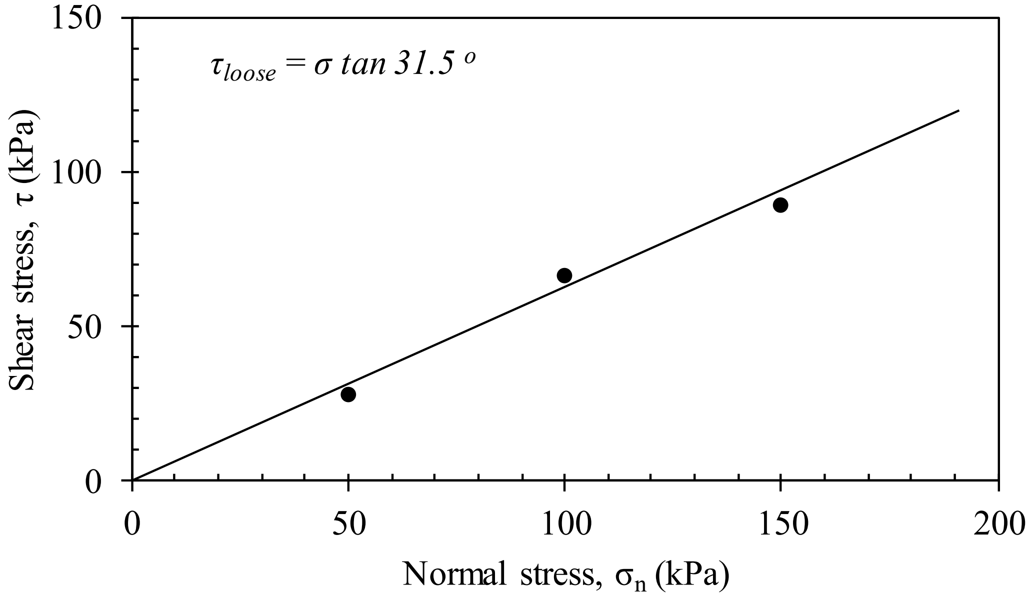

Figure 3.5: Shear stress versus normal stress.

3.3 Cement grout

In the drilled and grouted soil nail system, cement grout, with water cement (w/c) ratios varying from 0.40 to 0.50, is traditionally used as a grouting fluid, which provides corrosion protection to steel bars as well as improves the load transfer mechanism between the soil nails and the surrounding soils (Lazarte et al., 2003). A cement grout is a mixture of cement and water. It is also known as suspension grout, in which cement particles (inert material) suspend in water. The cement grout composed of a mixture of water and cement only is described here as neat cement grout due to the absence of any additives in the grout mix (Naudts et al., 2003; Rosquoët et al., 2003).

Basically, cement grout is a non-Newtonian fluid and exhibits Bingham fluid characteristics (Figure 3.6), i.e., once a threshold shear value (τ_o) has been reached the fluid behaves as a Newtonian fluid in which the viscosity/absolute viscosity (Newtonian viscosity) is constant with the rate of shearing. For the case of non-Newtonian fluids, the apparent viscosity, different from the Newtonian viscosity, changes with the shear rate and is a function of plastic viscosity and yield stress (Keong, 2006). The most important factor that affects the rheological properties (i.e., yield stress and apparent viscosity) of neat cement grout is the water cement (w/c) ratio (Raffle and Greenwood, 1961). Rosquoët et al. (2003) reported that the apparent viscosity and yield stress decrease exponentially as w/c ratio increases. Figure 3.7 illustrates the application of the cement grout in different fields based on the w/c ratio.

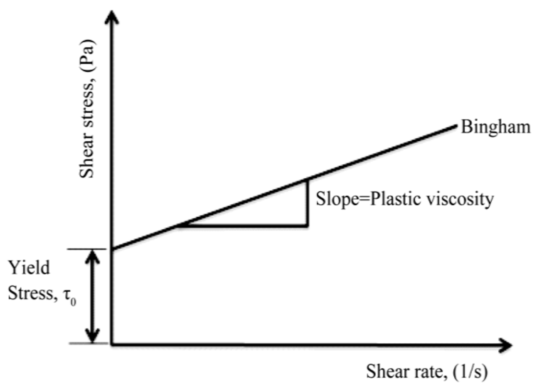

Figure 3.6: Bingham fluid model (adopted from Mohammed et al., 2014).

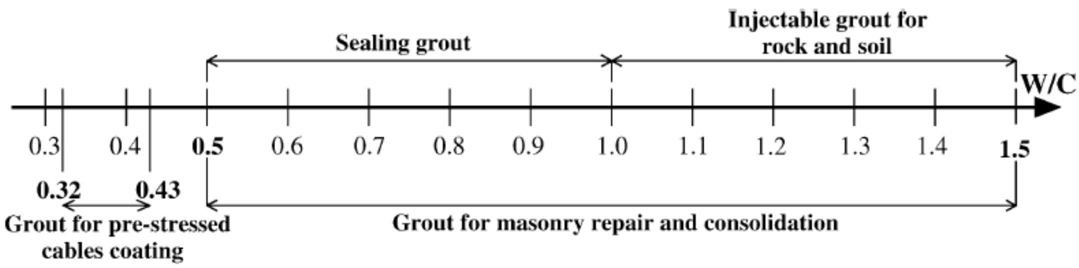

Figure 3.7: Various application of cement grout for a wide range of w/c ratios (adopted from Rosquoët et al., 2003).

For the neat cement grout used in this investigation, a locally available general purpose cement (Type-I Portland cement) is used. According to Boral cement (2017), the initial and final setting times of the cement were found to be 1.5-3.0 hours and 2.5–4.0 hours, respectively. One of the advantages of this cement is its initial setting time, which allows the cement grout to flow as a fluid for a relatively long time (approximately 1.5 hours) compared to other cements, for which the initial setting time is typically 30-45 minutes. A neat grout with a w/c ratio of 0.50 was selected and used for the experimental study of the pressure-grouted soil nail system based on the compressive strength, bleeding (i.e., segregation of clear water on the top surface of the grout during initial hydration process) and pressure filtration properties (i.e., expulsion of bleed water from the grout mixture due to pressurized injection) of this grout mixture. Wang et al. (2016) reported that neat cement grout with a w/c ratio of 0.50 developed higher compressive strength than that of the grout with a w/c ratio of 1.0. In addition, they also concluded that the grout with w/c ratio of 1.0 exhibited excessive pressure filtration due to pressurized injection of grout into sand compared to the w/c ratio of 0.50. In this study, the neat grout (w/c = 0.50) was prepared by mixing water and cement thoroughly with an electrical hand mixer, having an initial density of 1.84 Mg/m^3. According to Wang et al. (2017b), the prepared grout (w/c = 0.50) developed a compressive strength of 6.6 MPa, 23.73 MPa and 36.73 MPa after 24 hours, 7 and 28 days of curing, respectively.

Winterkorn and Pamukcu (1991) noted that the intrusion of grout slurry into the surrounding soil depends on the particle size distribution of the soil and the grout. They defined a relationship between the soil particle size, D_{15} (diameter for which 15% of particles are finer) and the grout particle size, D_{85} (diameter for which 85% of particles are finer), which was called the groutability ratio, N, as specified in Equation (3.1).

Winterkorn and Pamukcu (1991) recommended that the value of N should be greater than 24 to obtain successful grout penetration.

$$N = \frac{D_{15}^{soil}}{D_{85}^{grout}} \tag{3.1}$$

Figure 3.8 illustrates the grain size distribution of the cement slurry, which was analysed using SediGraph® III – a particle size analyser (Micromeritics, 2019). After obtaining the values of D_{15} and D_{85} from Figures 3.1 and 3.8 respectively, the value of N was calculated using Equation (3.1) and found to be approximately 12, which is smaller than the limiting value of 24 recommended by Winterkorn and Pamukcu (1991), possibly indicating unsuccessful grout penetration of this Stockton beach sand.

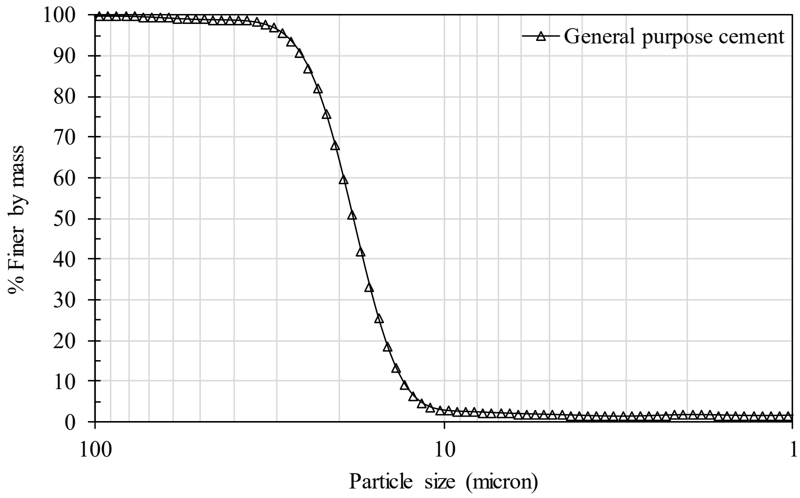

Figure 3.8: Particle size distribution curve for cement slurry.

3.4 Additive-mixed cement grout

Initially, the neat cement grout with w/c ratio of 0.50 was implemented for pressurized grouting in the soil nail systems since this grout is conventionally used for drilled and gravity grouted (low pressure grouting) soil nail systems, as reported by Lazarte et al. (2003). Bezuijen (2010) noted that pressurized cementitious grouts used in compaction/pressure grouting exhibit excessive pressure filtration (i.e., dehydration of the grout), thus impeding the flowability and workability of the injected grout. In addition, Naudts et al. (2003) described the neat cement grout as an unstable grout since it has poor resistance against the pressure filtration and forms a dehydrated grout pack for the pressurised grout injection. Consequently, the application of this type of grout in a pressure/compaction grouted soil nailing system might hamper the penetration of the injected grout significantly.

According to Warner (2004), however, the neat cement grout with a water cement (w/c) ratio greater than 0.35 usually exhibits significant shrinkage and low bond strength. Rosquoët et al. (2003) also reported that grouts with lower w/c ratios, varying from 0.32 to 0.43, are used for high bond strength applications, e.g., prestressed cable coating. Moreover, the viscosity of the grout increases exponentially with a decreasing w/c ratio (Raffle and Greenwood, 1961). Viscosity of the cement slurry is a measure of flowability, or fluidity, which is inversely related to the viscosity (Naudts et al., 2003; Fanchi, 2010). Thus, a grout with a low w/c ratio (i.e., more viscous grout) has a low flowability. Based on the factors (e.g., flowability, bond strength, and pressure filtration) mentioned previously, it can be said that, for pressurised grouting in a soil nailing system, the neat cementitious grout (w/c = 0.50) is not an effective grouting fluid. In addition, the Roads and Maritime Services (RMS) specification (2018) recommends using grouts with high bleed resistance, low shrinkage and high fluidity for soil nailing applications. Therefore, a special type of cement grout with an additive (BluCem HS200A) was introduced and used in this investigation to minimize the bleeding and shrinkage properties of the neat cementitious grout, as well as to increase its fluidity.

BluCem HS200A is a single component power additive formed by blending superplasticizers and suspension agents. The addition of this additive creates an ultra-flow cementitious grout (Bluey Technologies, 2017). A wide range of additive-mixed grouts, with water solid (cement + additive) ratio (w/s) varying from 0.30 to 0.50, was prepared by mixing 10% additive (by weight of cement powder) into a specified mass of cement-water mixture, in accordance with the Bluey Technologies (2017) specifications and mixing guidelines. Once the highly flowable cementitious grout was prepared, a Marsh funnel viscosity test (Fann, 2013) was conducted to evaluate the flowability, or the relative consistency, of the cementitious grouts and hence the Marsh funnel viscosity (reported as seconds) of the additive-mixed cement grout was compared with that of the neat cement grout (w/c = 0.50). Note that the Marsh funnel viscosity tests were performed at the ambient temperature of approximately 21ºC, on average. Table 3.2 compares the Marsh funnel viscosity of different cementitious grout compositions.

Table 3.2: Comparison of Marsh funnel viscosities of different cementitious grouts.

Grout type	Mix ratio		Grout density	Marsh funnel
	w/s	w/c	(Mg/m^3)	viscosity (second)
Neat grout	-	0.50	1.84	1036
Additive-mixed grout	0.50	0.52[a]	1.84	97
Additive-mixed grout	0.40	0.42[a]	1.95	215
Additive-mixed grout	0.30	0.32[a]	2.11	474

[a]Equivalent w/c ratio only of the additive-mixed grouts.

The results of the viscosity tests outlined in Table 3.2 show that the viscosity (1036 seconds) of the neat cement grout, with a w/c ratio of 0.50, was approximately 11 times higher than that (97 seconds) of the additive-mixed cement grout with a w/s ratio of 0.50 (an equivalent w/c ratio of 0.52), with the same grout density (1.84 Mg/m^3). In addition, the viscosities of the additive-mixed grouts for w/s ratios of 0.40 and 0.30 were approximately 21% and 46% of the neat grout viscosity, respectively, although the grout densities of the additive-mixed cement grouts were 1.10 and 1.15 times that (1.84 Mg/m^3) of the neat cement grout, respectively. Hence, the addition of this special type of additive into the neat cement grout increased the flowability of the grout significantly, which in turn transformed the neat cement grout from a low mobility grout to a high mobility grout. Similarly, Naudts et al. (2003) concluded that addition of admixtures (superplasticizers and dispersants) into neat cement grout reduces the viscosity and segregation of the grout. Interestingly, based on the viscosities of the additive-mixed grouts (Table 3.2), it can be argued that the amount of solid contents in the grout composition significantly affects the grout viscosity and the viscosity increases substantially with the increment of the grout density. Figure 3.9 illustrates that the viscosity increases exponentially as w/s ratio decreases, whereas fluidity increases with increasing w/s ratio. This is consistent with the findings reported by Raffle and Greenwood (1961) and Rosquoët et al. (2003). The fluidity of the cementitious grouts used in this study can be described as high, intermediate, low, and very low, depending on their measured viscosity values of 97, 215, 474, and 1036 seconds, respectively.

According to Bluey Technologies (2017), an additive-mixed cement grout with w/s ratio of 0.30 exhibits zero bleeding, high compressive strength, high bond strength, low shrinkage and high fluidity. Moreover, Bluey Technologies (2017) reported that the additive-mixed cement grout with w/s ratio of 0.30 develops a compressive strength of 40 MPa and 90 MPa after 24 hours, and 7 days curing, respectively. These values are much higher than the strengths of 6.6 MPa at 24 hours and 23.73 at 7 days resulting from a neat cement grout with w/c ratio of 0.50 used by Wang et al. (2017b) in a separate study of compaction-grouted soil nails. Hence, it can be said that the grout with a w/s ratio of 0.30 might be a stable and effective grout composition for pressure-grouted soil nail systems, which conforms to the performance requirements of the grout used for soil nailing specified by the Roads and Maritime Services (RMS) standards (RMS R64, 2018).

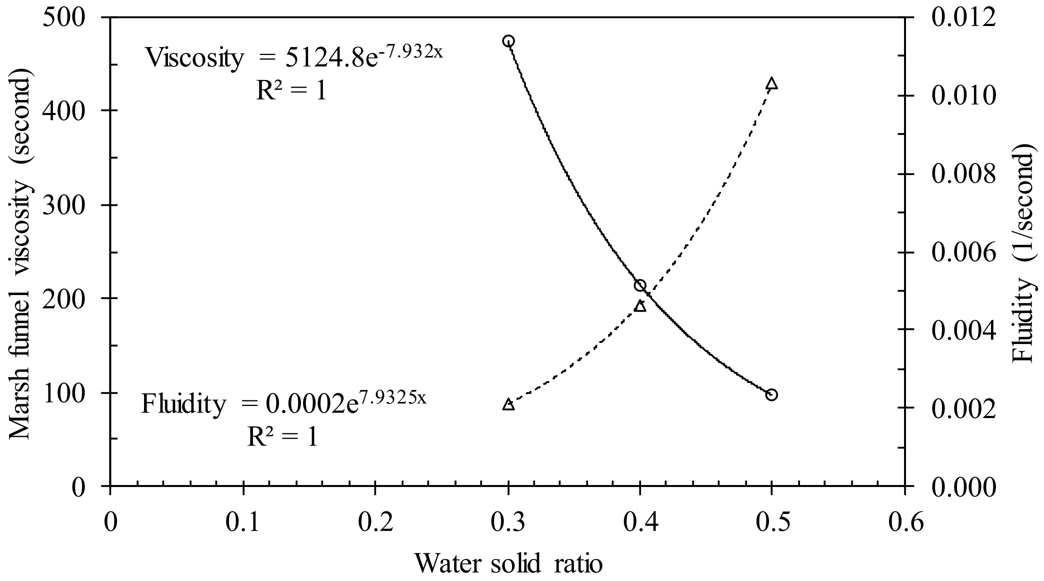

Figure 3.9: Evolution of viscosity and fluidity of the additive-mixed grout with respect to the w/s ratio.

Chapter 4 Apparatus, instrumentation, and test procedures

4.1 General

This chapter describes the experimental setup developed at the University of Newcastle to perform a physical model study of pressure-grouted soil nail systems with a view to providing a comprehensive outline of the instrumentation techniques and data acquisition system. In addition, this chapter also includes detailed test procedures for the pullout model study of the pressure-grouted soil nails.

4.2 Design and development of experimental setup

4.2.1 Background

The pullout resistance of a soil nail is influenced by several factors present in the actual field conditions, such as soil type, type of soil nail, method of nail installation, interface friction, relative density of the soil (and consequently the shear strength of the soil), overburden pressure (confining stress), inclination of the soil nails, degree of saturation of the soil and the grouting pressure, as well as the size of the grout inclusion, as described in Section 2.4 of Chapter 2.

A number of specially designed model-scale apparatuses have been developed in the laboratory for investigating the influence of the previously mentioned factors on the pullout resistance. However, most of the available setups are only applicable for conventional soil nails, for example, driven soil nails and drilled-and-grouted soil nails (Milligan et al., 1997; Franzen, 1998; Junaideen et al., 2004; Chu and Yin, 2005a; Pradhan et al., 2006; Yin and Su, 2006; Gurpersaud et al., 2013). In addition, Tokhi et al. (2017) and Sharma et al. (2019) have reported a pullout testing facility for studying screw nails along with conventional soil nails. Wang et al. (2017b) introduced a pullout device with a pressure grouting facility for study of an innovative compaction-grouted soil nail. In this apparatus, a pressure-controlled injection system was used whereby a predefined pressure was set in the injection pump system and the grout was injected at that set pressure for a certain period of time. However, the device was unable to control the flow rate of the injected grout. This is a major shortcoming because it is important to control the injection volume and to monitor pressure fluctuations during grouting (Bezuijen, 2010). By considering this issue, a special type of volume-controlled injection system was designed and developed to maintain a constant volumetric flow rate of the injected grout. In addition, in the newly developed test facility the exiting overburden pressure system (compressed air-filled rubber bag) reported by Wang et al. (2017b) was modified and redesigned to become a pressurized water-filled rubber bag with a facility to estimate the soil settlement indirectly from the volume of pressurized water contained in the bag. The design details of the new test facility developed for the pressure-grouted soil nail system are described in the following sections.

4.2.2 Details of the developed apparatus

The schematic layout of the experimental setup is shown in Figure 4.1. The apparatus consists of five major parts: (1) a volume-controlled injection system, (2) a pullout box, (3) an overburden (surcharge) pressure application system, (4) a pullout system, and (5) a data acquisition system. The key components and their functions are discussed in the following sections.

4.2.2.1 Grout injection system

The grout injection system was designed and fabricated for controlling the grout injection rate. The injection system is a piston pump and consists of a screw jack with a motor, a grout cylinder and a support frame, as shown in Figure 4.2. The screw jack capacity is 25 kN and the maximum stroke of the lifting screw (spindle) is 350 mm. The jack is bolted to the angle frame by facing the spindle upside down. A three-phase AC motor driven by an alternating current (AC) is coupled to the drive shaft of the screw jack for providing the necessary drive torques to the jack. The jack is a worm gear screw jack, which transfers the rotational motion to translatory motion (vertical movement). The travel rate of the jack is 0.25 mm/revolution for the worm gear ratio 24:1 (Zimm, 2015). Thus, the spindle experiences a displacement speed of 300 mm/min at 1200 rpm (revolutions per minute). A grout cylinder, 150 mm in diameter and 370 mm in height, is selected to accommodate the injection grout up to a maximum volume of 5 litres. A piston to pressurize the injection grout, 148 mm in diameter and fitted with two O-rings, is mounted inside the cylinder at the threaded end of the spindle (Figure 4.2). An air release valve is provided in the piston to eliminate the entrapped air while pressuring the grout.

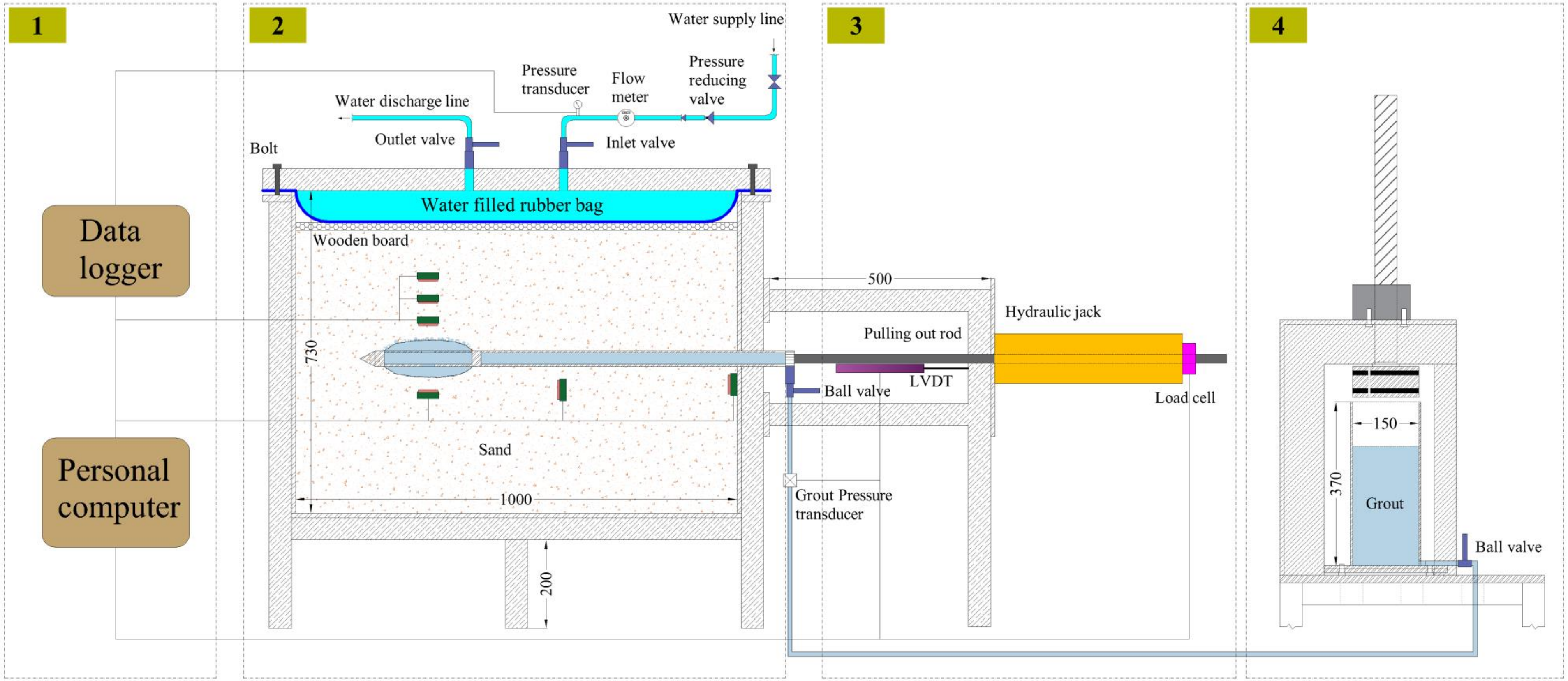

Figure 4.1: Schematic of the experimental setup: (1) data acquisition system; (2) physical model box including overburden pressure system; (3) pullout system; (4) volume-controlled grouting system (dimensions in mm).

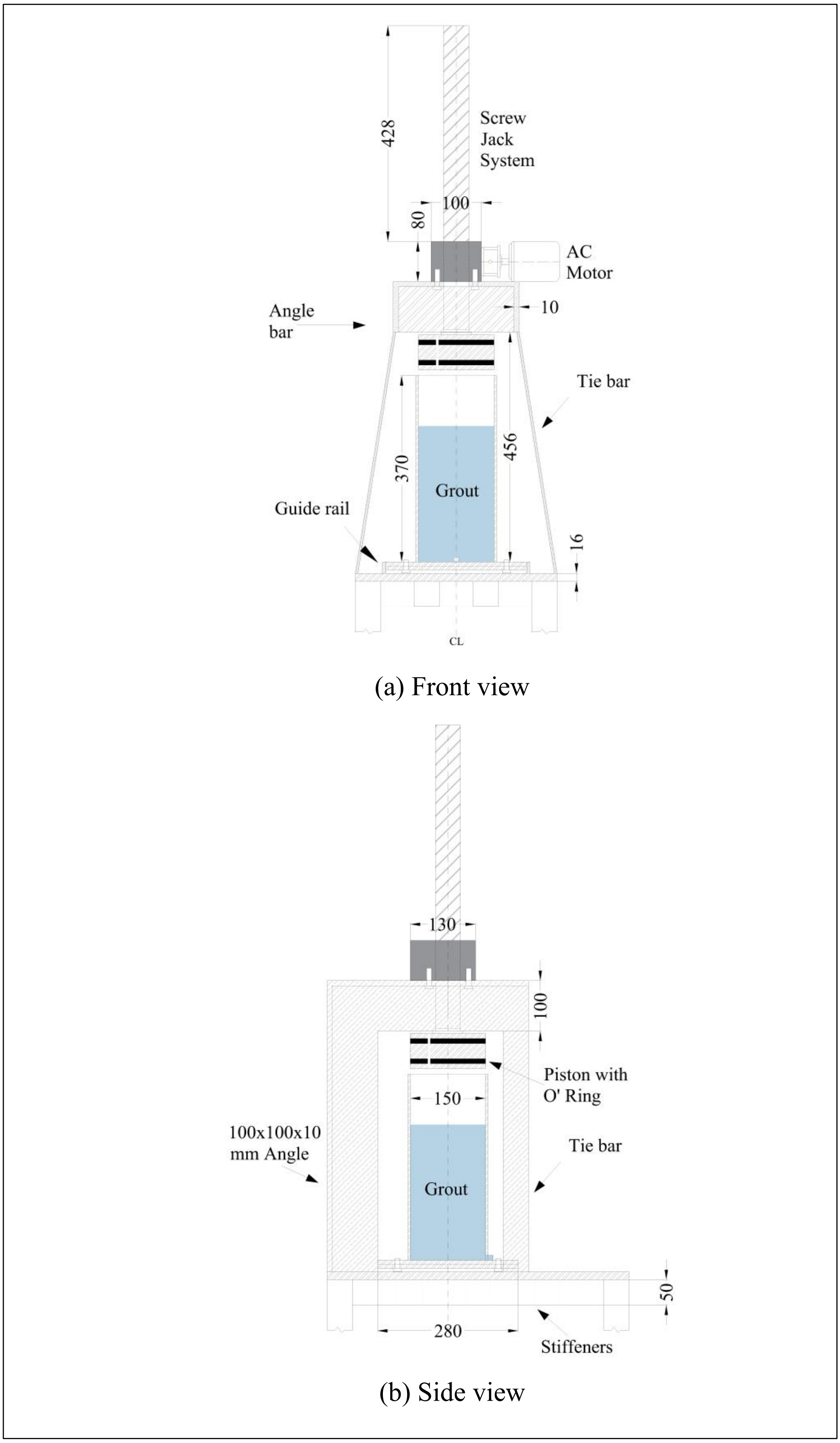

Figure 4.2: Details of the grout injection pump including screw-jack with piston, cylinder and support frame (dimensions in mm).

During grout injection, the AC motor always runs at a constant speed (rpm) and this speed can be varied by changing either the input voltage or frequency. In this study, a variable frequency driver (ACS150) was installed in the pump control unit for changing the input frequency supplied to the motor because the travel speed of the spindle is related to the speed (rpm) of the motor. Automation of the pump system was achieved by installing a switching panel to regulate the motor speed as well as to shift the direction of the spindle movement (Figure 4.3). The switching panel consists of five buttons: a regulator knob to adjust the speed of the motor, two push buttons (green in colour) for shifting upward and downward movements of the spindle, a latching button (red one between push buttons) to activate/deactivate the automatic up/down movement of the spindle, and an emergency-stop button (big one at the top of the switching panel) for safety purposes. With this automation, the grout can be injected using the regulator knob at different flow rates ranging from 0.5-7.5 litres/min. In addition, a string potentiometer (pot) is used to monitor the piston position over the grouting period, allowing estimation of the volume of injected grout. The pump is able to apply a maximum grout pressure of 2000 kPa. A diaphragm pressure transducer mounted at the outlet tube of the grout cylinder measures the grouting pressure.

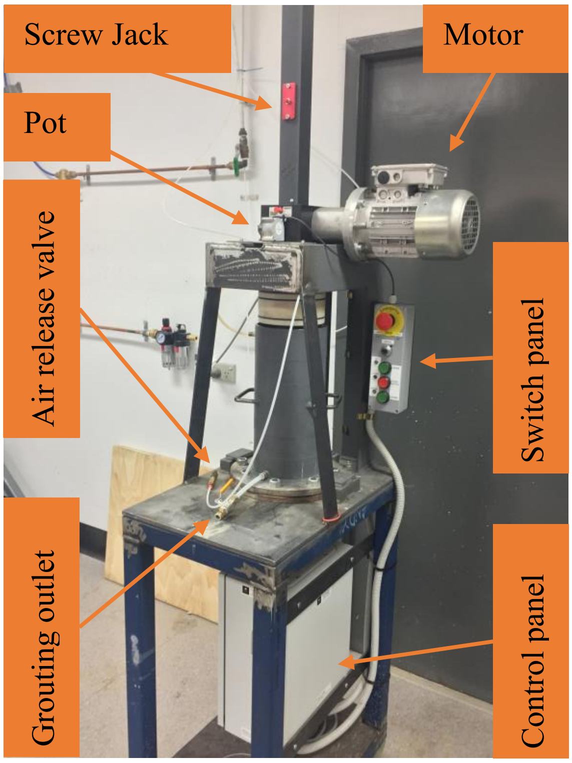

Figure 4.3: Photograph of the grout injection pump.

4.2.2.2 Pullout box

The pullout box works as a soil chamber, which accommodates the soil sample, the soil nail and the sensors used for instrumentation. The chamber was constructed by welding five mild steel plates, 10 mm thick, together to form the walls and the floor of an enclosed box. The box is reinforced with square steel tube stiffeners (50x50x4 mm) to minimize the bending deformations of the rigid boundaries during application of different overburden pressures (Figure 4.4). The lid (top cover) of the box was similarly constructed using steel plate reinforced with the steel stiffeners. The box has internal dimensions of 1000 mm in length, 600 mm in width and 730 mm in height. The size of the box was originally designed by Wang et al. (2017b) to reduce the boundary effects as well as to eliminate the difficulties of preparing huge volumes of soil samples for pullout testing. Palmeria and Milligan (1989) reported that the size of the pullout box can affect the pullout capacity of a buried reinforcement and a larger box had lower boundary effects. A crystal clear plastic sheet (thickness of 0.1 mm) lubricated with oil is attached on the interior sides of the box to minimise side friction (Palmeria and Milligan, 1989; Su 2006; Wang et al., 2017b). Two circular openings with diameters of 140 mm and 180 mm are provided at the middle of the front and back walls, respectively, with a height 350 mm from the bottom plate, to facilitate pre-drilling, driving and pullout of the soil nail. The diameters of the openings can be adjusted as required by mounting a circular plate with a specified hole diameter. In addition, a total of 22 small threaded holes were made in the side and front walls of the box at different heights, into which metal glands are installed to maintain water tightness, but also to allow access for the lead wires of the sensors used for instrumentation (Figure 4.4). A drainage layer of 50 mm thickness was prepared by compacting and levelling gravel at the bottom of the box, which was covered with a geotextile sheet to separate the soil sample from the drainage layer. Four valves are mounted at the level of the drainage layer for water supply to the soil sample or drainage, as needed. However, these valves were kept closed in the physical model tests performed in the present study.

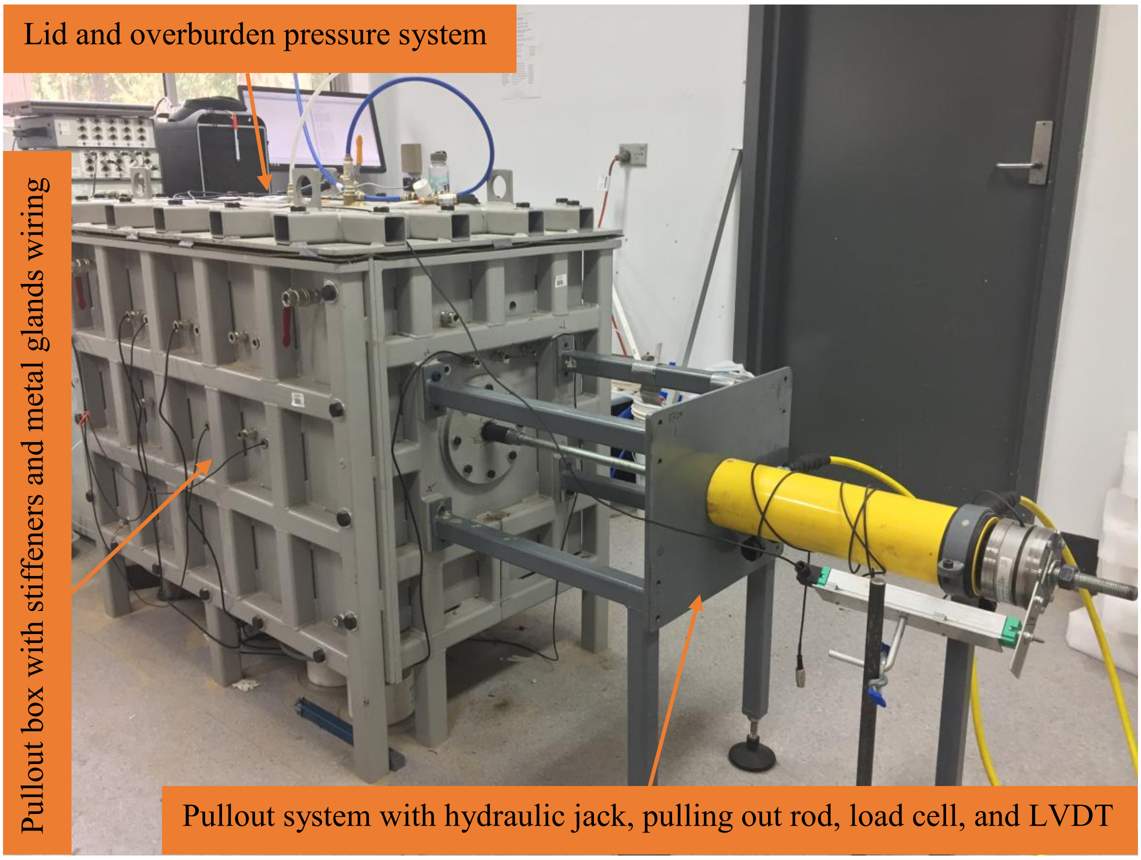

Figure 4.4: Photograph of the test facility showing pullout box, overburden pressure system, and pullout system.

4.2.2.3 Overburden pressure system

In many physical models of soil nail systems, an overburden pressure is applied by hydraulic jacks mounted on a rigid steel plate that rests on top of the soil surface (Junaideen et al., 2004; Pradhan et al., 2006; Tokhi et al., 2017; Sharma et al., 2019), or by fluid-filled rubber bags in which pressure is applied by pumping pressurized air (Wang et al. 2017b) or water (Palmeira and Milligan, 1989; Franzen, 1998; Chu and Yin, 2005a; Yin and Su, 2006) into the rubber diaphragm fixed under the lid of the box. A flexible rubber membrane is preferable for producing a uniform distribution of pressure on the top soil surface. In addition, it does not cause an overestimate of the pullout resistance by constraining dilatancy, as can occur with a rigid top plate loading system (Palmeira and Milligan, 1989). In the present study, a water-filled rubber cushion system was developed for applying surcharge pressure on the top surface of the soil sample compacted inside the box. A rubber sheet 3 mm thick is mounted under the top cover (lid) of the box to form a diaphragm, which separates the pressurized water from the soil surface. The diaphragm is air tightened and sealed against the extended edges of the walls of the box using M16 hexagonal bolts screwed to the brim stiffener of the box (Figure 4.5). A plywood sheet (17 mm thick) is placed under the rubber sheet in contact with the soil in an attempt to produce more uniform vertical soil displacements. Two valves are mounted on the top cover: one (inlet) for applying overburden pressure by pumping pressurized water into the rubber bag, and the other (outlet) is designed to release the water pressure after the pullout tests. A water supply line, from the existing tap water source in the laboratory, is connected to the inlet valve with a hydraulic pressure-reducing valve used to control the pressures of the source water (0-300 kPa). A check valve is installed downstream of the pressure-reducing valve to stop backflow into the reducing valve, as recommended by Caleffi (2018). In addition, a pressure transducer is inserted in the water line to monitor the digital reading of the applied overburden pressure during each test. Most importantly, a water flow meter is mounted on the water supply tube to measure the volume of pressurized water inside the rubber cushion during the application of an overburden pressure. In turn, these volume measurements are used to estimate the vertical settlement of the soil sample during the period of surcharge loading.

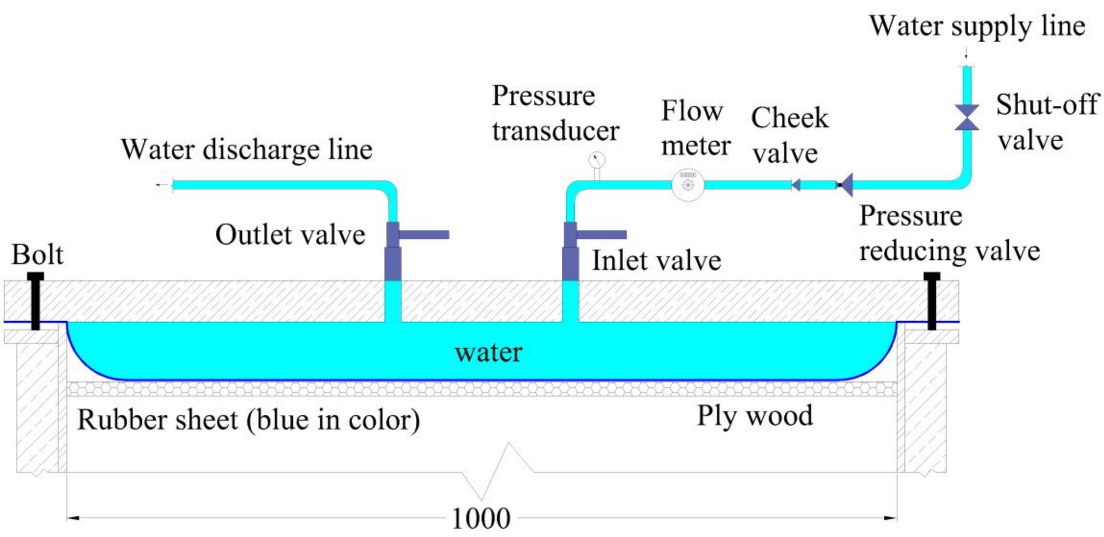

Figure 4.5: Schematic of the overburden pressure system

4.2.2.4 Pullout system

A pullout unit developed by Wang et al. (2017b) was only able to pull out a soil nail; this was redesigned in this investigation to add a driving facility of a soil nail to the unit. Thus, the modified pullout system is a "two-in-one" system, since it provides both the driving and pulling out of a soil nail (Figure 4.4 and Figure 4.6). Hence, the soil nail can easily be driven and extracted at different displacement rates ranging from 0.5 mm/min to 50 mm/min. The system consists of a reaction frame and a double-acting hydraulic cylinder with a hollow plunger (capacity of 300 kN), which is used for jacking/pulling out a soil nail as shown in Figure 4.4. The frame is connected to the front wall of the box with bolts (M10) to resist the pullout force. A set of three ball-joint-adjustable levelling feet are installed on the legs of the frame to allow alignment of the centre of the plunger along the centre of the opening located in the front wall of the pullout box. A threaded coupling rod (or pulling out rod, M16) is used to make a connection between the soil nail and the plunger. To provide the driving facility, the front wall of the box is attached to the reaction frame using four tension members, made of square steel tubes (25x25x2.5 mm), which are attached at both ends using bolts (M10), as illustrated in Figure 4.6. A double-acting hand pump is used for both driving and pulling out the nail. A hollow compression load cell of 100 kN capacity is attached to the plunger to monitor the driving and pullout forces. In addition, a linear variable displacement transducer (LVDT) is used to record the corresponding displacements.

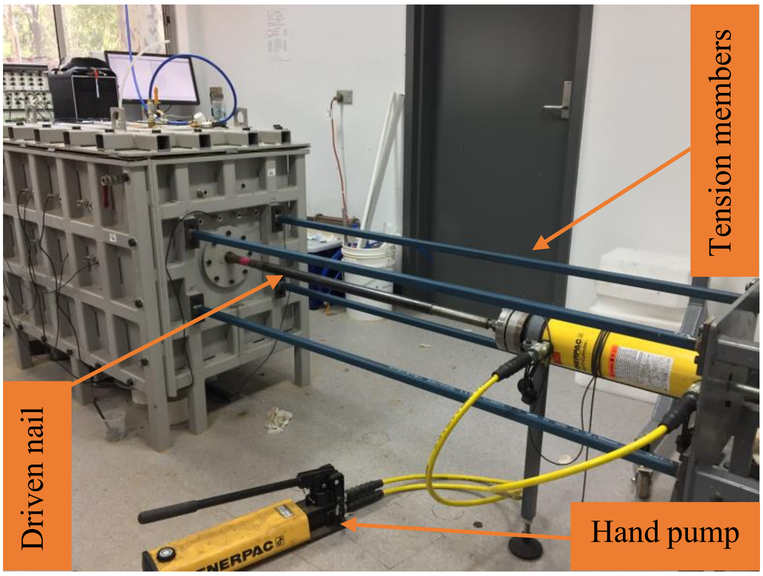

Figure 4.6: Photograph of the driving facility showing tension members, driven nail and hand pump.

4.2.2.5 Instrumentation system

In this study two types of transducers were utilised to monitor the soil response during the grout injection, jacking and pullout processes. The stress state conditions inside the soil were monitored using earth pressure cells (EPC). The soil pressure transducers used here are traditional diaphragm-type earth pressure cells (DEPC) that use strain gauge technology. In addition, the variation of water content in the soil sample was recorded by soil moisture sensors (SMS) and in this investigation the GS3 soil moisture sensors were used to measure the volumetric water content (VWC) inside the soil mass. The GS3 is a dielectric-based soil moisture sensor that uses electromagnetic fields to identify the dielectric permittivity of the surrounding soil. The GS3 is a robust probe whose data sensing accuracy is not affected by its orientation, and requires only a small volume of the soil for measuring the volumetric water content (Cobos, 2015; Decagon Devices, 2016). Furthermore, the volumetric water content readings monitored by the SMS can be used to estimate the soil dry density and the soil porosity using the simple relations reported by Bilskie (2001).

Figure 4.7 illustrates the basic layout of the main sensor locations, denoted by the prefix SL. In total, fourteen sensors were inserted in the soil sample, with each set consisting of eight pressure cells and six soil moisture sensors. The sensors located near the injection point (SL1 and SL3) are buried 50 mm below and above the soil nail surface, respectively, to observe the change of soil stress states and moisture contents during the grouting process. In addition, another two layers of sensors (SL5 and SL6) are buried just above SL1 to detect the zone of influence of grouting pressure up to a vertical distance of 150 mm from the injection point. To monitor the soil behaviour during the pullout process, additional sensors were embedded at the locations SL2 and SL4, which are 350 mm and 180 mm away (horizontally) from the centre of the injection point, respectively, with a vertical distance of 50 mm from the nail surface. Note that EPC2 located at SL2 is installed vertically, which makes it possible to measure the horizontal soil pressure changes adjacent to the soil nail.

In this physical model study EPC7 and EPC8 were mounted against the front and side walls, respectively, to measure the soil pressures at the boundaries of the box, as shown in Figure 4.7. EPC7 is located below the soil nail at the same distance as EPC2, whereas EPC8 is installed at the nail level at a horizontal distance of 700 mm from the front wall. All the soil pressure transducers were calibrated in sand based on their orientations and positions in the box, as described in detail by Bhuiyan et al. (2018). The SMSs used in the investigation were also calibrated for the sand sample, as reported by Bhuiyan et al. (2020). Table 4.1 outlines the details of the sensors used in this physical model study.

4.2.2.6 Data acquisition system

The data acquisition system consists of an intelligent universal input data logger (DT80 Series 3) and a powerful desktop computer. The robust data logger used in the acquisition system has the capacity to facilitate 35 analog channels (expandable up to 300), eight digital channels and four serial (SDI-12) channels. Thus, the smart logger is able to read versatile sensors (almost any sensor) based on the fundamental inputs such as voltage, current, resistance and frequency (dataTaker, 2011). The logger has plug and play facilities and therefore it can easily be connected to the computer by means of a USB communication port. A windows-based software, DeTransfer®, installed in the computer is used to supervise the logger and access the logged data stored in the internal memory. The software provides a terminal interface (send and receive windows) with macro buttons in which the send window is used to write built-in scripting commands that are sent into the logger to record and store the data continuously for the sensors connected to the specified channels, whereas the receive window allows the user to view real-time logged data in text format. The acquisition system has the ability to sample the data at the maximum speed of 25 Hz. However, in the present study, the sample speed (readings per unit time) was varied over the period of the testing (e.g., sample preparation stage, loading stage, grouting stage, and jacking/pullout stage), ranging from 0.07 Hz to 1.0 Hz.

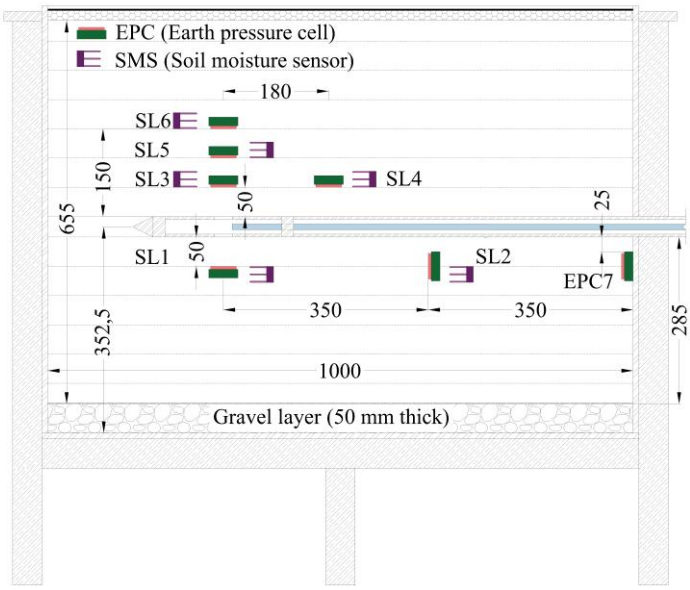

Figure 4.7: Basic layout of the sensors embedded around the soil nail (dimensions in mm) showing compaction layers (dotted lines).

Table 4.1: Details of the sensors used for instrumentation.

Sensor	Range	Accuracy	Location	Quantity
Grout pressure transducer	0-2000 kPa	±0.5%FS	Grout injection system	1
String pot	0-635 mm	±0.25%FS	Grout injection system	1
Load cell	0-100 kN	±0.5%FS	Pullout system	1
LVDT	0-200 mm	±0.05%FS	Pullout system	1
Overburden pressure transducer	0-1000 kPa	±0.25%FS	Surcharge system	1
Flow meter	0.25-6.5 litre/min	±1%FS	Surcharge system	1
Earth pressure cell	0-1000 kPa	±2%FS	soil	8
Soil moisture sensor	1-80 perm	±1-2%VWC	soil	6

Note: FS = Full-scale reading.

4.2.3 Important features of the developed apparatus

The key features of the developed experimental setup can be summarized as follows:

1. The developed overburden pressure system can be used as an easy alternative to the overburden systems developed by Yin and Su (2006) and Wang et al. (2017b), since it eliminates the need for a complex volume change gauge (Yin and Su, 2006) and the application of a linear guide system (Wang et al. 2017b), which can be susceptible to air leakage.
2. The volume-controlled injection system developed here can be used for a pressure-grouted soil nail system to evaluate the effects of grout injection rates and injected grouted volume on the pullout behaviour of soil nails.
3. The injection pump is also able to detect the fluctuations of injection pressures during pressured injection of grout at a constant flow rate.
4. The driving facility added to the experimental setup makes it possible to conduct an experimental study for the driven soil nail system.
5. The adjusted circular opening in the front wall of the box provides a facility to study the drilled and grouted soil nail.

4.2.4 Soil nail

In this investigation, two types of soil nails were used to evaluate the influences of grout injection rates, grout viscosities and injected grout volumes on the pullout behaviour of the soil nails. The following sub-sections describe the key components of the soil nails in detail.

4.2.4.1 Pre-buried soil nail

A special type of soil nail designed by Wang et al. (2017a) was used to investigate the effects of injection rates and grout viscosities on a pre-buried (embedded) soil nail, as illustrated in Figure 4.8. The nail consists of two parts: a hollow nail head with a tip and a hollow nail rod. The nail head and nail rod are joined together with a M30 threading. In addition, a bulkhead connector was attached at the end of the nail rod for fixing the grouting tube to the nail head. The grouting tube (10 mm diameter) is used to protect the hollow nail rod from being filled up with the grout and hence allowing reuse of the nail rod. The nail head consists of four holes positioned at the mid-length of the nail head, which act as injection outlets. A latex membrane with various lengths ranging from 50 mm to 200 mm is used as a liner around the grouting outlets to form a Tube-a-Manchette (TAM) for direct injection of the cement grout into sand. This is in contrast to the compaction-grouted soil nail for which an inflatable latex is used to prevent leakoff (permeation of water and solid particles of grout into the soil) of the injected grout (Wang et al. 2017a).

4.2.4.2 Driven and grouted soil nail

An innovative soil nail (described here as the x-Nail) was designed and manufactured in order to study a driven soil nail with a grouting facility. It combines the important features of a conventional driven (purely frictional) soil nail and a compaction-grouted soil nail. The innovative soil nail consists of three parts: (1) a hollow nail rod, (2) a hollow and grooved nail head with grouting outlets, and (3) a nail tip as shown in Figure 4.9. All parts were fabricated separately and connected together by screwing together the male-female threads. A tubing facility for grouting, similar to the pre-buried soil nail, was provided inside the x-Nail. An inflatable latex balloon (cylindrical in shape) with a length of 140 mm was fixed around the nail head by two O-rings, one at each end of the cylindrical membrane. The balloon was purposely used to prevent the grouting outlets from being blocked by the sand around the driven nail head and to control the shape of the grout bulb (hardened grout) formed around the nail head.

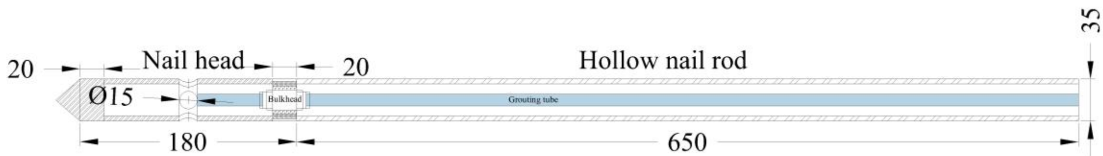

Figure 4.8: Sketch of the pre-buried soil nail (dimensions in mm).

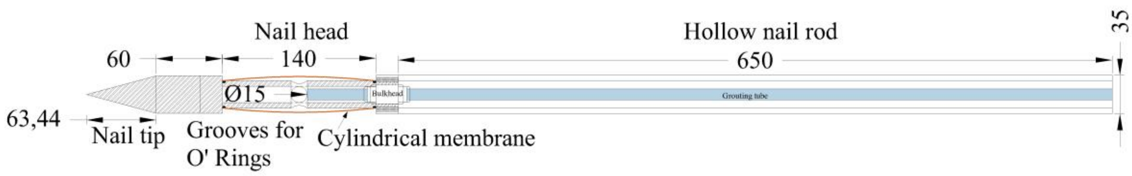

Figure 4.9: Sketch of the x-Nail (dimensions in mm).

4.3 Physical model test arrangement and procedures

A series of full-scale pullout tests were conducted with the developed experimental setup to quantify the influences of grout injection rates and grout viscosities on the pressurized grouting used for soil nailing systems. In addition, the developed test device was used to evaluate the performance of the innovative driven and grouted soil nail (the x-Nail) by executing multiple pullout tests. A general description of test preparation and procedure for physical study of the pressure-grouted soil nail system is outlined in the following subsections.

4.3.1 Sample preparation and installation of sensors

Prior to moist sample preparation, the sand used in this study was oven-dried and placed in storage containers for at least 24 hours to be cooled down to the ambient temperature. For preparing the moist sample, the mass of oven-dried sand required for a specified box height was calculated and the corresponding water mass was estimated from the desired water content of 3% (by weight of dry sand). After that, the measured masses of sand and water were poured into a mixer and mixed for 10 minutes to achieve a uniform mass of moist sand (Figure 4.10a). The unsaturated soil sample was then placed in the box and compacted manually by a steel plate rammer (of about 4.5 kg) to achieve an estimated relative compaction (CR) of 88% of the maximum dry density (1.70 Mg/m^3). Note that the moist sand was compacted inside the box in layers (35 mm to 50 mm thick), with a controlled dry density of 1.50 Mg/m^3. In total, 14 layers of compacted sand were used to fill the box and the maximum thickness of the compacted layer was limited to 50 mm to obtain a relatively uniform soil distribution (Figure 4.7). The layer height (thickness) was adjusted based on the positions of sensors and soil nail, as illustrated in Figure 4.7. The compacted sample was levelled by a hard wooden hand-float, and the finished layer surface was cross-checked by a plumb level (Figure 4.10b). This compaction process was repeated until the total height of the soil sample was 655 mm.

Once the compacted soil reached the height of a sensor position, the earth pressure cells (EPCs) and soil moisture sensors were installed by hand systematically at their predetermined positions, as outlined in Figure 4.7. Garnier et al. (1999) reported that the placement of earth pressure cells by hand in soil has a significant effect on the in situ stress measurement and they recommend taking appropriate care during installation of the cell in order to minimize the error in measured raw data. The EPCs, which register vertical pressures (particularly EPC1, 3, 4, 5 and 6), were placed on the compacted soil layer with a gentle placement force in order to ensure good contact occurred between the sensing face of the EPC and the soil surface. However, for the EPCs installed vertically (EPC2, 7 and 8), a small pit was dug into the compacted soil for the placement of the EPC and after insertion of the EPC, the surrounding was compacted slightly to ensure that soil-sensor contact was well established. Similarly, during the installation of the volumetric water content sensors, the SMS was embedded into compacted soil horizontally by digging a rectangular pit and fitting the body of the SMS. The excavated soil was used to cover the sensor prongs and compacted with appropriate measures to secure good contact between the sensor prongs and the soil surface, without allowing any air gaps that might affect the sensor raw readings, as reported by Cobos (2015). Figure 4.11 illustrates the placement of the EPC and SMS during the compaction process.

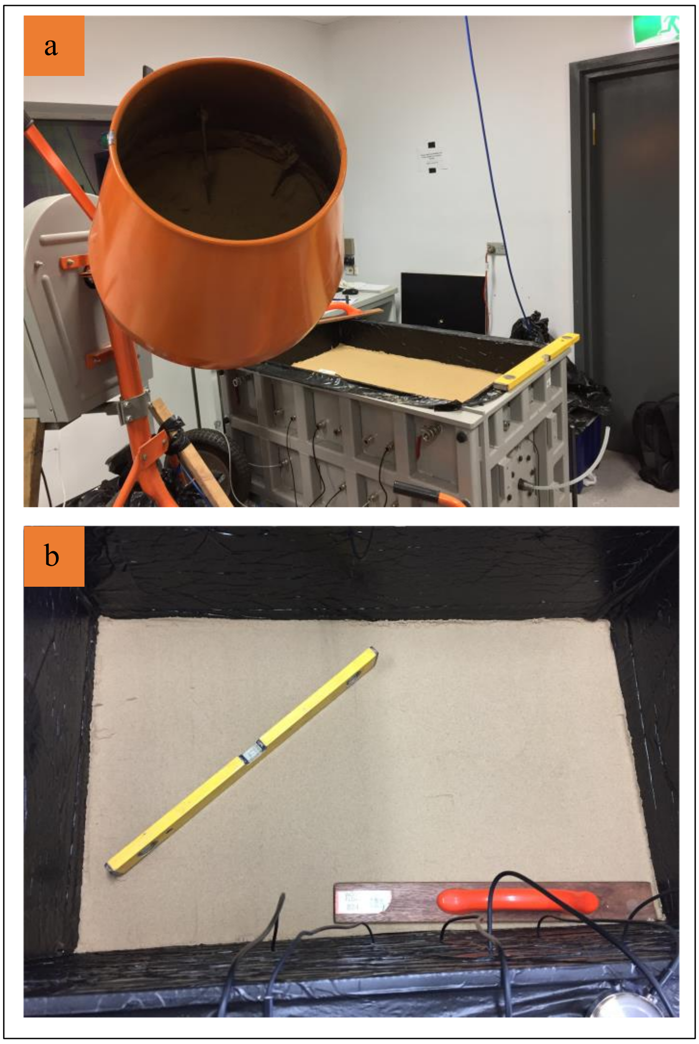

Figure 4.10: Photographs of (a) preparation of moist sand and (b) levelling of the compacted fill.

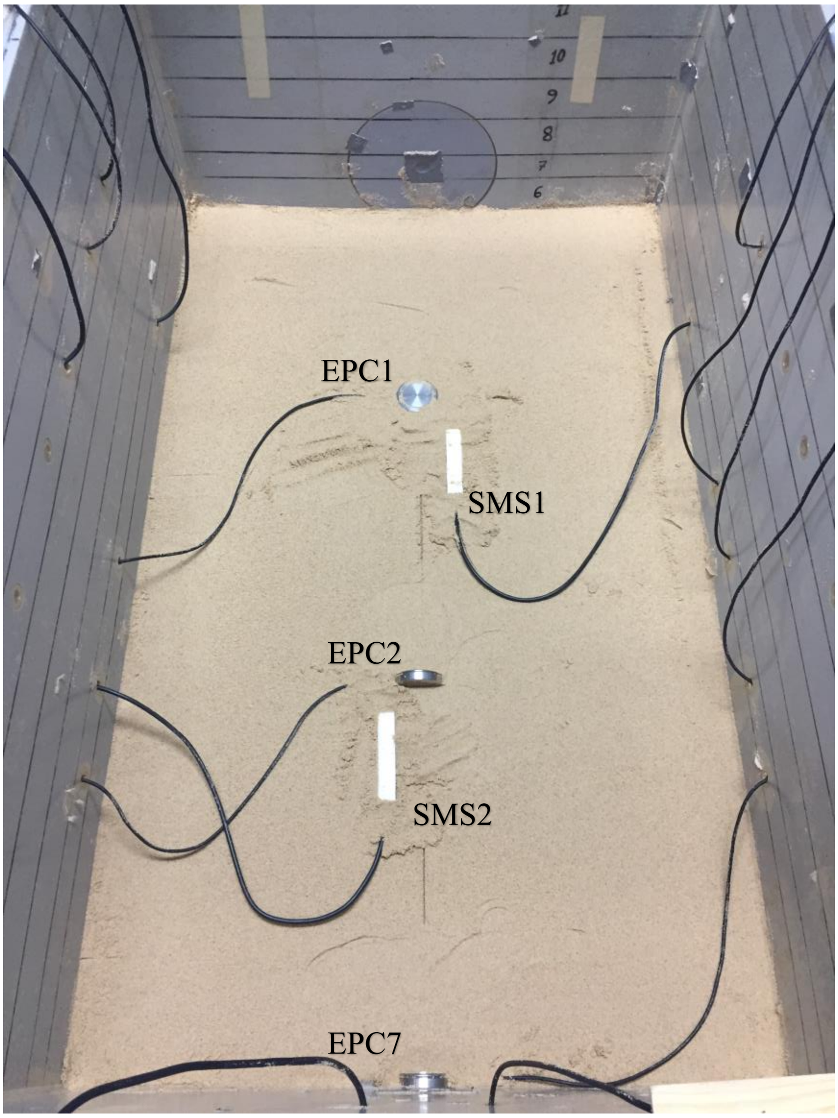

Figure 4.11: Photograph of installation of the sensors (EPC and SMS) during compaction process.

4.3.2 Soil nail installation and application of overburden pressure

During the compaction process, the pre-buried nail was also placed horizontally at a height of 335 mm from the bottom of the box (Figure 4.7). Additionally, the pre-buried nail was levelled carefully to minimize any bending effect during the pullout tests. In the current study, the pre-buried soil nails (Figure 4.12) were pre-installed to minimize the stress-state changes in the compacted soil. This represents an idealized undisturbed soil condition, since pre-drilling and nail driving disturb the surrounding soil conditions.

After placement of the soil sample up to the desired level (655 mm high), the hydraulic overburden pressure system was bolted to the top of the box, as illustrated in Figure 4.5. Before applying an overburden pressure, water was injected at very low pressure into the sealed rubber bag to remove entrapped air from the system. When the rubber bag was filled up with water, the air releasing valve was turned off and the volume of injected water was measured continuously by the digital flow meter to calculate the settlement of the compacted fill for a known applied surcharge pressure. The maximum water injection pressure was regulated to 100 kPa and checked by means of a mounted pressure transducer, which was kept constant during the test. After application of the overburden pressure, the sand box was left undisturbed for a maximum period of one hour to stabilize the stress states in the sand mass and thus the embedded sensors ultimately reached stable readings (Bhuiyan et al. 2019). Following the stabilization of the compacted fill, for the pre-buried soil nails only, the pressurised grout was injected directly into the sand by the volume-controlled grout injection pump at a specified injection rate.

In the case of the driven soil nails, with and without grouting facility, the compaction process and the installation of the sensors at the predetermined locations were done systematically, similar to the process used for the pre-buried soil nail. The x-Nail was subsequently jacked into the compacted soil mass after 1 hour of the application of the surcharge pressure (100 kPa). During the jacking process, the changes of soil stresses and water contents in the soil mass were monitored with the installed sensors, and the driving force and corresponding driving displacement were continuously recorded through the load cell and the LVDT attached to the jacking facility (Figure 4.13). After installation of the x-Nail, the setup was left undisturbed for 1 hour to stabilize the stress conditions in the soil mass due to any disturbance that may have resulted from the jacking process. After that, the cement grout was injected into the soil sample through the x-Nail at a specified injection rate to study the grouting effects on the pullout behaviour of the driven nail.

Figure 4.12: Photograph of placement of the pre-buried nail with Tube-a-Manchette (TAM) facility.

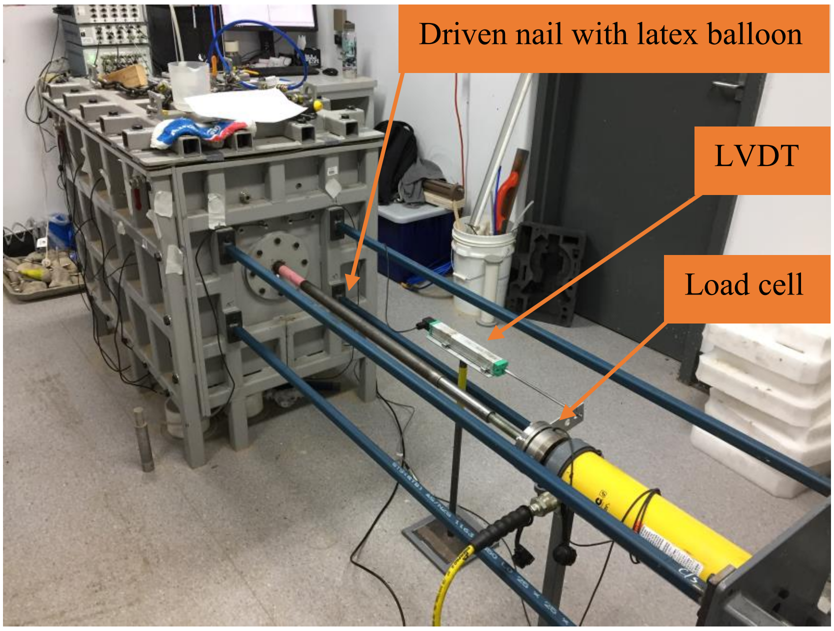

Figure 4.13: Photograph of installation of the x-Nail showing load cell and LVDT.

4.3.3 Injection of pressurized grout

For the grouting process, firstly one end of the grout-injection tube (10 mm diameter) with a bidirectional ball valve (valve #1) was connected to the grout cylinder via a push-in fitting and then the other end was connected to the grouting tube, situated inside the hollow soil nail, through a another bidirectional ball valve (valve #2) fitted with two push-in fittings at both ends. A tee fitting was mounted on the grout-injection tube (downstream of the valve #2) in order to install a diaphragm pressure transducer for monitoring the grouting pressure continuously over the grouting period. Figure 4.14 illustrates the experimental setup for the grouting process.

At the start of the grouting, a specific type of cement grout was prepared, as described in Chapter 4, and poured into the grout cylinder while the valve #1 was left closed in order to prevent the gravitation flow of the grout into the tubing system. Afterwards, the grout cylinder was placed centrally under the piston and the piston was moved down at a specified rate using the switching panel, as shown in Figure 4.3, to make good contact with the grout while the air release was kept open to drive out the entrapped air from the grout cylinder. Once the grout ran through the air release tubing, indicating the piston contact with the grout, the piston was paused for a while and the air release valve was shut off immediately. Finally, the upstream ball valve (#1) was turned on and the piston movement was resumed instantly for injecting a specified volume of grout. The piston displacement and the corresponding grouting pressure were recorded at 1 second intervals (1 Hz) using the instrumented volume-controlled injection pump system, as illustrated in Figure 4.14.

4.3.4 Pullout of soil nail

Following the injection of the grout for the pressure-grouted soil nails (i.e., pre-buried nail and x-Nail), the pullout tests were performed after approximately seven days of curing of the injected grout, developing the grout strength to approximately 65% and 90% of the 28-day compressive strength for the neat cement grout and additive-mixed cement grout respectively, as mentioned in Chapter 3 To accomplish the pullout test, the pullout facility was bolted against the front wall of the box and the free end of the pre-buried or driven soil nail was connected to the hydraulic jack by means of a pulling out rod, as illustrated in Figure 4.4. The pullout forces and the corresponding pullout displacements were recorded continuously by the installed load cell and the LVDT during the pullout process. The pullout displacement rate was maintained at 1 mm/min in accordance with the Federal Highway Administration (FHWA) guidelines (FHWA 1993). Note that prior to grouting of the x-Nail, an independent and additional pullout test of the driven nail was performed to evaluate its purely frictional pullout capacity arising from the interface friction between the nail and the surrounding soil.

Since the physical model tests were fully instrumented, the soil responses during the surcharging, jacking, grouting, and pullout processes were monitored continuously by the sensors installed in the sand box. The changes of soil stresses were recorded by the EPCs, and the variation of volumetric water contents, in-situ densities and soil conductivities were measured by the SMS.

4.4 Combination of pullout tests

In this physical model study, the pullout testing scheme was divided into three groups based on the research objectives. These groups were made to evaluate the influences of grout injection rates and viscosities on the pressure grouted soil nail system as well as to investigate the performance of the x-Nail developed in this experimental study. An overview of the test groups are described in the following subsections.

4.4.1 Test group 1 (effect of grout injection rate on pressure grouting)

The underlying objective of this test group was to evaluate the effects of grout injection rates on the pressure grouted soil nail system. To assess the grouting rate effect on the pullout resistance of the pressure grouted soil nail, the pressurized grout was injected through the pre-buried soil nail by the volume-controlled injection pump at different injection rates, viz. 4.0 L/min, 5.0 L/min and 6.5 L/min. The experimental details of this group are described in Chapter 5.

4.4.2 Test group 2 (effect of grout viscosity on pressure grouting)

The main aim of this group of tests was to examine the influences of the injecting grout viscosities on the pressure grouted soil nail system. To evaluate the effects of grout viscosities on the pullout capacity of the pressure grouted soil nail, a wide range of cement grouts with the w/c ratios varying from 0.30 to 0.50 were injected at a specified rate into the soil mass. Chapter 6 reports the detailed experimental investigation of Group 2.

4.4.3 Test group 3 (investigating the performance of the x-Nail)

The ultimate objective of this test group was to investigate the performance of the innovative driven soil nail (the x-Nail) compared to a conventional driven soil nail (purely frictional nail). To assess the pullout resistance of the x-Nail at different injected grout volumes, a special type of additive-mixed cement grout (w/c =0.32) was used and injected at a rate of 5.0 L/min with a controlled volume. The detailed experimental study of the x-Nail is described in Chapter 7.

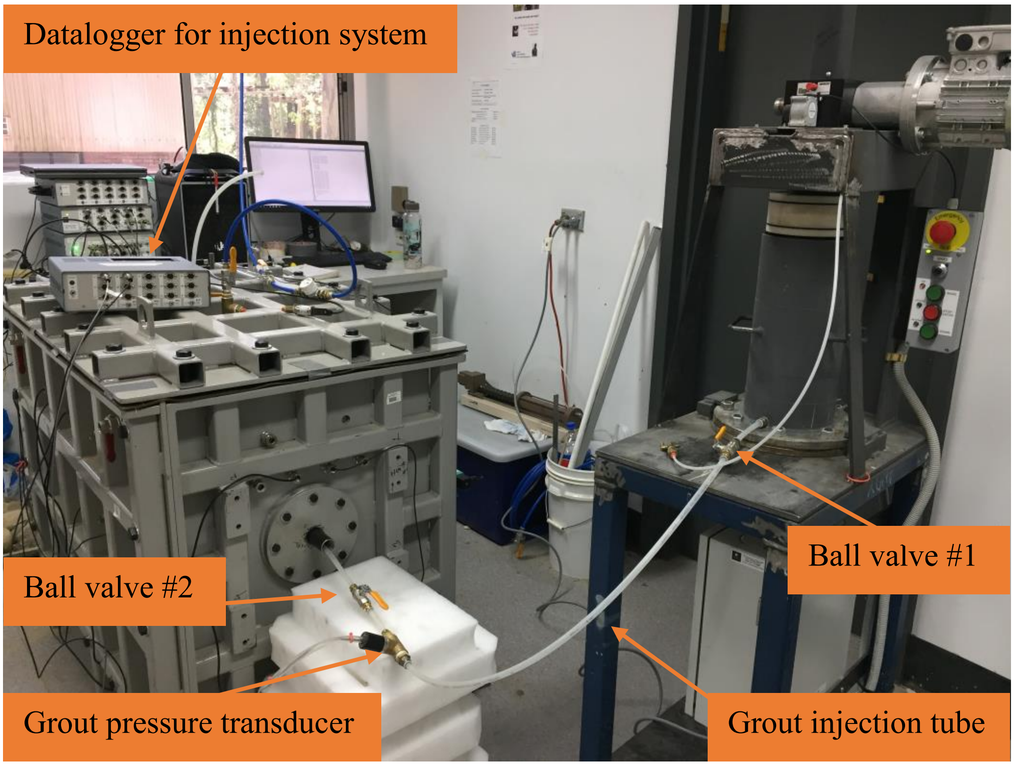

Figure 4.14: Photograph of the grouting setup.

Chapter 5 Influence of grout injection rate on pressure-grouted soil nail behaviour

5.1 General

In this chapter, a series of laboratory-scale pullout tests were conducted with the newly developed apparatus, as described in Chapter 4, to investigate the performance of pressure-grouted soil nails with the grout being injected at different rates. The apparatus allows the grout to be injected at different injection rates. A latex membrane is used as a liner around the grouting outlets of the pressure grouted soil nail to form a Tube-a-Manchette (TAM) for direct injection of grout into the surrounding soil. A neat cement grout with a w/c ratio 0.50 was used in this investigation. The soil responses (i.e., soil stress states and moisture contents) during the surcharging, grouting, and pullout processes are described here in detail.

5.2 Introduction

Pressure grouting is being progressively used for soil-nailed structures as an alternative to conventional gravity (or low pressure) grouting, since the pressure grouting technique has the ability to increase the bond strength significantly. Lazarte et al. (2003) reported that for a grouting pressure less than 350 kPa in a pre-drilled hole, the interface shear resistance could be as high as twice the resistance obtained from gravity grouting. A number of studies have reported that pressure grouting influences the soil-grout interaction behaviour and hence significantly enhances the pullout capacity of a pressure-grouted soil nail (also known as a compaction grouted soil nail) (Yin and Zhou, 2009; Yin et al., 2009; Zhou et al., 2011; Seo et al., 2012; Kim et al., 2013; Wang et al., 2017a). Generally, for the pressure grouted soil nail system, the pressurized grout was injected by a pressure-controlled injection system in which a desired pressure was set to inject the pressurized grout for a specific period of time.

Therefore, a detailed experimental study is required to investigate the effects of grout injection rates on pressure-grouted soil nail behaviour. In addition, a volume-controlled injection is important to control the injected grout volume as well as to monitor the fluctuations of injection pressure during the grouting process. In this investigation, the newly developed volume-controlled injection system, as described in Chapter 4, was used to evaluate the effects of grout injection rates on the pressure-grouted soil nail system. A pre-buried nail with a latex membrane 50 mm long placed around the grouting outlets of the nail was used to form a Tube-a-Manchette (TAM) for direct injection of pressurized grout into sand (Figure 4.12), as described in Chapter 4. The nail was pre-buried to minimize the disturbance of the surrounding soil since the pre-drilling and driving processes significantly disturb the surrounding soils (Su et al., 2010; Bhuiyan et al., 2020a). Since the physical model tests were fully instrumented, the soil responses during the surcharging, grouting, and pullout processes were monitored continuously by the sensors installed in the sand box. The changes of soil stresses were recorded by the earth pressure cells (EPC), and the variations of volumetric water contents, in situ densities and soil conductivities were measured by the soil moisture sensors (SMS). Figure 4.7 illustrates the basic layout of the sensors installed around the pre-buried soil nail. In addition, the pullout resistances of the soil nail grouted at different injection rates and the corresponding pullout displacements were measured by a load cell and a linear variable displacement transducer (LVDT), respectively. A general description of sample preparation and test procedure for physical model study of this pressure-grouted (pre-buried) soil nail system can be found in Section 4.3 of Chapter 4.

5.3 Experimental results

Three laboratory-scale physical model tests (designated as PT1, PT2, and PT3) were conducted on identical soil samples (i.e., dry density of 1.50 Mg/m^3 and moisture content of 3%) at an overburden pressure of 100 kPa to identify the effects of grout injection rates on the pullout capacity of compaction grouted (pre-buried) soil nails. In this study, the cement grout (w/c = 0.5) was injected by the specially developed grout pump at rates of 4.0 L/min, 5.0 L/min, and 6.5 L/min for the tests PT1, PT2, and PT3, respectively. In the following subsections, the typical results found from test PT3 during the compaction, surcharging, grouting, and pullout processes are presented in detail. A detailed comparison of the results for the tests (PT1, PT2, and PT3) will be described later in the Discussion section.

5.3.1 Compaction process

After compaction of the moist sand inside the box, the compacted soil sample was left undisturbed for a maximum period of 30 minutes to stabilize the moisture contents prior to the application of the overburden pressure (OP). Consequently, the readings of the soil moisture sensors (SMS) installed in the compacted fill reached the stabilized values within the period, as illustrated in Figure 5.1.

Figure 5.2 illustrates the typical volumetric water contents and dry densities measured by the soil moisture sensors (SMS) at the different locations of the compacted soil sample for the test PT3. It was found that the moisture content and dry density of the prepared soil sample (PT3) were relatively homogeneous at different locations, with an average value of 0.05 m^3/m^3 (equivalent to 3% gravimetric water content) and 1.50 Mg/ m^3, respectively. In addition, Figure 5.3 compares the variation of volumetric water contents at the different locations of the compacted soil sample for all tests (PT1, PT2, and PT3). It can be seen that the samples prepared for this physical model study had relatively uniform and identical moisture contents. The volumetric water contents measured by the SMSs varied only slightly from the average of approximately 0.05 m^3/m^3.

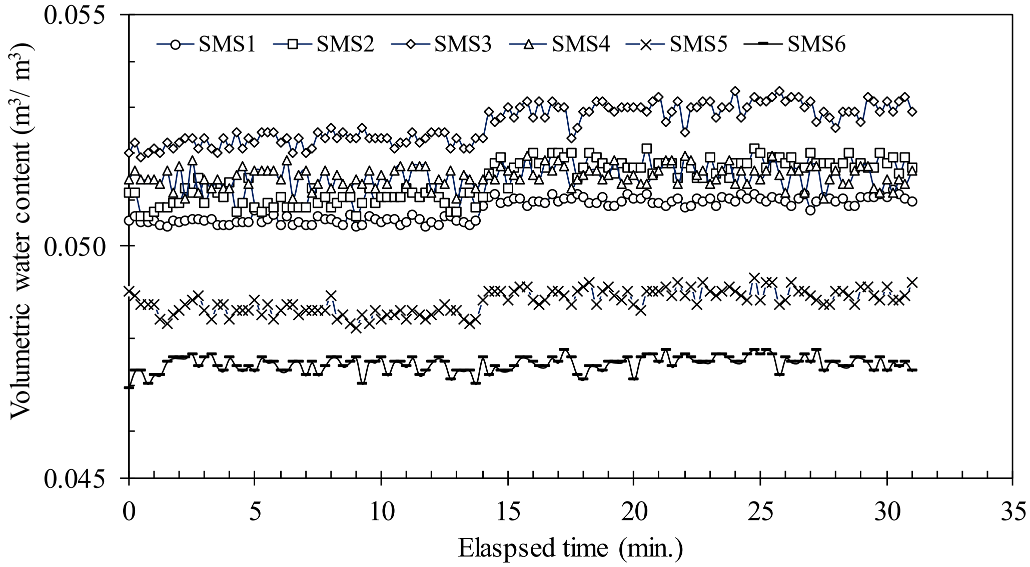

Figure 5.1: Typical variations of volumetric water contents after compaction process for PT3.

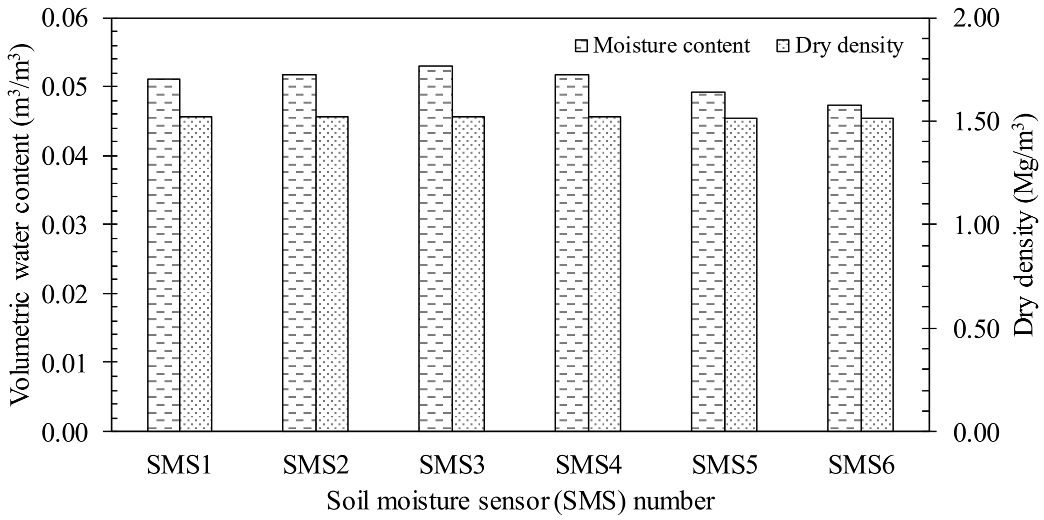

Figure 5.2: Typical changes of volumetric water contents and dry densities in compacted fill for PT3.

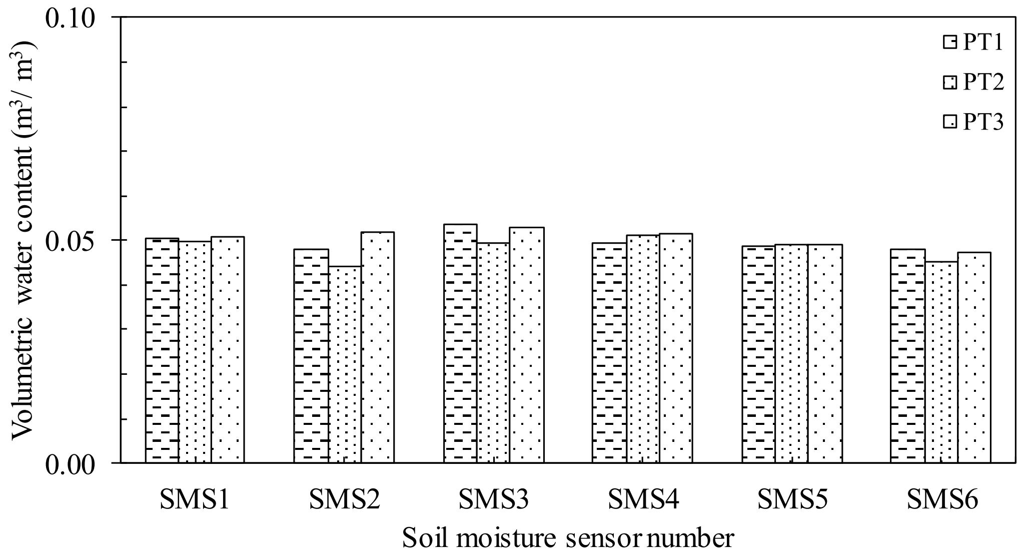

Figure 5.3: Comparison of volumetric water contents for all tests.

5.3.2 Surcharging process

As mentioned earlier (Chapter 4, subsection 4.2.2.3), the overburden pressure (OP) acting on the compacted soil samples was applied by the water-filled rubber cushion system and the corresponding settlements were estimated simply by dividing the volume of the pressurized water injected into the rubber cushion by the cross-sectional area of the box. Figure 5.4 shows the estimated settlements of the compacted soil samples during application of the overburden pressure. It can be observed that the vertical displacement of the soil surface increased gradually with the increment of the applied surcharge pressure and ultimately reached a stable value of approximately 2.5 mm, on average, within roughly 2 minutes, once the applied overburden pressure reached a maximum value of 100 kPa. In addition, it is noted that the final soil surface settlement (~2.5 mm) estimated by the modified surcharge pressure system was almost equal to the average measured value of approximately 2.3 mm, which was independently measured manually by a steel ruler after completion of the tests.

Figure 5.5 plots the variations in the induced soil stresses measured by the EPCs situated at different locations for an imposed surcharge pressure of 100 kPa. Figure 5.5 indicates that the induced earth pressures increased gradually and reached a steady state within a period of 1 hour from the start of surcharging, consistent with similar behaviour reported by Bhuiyan et al. (2019) for a pre-buried pressure-grouted soil nail with a TAM facility. Furthermore, it is seen that locations EPC2, EPC7, and EPC8 experienced lower pressures compared with the applied overburden pressure, and this may be a result of the orientation of the installed instruments, which is consistent with the findings of Garnier et al. (1999). EPC2 was installed vertically with the sensor facing parallel to the soil nail as illustrated in Figure 4.7 and recorded an earth pressure of approximately 25 kPa, whereas EPC7 and EPC8 were installed vertically at the mid height of the box in the transverse (front wall) and longitudinal (side wall) directions, respectively. Consequently, both of these EPCs attached on the boundaries monitored the lateral earth pressures of approximately 45 kPa, on average. At locations EPC1, EPC3, EPC4, EPC5, and EPC6, the earth pressure cells were installed horizontally in order to detect the vertical stresses. The stabilized soil pressures induced on EPC3 and EPC5 were in good agreement with the applied OP of 100 kPa. However, the pressure readings of EPC1, EPC4, and EPC6 were not consistent with the applied overburden pressure (100 kPa). For the applied vertical pressure of 100 kPa, EPC1 experienced approximately 20% lower induced earth pressure, whereas EPC4 and EPC6 recorded approximately 30% higher induced earth pressure. It is suspected that these errors (i.e., under- or over-registration) in measured data may have resulted from the placement effects (Garnier et al., 1999) and/or arching and inclusion effects (Bhuiyan et al. 2018b). Consequently, the earth pressures measured by the EPCs installed horizontally differ by roughly ± 20 to 30% from the applied overburden pressure.

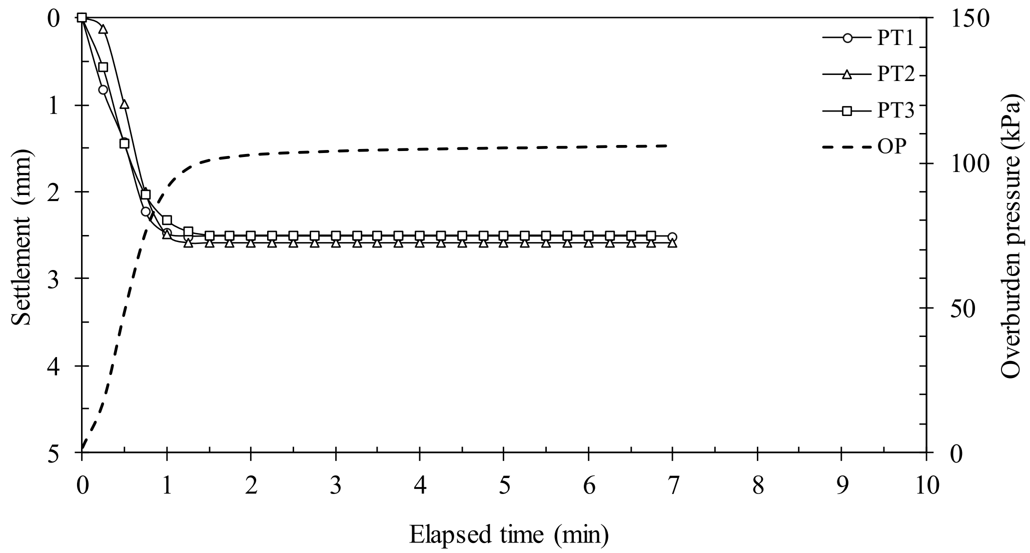

Figure 5.4: Settlement of soil surface during application of the overburden pressure (OP = 100 kPa).

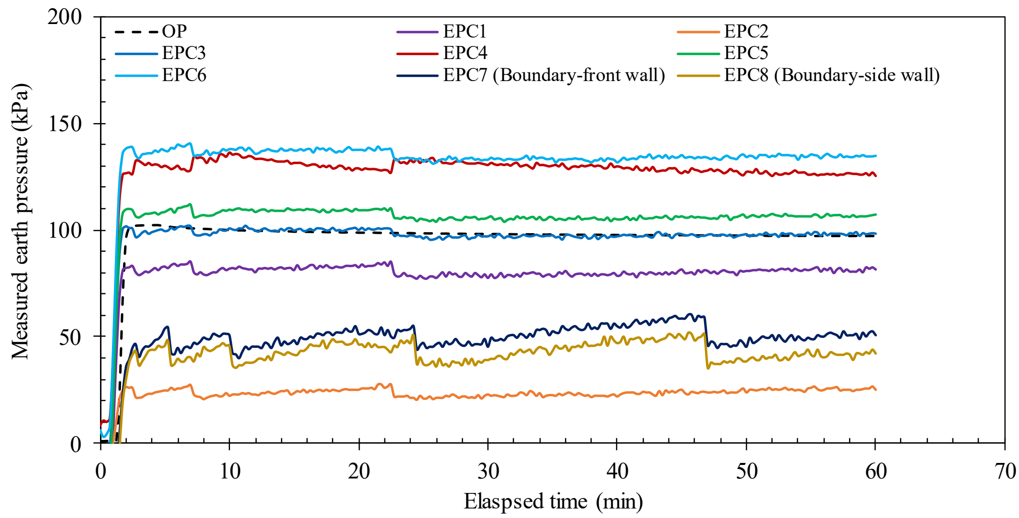

Figure 5.5: Typical changes in induced earth pressures over the surcharging process for PT3.

5.3.3 Grouting process

It is noted that in this investigation, neat cement grout (w/c = 0.50) was injected at the specified rates by the specially developed volume-controlled injection pump (Chapter 4, subsection 4.2.2.1), in contrast to the pressure-controlled injection pump adopted in an earlier study by Wang et al. (2017b). Figure 5.6 illustrates typical relationships between injection pressure and injected grout volume against injection time. The plots indicate that the grout injection pressure increased rapidly with the increment of the injected grout volume and then reached the ultimate pressure of approximately 1550 kPa once the grouting stopped completely at a maximum injection volume of about 800 ml for a specified injection rate of 6.5 L/min, followed by a gradual drop. This gradual drop in injection pressure may have resulted from the relaxation of the piston pressure applied to the grout since the piston pressure was not maintained once the grouting stopped.

The photograph inserted in Figure 5.6 shows a soil nail prior to being pre-buried with a latex membrane covering the injection outlets (thickness of 0.3 mm and length of 50 mm), as marked by a red rectangle. This membrane liner is used to protect the outlets from being filled by the compacted sand surrounding the pre-buried soil nail, effectively forming a Tube a Manchette (TAM) facility for direct injection of grout into the sand during the grouting process.

Figure 5.7 illustrates typical variations of soil stress states measured in the soil mass during the flow-controlled grouting process, which indicates that the grouting process significantly increases the earth pressures around the injection points. The vertical earth pressures induced on the EPCs (especially EPC1, EPC3, EPC5 and EPC6) located around the injection points increased virtually instantly from their stabilized values obtained after surcharging process and reached their peak values within a few seconds. The peak earth pressures were sustained for approximately only 5 to 10 seconds and then dropped rapidly to their residual or ultimate pressures, ranging from 180 to 260 kPa, once the grouting stopped at a maximum injection volume of about 800 ml (Figure 5.6). For the ultimate injection pressure of approximately 1550 kPa (Figure 5.6), EPC1, EPC3, EPC5, and EPC6 experienced peak induced pressures of approximately 980, 708, 602 and 481 respectively, which indicates that the soil mass near the injection points experiences the highest pressure induced by the grouting and the induced pressures decrease gradually with distance from the injection point. Therefore, it could reasonably be deduced that the compaction effects instigated by the pressure grouting are quite localized, as might have been expected. Wang et al. (2017b) reported similar behaviour of the induced earth pressures around the soil nail in their tests involving a pressure-controlled injection system. In the case of EPC4, it was found that the induced pressure initially dropped at the start of grouting and then increased slowly to a stable pressure (close to the overburden pressure) at the end of grouting. This sensor was installed horizontally 180 mm away from the injection outlets (Figure 4.7). The initial drop in pressure might have been the result of a slight rotation of the sensor caused by the injected grout bulk, displacing and compacting the soil mass around the injection holes. Conversely, the data recorded by EPC2, EPC7 and EPC8 increased insignificantly over the grouting period, which may have resulted from the injected grout volume compacting the soil mass in both the longitudinal and transverse directions.

Figure 5.8 shows the changes in volumetric water contents in the compacted fill after the grouting process against the stable moisture contents found after the application of the overburden pressure. It can be observed that the volumetric water content (VWC) measured by SMS1, located vertically 50 mm below the soil nail, increased from the initial stabilized value of approximately 0.050 m^3/m^3 to a maximum value of around 0.065 m^3/m^3 after the end of the grouting period. This sudden change in moisture content may be attributed to the release of bleed water from the pressurized neat cement grout. Interestingly, it was also found that no changes in moisture contents were registered the other SMSs, including SMS3, which was installed above the nail surface with a vertical distance of 50 mm. The unchanged reading of SMS3 found before and after grouting indicates that the bleed water probably naturally flows downward.

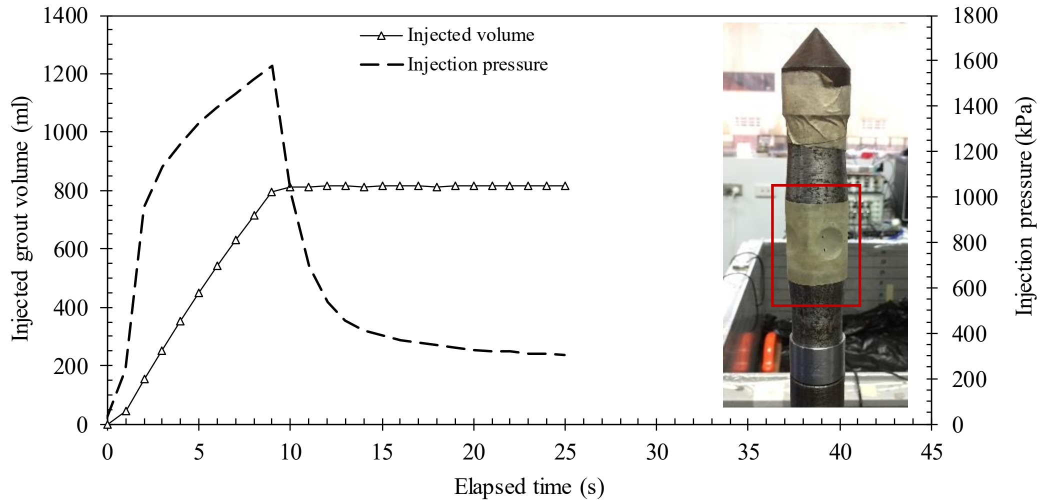

Figure 5.6: Typical variation of injection pressure and injected grout volume against time for the injection rate of 6.5 L/min (PT3).

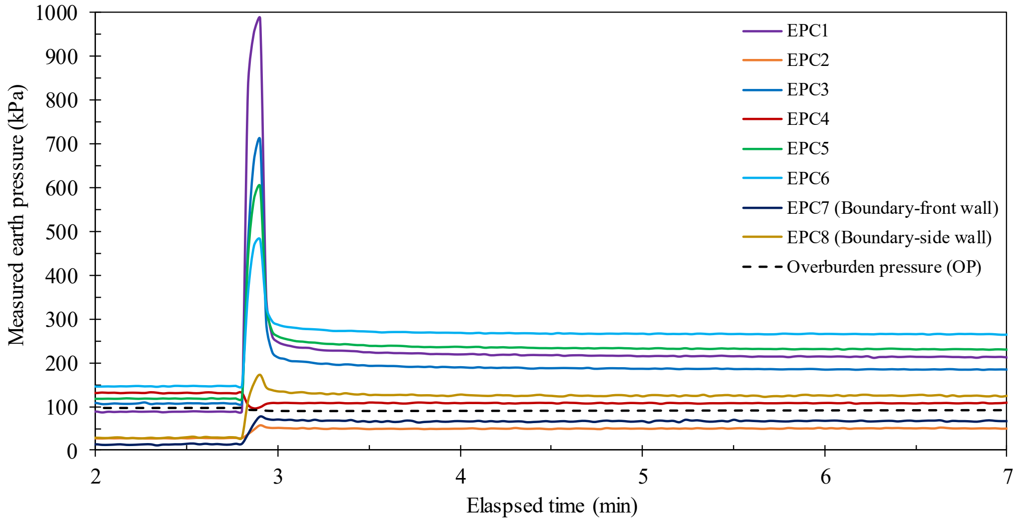

Figure 5.7: Typical variations of measured earth pressures during grouting process for PT3 (injection rate = 6.5 L/min).

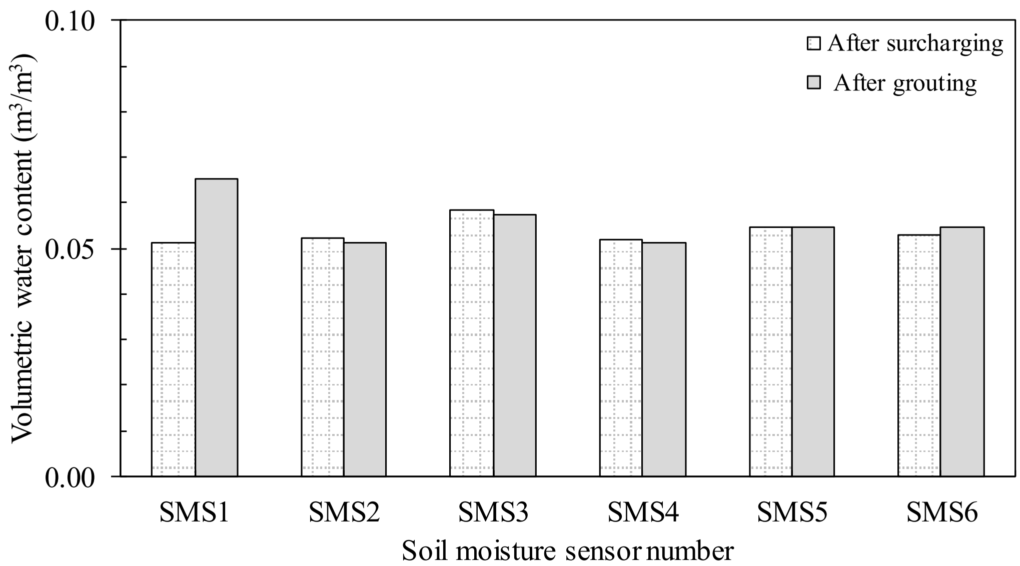

Figure 5.8: Comparison of volumetric moisture content during overburden and grouting process for PT3.

5.3.4 Pullout process

A typical plot of the pullout force versus pullout displacement is illustrated in Figure 5.9 together with the changes in earth pressures induced by the pullout process, also plotted against the pullout displacement. The pressure-grouted (pre-buried) soil nail was pulled out after 7 days of curing of the injected grout, which allowed it to develop a compressive strength of approximately 24 MPa (Wang et al., 2017b). The pullout force-pullout displacement plot presented in Figure 5.8 illustrates that the pullout force rose rapidly at the start of pulling out the grouted nail and then the force continued to grow more slowly with the advancement of the nail, and it ultimately reached a maximum value of approximately 33.5 kN after a significant amount of displacement (approximately 100 mm), consistent with similar behaviour reported previously by Wang et al. (2017b) for a compaction-grouted soil nail.

Figure 5.9 also reveals that the soil pressures induced during pullout on EPC1, EPC3, and EPC5, which were especially installed near the grout injection points, all reduced gradually from their initial values to almost zero reading after about 30 mm of pullout displacement. However, in the case of EPC6, located at a vertical distance of 150 mm from the injection point, the induced earth pressure reduced gradually from the initial value of about 260 kPa, achieved after grouting (Figure 5.7), to 27 kPa at the end of pullout displacement. This may be attributed to the stress relaxation on these EPCs (EPC1, EPC3, EPC5 and EPC6) resulting from the formation of a cavity in the compacted soil mass due to the inward displacement of the soil around the grouted bulb (hardened cement grout) as the nail was withdrawn. By contrast, the induced stresses on EPC2 and EPC7 increased gradually with increased pullout displacement. These EPCs were installed vertically, at horizontal distances of 350 and 700 mm, respectively, from the injection point, to measure the changes in the horizontal soil pressures during the pullout process. Therefore, the data recorded by EPC2 and EPC7 increased continuously from approximately 39 kPa, on average, to 326 and 260 kPa, respectively, over the pullout displacement (~100 mm). The increase in horizontal stress may have resulted from the densification and compression of the soil mass situated between the grout bulb and the EPC. The pressure induced on EPC4 increased gradually and reached a remarkably high value (~900 kPa) at the end of pullout displacement. This rise in vertical earth pressure may have resulted from the displacement and compaction of the soil situated in front of EPC4, providing passive resistance to the grout bulb during the pullout process.

However, the data recorded by EPC8, which was actually installed on the sidewall of the soil chamber, remain almost constant over the pullout period.

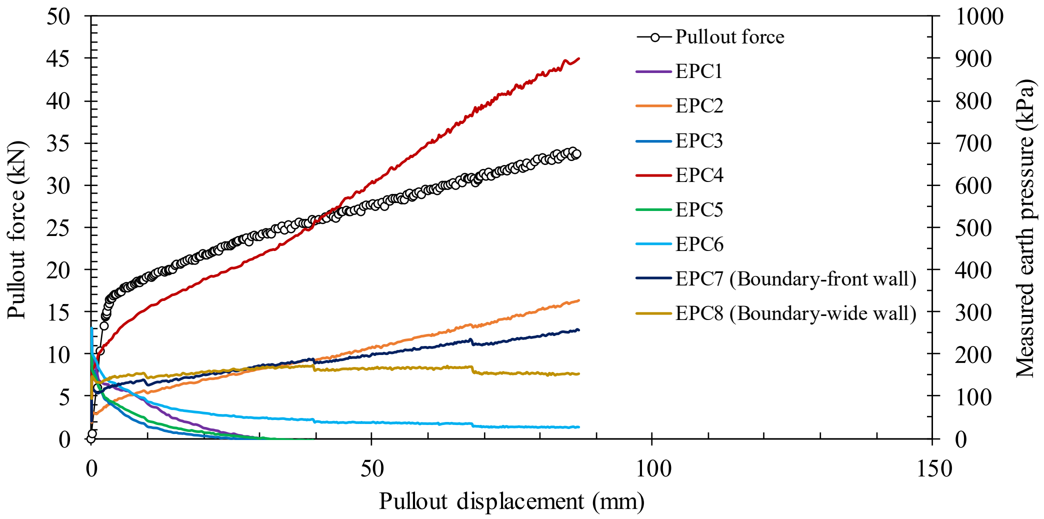

Figure 5.9: Pullout force and measured earth pressures against the pullout displacement for PT3.

5.4 Discussion

In this study, the overburden pressure system was modified so that the soil surface settlement could be estimated readily from the injected water volume recorded by a flow meter, as explained previously. The plots presented in Figure 5.4 illustrate the successful application of the modified overburden pressure system.

In addition, the test facility is able to quantify the effects of the rate of grout injection on the pressure grouted soil nail system. A comparison between the injected grout volume and injection pressure during the grouting period for the tests (PT1, PT2, and PT3) is illustrated in Figure 5.10. The injection pressure plots for the tests presented in Figure 5.10 show that the grout injection pressures increased gradually over the elapsed time and reached a maximum pressure within a few seconds, varying from 5 to 10 seconds. For the injection rates of 5.0 L/min (PT2) and 6.5 L/min (PT3), the maximum injection pressure was found to be approximately 1550 kPa, on average. Interestingly, for the injection rate of 4.0 L/min (PT1), the maximum injection pressure was approximately 1200 kPa. It is suspected that the injected pressure induced on the grout pressure transducer installed at the pre-buried nail end (Figure 4.13) may be affected by the piston speed. The rapid increase in injection pressure may be attributed to the clogging of the injection points embedded in the soil, which might have resulted from the formation of bonding between the cement grout and the relatively dry sand once the cement grout encountered the sand (Bhuiyan et al., 2019). In addition, for the test PT2, a sudden drop and rise in injection pressure indicates that the pressurized grout might instigate a small fracture in the compacted fill (Bezuijen and Tol, 2007).

Figure 5.10 also indicates that the volume of injected grout increased almost linearly with the increasing injection rate. The maximum volume of grout injected at 6.50 L/min was approximately 800 ml, followed by about 440 ml and 280 ml for the injection rates of 5.0 L/min and 4.0 L/min, respectively. These findings are consistent with the experimental results reported by Bezuijen (2010) for pressure grouting in sand. Bezuijen (2010) reported that the pressurized injection of cementitious grout into permeable soil, like sand, accelerated the expulsion of bleed water from the cement grout into the sand, which in turn formed a dehydration layer (filter cake) at the soil-grout interface. Because of the pressurized bleeding (pressure filtration) over time, the thickness of the filter cake increased and a plaster (thick layer of filter cake) formed with the sand, by filling the void spaces in the soil matrix (Bezuijen et al. 2007). Gafar et al. (2008) reported that the injection rate affected the filter cake formation and a slower injection rate accelerated the development of the plaster (thick filter cake), which consequently reduced the penetration of the grout as well as the compaction of the surrounding soil mass. Therefore, in the current study, it is likely that the formation of a thick dehydrated layer at the slower injection rate may have resulted in the injection of a smaller volume grout for a specified injection pressure. In addition, the formed plaster may have withstood the injection pressure, either fully or partially, and thus injection pressure could have built up instantaneously in the injection system without being effectively transferred to the surrounding soil mass (Bezuijen et al. 2007). This could be the reason for the relatively low induced pressures measured on the EPCs when the grout injection pressure was at its maximum value, as shown in Figure 5.7. Bhuiyan et al. (2019) confirmed the filter cake formation at the soil-grout interface by examining an excavated grout bulb.

In the case of the test PT1, to evaluate the injection pressure induced by the pressurized grouting at the injection points, a separate grout pressure transducer was installed at the nail tip end of the pre-buried soil nail, as shown in Figure 5.11. A comparison between the injection pressure recorded at the grouting end and the corresponding induced soil pressures on the EPCs located around the injection points over the grouting period is demonstrated in Figure 5.12. It can be observed that the maximum pressure induced by the grouting at the injection point was approximately 1200 kPa, which was consistent with the grouting pressure (~1200 kPa) of the test PT1, as illustrated in Figure 5.10. This confirms that the grouting pressure induced by the injection pump system (Figure 4.14) completely transfers through the grout paste to the injection points (i.e., grouting outlets) without any dissipation of energy inside the grouting tube.

The plots of induced earth pressures presented in Figure 5.12 indicate the earth pressures measured on the EPCs were much lower than the applied injection pressure, consistent with similar stress responses to the test PT3 (Figure 5.7). Interestingly, EPC1, which was embedded horizontally at a vertical distance of 50 mm from the injection points, registered almost 50% of the applied injection pressure. This decrease in induced earth pressure may have resulted from the seepage of the bleed water from the neat cement grout, as described earlier. Besides, it might be argued that the inconsistency between the applied injection pressure (~1200 kPa) and the induced earth pressure measured (~600 kPa) on EPC1 located 50 mm away from the injection points may be attributed to partial energy loss caused by the gap between the injection points and EPC1 location, as noted by Seo et al. (2012).

Figure 5.13 illustrates the variation of volumetric water content in the soil sample during the grouting process against the stable moisture contents found following the application of the overburden pressure. Figure 5.13 indicates that the volumetric moisture content recorded by SMS1, which was installed near the injection outlets at a vertical distance of 50 mm under the soil nail, increased from the stable value of around 0.050 m^3/ m^3, on average, to the maximum values of approximately 0.051 m^3/ m^3, 0.054 m^3/ m^3, and 0.065 m^3/ m^3 for the tests PT1, PT2, and PT3, respectively, over the grouting period. This sudden change in moisture content may have resulted from the release of bleed water from the pressurized grout. Based on the data presented in Figure 5.13, it can also be argued that the expulsion (seepage) of bleed water from the pressurized neat cement grout is directly and proportionally related to the injection rate, i.e., the higher the injection rate, the higher the seepage of bleed water.

Because the SMS sensors are able to monitor the conductivity of a soil mass together with its moisture content and temperature, infiltration of the pressurized cement grout into the permeable sand may also be inferred from the changes in soil conductivity observed during the grouting process. Figure 5.14 shows the variation in soil bulk conductivity around the injection outlets after the grouting process. It can be seen that the soil conductivity recorded by SMS1 (located below the nail) increases gradually from an initial stable value obtained after the surcharging process and reaches a maximum value over the grouting period. The increase in soil bulk conductivity was higher (~187 dS/m) for the test PT3, followed by the test PT2 (~70 dS/m) and PT1 (~20 dS/m), indicating a linear relationship between the conductivity and the grout injection rate. However, the conductivity readings recorded by SMS3 (located above the nail) for all tests remained constant over the same period. The changes in soil conductivity support the contention of gravitation flow of water from the grout into the soil matrix.

Figure 5.15 compares the variations of vertical earth pressures on EPC1, which was installed horizontally 50 mm below the nail surface with a horizontal distance of 700 mm from the front box wall, induced by the different processes (i.e., surcharging, grouting, and pulling out processes) of physical model tests. It can be observed that the induced vertical earth pressures on EPC1 increased from zero to approximately 75 kPa, on average, following application of the surcharge pressure (100 kPa) for all tests. This under-registration in measured data may be attributed to the placement effects (Garnier et al., 1999) and/or arching and inclusion effects (Bhuiyan et al. 2018b), as mentioned earlier. Figure 5.15 also demonstrates that the injection of pressurized grout into the compacted fill significantly increased the vertical soil pressures induced on EPC1, followed by a gradual drop over the grouting period. For an ultimate injection pressure of approximately 1550 kPa (Figure 5.10), it was found that the soil pressure induced on EPC1 rose quickly from an average stabilized value of about 80 kPa to the peak values of approximately 681 kPa and 987 kPa for the test PT2 and PT3, respectively. Conversely, for an applied injection pressure of about 1200 kPa (PT1), the peak induced earth pressure measured on EPC1 was approximately 622 kPa. The data of the peak induced earth pressures indicate that approximately 44% to 64% of the applied injection pressure was registered by EPC1, although the injection pressure was only maintained for a very short period of time, varying from 2-3 seconds (Figure 5.10). This discrepancy between the induced earth pressures measured on EPC1 and the injection pressures may be attributed to the location of EPC1, which was embedded 50 mm away from the injection point instead of being installed close to the injection point, and consequently this installation gap may result in a partial energy loss, as noted by Seo et al. (2012) in a separate study of a pressure-grouted soil nail where injection pressure was maintained using a pressure-controlled injection system for a long period of time. Once the grouting was completed, the peak induced earth pressures dropped gradually over the period and then reached the residual values of approximately 172 kPa, 193 kPa, and 207 kPa for the tests PT1, PT2, and PT3, respectively, which were significantly higher than the applied OP of 100 kPa.

In this investigation, the injection pump was paused immediately once the piston advancement stopped at a maximum injected grout volume for a specified injection rate and after that a shut off valve (#2) installed downstream of the pump, as illustrated in Figure 4.14, was closed instantly to minimize the drop in injection pressure within the grouted nail system. Therefore, it is suspected that the gradual drop in the peak induced pressure (Figure 5.15) after the grouting may have resulted from the dissipation of the injection pressure into the compacted fill over time. This is consistent with the findings of Seo et al. (2012), who reported that injection of pressurized grout (w/c = 0.5) into permeable soil accelerates the seepage (expulsion) of water from the grout paste into the soil, which results in development of seepage force, and the applied pressure of the seepage force to the soil mass decreases with time after the pressurized grouting. They also noted that the expanded grouted bulb (solidified grout) resists the rebounding of the enlarged cylindrical cavity formed by displacing and compacting the soil surrounding the injection points, thus developing the residual soil stresses in the compacted fill. Overall, the data of induced earth pressures including peak and residual soil stresses presented in Figure 5.15 indicates that the induced earth pressures increased virtually linearly with the increasing injected grouted volumes. In addition, it can be observed that the stabilized earth pressures (residual values) induced on EPC1 after grouting remained nearly constant over the curing period of 7 days.

Furthermore, during the pullout process, it can be observed that the confining stresses mobilized at the soil-grout interface increased insignificantly from an average stabilized value (~210 kPa) to an average value of about 226 kPa, followed by a gradual drop to almost zero pressure after a pullout displacement of approximately 100 mm. This drop in induced earth pressures may be attributed to the stress relaxation on EPC1 that resulted from the inward movement of the soil around the cavity formed by the expanded grout bulb once the nail was pulled out. Wang et al. (2017a) reported that the injection of pressurized grout into a soil mass densifies the soil surrounding the injection points and thus it is expected that the densified soil around the pressure grouted soil nail has the possibility to display dilatancy behaviour, i.e., the increase in soil volume as shear strain is mobilized (Milligan and Tei, 1998). Therefore, the increase in confining stress acting around the nail is possibly a result of the constrained dilatancy of the soil, consistent with the findings of Su et al. (2008).

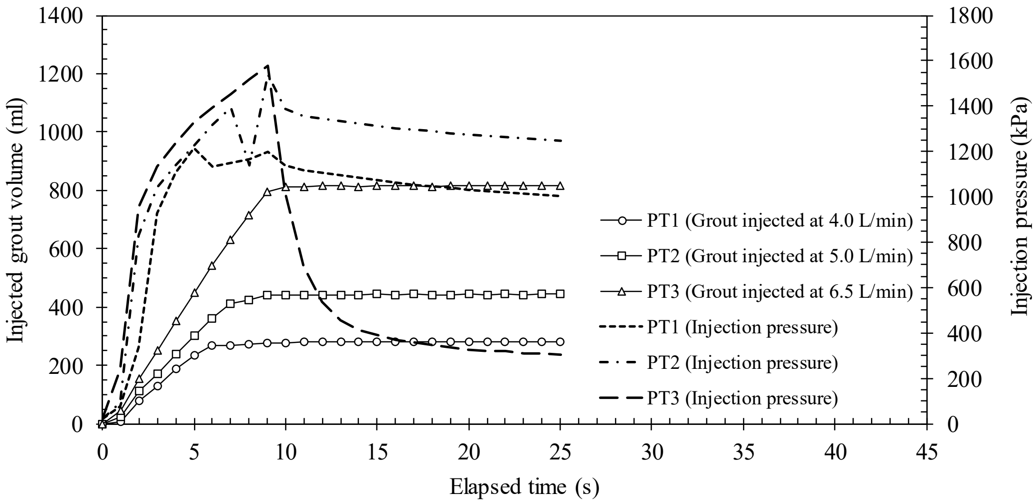

Figure 5.10: Variations of injected grout volume and injection pressure for all tests.

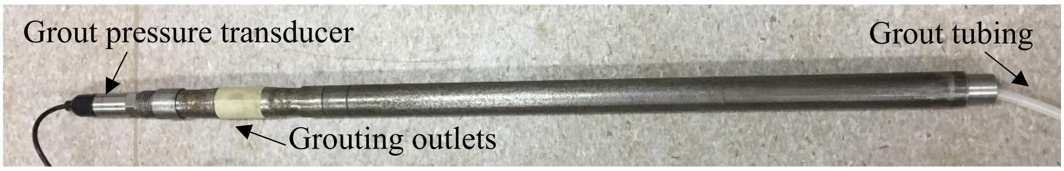

Figure 5.11: Photograph of a pre-buried soil nail with a grout pressure transducer installed near the grouting outlets (PT1).

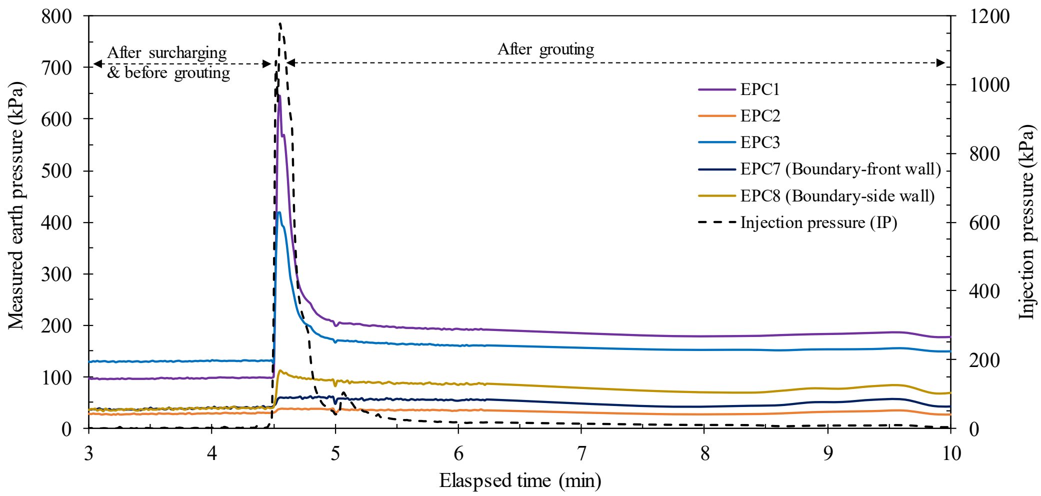

Figure 5.12: Evolution of injection pressure and earth pressure induced on the EPCs during the pressurized grouting for PT1.

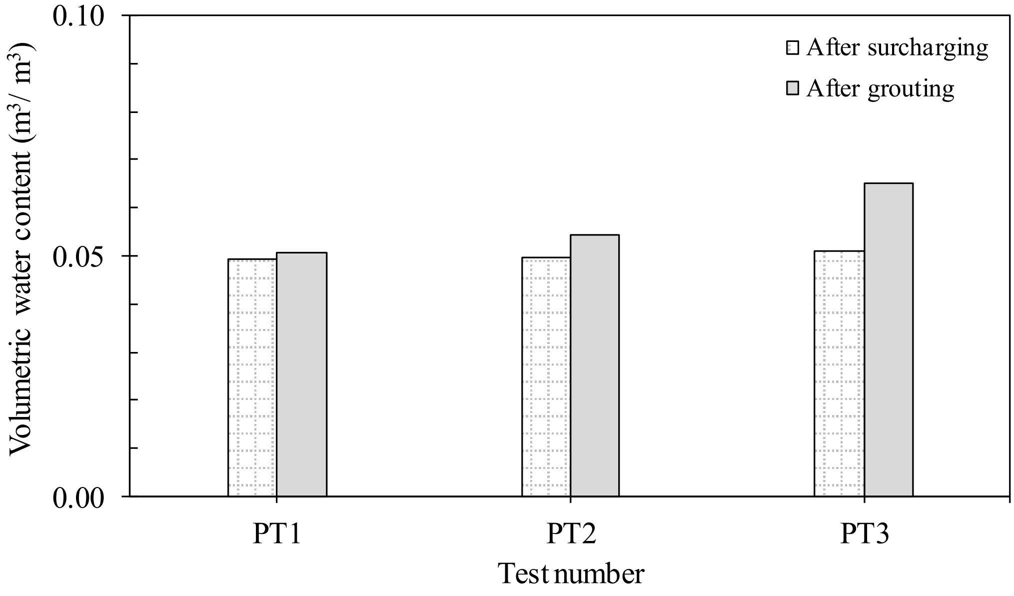

Figure 5.13: Comparison of volumetric moisture content recored by SMS1 during the overburden and grouting process for all tests.

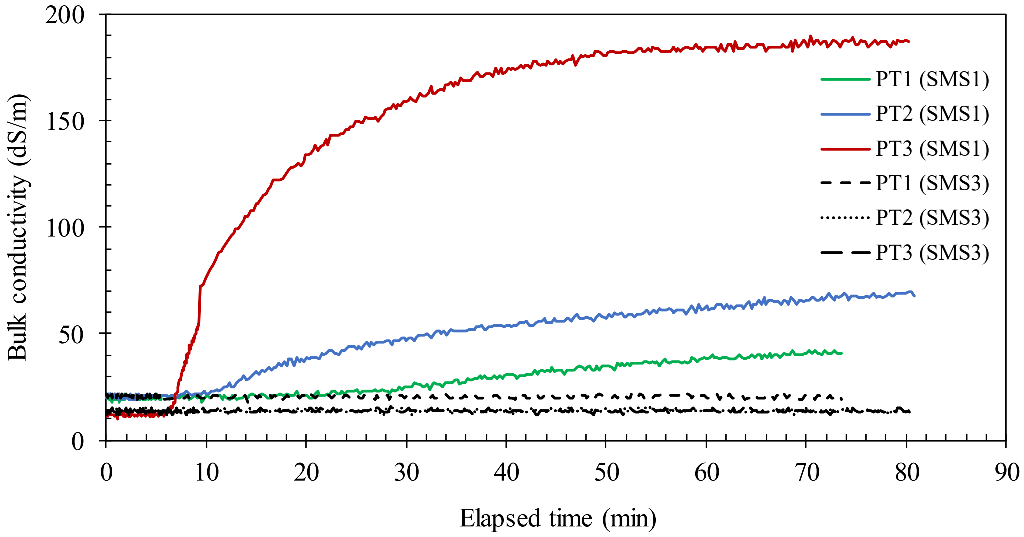

Figure 5.14: Variation of soil bulk conductivity around the grout injection points for all tests.

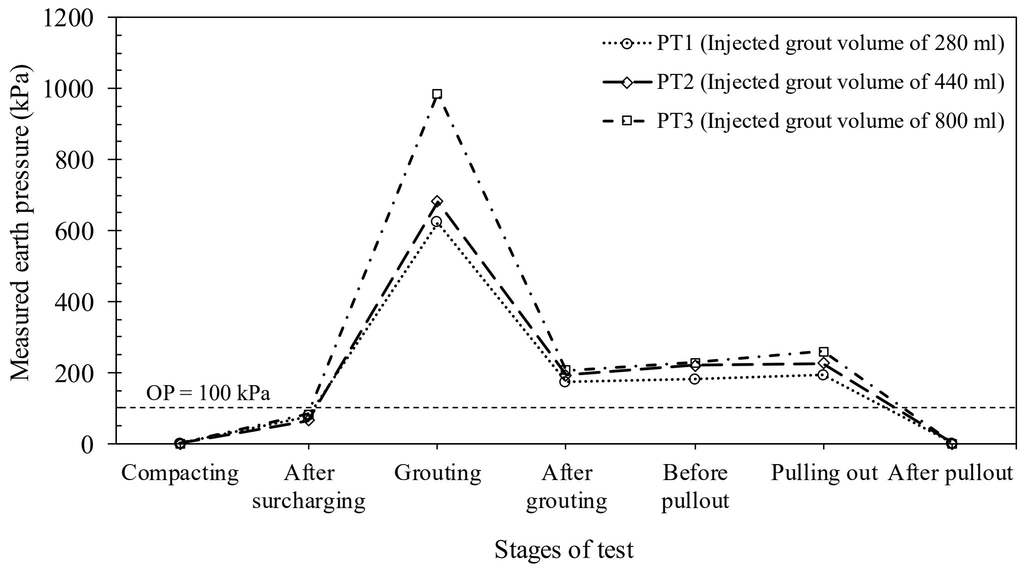

Figure 5.15: Comparison of vertical earth pressures induced on EPC1 at different stages of the tests showing overburden pressure line (horizontal dotted line).

In this study, pullout tests were conducted at a displacement rate of 1 mm/min, as recommended by FHWA (1993). As reported by Sharma et al. (2019) in a previous study, the effects of pullout displacement rates ranging from 0.6 to 2.4 mm/min on the mobilized pullout resistance were not significant. Figure 5.16 compares the pullout forces measured in this study involving pre-buried soil nails grouted at different injection rates. It was found that the pullout force increased with an increase in the injected grout volume. For example, the pullout force measured for PT3, with an injected grout volume of approximately 800 ml, was much higher (~33.5 kN) than that measured for PT2 (~22.0 kN) and PT1 (~15.0 kN), where the volumes of the injected grout were around 440 ml and 280 ml, respectively. Wang et al. (2017a) reported similar findings, where an incremental linear relationship was revealed between the grout volume and the corresponding pullout force for compaction-grouted soil nails. By comparing the pullout forces of the tests PT2 (~22.0 kN) and PT3 (~33.5 kN), where the injection pressure for both tests was approximately 1550 kPa (Figure 5.10), it might be argued that the pullout capacity of the pressure-grouted soil nail is predominantly influenced by the injected grout volume rather than the injection pressure, i.e., the higher the injected grout volume, the higher the pullout capacity.

In addition, in the load-displacement plots shown in Figure 5.16, the pullout forces of the (pre-buried) grouted soil nails indicate hardening behaviour. This phenomenon may be attributed to the passive resistance of the soil situated in front of the grout bulb. Ye et al. (2017) reported that nearly 80% of the pullout resistance arose from the expanded cement bulk of the compaction grouted soil nail, which indicates that the grouted soil nail actually behaves as an anchor rather than a frictional nail, with a substantial amount of end bearing resistance. Hsu and Liao (1998) reported that the pullout behaviour of a cylindrical anchor was greatly affected by the embedded depth (distance from ground surface to the anchor's top edge), and the pullout resistance showed hardening behaviour for an embedded depth of approximately 7 to 8 times the anchor diameter or more. Consequently, the displacement-hardening behaviour typically exhibited by, for example, compaction grouted soil nails and screw soil nails (Ye et al., 2017; Sharma et al., 2019), is governed by the end bearing.

Once the pullout tests were completed, the compacted soil was excavated to remove the grouted soil nail, allowing inspection of the grout bulb and the conditions of the soil surrounding the injection point. Visual inspection revealed that a layer of cemented sand was present at the bottom part of the cavity formed in the compacted soil by the movement of the grouted soil nail. These observations, together with the measured changes in moisture content and conductivity (Figures 5.13 and 5.14), confirm that bleeding and dehydration of cement grout occurred due to pressure filtration. After measuring the grout bulb dimensions (Figure 5.17), it was identified that the grout injected at a rate of 6.5 L/min (PT3) formed a grout bulb with an average diameter of approximately 92.5 mm and an average length of 103 mm. In contrast, the grout bulbs formed at the injection rates of 5.0 L/min (PT2) and 4.0 L/min (PT1) had average diameters of around 76.5 mm with an average length of 113 mm and 56.5 mm with an average length of 101 mm, respectively. These results indicate that the grout injected at the higher injection rate compacted the surrounding soil more by expansion in the radial direction. Clearly, the diameter of the grout bulb significantly influences the pullout force of this anchor-type nail by providing a substantial amount of end bearing resistance, as discussed earlier. Figure 5.18 illustrates the pullout force of the compaction-grouted soil nail almost linearly with increasing the grout bulb diameter. These findings are consistent with the numerical results reported by Ye et al. (2017).

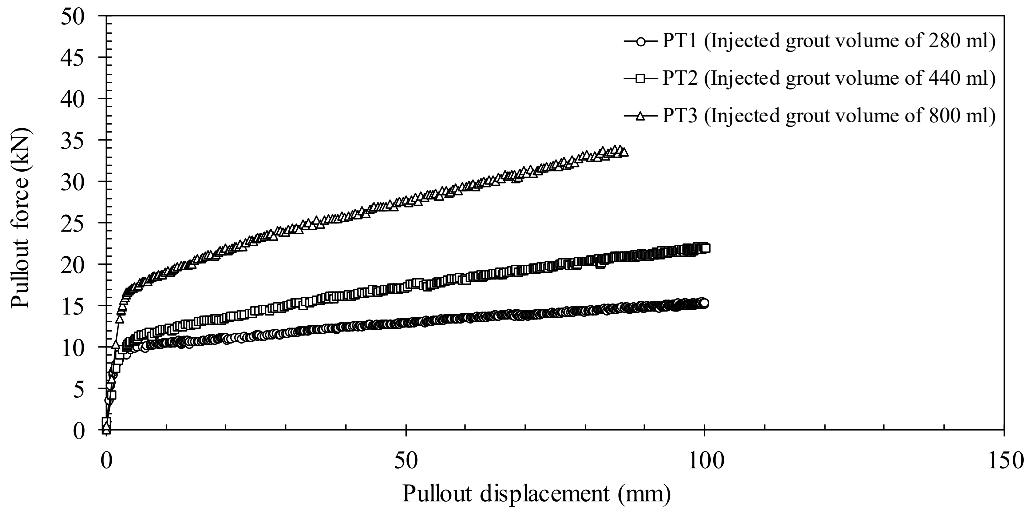

Figure 5.16: Pullout force versus displacement for all tests.

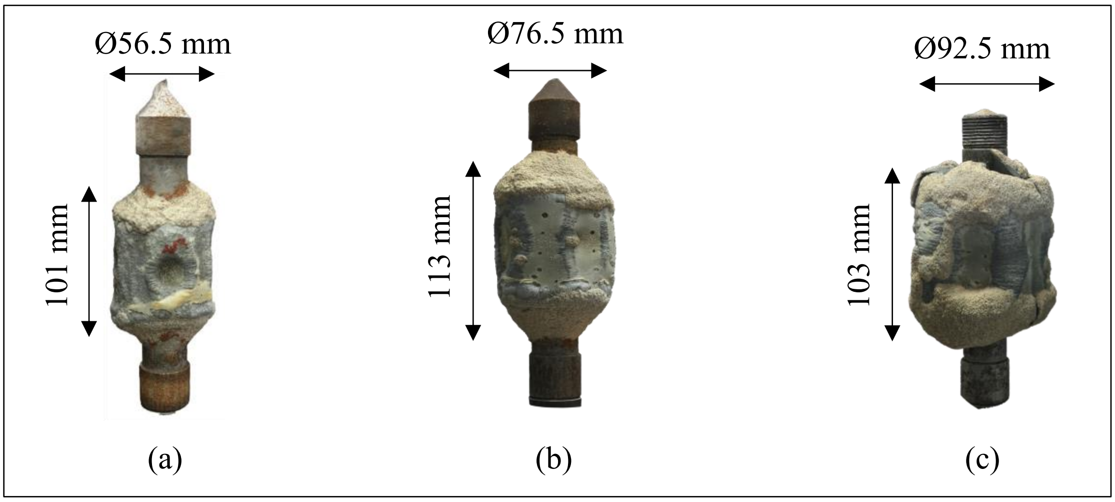

Figure 5.17: 3D Grout bulbs of the compaction-grouted (pre-buried) soil nails (a) PT1, (b) PT2, and (b) PT3.

Figure 5.19 shows the evolution of horizontal earth pressures induced on EPC2, installed vertically 25 mm below the nail with a horizontal distance of 350 mm from the injection point, during the pullout process for all tests. For the injected grout volume of about 800 ml (PT3, bulb diameter of 92.5 mm), it can be observed that the horizontal earth pressure measured on EPC2 increased gradually from an initial stable value (~ 30 kPa) to a maximum value of approximately 326 kPa after a pullout displacement of 100 mm. Similarly, for the test PT1 (bulb diameter of 56.5 mm) and PT2 (bulb diameter of 76.5 mm), the EPC2 readings increased with nail displacement and reached the maximum values of about 160 kPa and 265 kPa, respectively, at the end of pullout displacement. This increase in horizontal soil pressure measured on EPC2 may be attributed to the passive resistance of the soil situated in front of the grout bulb that is mobilized as the grouted nail is pulled out. Clearly, these findings confirm that the compaction-grouted soil nails investigated here exhibit a substantial amount of end bearing resistance due to the expanded grout bulb. In addition, on basis of EPC2 readings, it can be concluded that the end bearing resistance increases linearly when the diameter of grout bulbs is increased, i.e., the larger the diameter of grout bulb, the higher the pullout resistance, consistent with the results presented in Figure 5.18.

Figure 5.20 illustrates the variation of lateral earth pressure induced on EPC7 for all tests. Note that EPC7 was installed vertically on the box front wall with a vertical distance of 25 mm from the nail surface to detect the change in lateral earth pressure at the box boundary during the pullout process. The variations of induced lateral pressures on EPC7 with displacement show more or less a similar pattern to the pullout force-displacement plots shown in Figure 5.16. In particular, Figure 5.20 indicates that the induced lateral earth pressures increased rapidly from an initial stable value (~40 kPa) during the first few millimetres of nail displacement and these pressures continued to increase more gradually with further nail displacement, i.e., as the distance between the grout bulb and the front wall continued to reduce. It can be observed that the maximum induced lateral pressure (~260 kPa) for the larger diameter grout bulb (PT3, 92.5 mm in diameter) was much higher than that (~140 kPa) measured for the smallest grout bulb (PT1, 56.5 mm in diameter). These results indicate that boundary effects probably influenced the measured pressures, even though the centre of the grout bulb was initially approximately 700 mm away from the front wall of the box.

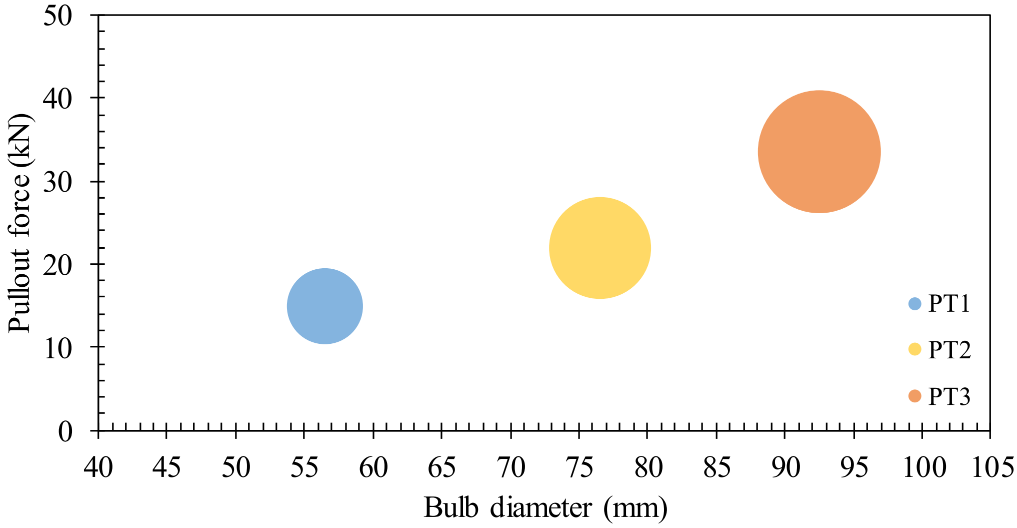

Figure 5.18: Pullout force versus grout bulb diameter for the compaction-grouted soil nails.

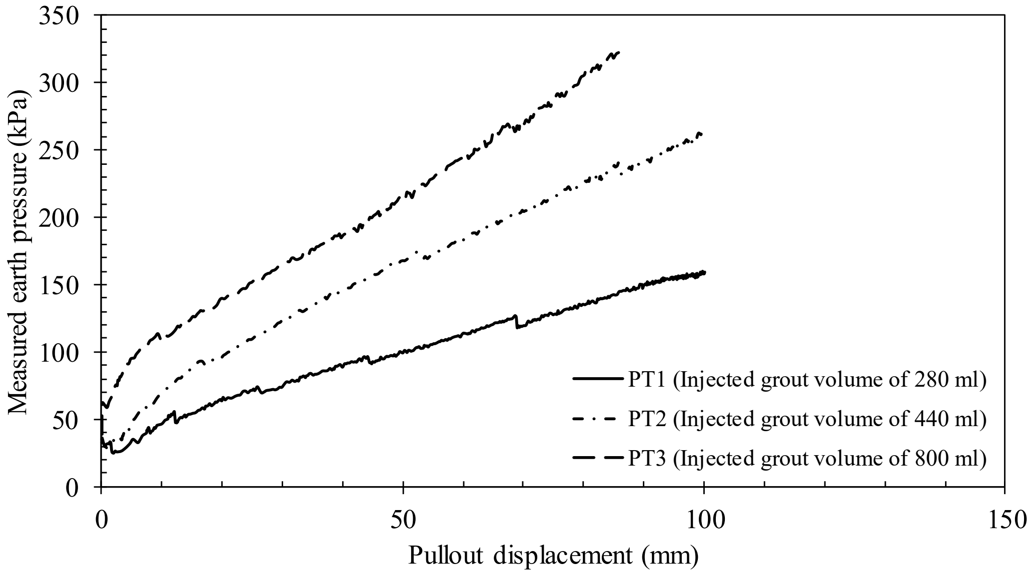

Figure 5.19: Comparison of earth pressure evolution induced on EPC2 during the pullout process for all tests.

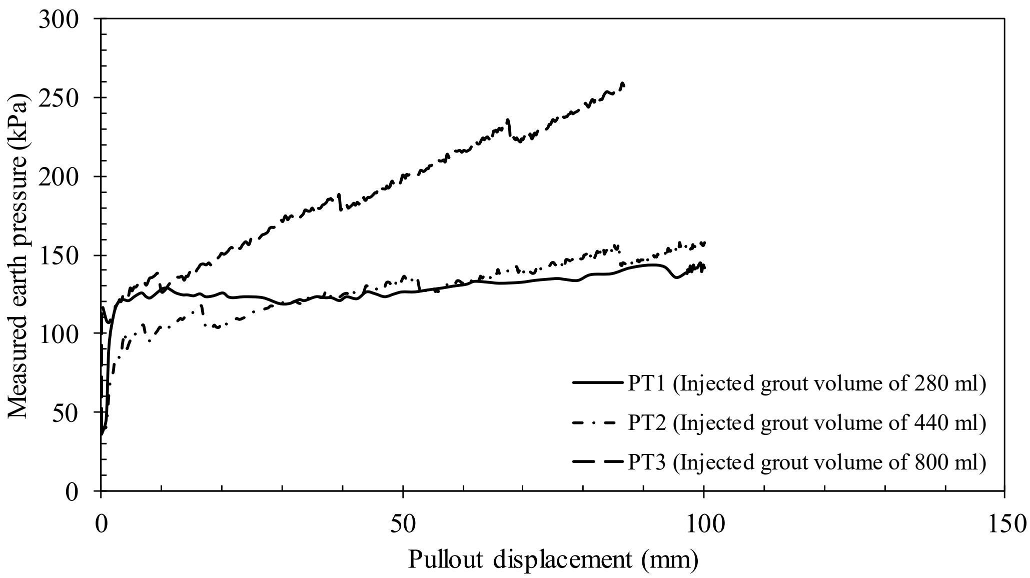

Figure 5.20: Variations in earth pressures on EPC7 during the pullout process for all tests.

5.5 Concluding remarks

In this chapter, physical model tests were conducted using the new test facility to study the behaviour of pressure-grouted soil nails, during which grout was injected directly into the sand at different injection rates. The physical model tests were conducted under fully instrumented conditions to monitor and record the soil responses during the grouting and pullout process. The advantages and capabilities of the developed apparatus are summarized as follows:

- The automatic grout injection pump of the developed test facility allows grout to be injected at different flow rates ranging from 0.5 to 7.5 L/min. Hence, the effect of grout injection rates on the subsequent behaviour of the pressure-grouted soil nails can be examined using this device. In addition, the variation of injection pressure and the injected grout volume over the grouting period can be monitored using this injection pump.
- The modified system for applying overburden pressure using a water-filled rubber cushion provides constant surcharge pressure over the period of testing and can also be used to estimate the surface settlement easily.

Based on the results obtained from a limited number of physical model tests, the following conclusions can also be drawn:

- Grout injection rates significantly influence the amount of grout injected into a soil mass. Due to pressure filtration (expulsion of bleed water under pressure) of neat cement grout, a thick filter cake (plaster) is formed in the soil at lower injection rates, which consequently reduces mobility of the grout as well as the injected grout volume. However, the volume of injected grout increases when injection rates are increased.
- The expulsion (seepage) of bleed water from the pressurized neat cement grout is directly and proportionally related to the injection rate, i.e., the higher the injection rate, the higher the seepage of bleed water.
- With the injection of pressurized grout directly into the soil mass, the normal stresses (confining stresses) acting at the grout-soil interface can be increased by approximately 100-150% of in situ soil stresses. The increase in confining stress is governed by the injected grout volume and an incremental relationship is observed between the injected grout volume and the corresponding confining stress.
- Pullout capacity of a pressure grouted soil nail is predominantly influenced by the injected grout volume, i.e., the size of the grout bulb. Consequently, for a higher injection rate, the grouted soil nail experiences a higher pullout capacity. The pressure grouted soil nail behaves as an anchor nail with a substantial amount of end bearing resistance. Therefore, the pullout force displays a displacement-hardening behaviour.

Chapter 6 Effect of grout viscosity in pressure-grouted soil nail system

6.1 General

This chapter focuses on the application of a special type of additive-mixed cement grout, as described in Chapter 3, in a pressure-grouted soil nail system. To evaluate the performance of the grout, including its bleeding and propagation under pressurized injection condition, a series of fully instrumented physical model tests was conducted. In this investigation a pre-buried soil nail with a Tube-a-Manchette (TAM) facility, as mentioned in Chapter 5, was used for direct injection of the pressurized additive-mixed grout into the soil surrounding the nail to evaluate the grout-soil interaction in sand. As a grouting fluid, three different grout compositions with water/solid (cement + additive) ratio (w/s) varying from 0.30 to 0.50 were used and the performance of these grouts were compared with a traditionally used neat cement grout (w/c = 0.50). The results obtained during the compaction, surcharging, compaction grouting, and pullout processes are described here in detail.

6.2 Introduction

Traditionally, neat cement grout with water cement (w/c) ratios varying from 0.42 to 0.50 is used for gravity and low pressure grouting in soil nailing systems (Su et al., 2007; Pradhan et al., 2006; Chu and Yin, 2005a,b; Yin et al., 2009; Yin and Zhou et al., 2009;). Seo et al. (2012) reported that the neat cement grout with a w/c ratio of 0.50, injected at high pressure (approximately 450 kPa) into permeable soil, exhibited excessive pressure filtration (i.e., seepage of water from the grout paste). The results obtained from the experimental investigation reported in Chapter 5 also confirm the expulsion of water from the grout paste during compaction grouting in sand. Wang et al. (2017a) reported a newly developed compaction-grouted soil nail system where highly pressurized neat grout (w/c = 0.50) was injected into a latex balloon (i.e., grout bag) formed with a membrane liner attached to the soil nail in order to prevent pressure filtration as well as to enhance the grout penetration. To evaluate the membrane liner effect on the grout penetration for a compaction-grouted soil nail system, Bhuiyan et al. (2019) investigated a comprehensive experimental study of a pre-buried soil nail with

TAM and grout bag facilities for simulating the injection of neat grout directly into sand and the grout bag (Wang et al., 2017a), respectively. They found that the injected grout volume for the soil nail with a TAM facility was much lower compared with the nail with a grout bag facility in which the seepage of neat grout was ceased. In addition, they argue that the pressurized grouting of neat grout into sand may have resulted in excessive pressure filtration, which in turn forms a dehydrated grout layer at the grout-soil interface, and thus hampers the penetration of this type of grout. According to Naudts et al. (2003), the neat cement grout is an unstable grout because of its poor resistance against the pressure filtration. In addition, the Roads and Maritime Services (RMS) specification (2018) recommends the application of high bleed resistance, low shrinkage and high fluidity grout for soil nailing.

Therefore, in this investigation, an additive-mixed cement grout was introduced for pressurized grouting into sand, and the performance of the grout with the w/s ratios varying from 0.30 to 0.50 was investigated with respect to the neat cement grout (w/c = 0.50). The Marsh funnel viscosities of the additive-mixed grouts for w/s ratios of 0.30, 0.40, and 0.50 were approximately 46%, 21%, and 9% of the neat grout viscosity (Table 3.2), indicating that the additive-mixed cement grouts are relatively highly fluid grouts, although the additive-mixed grout densities for w/s ratios of 0.30 (2.11 Mg/m^3) and 0.40 (1.95 Mg/m^3) were about 1.15 and 1.10 times that (1.84 Mg/m^3) of the neat grout, respectively. A pre-buried soil nail with a TAM facility was used to minimize the soil disturbance that resulted from the drilling and driving processes (Su et al., 2010; Bhuiyan et al., 2020a). In this study, grout was injected by the developed volume-controlled injected system, as described in Chapter 4, to monitor the change in injection pressure during the pressurized grouting, which makes it possible to monitor the change in injection pressure that might result from the fracture initiation caused by the pressurized injection of highly fluid grout into the compacted sand. With the fully instrumented physical model study (Figure 4.7), the soil responses, including stress states, moisture contents and soil bulk conductivities, were observed continuously, with the sensors embedded in the compacted soil at the different stages (especially the surcharging and grouting processes) of the physical model study. The soil moisture sensors (SMS) were used to register the variations in soil moisture content and soil bulk conductivities in the soil mass, and the changes of soil stresses were monitored with the earth pressure cells (EPC). An overall description of sample preparation and typical testing method for the pre-buried soil nail with a TAM facility can be found in Section 4.3 of Chapter 4.

6.3 Experimental results

A total of four physical model tests were conducted (labelled as VT1, VT2, VT3 and VT4) on identical unsaturated soil samples under controlled boundary conditions (i.e., dry density of 1.50 Mg/m^3, moisture content of 3% and overburden pressure of 100 kPa) to evaluate the performance (i.e., bleeding resistance, propagation and pressure transfer mechanism into the surrounding soil) of the additive-mixed cement grouts with w/s ratios ranging from 0.30-0.50. For the tests VT1, VT2, and VT3, the w/s ratios of the additive-mixed grout were 0.50, 0.40, and 0.30, respectively, and the pressurized grout was injected at a rate of 5.0 L/min. In the case of test VT4, the additive-mixed grout with a w/s ratio of 0.50 was injected at a rate 6.5 L/min to examine the injection rate effect on this type of grout. The typical results of this investigation are included in the following subsections and the results for all tests will be further described with detailed comparison in the Discussion section.

6.3.1 Compaction process

Following the compaction of the soil sample inside the soil chamber (Figure 4.10), the compacted fill was left untouched for about 30 minutes in order to stabilize the moisture contents in the compacted soil, and thereafter an overburden pressure of 100 kPa was applied to the soil. The plots of the typical variation of volumetric water contents (VWC) with time presented in Figure 6.1 indicate that the readings of the soil moisture sensors (SMS) embedded in the compacted fill reach relatively stable values after approximately 30 minutes.

A comparison between the typical volumetric water contents and dry densities monitored by the SMSs at different positions of the compacted soil is demonstrated in Figure 6.2. It is seen that the average volumetric water content and dry density of the compacted soil sample (VT1) are about 0.05 m^3/m^3 (equivalent to 3% gravimetric water content) and 1.50 Mg/ m^3, respectively, which indicates that the compacted soil sample is relatively homogeneous in terms of soil moisture and density. In addition, a comparison of volumetric water contents measured at different positions in the compacted soil samples for all tests (VT1-VT4) is shown in Figure 6.3. The data of the SMSs demonstrate that the unsaturated soil samples used for this investigation possess comparatively uniform and equal moisture contents, varying slightly from the average of around 0.05 m^3/m^3.

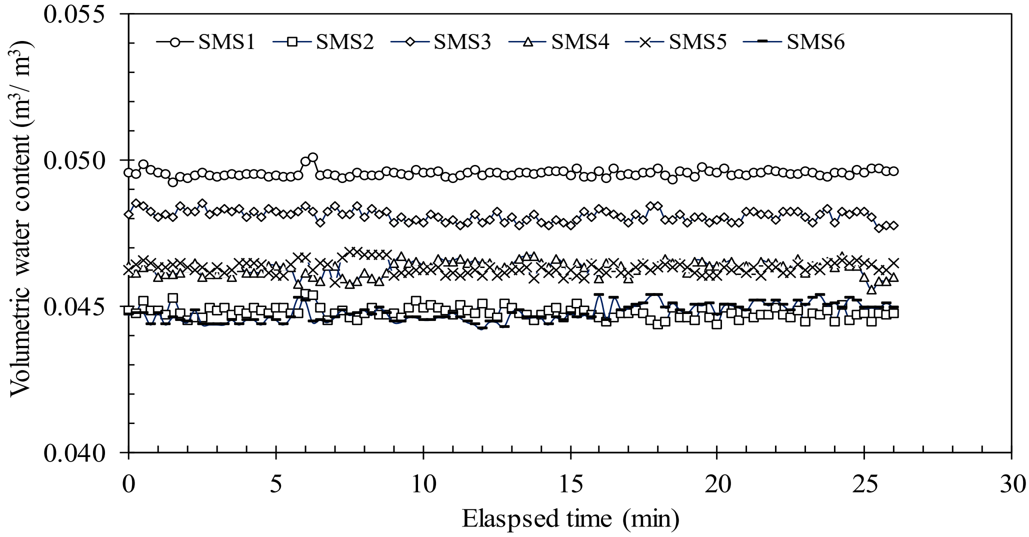

Figure 6.1: Typical variations of volumetric water contents in compacted fill with time following the compaction (VT1).

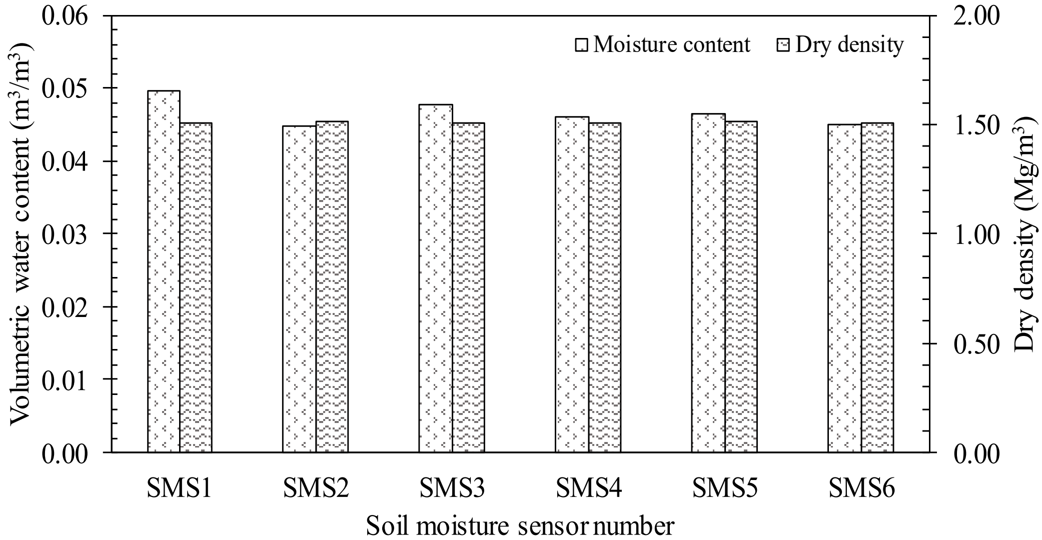

Figure 6.2: Typical changes in volumetric water contents and dry densities at different locations of compacted fill (VT1).

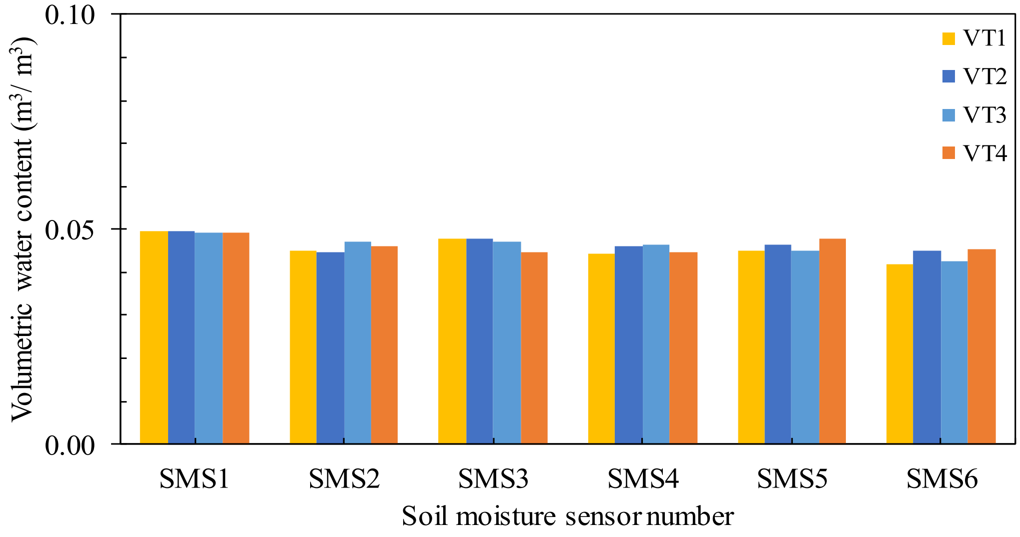

Figure 6.3: Comparison of volumetric water contents for all tests.

6.3.2 Surcharging process

Figure 6.4 illustrates the trend of induced earth pressure change at different locations in the compacted fill with time for a specified overburden pressure (OP) of 100 kPa. The trend of induced earth pressure demonstrates that the earth pressures increase gradually with time and reach the stabilized values within 1 hour after application of the surcharge pressure (100 kPa), consistent with the similar trend reported by Bhuiyan et al. (2019). Note that EPC1, EPC3, EPC4, EPC5, and EPC6 were installed horizontally to monitor the vertical soil pressures, whereas EPC2, EPC7, and EPC8 were installed vertically to record horizontal or lateral soil pressure, as shown in Figure 4.7. Overall, it is found that the vertical soil pressures induced on the EPCs (EPC1, EPC3, EPC4, EPC5, and EPC6) are not consistent with the applied surcharge pressure of 100 kPa. The vertical soil pressures measured by EPC3 and EPC5 are approximately 10% lower and 20% higher than the applied OP of 100 kPa, respectively. By contrast, for the 100 kPa overburden pressure, EPC4 and EPC6 register approximately 40% and 60% higher induced soil pressure, respectively. By comparing Figures 5.5 and 6.6, it is suspected that these significant degrees of error in induced pressures (especially over-registration) may be attributed to the placement effects (Garnier et al., 1999) if the arching and inclusion effects are disregarded (Bhuiyan et al. 2018b). In the case of EPC1, it is found that only 60% of the applied overburden pressure (100 kPa) is registered by EPC1, which was installed 50 mm below the injection point of the pre-buried nail with its sensing face vertically aligned with the centre of the injection point (15 mm in diameter), as illustrated in Figure 4.7. Therefore, the notably low value in induced earth pressure measured by EPC1 possibly results from the disruption of the applied surcharging pressure due to the position of the injection hole just above the sensing face and thus the applied pressure does not fully transfer onto the cell face. Interestingly, it is found that the readings of EPC7 and EPC8 are approximately 15 kPa and 6.5 kPa, on average, respectively, which are much lower than the value of approximately 50% of the applied surcharge pressure of 100 kPa, as expected (Figure 5.5). This indicates a serious placement problem, which may be a result of an improper compaction of the soil situated in front of the sensing faces of the cells, since a small pit was dug into the compacted fill for the placement of the EPC, as described in Subsection 4.3.1 of Chapter 4. Consequently, the applied load did not transfer effectively to the sensing faces of the EPCs. Hence, the readings of EPCs used in this investigation confirm the placement error in measured data caused by the manual installation of the EPCs. This is consistent with the findings of Garnier et al. (1999), who reported that the data measurement accuracy of an EPC is significantly affected by placement techniques (i.e., installation of cell by hand and placement device).

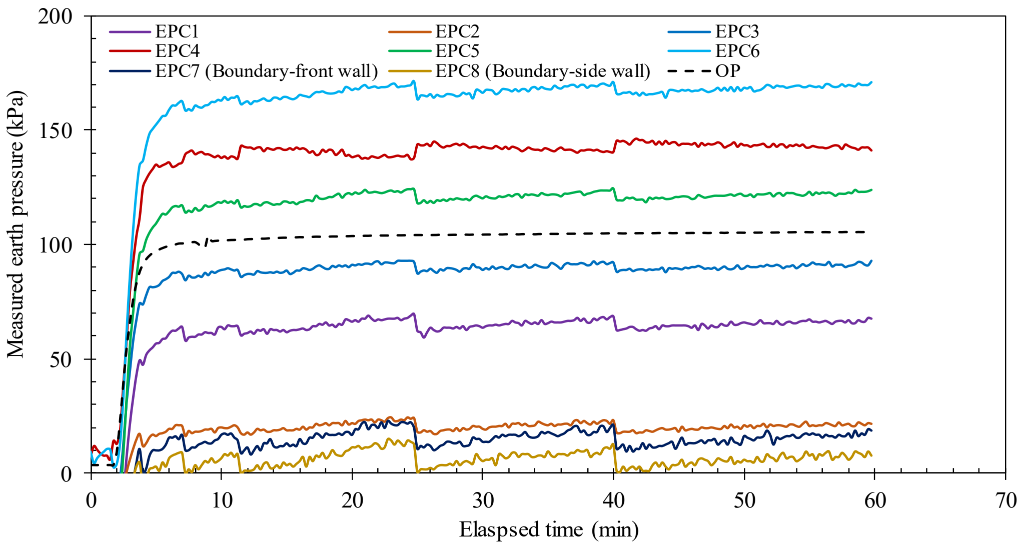

Figure 6.4: Typical changes in induced earth pressures with time over the surcharging process (VT1).

6.3.3 Grouting process

Once the induced earth pressures stabilized (i.e., after 1 hour of surcharging), the additive-mixed cement grout was injected into the pre-buried soil nails at the injection rates of 5.0 L/min and 6.5 L/min for the tests VT1-VT3 and VT4, respectively, by the volume-controlled grouting pump, as described in Subsection 4.2.2.1 of Chapter 4. A typical relationship between injected grout volume and corresponding injection pressure against grouting time is presented in Figure 6.5. It is seen that the injection pressure increases rapidly at the start of grout injection and then continues to rise very slowly as injection volume increases. Finally, the pressure reaches a maximum value of approximately1340 kPa once the injection stops totally at a maximum injected volume of approximately 950 ml, followed by a steady drop over the elapsed time. It is suspected that this drop in injection pressure may be attributed to the loss of pressure in the injection system because the injection pressure was not maintained once the grout injection stopped.

Figure 6.6 demonstrates the typical changes in soil stresses measured at different locations in the compacted fill induced by the pressurized grout process. It is seen that the induced earth pressures measured at locations EPC1, EPC3, EPC5, and EPC6 (i.e., near the grouting outlets) increase significantly over the grouting period compared with the other locations, e.g., EPC2, EPC4, EPC7, and EPC8. In the case of EPC1, EPC3, EPC5, and EPC6, for injection pressure of about 1350 kPa, the induced vertical earth pressure increases almost instantly from their stable values obtained after the application of surcharge pressure to the peak values of about 1020 kPa, 814 kPa, 743 kPa, and 587 kPa, respectively. The peak pressures induced on EPC3, EPC5, and EPC6, which were installed at the vertical distances of 50 mm, 100 mm, and 150 mm from the grouting outlets (injection points), indicate that the induced pressures reduce almost linearly with increasing distance from the injection point, consistent with the similar trend of the induced soil pressures reported by Bhuiyan et al. (2019) in a separate study of a pressure-grouted nail with a TAM facility. Once the grouting stopped at a maximum grout volume of about 950 ml (Figure 6.5), the peak pressures induced on EPC1, EPC3, and EPC5, located near the grouting outlets, decrease gradually to a residual value of almost zero pressure after approximately 3.5 minutes. However, for EPC6, the peak pressure drops steadily to a residual value of approximately 44 kPa over time, which is lower than the applied overburden pressure of 100 kPa. This may be a result of rebounding of the expanded cavity around the injection point formed by the pressurized injected grout, since the grout paste may not achieve a sufficient stiffness to constrain the rebounding (Seo et al., 2012) and thus the residual stresses developed at the grout-soil interface become zero after the grouting process. The reading of EPC4, which was installed horizontally at a horizontal distance of 180 mm from the injection point, shows a slight drop and rise in induced pressure at the start of grouting and then it remains almost constant over the elapsed time. This drop in induced pressure may be attributed to the uplift of the cell at the left side caused by the expanded grout bulk (Wang et al., 2017b). Moreover, the induced pressures measured by EPC2, EPC7, and EPC8, which were installed vertically to measure horizontal soil pressure, increases slightly from the initial stabilized values to their peak values and then remains almost constant with time, except for EPC8, which shows a gradual decrease from the peak value (~223 kPa) to residual value of 50 kPa over time. The increase in horizontally induced earth pressure indicates the insignificant compaction of soil mass in longitudinal and transverse directions for the injected grout volume.

Figure 6.7 illustrates the variations of volumetric water contents before and after the grouting process. It is seen that the volumetric water content (VWC) induced by the grouting process on SMS1, located at a vertical distance of 50 mm from the injection point (Figure 4.7), increases slightly from the initial stabilized value of about 0.050 m^3/m^3, obtained after the application of the surcharge pressure, to a maximum value of approximately 0.055 m^3/m^3 at the end of the grouting process. It is suspected that this slight increase in moisture content might have resulted from the expulsion of bleed water from the additive-mixed grout paste under pressurized injection. Importantly, it is also found that the readings of the other SMSs remain nearly unchanged, including SMS3, which was installed 50 mm above the injection point. The readings of SMS3 found after the surcharging and grouting processes indicate that the water released from the pressurized grout paste possibly flowed downwards due to gravity once the grouting stopped after a very short period of injection time (~15 seconds), as illustrated in Figure 6.5.

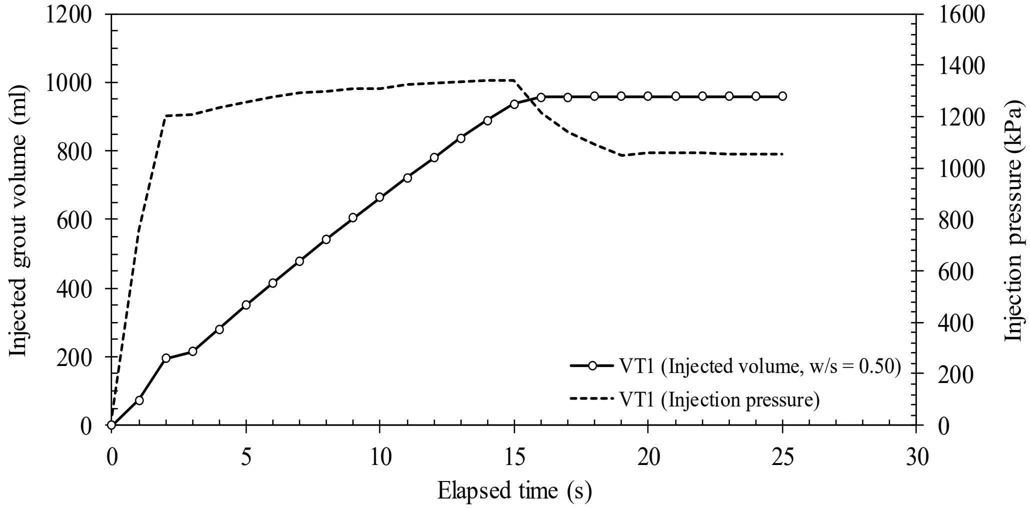

Figure 6.5: Typical variation of injection pressure and injected grout volume with time time for VT1.

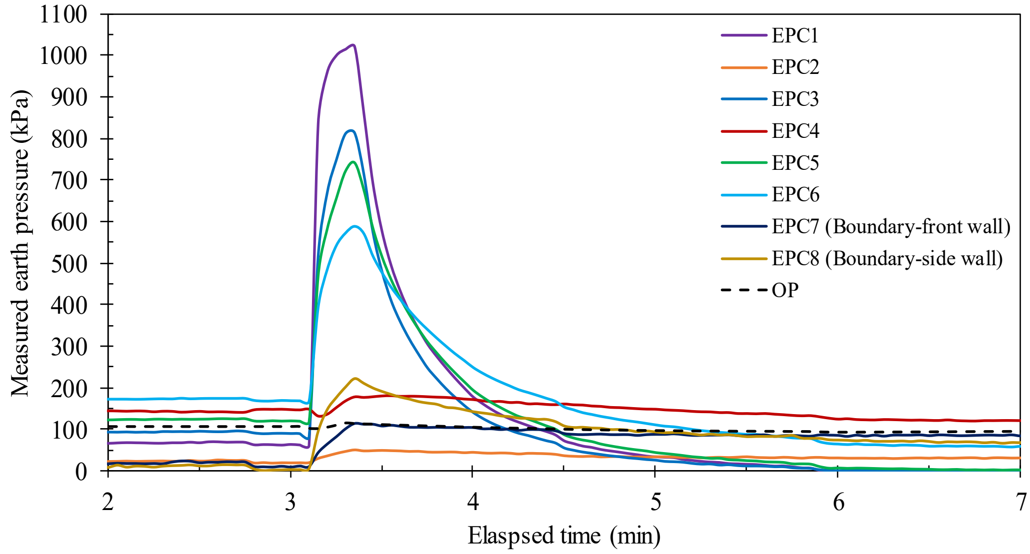

Figure 6.6: Typical changes in induced earth pressures during grouting process for VT1.

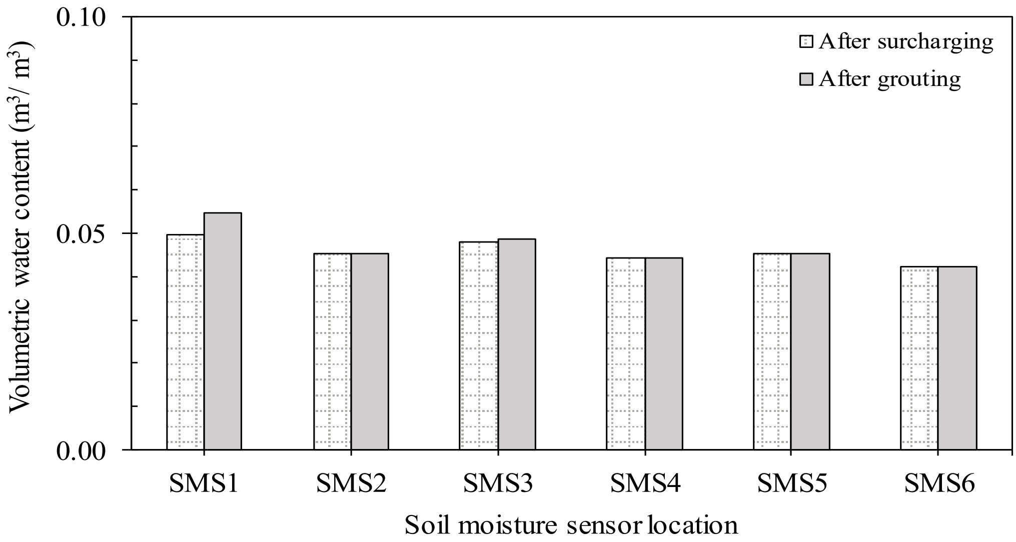

Figure 6.7: Comparison of volumetric water contents obtained after surcharging and grouting processes for VT1.

6.4 Discussion

Figure 6.8 illustrates a relationship between the injected grout volume and the injection pressure for the tests (VT1-VT3), where the additive-mixed cement grouts with w/s ratios ranging from 0.30 to 0.50 were injected at 5.0 L/min. The injection pressure plots presented in Figure 6.8 illustrate a similar trend in injection pressure change with time during the grouting process, showing a rapid increase in injection pressure within a very short period of time (5 to 15 seconds), followed by a steady drop over time. For the w/s ratios of 0.50 (VT1), 0.40 (VT2), and 0.30 (VT3), the maximum injection pressures induced by the flow-controlled grouting process were found to be about 1340 kPa, 1268 kPa, and 1274 kPa, respectively, indicating relatively equal injection pressures with a slight difference from the average value of approximately 1295 kPa.

It can also be found that the maximum injected grout volume for the highly fluid grout (VT1, viscosity of 97 seconds) was approximately 960 ml, followed by 900 ml for the intermediately fluid grout (VT2, viscosity of 215 seconds), and 330 ml for the moderately fluid grout (VT3, viscosity of 474 seconds). This indicates that the injected grout volume increases with decreasing grout viscosity, i.e., the higher the w/s ratio, the higher the grout propagation. This is consistent with the findings of Wang et al. (2016), who reported that the volume of the grout injected was higher for the higher w/c ratio (1.0) grout compared to the lower w/c ratio (0.50) grout where the neat cement grouts were injected at different specified injection pressures. Axelsson et al. (2009) noted that the higher water content in a grout mix keeps the cement particles more separated and thus reduces the risk of clogging (plugging of cement particles into the void spaces of the soil matrix) or filter cake formation (dehydrated layer at the grout-soil interface) under pressurized grouting condition. Hence, a higher w/c ratio grout exhibits better penetrability (injectability) before the blockage of the pathways. Therefore, it could reasonably be deduced that the higher cement contents (solid particles) in the grout mixes accelerate the clogging or filter cake formation over time, which in turn results in the stoppage of the propagation of the pressurized cementitious grouts into the soil mass. In addition, Kuhling et al. (1994) stated that a decrease in w/s ratio significantly increased the yield stress and accelerated rapid hardening of the grout (suspension), which consequently hampered the injectability of the suspension.

In order to evaluate the grout viscosity (i.e., resistance to flow) effect on grout injectability, the results of test PT2 obtained during the pressurized grouting process (reported in Chapter 5) are compared with the test VT1 in this chapter. Note that, for the tests PT2 and VT1, the injection fluids were a neat cement grout with a w/c ratio of 0.50 (viscosity of 1036 seconds) and an additive-mixed cement grout with a w/s ratio of 0.50 (viscosity of 97 seconds), respectively, having equal grout density of 1.84 Mg/m^3. In addition, the injection fluids were injected at a rate of 5.0 L/min into the identical soil samples (dry density of 1.50 Mg/m^3, moisture content of 3% and overburden pressure of 100 kPa). Figure 6.9 illustrates a comparison between grout injection volume and the corresponding injection pressure for the grouts with different viscosities over the grouting period. In Figure 6.9, it can be seen that the injection pressure induced by the pressurized grouting of the neat cement grout (PT2, viscosity of 1036 seconds) increases quickly to a maximum value of about 1540 kPa within roughly 9 seconds from the start of the grouting once the injection stopped entirely at a maximum injection volume of approximately 440 ml. By contrast, for the highly fluid grout (VT1, viscosity of 97 seconds), the injection pressure initially increases rapidly, similar to the PT2 at the start of grouting, and then continues to rise, but more slowly, as the volume of injected grout increases, and the pressure finally reaches a maximum value of approximately 1340 kPa within roughly 15 seconds once the grouting stopped completely at a maximum injected volume of about 960 ml. With the decreased viscosity, more grout could be injected at a specified injection rate and the volume (~960 ml) of the additive-mixed grout (high flowability, viscosity of 97 seconds) was almost 2 times that (~440 ml) of the neat cement grout (very low flowability, viscosity of 1036 seconds), indicating that the volume of grout injected (injectability) increases as fluidity increases. This is consistent with the findings of Nicholas and Goodings (2000), who reported that the highly pumpable (fluid) compaction grout (mixture of mineral aggregates, cement and bentonite) developed a larger grout bulb in cohesion-less soil. Lee et al. (2012) also pointed out that the increased viscosity of the pressurized cementitious grout reduces the grout penetration (injectability) into the soil mass.

Note that the Marsh funnel viscosity of the water used here for the grout mixes was found to be about 26 seconds, which is a typical viscosity of water (a Newtonian fluid, as described in Chapter 3). By comparing the viscosities of the water (viscosity of 26 seconds) and the neat cement grout (~40 times of water viscosity), it can be observed that the addition of the additive (BluCem HS200A, as mentioned in Chapter 3) into the neat cement grout transformed this highly viscous grout into a highly flowable grout, with a viscosity of 97 seconds (~3.7 times water viscosity), by reducing its viscosity significantly. Kuhling et al. (1994) reported that the addition of water into cement led to an instant agglomeration of the solids (i.e., enlargement of the cement particles), which made the grain size distribution of solids in the neat grout larger than the dry cement particles, and consequently reduced the injectability of the neat grout. However, they also found that the application of a suitable additive (dispersant) into the neat grout significantly reduced the yield stress and viscosity of the suspension as well as making the solids in the suspension noticeably finer by minimizing the agglomeration tendency of the solids significantly. Hence, they concluded that, for a specified injection rate, the neat grout with an additive could be injected into sand successfully at a lower injection pressure compare to the grout without additive.

In Figure 6.9, it can be found that the injection of the neat grout (PT2) stopped (at 9 seconds) relatively early compared to the fluid grout (VT1), which stopped at 15 seconds. This early stoppage of the grout propagation may be attributed to the agglomeration tendency of the neat grout, since the addition of the additive in the grout mixes reduces the accumulation of the cement particles under pressurized grouting conditions and thus more grout can be injected at a low injection pressure. The data presented in Figure 6.9 illustrates a good agreement with the findings of Kuhling et al. (1994). Moreover, Naudts et al. (2003) noted that the suspension with the higher viscosity required a higher injection pressure to flow the grout. This could be the reason for the higher injection pressure induced by the grouting of the highly viscous grout (PT2) compared to highly fluid grout (VT1).

Figure 6.10 compares the grout injection volumes and injection pressures for tests VT1 and VT4, where a highly fluid grout (w/s = 0.50, viscosity = 97 seconds) was injected at 5.0 L/min and 6.5 L/min, respectively. It can be observed that the maximum injection volumes for the injection rates of 5.0 L/min (VT1) and 6.5 L/min (VT4) were approximately 960 ml and 1600 ml, respectively, albeit the maximum injection pressure (~1340 kPa) for the test VT1 was moderately higher than that (~1200 kPa) found for the test VT4 once the grouting stopped entirely. These results confirm that the volume of grout injected increases with increases in the injection rate, consistent with the findings reported in Chapter 5 for the neat cement grout (w/c = 0.50). In addition, based on the injection pressure readings presented in Figure 6.10, it can be claimed that the injection pressure induced by the grouting does not have any significant effects on the volume of grout injected at a specified injection rate.

Figure 6.11 presents the changes in moisture contents at SMS1 location (50 mm below the injection point) before and after the grouting process for the tests VT1-VT3, in which the additive-mixed grouts with different w/s ratios ranging from 0.30 to 0.50 were injected at a specified flow rate of 5.0 L/min. In Figure 6.11, it is found that, for the tests VT1 (w/s = 0.50) and VT2 (w/s = 0.40), the volumetric moisture content (VWC) increases slightly from the average stabilized value of about 0.050 m^3/m^3 to the maximum values of about 0.055 m^3/m^3 and 0.052 m^3/m^3, respectively. However, the VWC (0.050 m^3/m^3) for the test VT3 (w/s = 0.30) remains virtually constant before and after the grouting process. As mentioned earlier (Figure 6.7), this increase in water content may be attributed to the dissipation of water from the pressurized grout paste, which will be further justified in the following paragraph using the change in soil conductivity induced by the grouting process. The VWC readings obtained after the pressurized grouting process indicate that the additive-mixed grout with a w/s ratio greater than 0.30 exhibits a significant degree of pressure filtration (i.e., expulsion of water from the cement grout under pressure) and the pressure filtration is directly and proportionally related to the grout w/s ratio, i.e., the higher the w/s ratio, the higher the pressure filtration. Hence, it can be asserted that the additive-mixed grout with a w/s of 0.30 is a zero bleed cementitious grout, consistent with the manufacturer's data (Bluey Technologies, 2017).

The soil moisture sensors (SMS) used in this investigation are "three-in-one" sensors, which are able to measure the bulk conductivity of the soil mass together with its volumetric moisture content (VWC) and temperature separately and concurrently (Bhuiyan et al. 2020b). Figure 6.12 demonstrates the changes in soil conductivity induced by the pressurized grouting on SMS1 (located 50 below the injection point) against elapsed time. It is seen that the soil bulk conductivities for the tests VT1 (w/s = 0.50) and VT2 (w/s = 0.40) increases gradually from an average stabilized value (~20 dS/m) achieved after the application of the surcharge pressure (100 kPa) and reaches the maximum values of approximately 77 dS/m and 53 dS/m, respectively, within a period of about 1 hour after the injection. However, the soil conductivity for the test VT3 (w/s = 0.30) remain unchanged over that period of time. These findings provide additional support to the conclusion made, based on the data presented in Figure 6.9, that the additive-mixed cementitious grout with a w/s ratio greater than 0.30 exhibits pressure filtration under pressurized injection of grout into sand.

Figure 6.13 compares the variations of the vertical earth pressures measured by EPC1 for the tests VT1-VT3 with the test PT2 (reported previously in Chapter 5), as induced by the pressurized injection of different types of cementitious grouts. Note that EPC1 was located vertically 50 mm and horizontally 700 mm away from the injection point and the front box wall, respectively. In Figure 6.13, it can be observed that the peak pressures induced on EPC1 for the pressurized injection of relatively fluid grouts with the w/s ratios of 0.50 (VT1, viscosity of 97 seconds) and 0.40 (VT2, viscosity of 215 seconds) drop rapidly to zero residual pressure within roughly 3 minutes and 7 minutes (secondary horizontal axis), respectively, once the grouting is stopped. By contrast, for the injection of comparatively viscous grout (VT3, viscosity of 474 seconds) with a grout density of 2.11 Mg/m^3, the peak pressure at EPC1 location reduces gradually with time and reaches a stable residual pressure of about 30 kPa within a period of about 47 minutes from the start of the grouting. In the case of test PT2, however, the peak pressure measured on EPC1 induced by the injection of the highly viscous grout (w/c = 0.50, viscosity of 1036 seconds) reduces to a residual value of approximately 195 kPa within several minutes after the grouting process, indicating a higher confining pressure at the grout-soil interface than the applied overburden pressure of 100 kPa. It is suspected that the higher residual stress may be attributed to the agglomeration and bleeding tendency of the highly viscous neat grout (w/c = 0.50) under pressurized injection, which in turn might solidify the grout paste without additive to some degree (Kuhling et al., 1994; Seo et al., 2012). Consequently, the neat grout paste may achieve a sufficient stiffness to restrain the rebounding of the enlarged cavity formed by shifting and compressing the soil surrounding the injection points during the pressurized injection of the grout into the compacted soil mass, resulting in the development of the residual soil stress at the grout-soil interface (Seo et al., 2012). Kuhling et al., (1994) pointed out that the addition of an additive to a neat grout mix remarkably reduced the agglomeration tendency and the yield stress of the neat grout by separating the cement particles in the suspension, which consequently made the grout highly flowable. Therefore, it could be argued that the highly fluid grouts (w/s rations of 0.50 and 0.40) may be unable to develop sufficient stiffness early to constrain the rebounding of the cavity, and the injected grout bulk might undergo deformation over time in asymmetric stress condition (i.e., K_o = 0.50). Thus, the zero residual pressure for the tests VT1 and VT2 might have resulted from stress relaxation around the injection point caused by the cavity rebounding. However, for the moderately fluid grout (VT3, w/s = 0.30), the grout paste may develop stiffness to some extent over time due to its comparatively high density (2.11 Mg/m^3), resulting in constraints on the rebounding of the cavity. This could be the reason for the relatively low residual soil pressure (~30 kPa) induced on EPC1.

Moreover, during the injection of grout at an injection rate of 5.0 L/min, the peak earth pressures induced on EPC1 for the VT1 was approximately 1020 kPa, followed by 925 kPa, 740 kPa, and 681 kPa for the test VT2, VT3, and PT2 respectively. This indicates that the induced pressure decreases with the increment of the grout viscosity. This phenomenon may be attributed to the agglomeration tendency of the viscous grouts (w/c = 0.50 and w/s = 0.30) since the viscous grout pastes have the ability to solidify quickly under pressurized injection compared to the fluid grout pastes (w/s = 0.40 and w/s = 0.50), and consequently the increased stiffness of the grout paste might have restrained the applied injection pressure partially without transferring it effectively onto the surrounding mass. Therefore, it is suspected that the lower value in peak pressures measured on EPC1 induced by the injection of viscous grouts (PT2 and VT2) may be governed by the grout consistency (i.e., viscosity) if the partial energy loss that caused the gap (50 mm) between the injection points and EPC1 is ignored (Seo et al., 2012).

Figure 6.14 illustrates the grout bulb (hardened grout) for all tests (VT1-VT4), which were excavated after the pullout tests of the grouted nails. Note that the pullout tests were performed after a curing period of 7 days in order to allow the grout pastes to develop a minimum compressive strength of 24 MPa (Bhuiyan et al., 2019). It is seen that the grout bulbs formed around the injection points for the tests VT1, VT2, and VT4 failed during the pullout testing and the bulbs were relatively flattened along the horizontal direct (i.e., lateral earth pressure direction). However, for the test VT3, the grout bulb was intact and nearly cylindrical in shape, as desired for all tests. Overall, the shape of the grout bulbs (especially, VT2 and VT4) found after excavation confirm the deformation of the grout pastes over the curing period along the vertical direction (i.e., surcharge pressure direction).

Figure 6.15 illustrates the pullout forces of the pressure grouted (pre-buried) soil nails with different injected grout volumes. For the test VT3 (injected volume of 330 ml), the pullout force increases quickly at the start of the nail pulling and then continues to increase with the displacement, and ultimately reaches a maximum value of about 21 kN at about 100 mm displacement. This is consistent with the findings of Wang et al. (2017b), who stated that the compaction-grouted (pre-buried) nail worked as an anchor and this anchored type of nail exhibited its maximum pullout capacity at a displacement of 100 mm. Bhuiyan et al. (2019) also noted that the pullout force of the pressure grouted (pre-buried) nail with TAM facility exhibited the displacement-hardening behaviour (i.e., increase in pullout force without any yield point). However, for the other grouted nails (VT1, VT2, and VT4), it is found that the pullout forces increase rapidly within the first few millimetres of pullout displacements, ranging from 8 mm to 20 mm, and then drop abruptly to almost a zero force. Clearly, this drop in pullout force resulted from the failure of the grout bulb during the pullout testing, as illustrated in Figure 6.14. In the case of VT1, with a grout injection volume of about 960 ml, the peak pullout force was found to be approximately 30 kN after a displacement of about 20 mm, indicating a rapid increase in pullout force compared to the test VT3. It is certainly presumed that this rapid increase in pullout force is attributed to the grout bulb size of the test VT1, which was much larger than the bulb of the test VT3 (Figure 6.14). Wang et al. (2017b) reported that the pullout of the compaction-grouted soil nail increased linearly by increasing the volume of grout injected. In Figure 6.14, a visual inspection of the grout bulb for VT1 revealed that a comparatively large cavity was formed inside the grout bulb during the pressurized injection of the highly fluid grout (w/s = 0.50), which in turn made a weak bonding at the nail-grout interface. Consequently, the larger grout bulb with a cavity has the possibility to fail during the pullout testing due to the stress concentration, since the larger grout bulb provides greater passive resistance, as discussed in Chapter 5.

Furthermore, for the injection volumes of 900 ml (VT2, w/s = 0.40) and 1600 ml (VT4, w/s = 0.50), the pullout forces exhibited more or less similar behaviour to the test VT1, increasing rapidly to the peak values of about 24 kN and 26 kN at displacements of 13 mm and 8 mm, respectively, followed by a sudden drop (Figure 6.15). By inspecting the grout bulbs visually presented in Figure 6.14, it is found that the bulbs of the tests

VT2 and VT4 were a relatively flattened cylindrical shape (i.e., compressed oval in cross sectional view) compared to the bulbs of VT1 and VT2. Therefore, it is suspected the early failure of the grouted nails (especially VT2 and VT4) may be attributable to the failure of the irregular (asymmetric) grout bulb formed by comparatively fluid grout, which fails easily due to a high stress concentration once the nails are mobilized. These findings indicate that the pullout capacity of the pressure-grouted nail is not only governed by the injected grouted volume, as claimed by Wang et al. (2017b) and Bhuiyan et al. (2019), but also depends on the shape of the grout bulb formed around the injection points. The grout bulbs with a flattened cylindrical shape and/or cavity have the higher possibility to fail early due to stress concentration, which ultimately results in failure of the grouted nail at very small displacement without mobilizing its maximum pullout capacity for a specified injected grout volume, and thus it lessens the efficiency of this nail system in terms of design and safety. Therefore, it can be argued that the application of the high density additive-mixed grout (w/s = 0.30) in pressure-grouted soil nail systems may be a good alternative injection fluid compared to highly fluid grouts with w/s ratios ranging from 0.40-0.50, due to its high compressive strength, zero bleeding, high bond strength, low shrinkage and high fluidity (Bluey Technologies, 2017), which conforms to the grout performance requirements stated by the Road and Maritime Services (RMS) standards (RMS R64, 2018) for soil nailing applications.

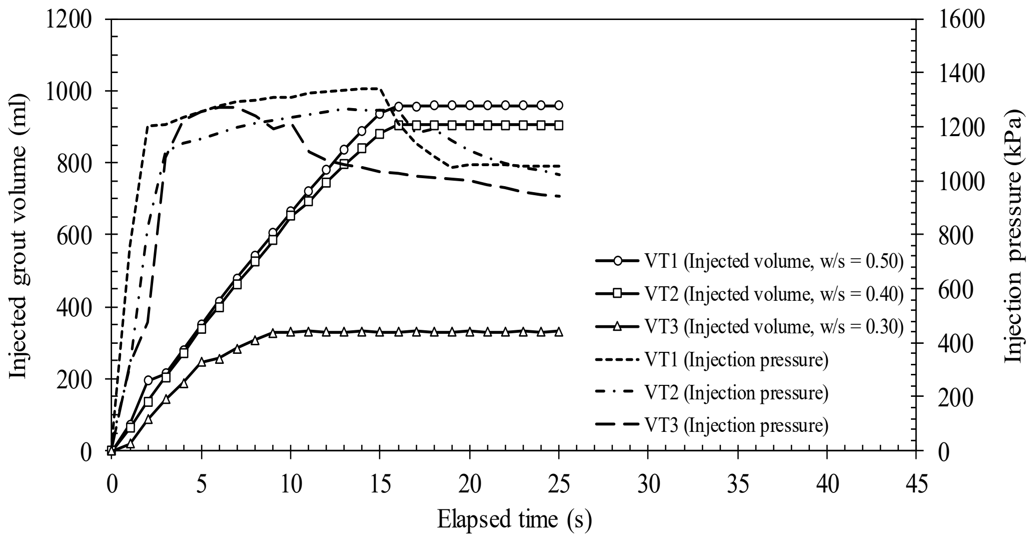

Figure 6.8: Evolution of injected grout volume and injection pressure for VT1-VT3.

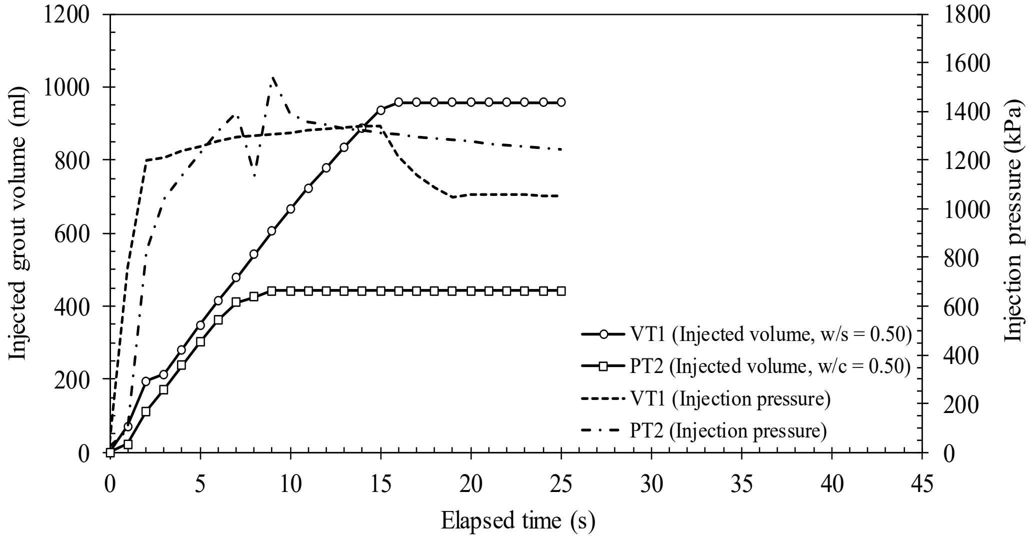

Figure 6.9: Comparison of injected grout volume and injection pressure for VT1 and PT2.

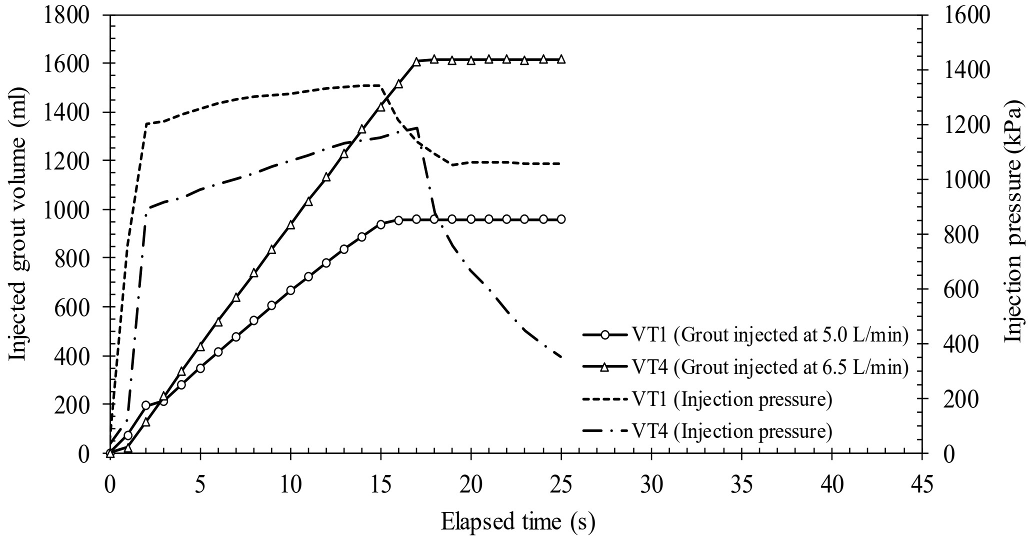

Figure 6.10: Comparison of injected grout volume and injection pressure for VT1 and VT4.

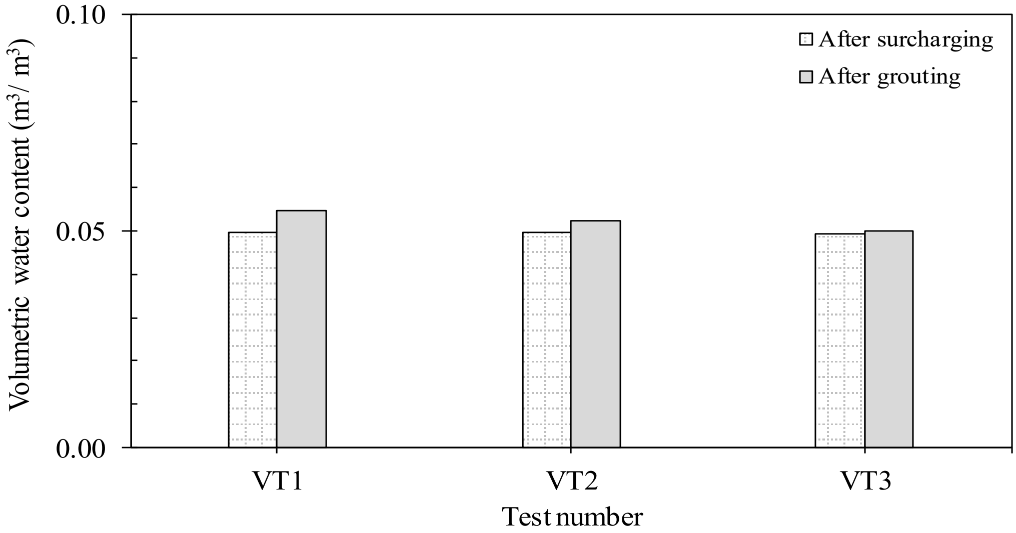

Figure 6.11: Comparison of volumetric moisture contents recorded by SMS1 for the tests, having different w/s ratios ranging from 0.30 to 0.50.

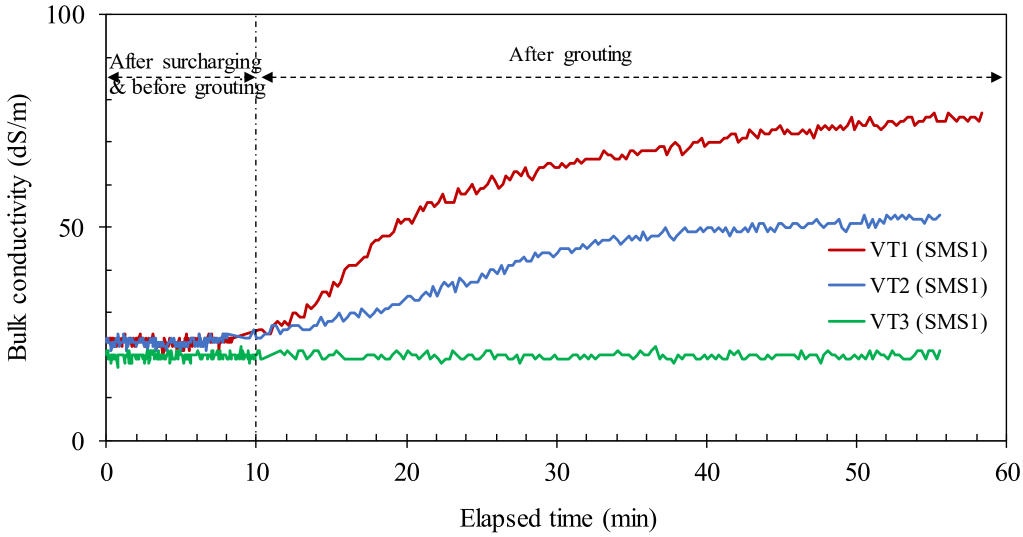

Figure 6.12: Evolution of soil bulk conductivity around the grout injection points for the tests, having different w/s ratios ranging from 0.30 to 0.50.

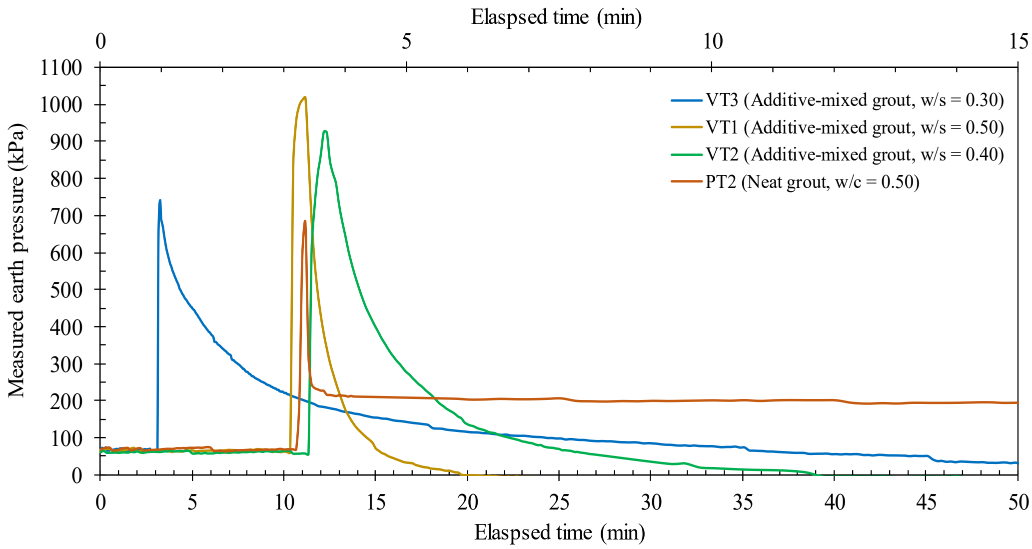

Figure 6.13: Evolution of vertical soil pressure induced on EPC1 during pressurized injection of different types of cementicious grouts.

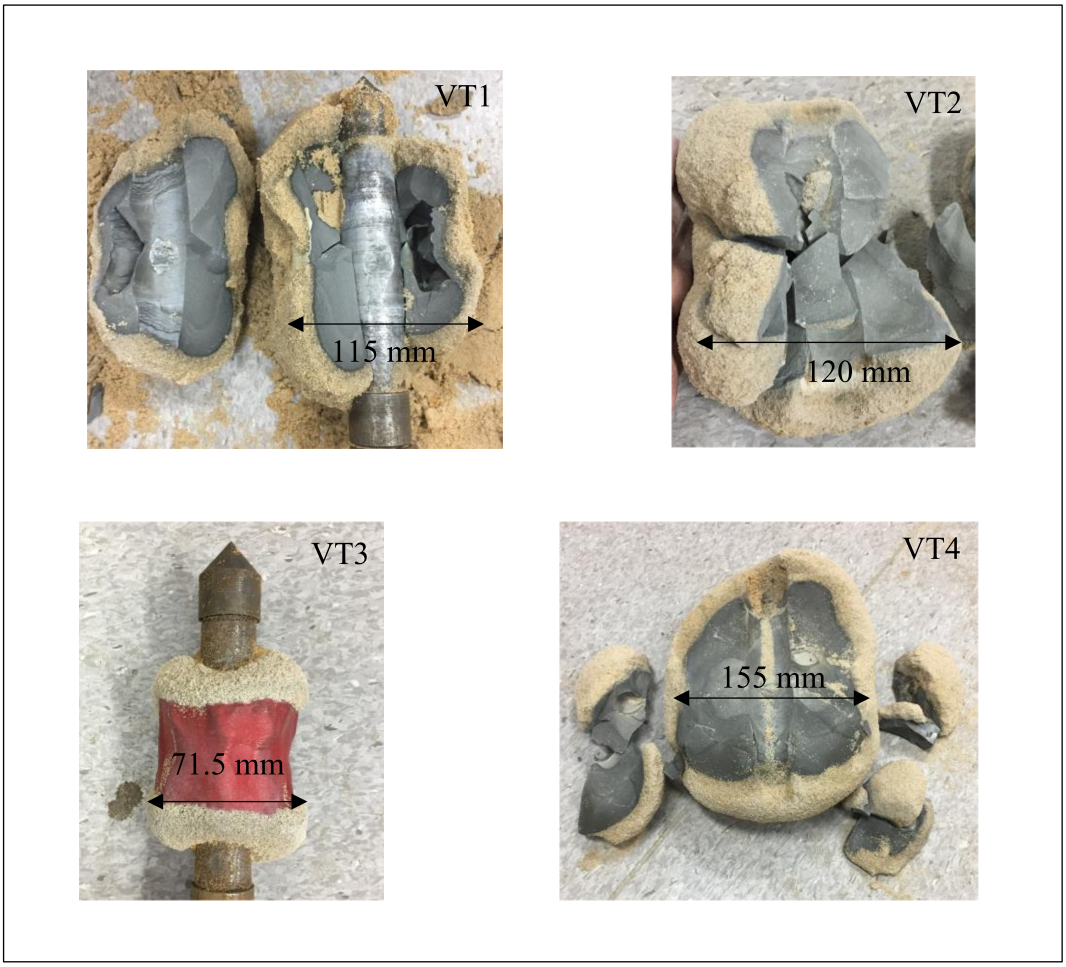

Figure 6.14: Shape of the grout bulbs for all tests showing approximate bulb width along the horizontal direction.

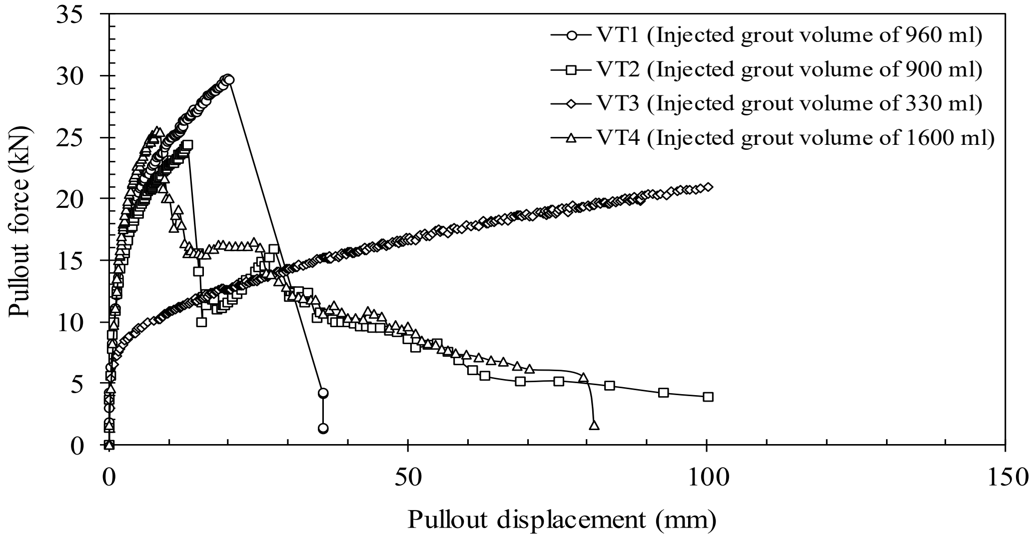

Figure 6.15: Pullout force versus displacement for all tests.

6.5 Concluding remarks

In this investigation, a series of fully instrumented physical model tests were conducted in order to evaluate the performances (i.e., bleeding resistance, propagation and pressure transfer mechanism into the surrounding soil) of the additive-mixed grouts with w/s ratios varying from 0.30-0.50 in a pressure-grouted soil nail system. The physical model tests were performed under identical soil sample conditions, having dry density of 1.50 Mg/m^3, moisture content of 3% and overburden pressure of 100 kPa. A pre-buried soil nail with a Tube-a-Manchette (TAM) facility was used for direct injection of the grouts into the sand at the specified injection rates. The findings of this comprehensive laboratory investigation can be summarized as follows:

- The w/s ratio of a grout mix greatly affects the injectability (penetration) of the grout into a soil mass. By increasing the w/s ratios of the grouts, the volume of grout injected increases.
- The dissipation of water (pressure filtration) from the additive-mixed grout paste under pressurized injection conditions is directly related to the w/s ratio, i.e., the higher the w/s ratio, the higher the pressure filtration. However, the additive-mixed grout with a w/s ratio of 0.30 does not exhibit any pressure filtration during

the pressurized grouting into sand. Therefore, it could be said that the additive-mixed grout with a w/s ratio greater than 0.30 is susceptible to pressure filtration.

- Application of an additive (a blend of superplasticizers and suspension agents) decreases the viscosity of the grout significantly by reducing the agglomeration tendency of the cement particles in suspension, and thus more grout, with the same w/s ratio, can easily be injected at a specified injection rate, i.e., the lower the viscosity, the larger the injectability.
- The pressure exerted by the grout onto the soil surrounding the injection point is influenced by the grout viscosity instead of its w/s ratio. The induced soil pressure instigated by the pressurized grouting process decreases with increments in grout viscosity.
- The grout bulks formed by the injection of highly fluid grouts with low grout densities (e.g., w/s = 0.40 and 0.50) behave as plastic masses, and deform under asymmetric stress conditions (i.e., $K_o = 0.5$) over the curing period and thus the solidified grouts form relatively flattened cylindrical shape bulbs compared to the high density grout (w/s = 0.30) with a moderate viscosity. The irregular grout bulb (deformed bulb) formed in the pressure-grouted nail system fails easily due to stress concentration at a very small pullout displacement without mobilizing its maximum pullout capacity for a specified grout injection volume.
- The volume of grout injected not only influences the pullout capacity of pressure-grouted nails, but the shape of the bulb formed inside the compacted fill also affects this type of nail performance. In order to form a cylindrically-shaped grout bulb (effective shape), it is therefore recommended that the high density additive-mixed grout with a moderate viscosity (e.g., w/s = 0.30) be applied as an effective injection fluid for this pressure-grouted soil nail system because of its high bleed resistance, high compressive strength, high bond strength, low shrinkage and high fluidity.

Chapter 7 Performance of an innovative driven and compaction-grouted soil nail

7.1 General

This chapter represents an experimental investigation of a newly developed driven and compaction-grouted soil nail (termed here as x-Nail). The innovative x-Nail is a hybrid soil nail, which combines the facilities and capabilities of a purely friction driven nail and a compaction-grouted nail, as described in Subsection 4.2.4.2 of Chapter 4. The innovative design makes it possible to drive the x-Nail into in situ ground with a latex balloon that is used for compaction grouting, in order to form a grout bulb at the driven end of the nail to improve its pullout resistance. For compaction grouting, a special type of additive-mixed cement grout (w/c = 0.32) was used in this investigation because of its zero bleeding and high bond strength, as mentioned in Section 3.4 of Chapter 3. A series of five fully instrumented pullout model tests were conducted to examine the performance of the x-Nail compared to a purely frictional soil nail. The experimental results obtained at different stages (i.e., compaction, driving, surcharging, grouting, and pullout processes) of the physical model study are described here in detail.

7.2 Introduction

Conventionally, soil nails are inserted into the ground by two types of frequently used methods, viz. driving and drilling-grouting techniques, based on the soil conditions, project cost and construction flexibility (Geo, 2008). Currently, however, the drilled and grouted soil nail is the most popular nailing technique and commonly used in practice because of its higher pullout resistance compared to the driven soil nail (Franzen, 1998; Lazarte et al., 2003; Kim et al., 2014; Zhou, 2015).

Wang et al. (2017a) noted that the injection of high pressure grout directly into the pre-drilled holes may initiate unintended fractures into the surrounding soil as well as cause it to exhibit pressure filtration (i.e., permeation of water from the grout), which may result in uncontrolled grout injection and contamination of the surrounding soil. To mitigate these issues, Wang et al. (2017a) proposed a compaction-grouted soil nail system in which a latex balloon attached to the soil nail was used to control the injection of the pressurized grout and consequently to compact the surrounding soil. Unlike the drilled and grouted soil nails, a small size pre-drilled hole is required for the installation of the newly developed compaction-grouted soil nail. It is thus also a drilled and grouted soil nail.

However, Su et al. (2010) reported that the pre-drilling into the ground altered the effect of the overburden pressure on the installed soil nail and following the drilling process, thus the overburden pressure (i.e., effective vertical stress) applied on the compacted soil decreased to almost zero at the nail/soil interface due to the stress release at the top of the hole. Consequently, the normal stress acting around the grouted nail drops, which ultimately reduces the pullout resistance of the grouted nail. Therefore, the pullout resistance of the drilled and grouted soil nail completely depends on the acting normal stress around the drilled hole instead of the applied overburden pressure (Su et al. 2008). In addition, Schlosser (1982) observed that the normal stress acting at the nail-soil interface was almost equal to the applied overburden pressure for the driven soil nail, whereas the value of acting normal stress could be very low for the drilled and grouted soil nail and the value remained nearly constant with respect to the soil depth (i.e., overburden pressure).

Traditionally, neat cement grout (w/c = 0.40 to 0.50) is recommended for the grouted soil nail system in which the nail is grouted by gravity or low pressure grouting (Lazarte et al., 2003). However, the cement grout used in compaction (or pressure) grouting exhibits significant pressure filtration, which consequently hampers the flowability and workability of the pressurised grout (Wang et al., 2016; Bezuijen, 2010). On basis of flowability, bond strength, and pressure filtration (Chapter 3, Section 3.4), therefore, it can be said that the application of a cement grout with a w/c ratio of 0.50 used previously by Wang et al. (2017a) for a compaction-grouted soil nail is not a suitable grouting fluid for high pressure grouting. Moreover, the Roads and Maritime Services (RMS) specification (2018) recommends that the grout used for soil nailing applications should have high bleed resistance, low shrinkage and high fluidity. Thus, a special type of additive-mixed cement grout with a water to solid (cement + additive) ratio of 0.30 was introduced in this investigation to conform to the RMS requirements.

In this study, an innovative soil nail (described here as the x-Nail) has been developed in order to study a driven soil nail with a grouting facility (Figure 4.9). The developed soil nail combines the facilities and capabilities of a purely friction driven nail (Franzen, 1998) and a compaction-grouted soil nail (Wang et al., 2017a). The innovative design makes it possible to drive the x-Nail into the ground in-situ with a latex balloon that is used for compaction grouting in order to form a grout bulb at the driven end of the nail. Thus, the newly developed soil nail minimizes the pre-drilling effects at the nail/soil interface and maximizes the compaction of the surrounding soil in two ways: (1) by driving process and (2) by pressure grouting process.

In this work, a physical model was developed in the laboratory to conduct a detailed experimental study on the pullout resistance mechanism of the innovative driven and grouted soil nail, since a laboratory pullout test is considered to be a practical way to investigate the pullout response of a soil nail under different controlled boundary conditions (Zhou, 2015). A detailed description of the sample preparation and testing procedure for the physical model study of this x-Nail system, with and without grouting facility, can be found in Section 4.3 of Chapter 4. In order to investigate the pullout behaviour of the grouted driven nail at different injected grout volumes, a number of fully instrumented pullout tests were performed in sand after injecting the additive-mixed grout at a specified injection rate and controlled volume, using a specially designed large pullout box with driving, grouting and pullout facilities. The soil responses (variations of soil stresses and moisture contents) and the nail-soil interaction were continuously monitored with the installed total earth pressure cells (EPC) and soil moisture sensors (SMS) buried in the compacted sand during the soil compaction, nail driving, grouting and pullout process. The basic layout of the sensors installed around the pre-buried soil nail is illustrated in Figure 4.7. In addition, the driving and pullout forces were recorded with a load cell, and the corresponding displacements were recorded by a linear variable displacement transducer (LVDT) attached to the pullout facility (Figures 4.4 and 4.13). Finally, the performance of the driven and grouted soil was evaluated with respect to the purely frictional driven soil nail. Some preliminary results of this experimental investigation have been published by Bhuiyan et al. (2020a).

7.3 Experimental results

To investigate the effect of injected grout volume on the pullout resistance of the x-Nail, and to compare the performance of the grouted x-Nail with the purely frictional soil nail (i.e., ungrouted x-Nail), a series of five pullout tests were performed on identical unsaturated soil samples having the same dry density (1.50 Mg/m^3), moisture content (3%) and overburden pressure (100 kPa). On the basis of the injected grout volumes, the pullout tests of the x-Nail, with and without grouting, are labelled here as DT1, DT2, DT3, DT4, and DT5 for a grout injection volume of 0 ml (i.e., purely friction driven nail), 170 ml, 220 ml, 270 ml, and 350 ml, respectively. The typical results obtained at different stages of the physical model tests (DT1 and DT2) are presented in detail in the following subsections. A detailed comparison of the results for 5 tests will be reported in the Discussion section.

7.3.1 Compaction process

The soil sample with a water content of approximately 3% was prepared and compacted inside the pullout box in accordance with the procedures outlined in Section 4.3 of Chapter 4. Once the compaction was completed, the moist sand was left undisturbed for approximately 30 minutes to stabilize the moisture contents before the application of overburden pressure (OP). Thus, the soil moisture sensors (SMS) installed at the different locations in the compacted fill register the stable values within the period, as shown in Figure 7.1.

In addition, Figure 7.2 illustrates typical variations of the volumetric water contents (VWC) and dry densities recorded by the SMSs at the different locations of the compacted fill for the test DT2. It can be found that the average volumetric water content and dry density of the prepared soil sample are approximately 0.05 m^3/m^3 (equivalent to 3% gravimetric water content) and 1.50 Mg/m^3, respectively, indicating a relatively homogeneous compacted soil sample.

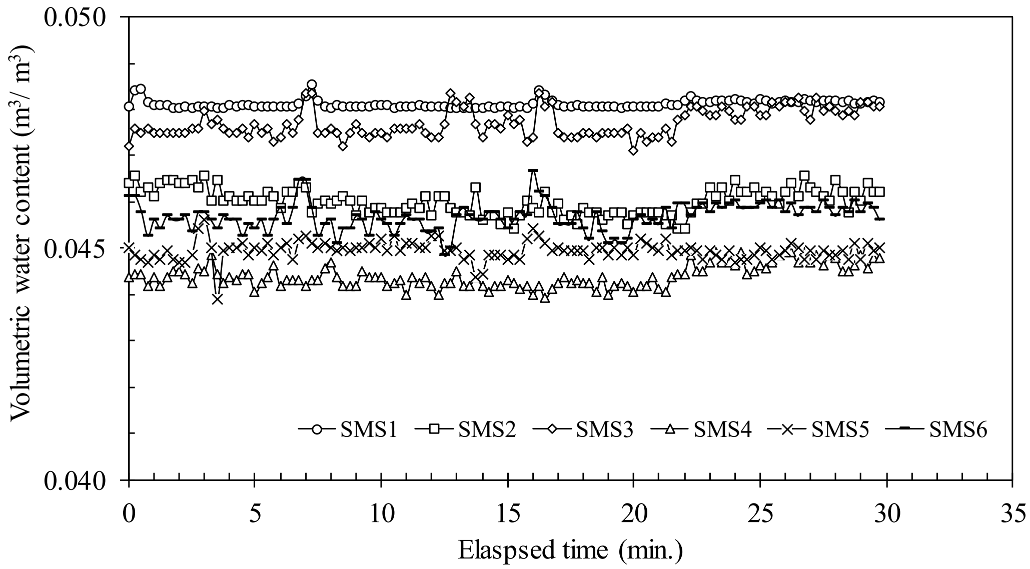

Figure 7.1: Typical fluctuations of volumetric water contents after compaction process for DT2.

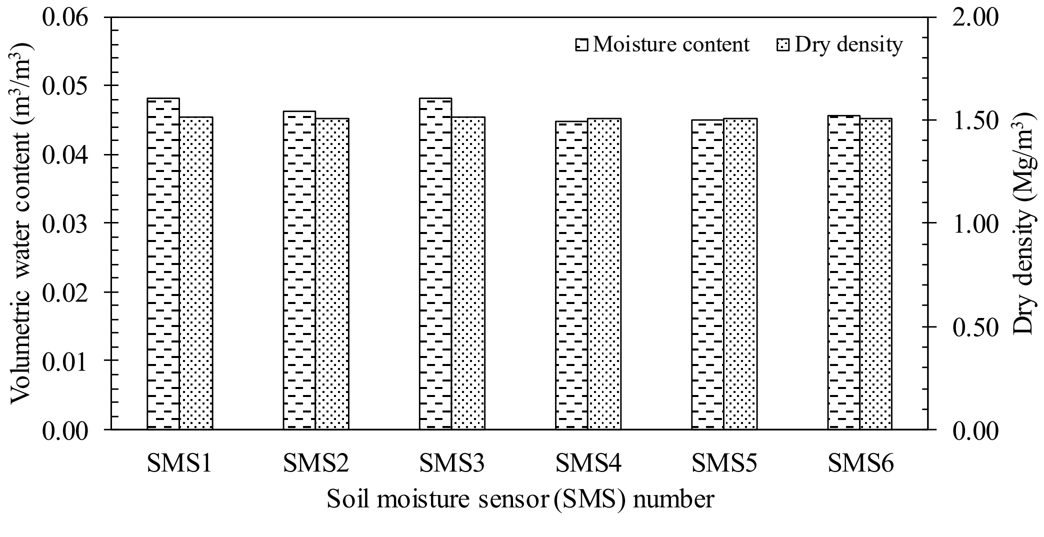

Figure 7.2: Typical variations of volumetric water contents and dry densities in compacted sand for DT2.

7.3.2 Surcharging process

Figure 7.3 illustrates the changes in soil pressures induced on the EPCs located at different positions for an applied overburden pressure (OP) of 100 kPa. The plots of induced soil pressures indicate that the earth pressures measured by the EPCs increased progressively and reached a stable state within 1 hour after application of the overburden pressure. The stabilized soil pressures induced on EPC1, EPC 4 and EPC5, which were installed horizontally to monitor the vertical soil pressure, are nearly in good agreement with the applied overburden pressure of 100 kPa. However, the earth pressures recorded by EPC3 and EPC6 are not consistent with the overburden pressure (OP = 100 kPa), experiencing approximately 10% lower and 15% higher induced earth pressures from the 100 kPa overburden pressure, respectively. It is suspected that these errors (i.e., under- or over-registration) in measured data may have resulted from the placement effects (Garnier et al. 1999) and/or arching and inclusion effects (Bhuiyan et al. 2018b). Furthermore, the horizontal earth pressure measured by EPC2, which was installed vertically facing the sensing area parallel to the nail, as shown in Figure 4.7., are approximately 25 kPa. By contrast, EPC7 and EPC8, which were installed at the mid heights of the front and side walls of the box, respectively, register the lateral earth pressures of approximately 45 kPa, on average. Thus, the coefficient of lateral earth pressure can be estimated to be almost 0.45, which is very close to the Jaky (1944) coefficient earth pressure at rest (K_o = 1- sin Ø) of 0.48 for a friction angle of 31.5°. The lateral earth pressures induced on the vertically installed sensors (EPC2, EPC7, and EPC8) signifies that the installation orientation of the earth pressure cell significantly affects the EPC readings, which is consistent with the findings reported by Garnier et al. (1999).

Figure 7.4 demonstrates the vertical displacements of the compacted fills for all tests during the surcharging process. The settlements are estimated by dividing the volume of the pressurized water injected into a water-filled rubber cushion system, which was measured by a flow meter as described earlier in Chapter 4, by the cross-sectional area of the box. From Figure 7.4, it is found that the soil surface settles gradually with increases in the overburden pressure and quickly reaches a stable value of about 2.5, on average, after roughly 4 minutes once the overburden pressure is applied to a desired value of 100 kPa.

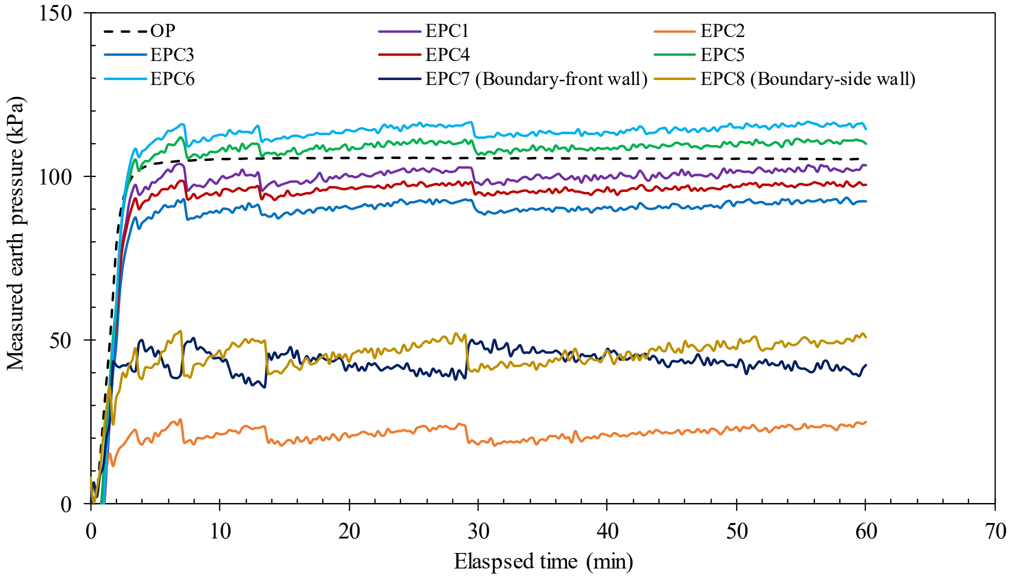

Figure 7.3: Typical variations of induced earth pressure after application of the overburden pressure (OP = 100 kPa) for DT2.

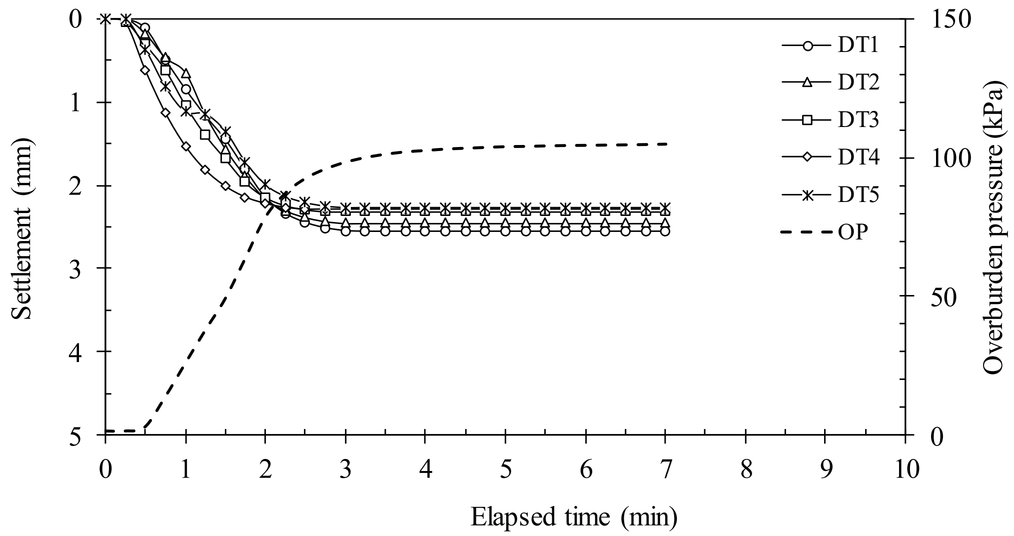

Figure 7.4: Surface settlement during application of the overburden pressure (OP = 100 kPa).

7.3.3 Driving process

The x-Nail was driven into the compacted fill after 1 hour of the application of the overburden pressure. The results obtained during the driving process of the x-Nail are illustrated in Figure 7.5. It indicates the driving force of the nail increases progressively and reaches a maximum force (approximately 7 kN) after a driving displacement of approximately 400 mm. This force remains nearly constant with further advancement of the driven nail. The changes in soil stress states induced by the x-Nail driving process are also plotted in Figure 7.5. It can be seen that the installation of the driven soil nail significantly disturbs the stabilized earth pressures obtained after application of the initial overburden pressure (100 kPa). During the driving process, the horizontal soil pressure induced on EPC2 increases gradually from a stable pressure of approximately 25 kPa to a peak value of approximately 257 kPa, and then drops significantly to a residual value of about 25 kPa after the insertion of the entire soil nail (800 mm long). EPC2 was installed vertically 25 mm below the driven nail with a horizontal distance of 350 mm away from the driving point (i.e., the front wall of the box in Figure 4.7). Interestingly, EPC2 recorded its maximum induced earth pressure at a driving displacement of approximately 253 mm, i.e., before the nail tip reached the location of EPC2, and subsequently the induced pressure dropped abruptly. The measured pressure continued to decrease once the tip of the nail passed the position of EPC2. This type of stress response might be due to compaction of the soil mass in front of the nail tip during the jacking process. EPC4, which was located horizontally 520 mm away from the driving point and EPC1 located 700 mm away from the driving point experienced similar stress behaviour to EPC2. The soil pressures induced on EPC4 and EPC1 rose from the initial stabilized value of 100 kPa to the peak pressures of approximately 500 kPa and 594 kPa, respectively, followed by a rapid drop as the nail tip passed the sensor locations. The other EPCs (especially EPC3, EPC5, and EPC6) positioned 700 mm away from the driving point experienced a gradual rise and then a drop in induced earth pressures during the driving process. The behaviour of EPC3, EPC5, and EPC6 may have resulted from stress redistribution around the soil nail caused by the soil disturbance during the driving process. In addition, it can be found that the peak pressures recorded by EPC3, EPC5 and EPC6 during the driving process were approximately 569 kPa, 435 kPa and 379 kPa respectively, indicating a decrease in the induced soil pressure with increasing vertical distance of the EPC location from the driven nail, as might have been expected. This is consistent with the findings of Sharma et al. (2019), who noted that the increase in induced earth pressure instigated by the nail installation process was negligible at a vertical distance of 230 mm from the nail surface. With respect to EPC8, located at the mid height of the box side wall, the induced pressure increased slowly from a stable pressure of approximately 45 kPa to a peak pressure of approximately 157 kPa at a driving displacement of approximately 672 mm. Subsequently, the increased earth pressure decreased slightly to a residual pressure of 130 kPa, which reflects the compaction of the soil mass caused by driving of the soil nail. The readings of EPC7, which was installed vertically on the front wall of the box at a vertical distance 25 mm from the nail surface (Figure 4.7), remains unchanged during nail installation, except for a small rise at the start of nail driving. The vertical dotted lines in the Figure 7.4 illustrate the positions of the EPCs from the driving point (taken to be 0 mm).

Figure 7.6 illustrates the typical stress responses in the compacted fill after installation of the driven nail. It can be observed that the stable states within the soil mass obtained after 1 hour of application of the overburden pressure (100 kPa) significantly changes from the initial stable values to the final stabilized values, either increasing or decreasing, within a period of 1 hour once the nail insertion is completed. After the driving process, the induced pressures measured by the EPC1, EPC3, EPC4, EPC5, and EPC6 drop from an initial stable value of about 100 kPa, on average, to the final stabilized values of approximately 21 kPa, 14 kPa, 12 kPa, 52 kPa, and 77 kPa, respectively. Interestingly, the drops in induced pressures are higher for the sensors located near the driven nail, i.e., the higher the vertical distance from the nail, the lower the pressure drop. However, in the case of EPC8, the induced soil pressure rose from an initial stabilized pressure (~45 kPa) to a final stable pressure of approximately 130 kPa. In addition, the final stabilized readings measured by the EPC2 and EPC7 after the nail driving are almost equal to the initial stable values obtained before the start of the nail driving.

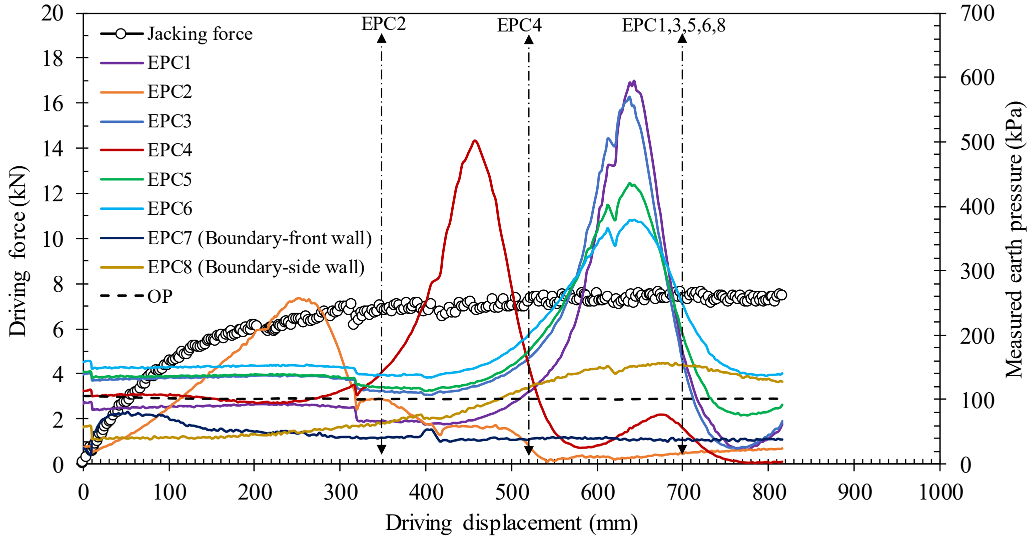

Figure 7.5: Evolution of driving force and measured earth pressures against the driving displacement for DT2 showing the EPC positions (vertical dotted line).

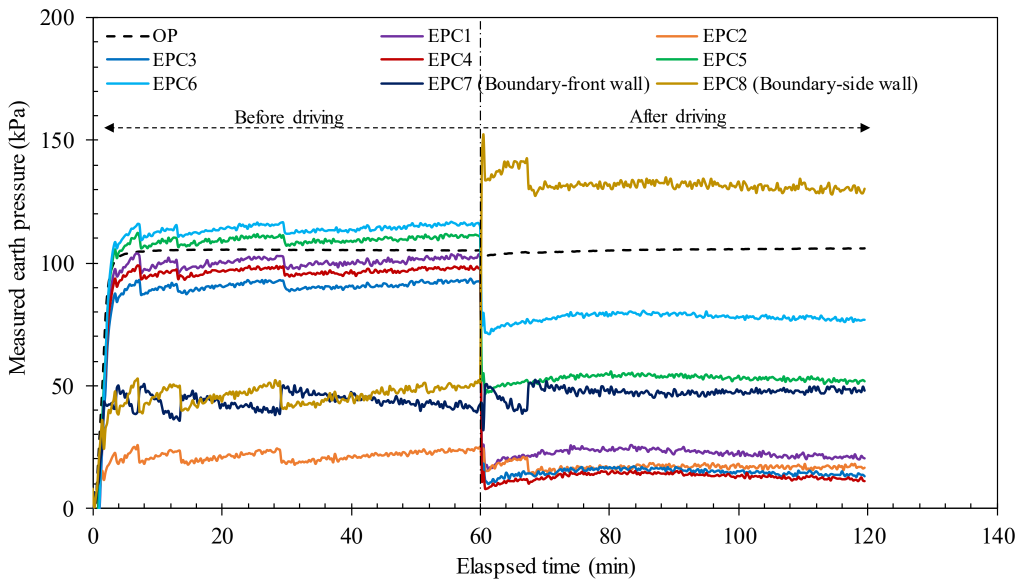

Figure 7.6: Typical changes in soil stress states induced by the nail driving process.

7.3.4 Grouting process

For the grouted x-Nails (DT2, DT3, DT4 and DT5), after 1 hour of installation of the x-Nail the additive-mixed cement grout was injected into the grout bag of the x-Nail at an injection rate of 5.0 L/min by the developed volume-controlled injection pump. The plots presented in Figure 7.7 illustrate typical variations of pressurized grout volumes and the corresponding injection pressures during pressure grouting of the x-Nail (DT2). It can be observed that the injection pressure increases rapidly with increasing injected grout volume and subsequently reaches an ultimate pressure of approximately 1400 kPa as the grout injection entirely stops at a specified injected volume (~170 ml), followed by a gradual drop. This steady drop in injection pressure is expected to occur in the injection pump, since the piston pressure applied to the grout was not maintained as the pressurized injection stopped.

The typical soil stress variations induced by the pressurized grouting are presented in Figure 7.8, which illustrates how grouting significantly increases the induced earth pressures at different locations in the soil mass. It is found that the earth pressures induced on the EPCs (especially, EPC1, EPC3, EPC5, and EPC6) located around the injection points increased nearly instantly and reached their peak values in the first few seconds of the start of grouting. Once the grouting was stopped at an injection volume of approximately 170 ml, the peak pressures dropped gradually and continued to reduce over time, and then ultimately reached their residual pressures after approximately 3 hours. During the pressure grouting process, for an injection pressure of about 1400 kPa, the vertical earth pressures induced on EPC1 and EPC3, positioned vertically 50 mm away from the injection points, increased sharply from a stabilized value of approximately 34 kPa, on average, obtained after the driving process (Figure 7.6) to the peak pressures of approximately 562 kPa and 500 kPa, respectively, and then decrease gradually over time to the residual values of about 65 kPa and 50 kPa, respectively, once the grouting was stopped immediately after injecting the desired amount of grout (~170 ml). Similarly, for EPC5 and EPC6, located vertically100 mm and 150 mm away from the injection points, the induced vertical soil pressures increase abruptly from the stable values of approximately 74 kPa and 129 kPa to the peak values of about 439 kPa and 411 kPa, followed by a steady drop to the residual pressures of roughly 101 kPa and 153 kPa, respectively. The peak pressure readings at the EPC3, EPC5, and EPC6 locations indicate that the induced soil pressures decreased virtually linearly with the increment of the distance from the injection points, consistent with the soil responses induced by the nail driving process as described above. The decrease in induced soil pressure with increasing distance from the injection point is consistent with the results reported previously by Wang et al. (2017a) for a compaction-grouted soil nail. With respect to EPC2, EPC4, and EPC7, it is found that the induced soil pressures increase slightly and remain constant over time, indicating insignificant compaction of soil mass in the longitudinal direction for the injected grout volume. However, for EPC8, the measured earth pressure increased quickly from a stabilized value of approximately 130 kPa to a peak value of about 192 kPa and then finally reduced steadily to the stabilized value (~130 kPa). Thus, it might be argued that the compaction effects induced by the pressurized grouting are relatively localized.

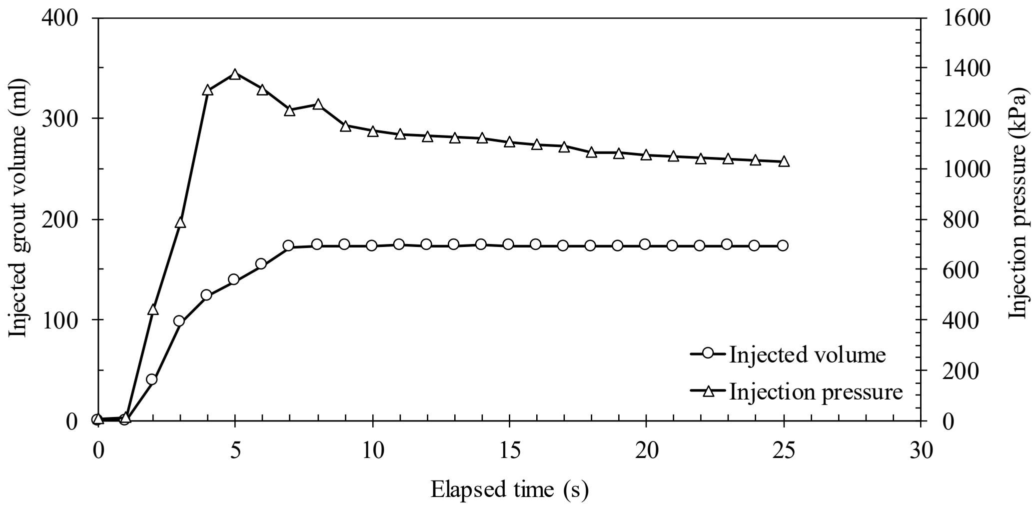

Figure 7.7: Typical variations of injection pressure and injected grout volume over the grouting time for an injection rate of 5.0 L/min (DT2).

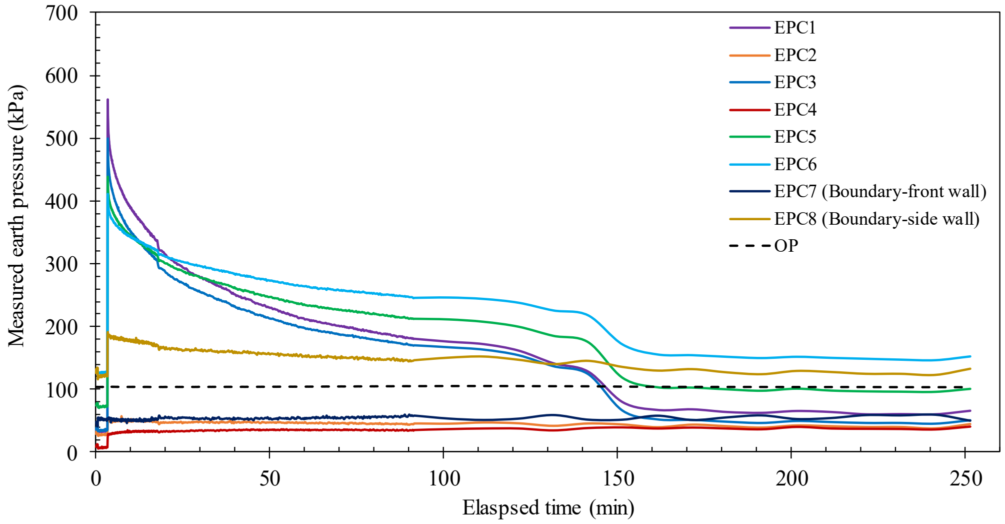

Figure 7.8: Typical changes in earth pressures induced by the pressure grouting process for DT2.

7.3.5 Pullout process

Once the insertion of the driven soil nail was completed, for the test DT1, a pullout test was conducted after 1 hour to evaluate the purely frictional capacity of the ungrouted x-Nail. Figure 7.9 illustrates the typical variations of pullout force against the pullout displacement of the purely frictional soil nail. The pullout force/pullout displacement plot shows that the pullout force increases steadily with the advancement of the pullout displacement and reaches a stable value of approximately 1.00 kN, on average, which is almost equal to the estimated pullout force of 1.04 kN calculated by the simplified analytical method proposed by Jewell (1990). Figure 7.9 also plots the variation of induced earth pressures recorded by the EPCs during the pullout process of the driven, purely frictional soil nail. For EPC1 and EPC3 installed around the injection points, with a vertical distance of 50 mm from the nail, the pressure readings initially increase insignificantly from a zero pressure to a peak value of approximately 50 kPa after a pullout displacement of approximately 60 mm. Subsequently, the readings drop gradually to a residual value of approximately 25 kPa, on average, at the end of the pullout process (100 mm displacement). By contrast, the earth pressures induced on EPC2, EPC4, EPC5, EPC6, EPC7, and EPC8 remain almost constant over the pullout displacement of 100 mm, apart from an insignificant rise and drop at the start of nail pulling.

In contrast to the purely frictional driven nail (DT1), the driven and grouted x-Nails (DT2, DT3, DT4, and DT5) were pulled out after 7 days of curing of the injected additive-mixed cement grout, allowing the grout to develop a compressive strength of about 90

MPa. Figure 7.10 presents the typical curves of the pullout force and the changes in soil stresses at various locations recorded during the pullout of the grouted x-Nail (DT2). The pullout force/displacement curve in this figure indicates that the pullout force of the grouted driven nail increases quickly at the start of the pulling and subsequently the force continues to rise, but at a slower rate, with increasing pullout displacement. The pullout force finally reaches a maximum value of approximately 10.0 kN at about 100 mm of pullout displacement. This is consistent with the results of Wang et al. (2017b), who reported that the compaction-grouted soil nail exhibited its maximum pullout force at a pullout displacement of 100 mm. For an injected grout volume of approximately 170 ml, it is found that the induced pressures on most EPCs (e.g., EPC1, EPC3, EPC5, and EPC6), which were installed around the injection points, increases slightly from the stabilized values (Figure 7.8) to the peak values after a small amount of displacement (approximately 7 mm) and then decreases gradually as the pullout displacement increased (Figure 7.10). EPC1, EPC3, and EPC5 particularly recorded zero induced pressure at about 100 mm pullout displacement. This drop in induced pressures may be related to the stress relaxation on the EPCs, which might have resulted from the inward movement of the surrounding soil of the grout bulb (hardened grout) in the compacted fill as the grouted nail was pulled out. In the case of EPC6, it can be observed that the induced earth pressure reduces gradually from the initial value of about 136 kPa to 28 kPa over the pullout displacement of 100 mm. Similarly, the lateral earth pressure induced on EPC8 slightly reduces from about 120 kPa to 73 kPa during the pullout process. This may have resulted from stress redistribution occurring in the soil mass due to the movement of the grout bulb. The data recorded by EPC4 increases significantly and reaches a peak value of approximately 386 kPa at a displacement of about 55 mm, followed by a gradual drop to a residual value of about 150 kPa after a displacement of 100 mm. This rise and drop in induced vertical soil stress may be attributed to the compaction and displacement, respectively, of the soil situated in front of EPC4, consistent with the similar stress responses observed by Wang et al. (2017b) for a compaction-grouted soil nail. By contrast, the earth pressure induced on EPC2 increases steadily from a stabilized value of about 40 kPa to 174 kPa at about 100 mm displacement. However, the readings of EPC7 slightly increase from an initial value of about 50 kPa to a maximum value of approximately 100 kPa at the end of pullout displacement.

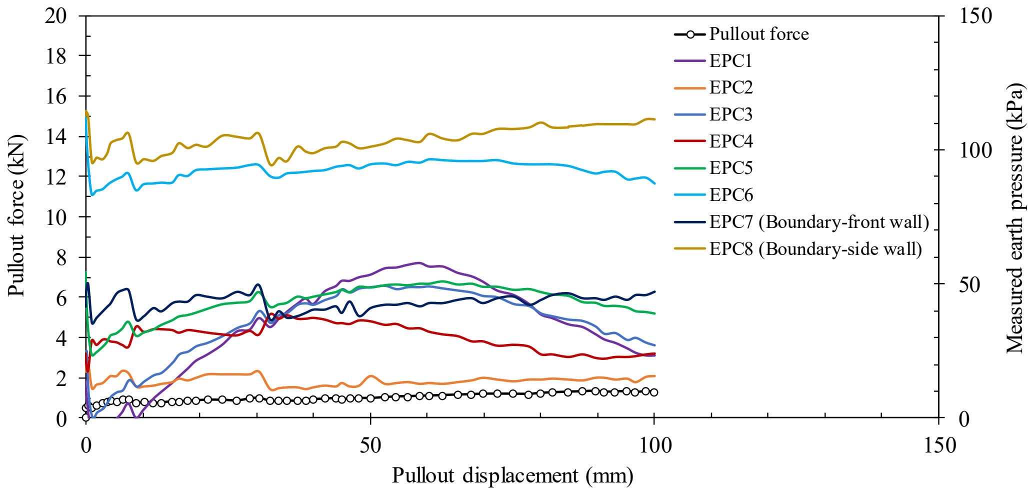

Figure 7.9: Pullout force and measured earth pressures against the pullout displacement for purely frictional driven nail (DT1).

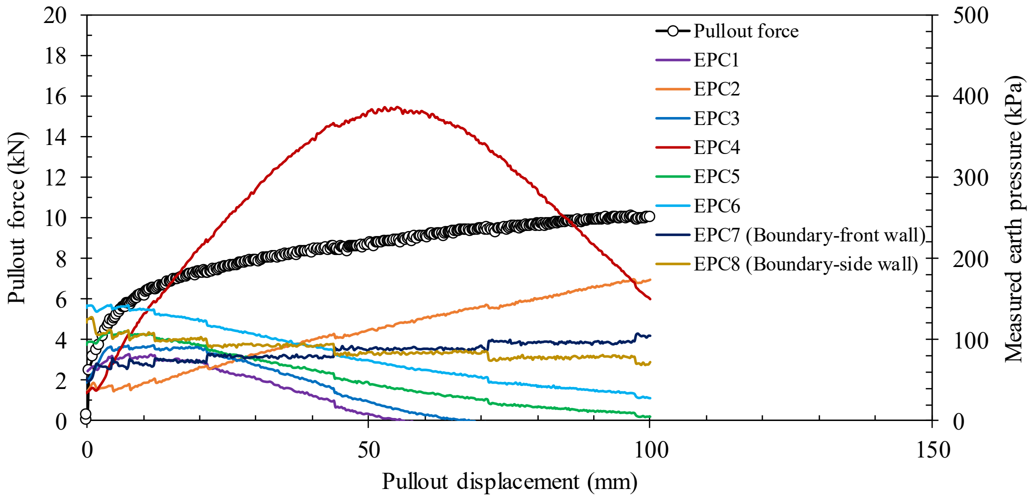

Figure 7.10: Pullout force and measured earth pressures against the pullout displacement for DT2.

7.4 Discussion

The laboratory pullout test is considered to be a promising technique to examine the pullout resistance of a soil nail under different controlled conditions. In this investigation, five pullout tests were conducted to identify the performance of the innovative driven soil nail with respect to the frictional driven soil (conventional driven nail) under identical sample conditions, with the dry density of 1.50 Mg/m^3, moisture content of 3%, and overburden pressure of 100 kPa.

Figure 7.11 presents plots of the driving (installation) force versus the driving displacement for different driving speeds (installation rates) for all tests. The plots compare the installation forces of the innovative driven soil nails (the x-Nail) inserted at different installation rates, or driving speeds, ranging from 10-15 mm/min. Generally, for all tests, it is seen that the driving force of the x-Nail increases gradually and first reaches a maximum value varying from approximately 6 kN to 7 kN, on average, at a driving displacement of approximately 400 mm. After that, the maximum driving force remains approximately constant with increasing driving displacement. Since the tests were conducted on identical soil samples with an overburden pressure of 100 kPa, the plots presented in Figure 7.11 indicate that the installation rates do not show any significant influence on the driving resistance, at least over the relatively narrow range of speeds investigated here. These results are in good agreement with the findings reported by Sharma et al. (2019) for conventional driven soil nails, who concluded that the installation force of a driven soil nail was not affected by the driving speed, and the force was directly related to the inserted surface area of the nail and the applied overburden pressure.

In this study, the pressurized grout was injected into the balloon through the nail at a specified injection rate (5.0 L/min) to expedite the grouting with the sufficient injection pressure under controlled volume conditions. Figure 7.12 compares the variations of the injected grouted volume and the corresponding injection pressure for the grouted x-Nails (DT2-DT5) over the grouting period. It was found that the injection pressures for all tests showed more or less similar behaviour during the grouting process, rapidly reaching an ultimate pressure (~1400 kPa), followed by a gradual drop over the elapsed time. This demonstrates that the grout was successfully injected by controlling the injection volume at a constant injection pressure of approximately 1400 kPa. However, in a previous study, Bhuiyan et al. (2019) found that the volume of the injected grout predominantly influenced the pullout resistance of the grouted soil nail compared to the grout injection pressure.

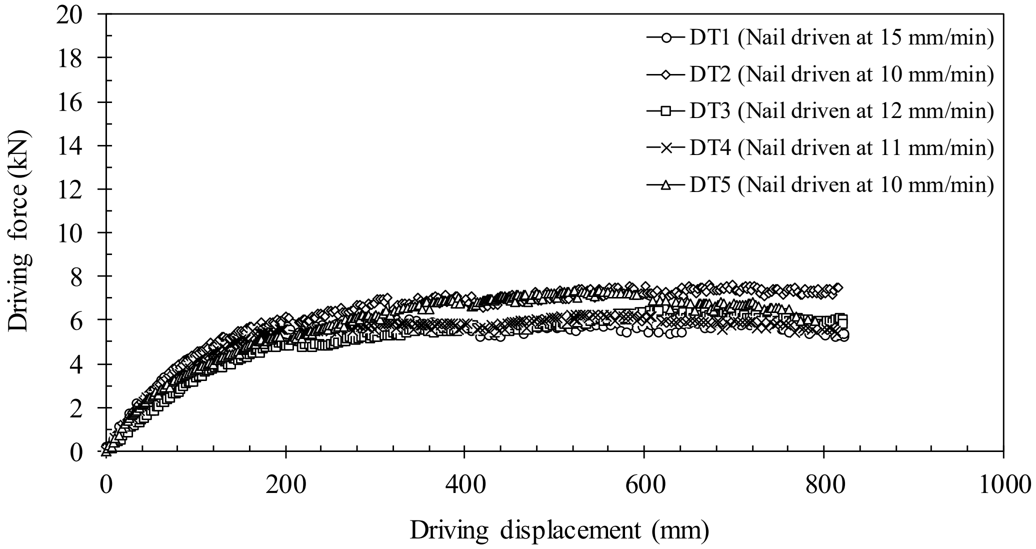

Figure 7.11: Driving force versus driving displacement for the x-Nail at different installation rates.

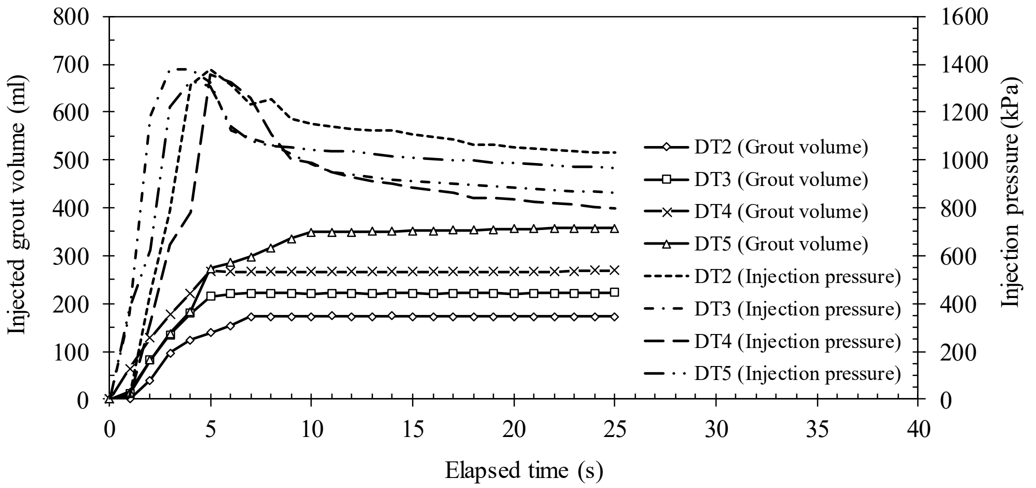

Figure 7.12: Evolution of injected grout volume and injection pressure for tests T2-T5.

Figure 7.13 compares the changes in vertical soil pressure on EPC1, which was installed at a horizontal distance of 700 mm from the front box wall and at a vertical distance of 50 mm from the driven nail surface, induced by the different processes (particularly driving, grouting, and pulling out processes) of physical model tests. It can be found the insertion of the driven nail significantly increased the vertical soil stress induced on EPC1 from a stable value of approximately 100 kPa to an average peak value of about 560 kPa and then dropped significantly to a lower residual value than the applied surcharge pressure (100 kPa) after the installation of the entire nail. This decrease in induced earth pressure might have resulted from stress redistribution initiated by the soil disturbance during the nail installation process (Figure 7.5). Sharma et al. (2019) observed that installation of a driven nail into a compacted soil mass densified the soil surrounding the nail, which in turn increased the normal stress (i.e., confining stress) acting at the nail-soil interface. Consequently, the driven soil nail (purely frictional nail) provided higher pullout forces compared with the pre-buried frictional nail, which was placed in the soil mass during the compaction process of the soil. In addition, Bhuiyan et al. (2020a) demonstrated that the driven and grouted soil nail exhibited approximately 12% higher pullout force compared with the pre-buried grouted nail for an injected grout volume of around 500 ml.

During the grouting process, it was also found that the vertical pressure induced on EPC1 increased rapidly from an average value of about 21 kPa to an average peak value of 626 kPa (Figure 7.13) and subsequently decreased to a lower value (~37 kPa) over the period. Interestingly, for an ultimate injection pressure of approximately 1400 kPa (Figure 7.12), the peak earth pressure recorded by EPC1 for all the grouted soil nails was less than 50% of the applied injection pressure. In this study, the injection pressure was only maintained for a very short period of time, ranging from 3-6 seconds, as illustrated in Figure 7.12, and the injection pump was stopped within a few seconds once the desired amount of grout was injected. Consequently, it resulted in a pressure loss in the injection pump system due to the relaxation of the piston pressure applied to the injecting grout (Figure 7.12). This quick pressure loss in the pump system might be the reason for the relatively low induced earth pressure recorded by EPC1. In addition, once the pressurized grouting was stopped after injection of a specified volume of grout, a ball valve (shut off valve) installed on the grout-injection tube near the soil nail (Figure 4.14) was closed immediately to prevent the back flow of the pressurized grout injected into the balloon as well as to minimize the injection pressure developed in the compacted fill. Therefore, it is believed that the gradual drop in the peak induced earth pressure (Figures 7.8 and 7.13) following the grouting may have resulted from the dissipation of the injection pressure into the compacted soil over time. This is consistent with the findings of Wang et al. (2017a, b), who noted that the induced earth pressure around the injection points decreased shortly after the compaction grouting. They also claimed that the pressurized grouting significantly compacted the surrounding soil and thus increased the dry density surrounding the injection points.

Figure 7.13 also illustrates a gradual rise and drop in induced soil pressure measured by EPC1 during the pulling out of the grouted and ungrouted x-Nails. It can be seen that the stabilized soil pressure induced on EPC1 after grouting remains almost constant over the curing period of 7 days for the grouted nails. This possibly indicates that the grout bulb formed after curing of the additive-mixed cement grout used here is not significantly affected by the grout shrinkage effects, which could otherwise instigate a decrease in induced soil pressure at the soil-grout interface, as suspected. In addition, the induced pressure readings of EPC1 for all tests demonstrate that the densification or compaction effects instigated by the driving and pressure grouting processes are quite localized. As mentioned earlier, it is suspected that the increase in the soil stress induced by the driving and grouting processes is redistributed into the compacted soil over time and, consequently, the ultimate confining stresses (normal stresses) acting around the nails at the beginning of the pullout tests are significantly lower than the applied OP (100 kPa). Moreover, it can be seen that the confining stresses acting around the nails increased slightly during the pullout process and reached the peak earth pressures of approximately 58kPa, 83 kPa, 126 kPa, 150 kPa, and 161 kPa for test DT1, DT2, DT3, DT4, and DT5, respectively, followed by a gradual drop to almost zero pressure after approximately 100 mm pullout displacement. This drop in the induced pressures is expected to occur due to the formation of a cavity around the grout bulb (hardened grout) in the compacted fill as the grouted nail is withdrawn and, consequently, the soil stresses induced on EPC1 are released. Figure 7.14 illustrates the grouted x-Nail with a typical grout bulb. During the pullout process, interestingly, it is seen that the confining stresses at the nail-soil interface increase virtually linearly with the increment of the injected grout volumes. By increasing the injected grouted volumes into the latex balloon, the grout bulbs are expected to enlarge in diameter by displacing and compacting the soil surrounding the injection points, thus densifying the surrounding soil more (Wang et al. 2017a). Therefore, it is believed that the densified soil in the vicinity of the nail has the possibility of exhibiting dilatancy behaviour (i.e., the increase in soil volume as shear strain is mobilized), as reported by Milligan and Tei (1998). Hence, the confining stress mobilized at the nail-soil interface is expected to be increased by constrained dilatancy of the soil. This increase in normal stress is consistent with the findings reported by a number of researchers (Luo et al. 2000; Chai and Hayashi 2005; Su et al. 2008), who demonstrated that normal stress acting around the nail increased due to constrained dilatancy of the granular soils.

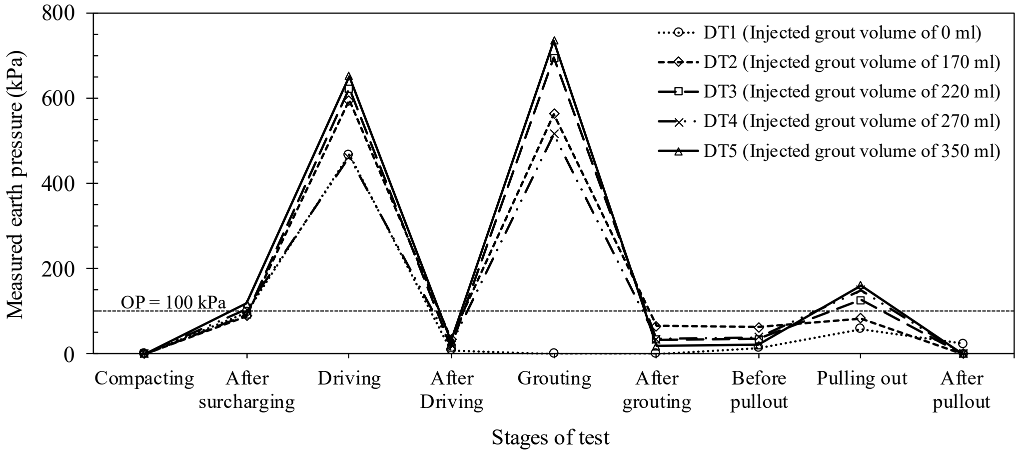

Figure 7.13: Comparison of vertical earth pressures induced on EPC1 at different stages of the tests showing overburden pressure line (horizontal dotted line).

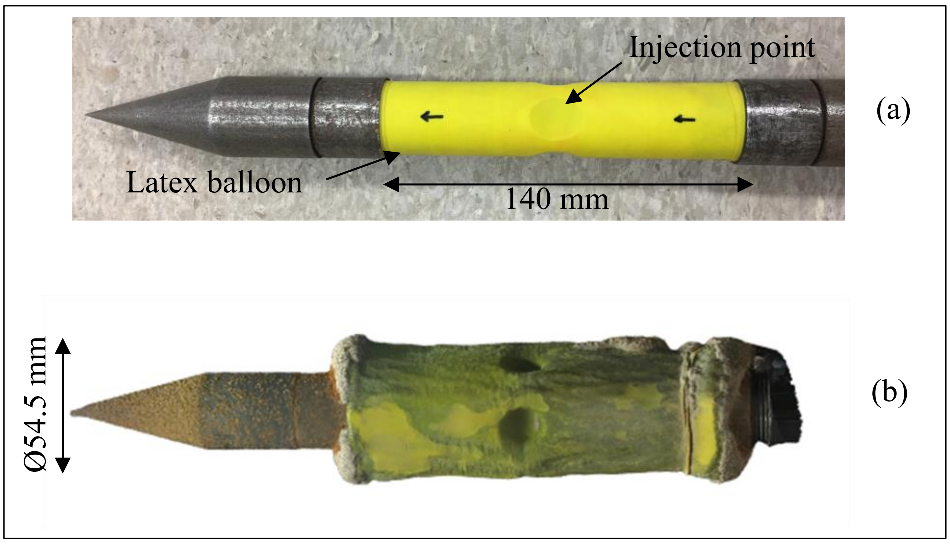

Figure 7.14: Photograph of (a) the x-Nail with grouting facility and (b) the grouted nail showing 3D grout bulb.

In addition, a comparison of pullout forces for the driven soil nails with and without grouting is illustrated in Figure 7.15. From the load-displacement plots presented in Figure 7.15, it can be observed that the pullout force of the ungrouted x-Nail (i.e., purely frictional driven nail) increases rapidly to a maximum value of only about 1.0 kN within the first few millimetres of nail displacement, and then remains almost constant up to the end of the pullout process. This indicates that the ungrouted x-Nail behaves as a conventional driven soil nail (i.e., purely frictional soil nail) in which the pullout resistance results totally from the frictional resistance developed at the nail-soil interface (Franzen, 1998; Junaiden et al., 2004). This finding is consistent with the experimental results reported by Sharma et al. (2019) for a conventional driven soil nail. By contrast, for the grouted x-Nails, the pullout force increases significantly in the first few millimetres of nail displacement and reaches a maximum value after a significant pullout displacement (~100 mm). It is found that the pullout capacity is higher (~19.0 kN) for the test DT5 with an injected grout volume of 350 ml, followed by the test DT4 (~16.5 kN), DT3 (~13.0 kN), and DT2 (~10.0 kN) with injected grout volumes of 270 ml, 220 ml, and 170 ml, respectively. This indicates that the pullout forces of the grouted x-Nails increase almost linearly with the increment of the injected grout volume. This is consistent with the experimental results reported by Bhuiyan et al. (2019), who claimed that the pullout resistance of the compaction-grouted soil nail was a function of the injected grout volume, i.e., the higher the injected grout volume, the higher the pullout resistance. Table 7.1 summarizes the maximum pullout capacities and the corresponding average grout bulb sizes for the x-Nails where the average bulb length was approximately 144 mm.

By comparing the pullout forces of the grouted x-Nails with respect to the purely frictional nail (Table 7.1), it is found that more than 90% of the pullout force is contributed by the expanded grout bulb, which provides the end bearing resistance. Figure 7.16 shows a detailed comparison between the frictional and end bearing resistances for all tests. It can be observed that approximately 10% of pullout force is resisted by the frictional resistance for the test T2, followed by the test T3 (8%), T4 (6%), and T5 (5%), indicating the contribution of the interface frictional resistance to the pullout force becomes negligible with increasing grout volume. These findings are consistent with the numerical results of Ye et al. (2017), who reported that almost 80% of the pullout force of a compaction-grouted (pre-buried) soil nail was resisted by its expanded grout bulb. The grout bulb diameters presented in Figure 7.17 demonstrate that the end bearing resistance of the driven and grouted soil nail increases almost linearly with the increment of the bulb diameter (i.e., increasing grout volume). Hence, it may reasonably be deduced the grouted x-Nail fundamentally acts as an anchor, where the end bearing resistance prevails, instead of as a purely frictional soil nail. From Table 1, it can also be observed that the grouted x-Nail exhibited approximately 1800% higher pullout capacity compared with the conventional driven nail for the test T5, followed by about 1550% (T4), 1200% (T3), and 900% (T2). The high pullout capacity of the grouted x-Nail probably resulted from the end bearing resistance of the grouted section, as previously described, but also possibly from densification of the soil mass immediately surrounding the soil nail during driving, which in turn would have increased the effective normal stress acting on the nail, as found by Sharma et al. (2019).

Moreover, for the grouted x-Nails, the pullout force/displacement plots presented in Figure 7.15 indicate the pullout force exhibited displacement-hardening behaviour after a rapid increase without any yield point. The grouted x-Nail is expected to experience this phenomenon since it behaves as an anchor, as described earlier. Thus, the soil located in front of the grout bulb provides a substantial amount of passive resistance to the grouted x-Nail. Hsu and Liao (1998) reported that the pullout resistance of a cylindrical anchor embedded at a depth (distance between the anchor's top edge and the ground surface) of about 7 to 8 times the anchor diameter, or greater, demonstrates the hardening behaviour. Consequently, the compaction-grouted soil nail (Wang et al., 2017a, b) and screw soil nail (Tokhi et al., 2017; Sharma et al., 2019) typically display the hardening behaviour, which is ruled by the end bearing. Due to the substantial end bearing resistance of the grouted x-Nail, it is expected that the newly developed nail can be a promising alternative for in-situ soil reinforcement and it is also capable of withstanding a relatively large displacement before failure.

Table 7.1: Comparison of the pullout capacity of the x-Nails.

Test number	Bulb dia. (mm)	Pullout force (kN)	Frictional resistance (kN)	End bearing resistance (kN)
DT1	N/A	1.0	1.0	0.0
DT2	44.0	10.0	1.0	9.0
DT3	48.0	13.0	1.0	12.0
DT4	51.0	16.5	1.0	15.5
DT5	54.5	19.0	1.0	18.0

Note: N/A = not available.

Interestingly, for an injection pressure of about 1400 kPa (Figure 7.12), it was found the pullout resistance of the driven and grouted soil nails increased with increasing injected grouted volume (Figure 7.15). However, Wang et al. (2017a) reported an incremental relationship between the injection pressure and the corresponding pullout resistance for a compaction-grouted (pre-buried) soil nail. They adopted a pressure-controlled injection system, which was unable to control the volume of the injected grout for a specified injection pressure. Hence, from the plots presented in Figures 7.12, 7.15, and 7.17, it can be claimed that the pullout capacity of the compaction-grouted soil nail is directly and proportionally related to the volume of the injected grout rather than the injection pressure, which might have an indirect influence on this anchor-type nail.

The changes in induced earth pressure recorded by EPC2 during the pullout process for all tests are shown in Figure 7.18. Note that EPC2 was installed vertically with a vertical distance of 50 mm from the nail and a horizontal distance of 350 mm from the injection point in order to measure the induced horizontal soil pressure in front of the expanded grout bulb during the pulling out of a nail. For the grouted x-Nail with an injected grout volume of about 350 ml (DT5), it is found that the induced soil pressure on EPC2 increases gradually from an initial average value (~30 kPa) to a maximum value (~395 kPa) at approximately 100 mm of pullout displacement, whereas, for the test DT1, the induced soil pressure measured by EPC2 is virtually constant over the pullout period. The readings of EPC2 for the DT2, DT3, and DT4 exhibit similar behaviour to the test T5, increasing to a maximum pressure after a displacement of 100 mm. However, the maximum induced pressures on EPC2 were approximately 174 kPa, 195 kPa, and 212 kPa for the injected grout volumes of approximately 170 ml (T2), 220 ml (T3), and 270 ml (T4), respectively. The increase in the horizontal earth pressure induced on EPC2 possibly results from the passive resistance of the soil located in front of the grout bulb mobilized as the grouted nail is withdrawn. These findings confirm that the grouted x-Nails experience a significant amount of end bearing resistance compared with the purely frictional soil nail. Based on the induced horizontal pressure readings of EPC2, it can be concluded that the larger diameter grout bulb (DT5, diameter of 54.5 mm) provides much higher bearing resistance compared to the small diameter grout bulb (DT2, diameter of 44 mm), consistent with the results presented in Figure 7.17.

Figure 7.19 illustrates the variations of induced lateral earth pressure on EPC7, mounted vertically on the box front wall 25 mm below the nail surface, for all tests. The changes in lateral earth pressure induced on EPC7 with displacement illustrates more or less a similar pattern to the variations of horizontal earth pressure induced on EPC2 presented in Figure 7.18. Clearly, Figure 7.19 demonstrates that the induced lateral earth pressures increase slightly from an initial value to a maximum value after a pullout displacement of 100 mm for the grouted x-Nails. However, in the case of the purely frictional soil nail (T1), the lateral earth pressure (~45 kPa) induced on EPC7 remains almost constant during the pullout process, indicating no boundary effects on the measured earth pressures. It can be observed that the maximum induced pressures for the test DT2, DT3, DT4, and DT5 are approximately 104 kPa, 128 kPa, 137 kPa, and 167 kPa, respectively. This indicates that the boundary effects are influenced by the injected grout volume (i.e., the size of grout bulb); with an increased grout bulb diameter, the influence of boundary effects increases on EPC8.

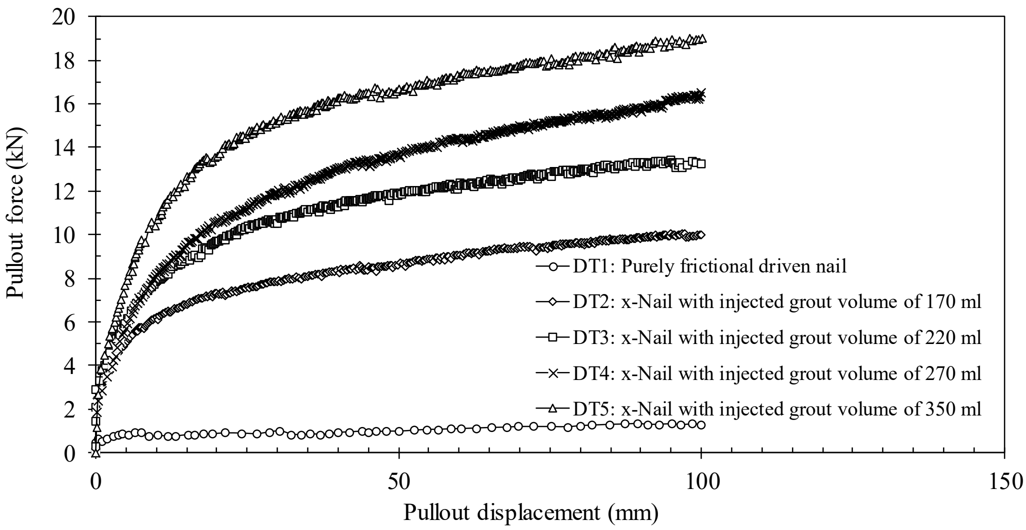

Figure 7.15: Pullout force versus displacement for the x-Nails.

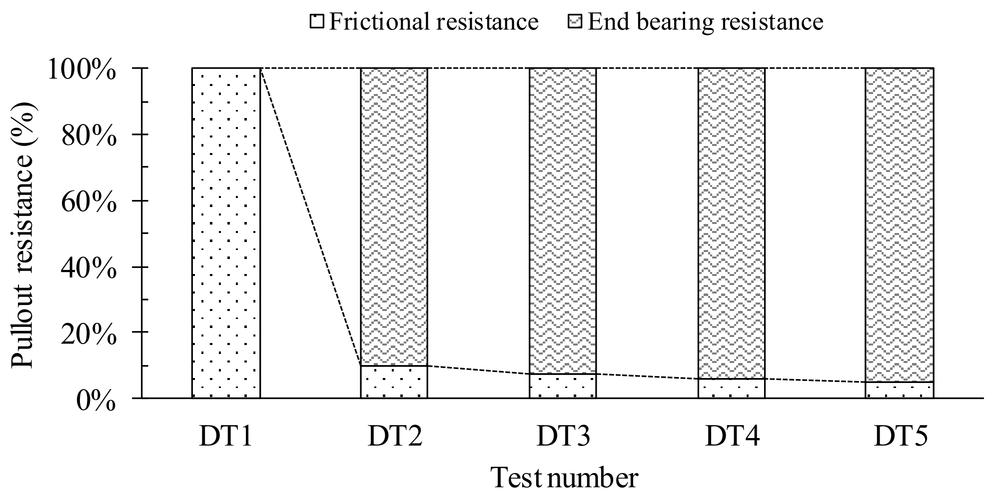

Figure 7.16: Percentage of pullout force resisted by the frictional and end bearing resistance for the x-Nails.

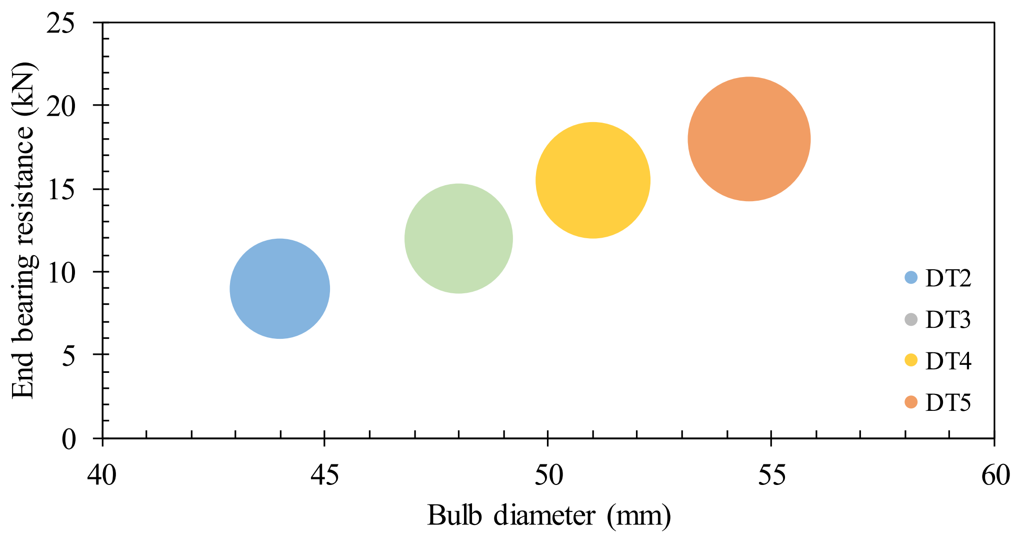

Figure 7.17: End bearing resistance versus bulb diameter for the grouted x-Nails.

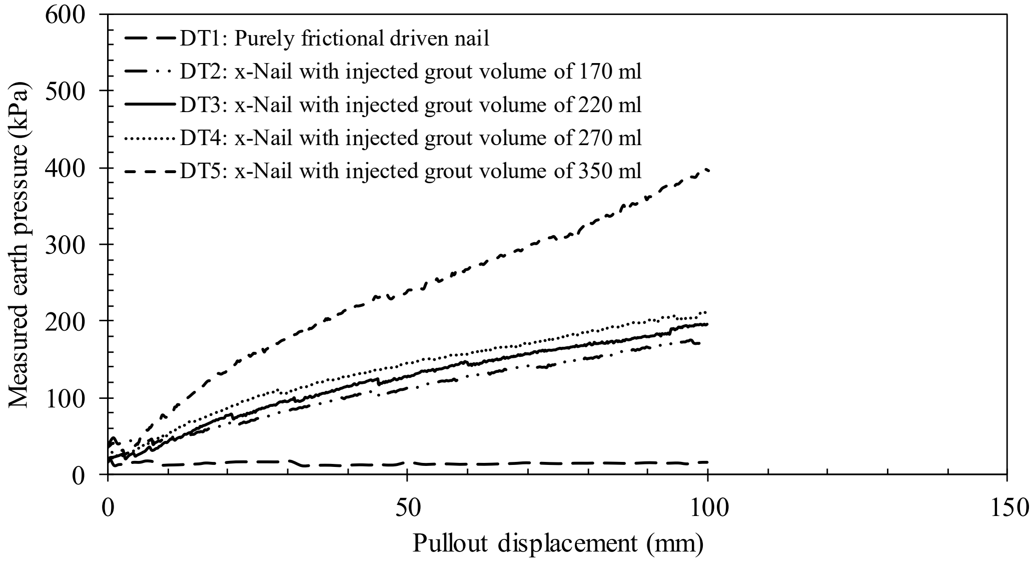

Figure 7.18: Evolution of earth pressure induced on EPC2 during the pullout process.

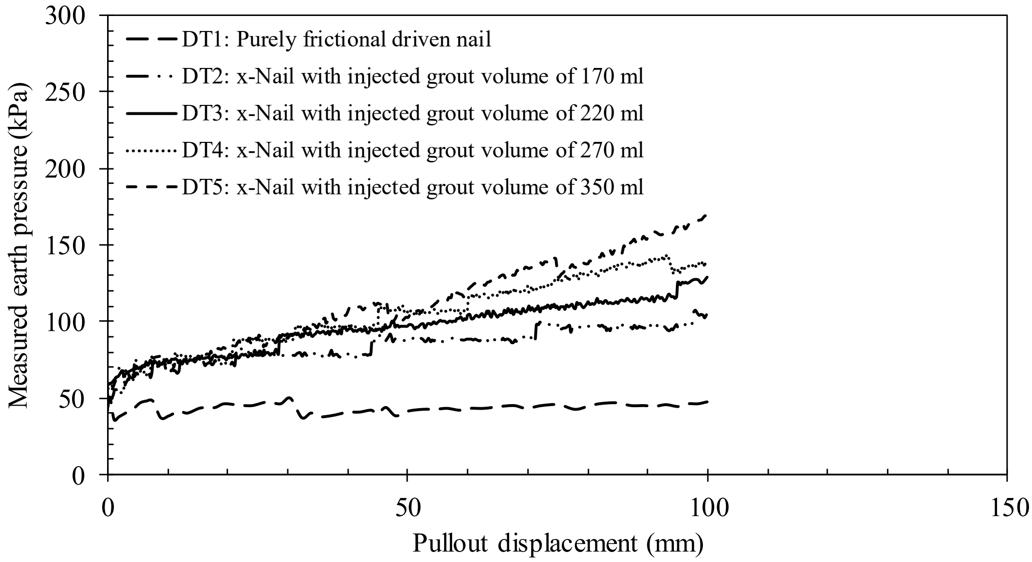

Figure 7.19: Evolution of earth pressure induced on EPC7 during the pullout process.

7.5 Concluding remarks

In this study, an innovative soil nail (the x-Nail) was designed and developed, which combines the facilities and capabilities of a driven nail and a compaction-grouted soil nail. The innovative design makes the x-Nail possible to drive into the soil with a latex balloon that is used for compaction grouting in order to form a grout bulb at the driven end of the nail to improve its pullout resistance. To quantify the performance of the newly developed soil nail with respect to the driven nail, a series of fully instrumented physical model tests were conducted under identical sample conditions, with a dry density of 1.50 Mg/m3, moisture content of 3%, and overburden pressure of 100 kPa. In addition, a special type of additive-mixed cement was used for pressurised grouting in this investigation because of its zero bleeding, low shrinkage and high fluidity. The following conclusions can be drawn on the basis of the experimental results obtained from this comprehensive physical model study:

- The additive applied into the cementitious grout (w/c = 0.32) decreases its viscosity significantly, which ultimately transforms the neat cement grout from a low flow grout to an ultra-high flow grout. The Marsh funnel viscosity of the neat cement grout with a w/c ratio of 0.5 is almost 2 times that of the additive-mixed cement grout (w/c = 0.32), while the density of the cement grout with an additive is found to be 1.15 times of that of the neat cement grout. The constant induced soil pressure around the grout bulb over the curing period of 7 days possibly indicates that the additive–mixed cement grout used in this investigation is not significantly affected by the grout shrinkage effects. Thus, the additive-mixed cement can be used in pressure-grouted soil nailing systems as an alternative to the traditionally used neat cement grout due to its high fluidity, low shrinkage and high compressive strength.
- The pullout system developed for this apparatus is a “two-in-one” system, which combines the driving and pulling out facilities for a soil nail. The nail driving process significantly disturbs and compacts the soil surrounding the driven nail. In addition, the driving force of a driven nail is not affected by the driving speed (installation rate).
- Pullout capacity of the grouted x-Nail is much higher compared with the conventional driven (purely frictional) soil nail. The pullout capacity of the

grouted driven nail increases almost linearly with increases in the injected grout volume (i.e., the grout bulb size). For injected grout volumes of about 480 ml, 400 ml, 350 ml, and 300 ml, the pullout forces of the grouted x-Nails are found to be almost 19, 16.5, 13, and 10 times, respectively, that of the ungrouted x-Nail (i.e., purely frictional nail).

- Pullout force of the grouted nail is directly and proportionally related to the diameter of the expanded grout bulb. The grout bulb provides a significant amount of end bearing resistance that results from the passive resistance of the soil situated in front of the bulb. Nearly more than 90% of pullout force is resisted by the expanded grout bulb and the end bearing resistance increases with increasing grout bulb diameter, i.e., the larger the bulb diameter, the higher the pullout resistance. Thus, the driven and grouted nail acts as an anchor instead of a frictional nail. Consequently, the pullout resistance shows a displacement-hardening behaviour.
- The conventional driven soil nail does not exhibit any end bearing resistance and 100% of pullout forces arise from the frictional resistance at the nail-soil interface.
- The innovative driven-grouted soil nail (x-Nail), which combines the facilities of conventional driven (purely frictional) and compaction grouted soil nails, maximizes the compaction effects on the surrounding soil in two ways: (1) by the driving process and (2) by the pressure grouting process. In addition, the x-Nail exhibits a substantial end bearing resistance. Overall, it could be said that the x-Nail is a promising alternative means of soil reinforcement, which might be capable of withstanding a relatively large deformation before failure.

Chapter 8 Conclusions and recommendations

8.1 General

This thesis focuses on the development of a test facility to conduct a physical model study of a pressure-grouted soil nail system in order to evaluate the grout injection rate and grout viscosity effects on the formation of the grout body (i.e., grout bulk) and its interaction with the surrounding soils. In addition, an innovative driven and grouted soil nail was proposed in this research program and its performance in terms of pullout resistance was investigated with respect to a conventional driven soil nail. The results obtained from this research are presented and discussed in Chapters 5, 6, and 7 with the specific conclusions of each experimental investigation. In this chapter, a number of general conclusions are summarized on the basis of the experimental results and some recommendations are outlined for future study.

8.2 Conclusions

Based on the performance of the test facility, the following major conclusions and competitive advantages can be summarized as follows:

- The automatic grout injection pump of the developed test facility allows grout to be injected at different flow rates ranging from 0.5 to 7.5 L/min. Hence, the effect of grout injection rates on the subsequent behaviour of the pressure-grouted soil nails can be examined using this device. In addition, the variation of injection pressure and the injected grout volume over the grouting period can be monitored using this injection pump.
- The modified system for applying overburden pressure using a water-filled rubber cushion provides constant surcharge pressure over the period of testing and can also be used to estimate the surface settlement easily.
- The updated pullout system is a "two-in-one" system, which makes the apparatus able to study the conventional driven soil nail.

Based on the results of the experimental investigation conducted in this thesis, the following conclusions can also be drawn:

- Grout injection rates significantly influence the amount of grout injected into a soil mass and the volume of injected grout into a soil mass increases when the injection rate is increased.
- The expulsion of water (i.e., pressure filtration) from the pressurized neat cement grout is directly and proportionally related to the injection rate, i.e., the higher the injection rate, the higher the pressure filtration.
- As expected, the increase in confining stress (i.e., normal stress acting at the grout-soil interface) is governed by the injected grout volume, and the confining stress increases with the increased injected grout volume (i.e., increased grout body).
- Pullout capacity of a pressure-grouted soil nail is predominantly influenced by the injected grout volume (i.e., the size of the grout body) rather than the injection pressure, and thus the grouted nail shows a higher pullout resistance for a higher injection rate.
- Addition of an additive (a blend of superplasticizers and suspension agents) decreases the viscosity of the grout significantly by reducing the agglomeration tendency of the cement particles in suspension. The viscosity of cementitious grout increases exponentially as water solid (w/s) ratio decreases, whereas fluidity increases with increasing w/s ratio.
- The water solid (w/s) ratio of a grout mix is a key factor for the penetration of the grout into a soil mass (referred as injectability). Consequently, more grout can be injected in a pressure-grouted soil nail system at a specified injection rate by increasing the w/s ratio, i.e., the lower the viscosity, the larger the injectability.
- The pressure filtration (dissipation of water) from the additive-mixed grout paste under pressurized injection conditions is directly related to the w/s ratio, i.e., the higher the w/s ratio, the higher the pressure filtration. However, the additive-mixed grout with a w/s ratio of 0.30 does not exhibit any pressure filtration during the pressurized grouting into sand, indicating that the additive-mixed grout with a w/s ratio greater than 0.30 is susceptible to the pressure filtration.
- The pressure exerted by the grout onto the soil surrounding the injection point is influenced by the grout viscosity rather than its w/s ratio. The induced soil

pressure instigated by the pressurized grouting process decreases with the increments in grout viscosity.

- For the injection of highly fluid grouts with low grout densities (e.g., w/s = 0.40 and 0.50) in a pressure-grouted nail system, the grout bodies formed around the injection points deform under asymmetric stress conditions (i.e., K_o = 0.5) over the curing period, and thus they become relatively flattened, cylindrically-shaped bulbs compared to the high density grout (w/s = 0.30) with a moderate viscosity. Hence, these irregular grout bulbs (deformed bulbs) fail easily due to stress concentration at a very small pullout displacement without mobilizing the maximum pullout capacity for a specified grout injection volume, which indicates that the pullout resistance of the pressure-grouted nail is not only influenced by the injected grout volume but it also affected by the shape of the bulb.
- In order to form a cylindrically-shaped grout bulb (effective shape), it is therefore recommended that the high density additive-mixed grout with a moderate viscosity (e.g., w/s = 0.30) may be applied as an effective injection fluid for the pressure-grouted soil nail system because of its high bleed resistance, high compressive strength, high bond strength, low shrinkage and high fluidity. Moreover, this additive-mixed cementitious grout with a w/s ratio of 0.30 can be an alternative to the traditional neat cement grout used in pressure-grouted soil nail systems.
- For the innovative x-Nail, it is found that the pullout force of the grouted x-Nail is much higher compared with the conventionally driven (purely frictional) soil nail. The pullout force of the grouted driven nail increases almost linearly with increases in diameter of the grout bulb (i.e., the larger the bulb diameter, the higher the pullout force) since the grout bulb provides a significant amount of end bearing resistance that results from the passive resistance of the soil situated in front of the bulb. Almost 90% of pullout force is resisted by the expanded grout bulb. Consequently, the grouted x-Nail works as an anchor instead of a frictional nail and shows a displacement-hardening behaviour in pullout force. Overall, it could be said that the x-Nail is a promising alternative means of soil reinforcement that might be capable of withstanding a relatively large deformation before failure.

8.3 Recommendations for future study

The scope of this research was limited to the experimental study. There is scope to do further research on the pressure grouted soil nail, as follows:

1. To investigate the interaction behaviour of the pressurized cementitious grout in cohesionless soils, further experimental and numerical studies are required. For numerical investigation, the extended finite element method (XFEM) can be employed to investigate the effects of grout injection rates and viscosities, and thus the grout penetration, pressure filtration and load transfer mechanism can be investigated in detail via numerical simulation.
2. An extended cylindrical soil chamber has already been designed and fabricated, which can be connected to the circular opening made on the front wall of the test box. This will allow the movement of the soil situated adjacent to the front wall of the box and thus minimize the boundary effects that are expected to develop during the pullout process. Therefore, further experimental study is necessary using this chamber to quantify the influence of the boundary effects on grout volume increase on the pullout capacity of the anchor-type nail.
3. In the innovative x-Nail system, the push-in plugs can be employed at the injection points instead of a grout bag facility for direct injection of grout into the soil which has the possibility of minimizing the risk of membrane breakage during the driving process of the x-Nail with a latex membrane. A detailed experimental study needs to be conducted for the x-Nail with a push-in plug set installed around the nail head.
4. To evaluate the performance of the x-Nail in clayey soil, further experimental study is required.
5. An extensive theoretical study is required to develop an analytical model for the innovative driven and grouted soil nail.
6. A numerical modelling tool, e.g., the discrete element method (DEM), can be used to simulate the driving, grouting and pulling out behaviour of the x-Nail in soil. It is suggested that the DEM could be an effective tool compared with Finite Element Method (FEM) for simulating the discontinuum medium (e.g., soil).

7. Further study is required to update and redesign the existing grout bag facility of the x-Nail before its practical application. An inflatable latex membrane (cylindrical in shape) was attached around the nail head using two O-rings, which has the possibility to fail during the driving and/or grouting process.
8. Furthermore, there is scope to investigate the effects of overburden pressure and moisture content on the pullout behaviour for this type of soil nail. A detailed experimental and field study could be conducted to understand the creep behaviour of the x-Nail as well.

References

Ajalloeian, R., Yu, H. S., & Allman, M. A. (1996). Physical and mechanical properties of stockton beach sand. In M.B. Jaksa, W.S. Kaggwa, & D.A. Cameron (Eds), *7th Australia New Zealand Conference on Geomechanics: Geomechanics in a Changing World* (pp. 60-65). Retrieved from https://search.informit.com.au/documentSummary;dn=551255861887012;res=IELENG;type=pdf

Axelsson, M., Gustafson, G., & Fransson, Å. (2009). Stop mechanism for cementitious grouts at different water-to-cement ratios. *Tunnelling and Underground Space Technology, 24*(4), 390-397. https://doi.org/10.1016/j.tust.2008.11.001

Aziz, E. S., & Stephens, T. J. (2013). Cost and schedule savings from directly-driven soil nail and innovative fascia systems. In C. Meehan, D. Pradel, M. Pando & J. Labuz (Eds.), *Geo-Congress 2013: Stability and Performance of Slopes and Embankments III* (pp. 1704-1718). https://doi.org/10.1061/9780784412787.171

Bang, S., Shen, C. K., & Romstad, K. M. (1980). Analysis of an earth-reinforcing system for deep excavation. *Transportation Research Record* (749), 21-26. Retrieved from https://www.scopus.com/inward/record.uri?eid=2-s2.0-0019213876&partnerID=40&md5=92702dbb764cde833a0dbd47aa8d1169

Bezuijen, A. (2010). *Compensation grouting in sand-experiments, field experiences and mechanisms* (Doctoral dissertation). Retrieved from http://resolver.tudelft.nl/uuid:5c19254c-6a3f-49da-845d-329fae1a3ca8

Bezuijen, A., Sanders, M., Den Hamer, D., & Van Tol, A. (2007). Laboratory tests on compensation grouting, the influence of grout bleeding.In J. Barták, I. Hrdina, G. Romancov, & J. Zlámal (Eds), *Underground Space-The 4th Dimension of Metropolises, Proceedings of the World Tunnel Congress 2007 and 33rd ITA/AITES Annual General Assembly* (pp. 395-401). Retrieved from https://www.taylorfrancis.com/books/e/9780429107238/chapters/10.1201/NOE0415408073-44

Bezuijen, A., & van Tol, F. (2007). Compensation grouting in sand, fractures and compaction. *14th European Conference on Soil Mechanics and Geotechnical Engineering* (pp. 1257-1262).

Bhuiyan, M. Z. I., Wang, S., Sloan, S. W., Sheng, D., & Ming, L. K. (2018a). Gravity grouting and its future alternative for soil reinforcement systems. In W. Wu & H.S. Yu (Eds), *Proceedings of China-Europe Conference on Geotechnical Engineering* (pp. 898-901). https://doi.org/10.1007/978-3-319-97115-5_4

Bhuiyan, M. Z. I., Wang, S., Sloan, S. W., Sheng, D., & Michel, H. (2018b). Calibration of earth pressure cell for a specified laboratory application. In Z. Hossain, B.B.K. Huat, V. Anggraini, & J. Shiau (Eds), *8th International Conference on Geotechnique, Construction Materials and Environment* (pp. 263-268). Retrieved from http://eprints.usq.edu.au/id/eprint/35187

Bhuiyan, M. Z. I., Wang, S., Sloan, S. W., Carter, J., & Raka, T. M. (2019). Effects of grout injection techniques in pressure grouted soil nail system. *7th International Symposium on Deformation Characteristics of Geomaterials* (pp. 1-6). https://doi.org/10.1051/e3sconf/20199217010

Bhuiyan, M. Z. I., Wang, S., Carter, J. P., & Raka, T. M. (2020a). An innovative driven soil nail (X-Nail): A promising alternative to conventional soil nails. *Geo-congress 2020*, (pp. 383-393). https://ascelibrary.org/doi/abs/10.1061/9780784482797.038

Bhuiyan, M. Z. I., Wang, S., Carter, J. P., & Raka, T. M. (2020b). Calibration and assessment of capacitance-based soil moisture sensors. *Geo-Congress 2020* (pp. 754-766). https://ascelibrary.org/doi/abs/10.1061/9780784482797.074

Bilskie, J. (2001). *Soil water status: Content and potential*. Retrieved from https://s.campbellsci.com/documents/us/technical-papers/soilh20c.pdf

Bluey Technologies (2017). *BluCem HS200A PT cable grout additive*. QLD, Australia: Bluey Technologies. Retrieved from https://www.bluey.com.au/products/blucem-hs200a

Boral Cement (2017). *General purpose cement - Product data sheet*. Retrieved from http://www.boral.com.au/productcatalogue/product.aspx?product=2268

Bruce, D. A., & Jewell, R. A. (1986). Soil nailing: Application and practice - Part 1. *Ground Engineering, 19*(8), 10-15.

Bruce, D. A., & Jewell, R. A. (1987). Soil nailing: Application and Practice - Part 2. *Ground Engineering, 20*(1), 21-33.

Burgoyne, C., & Balafas, I. (2007). Why is FRP not a financial success? *8th International Conference on FRP Reinforcement for Reinforced Concrete Structures* (pp. 1-10). Retrieved from http://www-civ.eng.cam.ac.uk/cjb/papers/cp74.pdf

Byrne, J. R., Chassie, R. G., Keeley, J. W., Bruce, D. A., Nicholson, P., Walkinshaw, J. L., Ludwig, C. (1993). *FHWA tour for geotechnology - Soil nailing* (FHWA-PL-93-020).

Caleffi International (2018). *Inclined Pressure Reducing Valves: Installation, commissioning and servicing instructions*. Retrieved from https://www.caleffi.com/sites/default/files/file/38538.10.pdf

Cartier, G., & Gigan, J. P. (1983). Experiments and observations in soil nailing structures. *Proceedings of the 8th European Conference on Soil Mechanics and Foundation Engineering* (pp. 473-476).

Chai, X. J., & Hayashi, S. (2005). Effect of constrained dilatancy on pull-out resistance of nails in sandy clay. *Proceedings of the Institution of Civil Engineers - Ground Improvement, 9*(3), 127-135. doi:10.1680/grim.2005.9.3.127

Cheng, Y. M., Au, S. K., Pearson, A. M., & Li, N. (2013). An innovative Geonail system for soft ground stabilization. *Soils and Foundations, 53*(2), 282-298. doi:10.1016/j.sandf.2013.02.009

Cheng, Y. M., Au, S. K., & Yeung, A. T. (2016). Laboratory and field evaluation of several types of soil nails for different geological conditions. *Canadian Geotechnical Journal, 53*(4), 634-645. doi:10.1139/cgj-2015-0267

Cheng, Y. M., Choi, Y. K., Yeung, A. T., Tham, L. G., Au, A. S. K., Wei, W. B., & Chen, J. (2009). New soil nail material-pilot study of grouted GFRP pipe nails in Korea and Hong Kong. *Journal of Materials in Civil Engineering, 21*(3), 93-102. doi:10.1061/(Asce)0899-1561(2009)21:3(93)

Chu, L. M. (2003). *Study on the interface shear strength of soil nailing in completely decomposed granite (CDG) soil* (Master's thesis). Retrieved from http://hdl.handle.net/10397/2135

Chu, L. M., & Yin, J. H. (2005a). A laboratory device to test the pull-out behavior of soil nails. *Geotechnical Testing Journal, 28*(5), 499-513. https://doi.org/10.1520/GTJ12212

Chu, L. M., & Yin, J. H. (2005b). Comparison of interface shear strength of soil nails measured by both direct shear box tests and pullout tests. *Journal of Geotechnical* *and Geoenvironmental Engineering, 131*(9), 1097-1107. doi:10.1061/(Asce)1090-0241(2005)131:9(1097)

Cobos, D. (2015). *Measurement volume of Decagon volumetric water content sensors*. Retrieved from http://manuals.decagon.com/Application%20Notes/14955_VWC%20Sensor%20Measurement%20Volumes_Web.pdf

Coduto, D. P. (1999). *Geotechnical engineering: Principles and practices*. Upper Saddle River, NJ: Prentice Hall.

DataTaker (2011). *DT80 Series 3 Data Logger* (Techncial information). Retrieved from https://www.dataloggerinc.com/wp-content/uploads/2016/09/dt80-intelligent-universal-input-data-logger.pdf

Deardorff, D. (2014). *An introduction to helical soil nails*. Retrieved from https://dc69b531ebf7a086ce97-290115cc0d6de62a29c33db202ae565c.ssl.cf1.rackcdn.com/319/AnIntroToHelicalSoilNails.pdf

Deardorff, D., Moeller, M., & Walt, E. (2010). Results of an instrumented helical soil nail wall. In In R. Finno, Y. Hashash, & P. Arduino (Eds.), *Earth Retention Conference 3* (pp. 262-269). https://doi.org/10.1061/9780784411285

Decagon Devices (2016). *GS3 water content, EC, and temperature sensors.* Retrieved from http://manuals.decagon.com/Manuals/13822_GS3_Web.pdf

Dey, A. (2015). Issues and aspects of soil nailing. *QIP-STC Challenges and Recent Advances in Geotechnical Engineering Research and Practice (pp. 1-21). Retrieved from* http://citeseerx.ist.psu.edu/viewdoc/download?doi=10.1.1.712.6886&rep=rep1&type=pdf

Drooff, E. R., Tavares, P. D., & Forbes, J. (1995). Soil fracture grouting to remediate settlement due to soft ground tunneling. *12th Rapid Excavation and Tunneling Conference* (pp. 21-40). Retrieved from https://www.tib.eu/en/search/id/BLCP%3ACN012010023/Soil-Fracture-Grouting-to-Remediate-Settlement/

Essler, R. D., Drooff, E. R., & Falk, E. (2000). Compensation grouting: Concept, theory and practice. Geo-Denver 2000 (pp. 1-15). Retrieved from https://ascelibrary.org/doi/pdf/10.1061/40516(292)1

Fanchi, J. R. (2010). *Integrated reservoir asset management*. Boston, MA: Gulf Professional Publishing.

Fann Instrument Company (2013). *Marsh Funnel Viscometer instructions*. Retrieved from https://www.fann.com/content/dam/fann/Manuals/Marsh_Funnel_Instruction.pdf

FHWA (1993). *Recommendations clouterre 1991 (English translation): Report on the French national research project clouterre*. Retrieved from https://ntrl.ntis.gov/NTRL/dashboard/searchResults/titleDetail/PB94109980.xhtml

Franzen, G. (1998). *Soil nailing - A laboratory and field study of pullout capacity* (Doctoral dissertation). Retrieved from https://research.chalmers.se/en/publication/845

Franzen, G., & Jendeby, L. (2001). Prediction of pullout capacity of soil nails. *15th International Conference on Soil Mechanics and Geotechnical Engineering* (pp. 1743-1747). Retrieved from https://www.issmge.org/uploads/publications/1/30/2001_03_0016.pdf

Gässler, G. U. (1983). Discussion of "Ground movement analysis of earth support system: Field measurements of an earth support system" C. K. Shen, S. Bang, K. M.

Romstad, L. Kulchin, and J. S. DeNatale (Dec., 1981). *Journal of Geotechnical Engineering, 109*(3), 488-490. doi:10.1061/(ASCE)0733-9410(1983)109:3(488.2)

Gafar, K., Soga, K., Bezuijen, A., Sanders, M., & Van Tol, A. (2008). Fracturing of sand in compensation grouting. In C.W.W. Ng, H.W. Huang, & G.B. Lie (Eds), *2008 6th International Symposium of Geotechnical Aspects of Underground Construction in Soft Ground* (pp. 281-286), Retrieved from https://www.issmge.org/uploads/publications/6/12/2008_033.pdf

Garnier, J., Ternet, O., Cottineau, L.-M., & Brown, C. (1999). Placement of embedded pressure cells. *Geotechnique, 49*(3), 415-421. https://doi.org/10.1680/geot.1999.49.3.415

GEO (2008). *Geoguide 7 - Guide to soil nail design and construction* (Report No. 197). Retrieved from https://www.cedd.gov.hk/filemanager/eng/content_118/eg7_200803.pdf

Guilloux, A., & Schlosser, F. (1982). Soil nailing: Practical applications. In A. S. Balasubramaniam (Ed), *Symposium on Recent Development in Ground Improvement Technique* (pp. 389-397).

Gurpersaud, N., Vanapalli, S. K., & Sivathayalan, S. (2013). Semiempirical method for estimation of pullout capacity of grouted soil nails in saturated and unsaturated soil environments. *Journal of Geotechnical and Geoenvironmental Engineering, 139*(11), 1934-1943. doi:10.1061/(ASCE)GT.1943-5606.0000883

HA68/94 (1994). *Design methods for the reinforcement of highway slopes by reinforced soil and soil nailing techniques*.

Heymann, J. E., Rohde, A. W., Schwartz, W., & Friedlander, E. (1992). Soil nail pullout resistance in residual soils. In H. Ochiai, S. Hayashi, & J. Otani (Eds), *International Symposium on Earth Reinforcement Practice* (pp. 487-492). Retrieved from https://www.tib.eu/en/search/id/BLCP%3ACN003511649/Soil-nail-pull-out-resistance-in-residual-soils/

Hong, C.-Y., Zhang, Y.-F., Guo, J.-W., & Li, G.-Y. (2016). Experimental study on the influence of drillhole roughness on the pullout resistance of model soil nails. *International Journal of Geomechanics, 16*(2), 04015047. doi:10.1061/(ASCE)GM.1943-5622.0000491

Hong, Y.-S., Wu, C.-S., & Yang, S.-H. (2003). Pullout resistance of single and double nails in a model sandbox. *Canadian Geotechnical Journal, 40*(5), 1039-1047. https://doi.org/10.1139/t03-048

Hsu, S., & Liao, H. (1998). Uplift behaviour of cylindrical anchors in sand. *Canadian Geotechnical Journal, 35*(1), 70-80. https://doi.org/10.1139/t97-067

Jaky, J. (1941). The coefficient of earth pressure at rest. *Journal Society of Hungarian Architects and Engineers, 78*(22), 355–358.

Jewell, R. A. (1990). P3/12 Review of theoretical models for soil nailing. In A. McGown, K. Yeo & K.Z. Andrawes (Eds), *International Reinforced Soil Conference* (pp. 265-275).

Jewell, R. A., & Wroth, C. P. (1987). Direct shear tests on reinforced sand. *Geotechnique, 37*(1), 53-68. doi:10.1680/geot.1987.37.1.53

Johnson, P. E., Card, G. B., & Darley, P. (2002). *Soil nailing for slopes*. Retrieved from: https://trl.co.uk/sites/default/files/TRL537.pdf

Junaideen, S. M. (2001). *The design and performance of a pressure chamber for testing soil nails in loose fill* (Master's thesis). Retrieved from http://hdl.handle.net/10722/33603

Junaideen, S. M., Tham, L. G., Law, K. T., Lee, C. F., & Yue, Z. Q. (2004). Laboratory study of soil-nail interaction in loose, completely decomposed granite. *Canadian Geotechnical Journal, 41*(2), 274-286. doi:10.1139/T03-094

Juran, I. (1987). Nailed-soil retaining structures: Design and practice. *Transportation Research Record*, 139-150. Retrieved from http://onlinepubs.trb.org/Onlinepubs/trr/1987/1119/1119-019.pdf

Keong, K. S. (2006). *Properties of cement based permeation grout used in ground engineering* (Master's thesis). Retrieved from https://core.ac.uk/download/pdf/48633813.pdf

Kim, T.-C., Liu, J., & Lee, S. (2014). Soil nailing for highway construction and maintenance in Ontario. *Geo Regina 2014* (pp. 1-8).

Kim, Y., Lee, S., Jeong, S., & Kim, J. (2013). The effect of pressure-grouted soil nails on the stability of weathered soil slopes. *Computers and Geotechnics, 49*, 253-263. doi:10.1016/j.compgeo.2012.12.003

Koerner, R. M. (1984). *Construction and geotechnical methods in foundation engineering*. Michigan: McGraw-Hill.

Kuhling, G., Tax, M., & Schulze, B. (1994). New additives for microfine grouts with low water: Cement ratios. *13th International Conference on Soil Mechanics and Foundation Engineering* (pp. 1171-1177). Retrieved from https://www.tib.eu/en/search/id/BLCP%3ACN003381596/New-Additives-for-Microfine-Grouts-with-Low-Water/

Lazarte, C. A., Elias, V., Espinoza, R. D., & Sabatini, P. J. (2003). *Geotechnical Engineering Circular No. 7: Soil Nail Walls* (FHWA0-IF-03-017).

Lazarte, C. A., Robinson, H., Gómez, J. E., Baxter, A., Cadden, A., & Berg, R. (2015). *Soil nail walls - Reference manual* (FHWA-NHI-14-007). Retrieved from https://www.fhwa.dot.gov/engineering/geotech/pubs/nhi14007.pdf

Lee, S.-W. (2002). The use of compensation grouting in tunnelling: A case study. *Proceedings of the Institution of Civil Engineers-Geotechnical Engineering, 155*(2), 101-109. Retrieved from https://www.icevirtuallibrary.com/doi/pdf/10.1680/geng.2002.155.2.101

Lee, S.-W., Kim, T.-S., Sim, B.-K., Kim, J.-S., & Lee, I.-M. (2012). Effect of pressurized grouting on pullout resistance and group efficiency of compression ground anchor. *Canadian Geotechnical Journal, 49*(8), 939-953. doi:10.1139/t2012-059

Littlejohn, G. (1980). Design estimation of the ultimate load-holding capacity of ground anchors. *Ground Engineering, 13*(8).

Littlejohn, S. (2003). The development of practice in permeation and compensation grouting: A historical review (1802–2002): Part 1 permeation grouting. In L.F. Johnsen, D.A. Bruce, & M.J. Byle, (Eds), *Grouting and Ground Treatment, 3rd International Conference on Grouting and Ground Treatment* (pp. 50-99). https://doi.org/10.1061/40663(2003)3

Luo, S. Q., Tan, S. A., & Yong, K. Y. (2000). Pull-out resistance mechanism of a soil nail reinforcement in dilative soils. *Soils and Foundations, 40*(1), 47-56. doi:10.3208/sandf.40.47

Luo, S. Q., Tan, S. A., Cheang, W., & Yong, K. Y. (2002). Elastoplastic analysis of pull-out resistance of soil nails in dilatant soils. *Proceedings of the Institution of Civil Engineers - Ground Improvement, 6*(4), 153-161. doi:10.1680/grim.2002.6.4.153

McIlveen, A. (n.d.). *Ballistic soil nailing*. Retrieved from //www.tmr.qld.gov.au/-/media/busind/techstdpubs/Supporting-documents/Queensland-roads-technical-journal/September-2010/05Balisticnailsoilingedition9page615.pdf?la=en BALLISTIC SOIL NAILING

Micromeritics (2019). SediGraph III PLUS Particle Size Analyzer. Retrieved from https://www.micromeritics.com/Repository/Files/SediGraph_III_Plus_1.pdf

Milligan, G. W. E., Chang, K. T., & Morris, J. D. (1997). Pull-out resistance of soil nails in sand and clay. *3rd International Conference on Ground Improvement Geosystems* (pp. 414-422). Retrieved from https://trid.trb.org/view/635517

Milligan, G. W. E., & Tei, K. (1998). The pull-out resistance of model soil nails. *Soils and Foundations, 38*(2), 179-190. doi:10.3208/sandf.38.2_179

Mohammed, M. H., Pusch, R., Knutsson, S., & Hellström, G. (2014). Rheological properties of cement-based grouts determined by different techniques. *Engineering, 6*(05), 217.

Moradi, G., & Zadkarim, S. (2016). Field study of the effect of grout used on tensile strength and creep behavior of grout nails in green marl. *The Electronic Journal of Geotechnical Engineering, 21*(2), 521-532. Retrieved from http://www.ejge.com/2016/Ppr2016.0064ma.pdf

Naudts, A., Landry, E., Hooey, S., & Naudts, W. (2003). Additives and admixtures in cement-based grouts. *3rd International Conference on Grouting And Ground Treatment* (pp. 1180-1191). https://doi.org/10.1061/40663(2003)66

Nichols, S. C., & Goodings, D. J. (2000). Effects of grout composition, depth and injection rate on compaction grouting. *Geo-Denver 2000: Advances in Grouting and Ground* (pp. 16-31). https://doi.org/10.1061/40516(292)2

Nomoto, T. S. T., Nomoto, M., & Hagiwara, Y. A. (2000). Compensation grouting at the Docklands Light Railway Lewisham Extension project. In K.K. Fujita, O. Kusakabe, & Y. Miyazaki (Eds), *International Symposium on Geotechnical Aspects of Underground Construction in Soft Ground* (pp. 319-324). Retrieved from http://publications.eng.cam.ac.uk/329900/

NRCS (2016, November 16). Review of Relative Density Principles. https://www.wcc.nrcs.usda.gov/

Ortigao, J. (1996). FRP applications in geotechnical engineering. *ASCE 4th Materials Engineering Conference* (pp. 535-544). Retrieved from https://cedb.asce.org/CEDBsearch/record.jsp?dockey=0102918

Palmeria, E., & Milligan, G. (1989). Scale and other factors affecting the results of pull-out tests of grids buried in sand. *Geotechnique, 39*(3), 511-542. https://doi.org/10.1680/geot.1989.39.3.511

Parsapajouh, A., Litkouhi, S., & Amini, B. (2012). A case study on excavation stabilization using ground anchors and high pressure injection. In L.F. Johnsen, D.A. Bruce, & M.J. Byle (Eds), *Grouting and Deep Mixing 2012*, *4th International Conference on Grouting and Deep Mixing* (pp. 1115-1123). https://doi.org/10.1061/9780784412350

Potyondy, J. G. (1961). Skin friction between various soils and construction materials. *Geotechnique, 11*(4), 339-353. doi:10.1680/geot.1961.11.4.339

Pradhan, B. (2003). *Study of pullout behaviour of soil nails in completely decomposed granite fill* (Master's thesis). Retrieved from http://hdl.handle.net/10722/31203

Pradhan, B., Tham, L. G., Yue, Z. Q., Junaideen, S. M., & Lee, C. F. (2006). Soil–nail pullout interaction in loose fill materials. *International Journal of Geomechanics, 6*(4), 238-247. doi:10.1061/(ASCE)1532-3641(2006)6:4(238)

Pun, W., & Shiu, Y. (2007). Design practice and technical developments of soil nailing in Hong Kong. *27th Annual Seminar: Geotechnical Advancements in Hong Kong Since 1970s*. Hong Kong Institution of Engineers, Geotechnical Division, Hong Kong.

Raffle, J. F., & Greenwood, D. A. (1961). The relationship between the rheological characteristics of grouts and their capacity to permeate soils. *5th International Conference on Soil Mechanics and Foundation Engineering* (pp. 789-793).

RMS. (2018). QA specification R64: Soil nailing. Roads And Maritime Services, New South Wales, Australia. Retrieved from https://www.rms.nsw.gov.au/business-industry/partners-suppliers/documents/specifications/r064.pdf

Rosquoët, F., Alexis, A., Khelidj, A., & Phelipot, A. (2003). Experimental study of cement grout: Rheological behavior and sedimentation. *Cement and Concrete Research, 33*(5), 713-722. https://doi.org/10.1016/S0008-8846(02)01036-0

Samaiklang, W., & Fuenkajorn, K. (2013). Mechanical and hydraulic performance of cement grouts from five suppliers in Thailand. *7th International Conference on Materials, Mining And Petroleum Engineeirng* (pp. 45-51). Retirieved from http://mining.eng.cmu.ac.th/wp-content/uploads/2013/11/Material-Sciences_8_PaperID-98.pdf

Schlosser, F. (1982). Behaviour and design of soil nailing. *Symposium on Recent Developments in Ground Improvement* (pp. 399-413).

Schlosser, F., & Unterreiner, P. (1991). Soil nailing in France: Research and practice. *Transportation Research Record, 1330*, 72-79. http://onlinepubs.trb.org/Onlinepubs/trr/1991/1330/1330-009.pdf

Seo, H. J., Jeong, K. H., Choi, H., & Lee, I. M. (2012). Pullout resistance increase of soil nailing induced by pressurized grouting. *Journal of Geotechnical and Geoenvironmental Engineering, 138*(5), 604-613. doi:10.1061/(Asce)Gt.1943-5606.0000622

Sin Dong Geological Engineering. (n.d.) Range of soil by grouting method [Graph]. Retrieved February 2020 from https://web.archive.org/web/20200212064744/https://www.sindong.com.sg/wordpress/wp-content/uploads/2014/12/Range-of-Soil-by-Grouting-Method1.png. Singapore: http://www.sindong.com.sg/wordpress/?page_id=10.

Sharma, M., Samanta, M., & Sarkar, S. (2019). Novel laboratory pullout device for conventional and helical soil nails. *Geotechnical Testing Journal, 42(5), 1314-1335.* doi:10.1520/GTJ20170319

Sharma, M., Samanta, M., & Sarkar, S. (2017). Laboratory study on pullout capacity of helical soil nail in cohesionless soil. *Canadian Geotechnical Journal, 54*(10), 1482-1495. doi:10.1139/cgj-2016-0243

Shiu, Y. K., & Chang, G. W. K. (2006). *Effects of inclination, length pattern and bending stiffness of soil nails on behaviour of nailed structures* (GEO report No. 197). Retrieved from https://www.cedd.gov.hk/filemanager/eng/content_352/er197links.pdf

Standards Australia. (2009). *Methods of testing soils for engineering purposes. Method 3.6.1: Soil classification tests—Determination of the particle size distribution of a soil—Standard method of analysis by sieving*. (AS 1289.3.6.1-2009). Sydney, NSW: Standards Australia

Standards Australia. (2003). *Soil compaction and density tests—Determination of the dry density/moisture content relation of a soil using standard compactive effort* (AS1289.5.1.1-2003). Sydney, NSW: Standards Australia.

Standards Australia. (1998). *Methods of testing soils for engineering purposes. Soil strength and consolidation tests—Determination of the dry density/moisture content relation of a soil using standard compactive effort* (AS1289.6.2.2-1998). Sydney, NSW: Standards Australia.

Standards Australia. (2001). *Soil strength and consolidation tests—Determination of permeability of a soil—Constant head method for a remoulded specimen* (AS 1289.6.7.1-2001). Sydney, NSW: Standards Australia.

Stephens, T. J., Holtz, R. D., & Aziz, E. S. (2013). Construction and initial performance of a full-scale excavation supported by spiralnail groutless soil nails. In A.W. Stuedlein & B.R. Christopher (Eds), Geo-congress 2013: *Sound Geotechnical Research to Practice* (pp. 525-538). https://doi.org/10.1061/9780784412770.035

Stocker, M. F., Korber, G. W., Gassler, G., & Gudehus, G. (1979). Soil nailing. *International Conference on Soil Reinforcement* (pp. 469-474).

Su, L.-J., Chan, T. C. F., Shiu, Y. K., Cheung, T., & Yin, J.-H. (2007). Influence of degree of saturation on soil nail pull-out resistance in compacted completely decomposed granite fill. *Canadian Geotechnical Journal, 44*(11), 1314-1328. doi:10.1139/T07-056

Su, L.-J., Chan, T. C. F., Yin, J.-H., Shiu, Y. K., & Chiu, S. L. (2008). Influence of overburden pressure on soil–nail pullout resistance in a compacted fill. *Journal of Geotechnical and Geoenvironmental Engineering, 134*(9), 1339-1347. doi:10.1061/(ASCE)1090-0241(2008)134:9(1339)

Su, L. J. (2006). *Laboratory pull-out testing study on soil nails in compacted completely decomposed granite fill* (Doctoral dissertation). Retrieved from http://ira.lib.polyu.edu.hk/handle/10397/3820

Su, L. J., Yin, J. H., & Zhou, W. H. (2010). Influences of overburden pressure and soil dilation on soil nail pull-out resistance. *Computers and Geotechnics, 37*(4), 555-564. doi:10.1016/j.compgeo.2010.03.004

Tex-142-E (1996). Laboratory classification of soils for engineering purposes. USA: Texas Department of Transportation. Retrieved from http://ftp.dot.state.tx.us/pub/txdot-info/cst/TMS/100-E_series/pdfs/soi142.pdf

Tokhi, H., Ren, G., & Li, J. (2016). Laboratory pullout resistance of a new screw soil nail in residual soil. *Canadian Geotechnical Journal, 55*(5), 609-619. doi:10.1139/cgj-2017-0048

Vermeer, P. A. (1990). The orientation of shear bands in biaxial tests. *Geotechnique, 40*(2), 223-236. doi:10.1680/geot.1990.40.2.223

Walker, A., Pearlman, S., & Kartofilis, D. (1997). Advances in grouting technology. *World Tunnelling and Subsurface Excavation, 10*(9).

Wang, Q., Wang, S. Y., Sloan, S. W., Sheng, D. C., & Pakzad, R. (2016). Experimental investigation of pressure grouting in sand. *Soils and Foundations, 56*(2), 161-173. doi:10.1016/j.sandf.2016.02.001

Wang, Q., Ye, X., Wang, S., Sloan, S. W., & Sheng, D. (2017a). Experimental investigation of compaction-grouted soil nails. *Canadian Geotechnical Journal, 54*(12), 1728-1738. doi:10.1139/cgj-2017-0063

Wang, Q., Ye, X., Wang, S., Sloan, S., & Sheng, D. (2017b). Development of a model test system for studying the behaviour of a compaction grouted soil nail under unsaturated conditions. *Geotechnical Testing Journal, 40*(5), 776-788. doi:10.1520/GTJ20160229

Warner, J. (2004). *Practical handbook of grouting: Soil, rock, and structures*. John Wiley & Sons.

Winterkorn, H. F., & Pamukcu, S. (1991). Soil stabilization and grouting. In H.-Y. Fang (Ed.), *Foundation Engineering Handbook* (pp. 317-378). Boston, MA: Springer US.

Wood, T. A., Jayawickrama, P. W., & Lawson, W. D. (2009). Instrumentation and monitoring of an MSE/soil nail hybrid retaining wall. In M. Iskander, D.F. Laefer,

& M.H. Hussein (Eds), *Contemporary topics in ground modification, problem soils, and geo-support* (pp. 177-184). https://doi.org/10.1061/9780784410233

Ye, X., Wang, S., Wang, Q., Sloan, S. W., & Sheng, D. (2017). Numerical and experimental studies of the mechanical behaviour for compaction grouted soil nails in sandy soil. *Computers and Geotechnics, 90*, 202-214. doi: 10.1016/j.compgeo.2017.06.011

Ye, X., Wang, Q., Wang, S., Sloan, S., & Sheng, D. (2019a). Performance of a compaction-grouted soil nail in laboratory tests. *Acta Geotechnica, 14*(4), 1049-1063. doi:10.1007/s11440-018-0693-y

Ye, X., Wang, S., Wang, Q., Sloan, S. W., & Sheng, D. (2019b). The influence of the degree of saturation on compaction-grouted soil nails in sand. *Acta Geotechnica, 14*(4), 1101-1111. doi:10.1007/s11440-018-0706-x

Ye, X., Wang, S., Xiao, X., Sloan, S., & Sheng, D. (2019c). Numerical study for compaction-grouted soil nails with multiple grout bulbs. *International Journal of Geomechanics, 19*(2), 04018193. doi:10.1061/(ASCE)GM.1943-5622.0001342

Yeo, K., & Leung, S. (2001). Soil nail design with respect to Hong Kong conditions. *Landmarks in Earth Reinforcement, 1*, 759-764.

Yeung, A. T., Cheng, Y. M., Tham, L. G., Au, A. S., So, S. T., & Choi, Y.-K. (2007). Field evaluation of a glass-fiber soil reinforcement system. *Journal of Performance of Constructed Facilities, 21*(1), 26-34. doi:10.1061/(ASCE)0887-3828(2007)21:1(26)

Yin, J.-H., & Zhou, W.-H. (2009). Influence of grouting pressure and overburden stress on the interface resistance of a soil nail. *Journal of Geotechnical and Geoenvironmental Engineering, 135*(9), 1198-1208. doi:10.1061/(ASCE)GT.1943-5606.0000045

Yin, J. H., Su, L. J., Cheung, R. W. M., Shiu, Y. K., & Tang, C. (2009). The influence of grouting pressure on the pullout resistance of soil nails in compacted completely decomposed granite fill. *Geotechnique, 59*(2), 103-113. doi:10.1680/geot.2008.3672

Yin, X. H., & Su, L. J. (2006). An innovative laboratory box for testing nail pull-out resistance in soil. *Geotechnical Testing Journal, 29*(6), 451-461. https://doi.org/10.1520/GTJ100216

Zhang, L. L., Zhang, L. M., & Tang, W. H. (2009). Uncertainties of field pullout resistance of soil nails. *Journal of Geotechnical and Geoenvironmental Engineering, 135*(7), 966-972. doi:10.1061/(ASCE)GT.1943-5606.0000014

Zhou, W.-H. (2015). Pullout resistance of grouted soil nails. In B. Indraratna, J. Chu, & C. Rujikiatkamjorn (Eds.), *Ground improvement case histories* (pp. 533-571). Australia: Butterworth-Heinemann.

Zhou, W.-H., Yin, J.-H., & Hong, C.-Y. (2011). Finite element modelling of pullout testing on a soil nail in a pullout box under different overburden and grouting pressures. *Canadian Geotechnical Journal, 48*(4), 557-567. doi:10.1139/t10-086

Zhu, H.-H., Yin, J.-H., Yeung, A. T., & Jin, W. (2011). Field pullout testing and performance evaluation of GFRP soil nails. *Journal of Geotechnical and Geoenvironmental Engineering, 137*(7), 633-642. doi:10.1061/(ASCE)GT.1943-5606.0000457

ZIMM. (2015). *Product specific information*. Retrieved 13 January 2019, from https://zimmscrewjacks.com/product/25-kn-30x6-s-trapezoidal-screw/